



Universitat Autònoma de Barcelona

ADVERTIMENT. L'accés als continguts d'aquesta tesi queda condicionat a l'acceptació de les condicions d'ús establertes per la següent llicència Creative Commons:  http://cat.creativecommons.org/?page_id=184

ADVERTENCIA. El acceso a los contenidos de esta tesis queda condicionado a la aceptación de las condiciones de uso establecidas por la siguiente licencia Creative Commons:  <http://es.creativecommons.org/blog/licencias/>

WARNING. The access to the contents of this doctoral thesis it is limited to the acceptance of the use conditions set by the following Creative Commons license:  <https://creativecommons.org/licenses/?lang=en>

The background features abstract geometric shapes in shades of orange and purple. A large orange shape is in the top left, and a large purple shape is in the bottom right. The text is centered over the white space.

ENGINEERING ALL-IN-ONE PROTEIN-BASED NANOPARTICLES FOR TARGETED CANCER THERAPIES

Laura Sánchez García
PhD Thesis 2019

Doctorat en Biotecnologia

Engineering all-in-one protein-based nanoparticles for targeted cancer therapies

Tesi doctoral 2019

Departament de Genètica i de Microbiologia
Facultat de Biociències



Memòria presentada per la Laura Sánchez García per optar al grau de Doctora en Biotecnologia per la Universitat Autònoma de Barcelona

Laura Sánchez García

Vist i plau dels directors de la tesi:

Antonio Villaverde Corrales

Esther Vázquez Gómez

Ugutzu Unzueta Elorza

Aquest treball ha estat realitzat principalment a l'Institut de Biotecnologia i de Biomedicina, Vicent Villar i Palasí, sota la direcció dels doctors: Antonio Villaverde Corrales, Esther Vázquez Gómez i Ugutz Unzueta Elorza. Una part, però, ha estat duta a terme a la Univerza v Novi Gorici (Eslovènia) sota la supervisió del professor Ario de Marco.

A todos aquellos que me han animado y apoyado durante la tesis,



CONTENTS



ABBREVIATIONS	5
INTRODUCTION	9
1. CANCER TREATMENT AND NANOMEDICINE	9
2. NANOCARRIERS	10
3. CELL-TARGETED DRUG DELIVERY	16
3.1. PASSIVE TARGETING.....	16
3.2. ACTIVE TARGETING.....	21
3.3. CANCER CELL-TARGETING.....	25
4. CARRIER-FREE SELF-ASSEMBLING NANODRUGS	28
4.1. SINGLE-STEP PRODUCTION OF PROTEIN-BASED NANODRUGS.....	30
5. RECOMBINANT PROTEINS	30
5.1. PROTEIN ASSEMBLIES.....	33
5.2. SELF-ASSEMBLING MULTIFUNCTIONAL PROTEINS.....	36
6. CYTOTOXIC PROTEINS AS ANTITUMORAL DRUGS	40
7. OVERVIEW	45
OBJECTIVES	49
RESULTS	53
REVIEW 1	53
ARTICLE 1	65
ARTICLE 2	81
DISCUSSION	101
CONCLUSIONS	125
ANNEXES	129
ANNEX 1: REVIEW 2	129
ANNEX 2: ARTICLE 3	149
ANNEX 3: ARTICLE 4	161
ANNEX 4: ARTICLE 5	173
ANNEX 5: ARTICLE 6	187
ANNEX 6: OTHER PUBLICATIONS	203
ANNEX 7: EUROPEAN PATENT	205
REFERENCES	215

ABBREVIATIONS

ADC: antibody-drug conjugate

bFGF: basic fibroblast growth factor

CC: coiled coil

CD19: cluster of differentiation 19

CD44: cluster of differentiation 44

CNS: central nervous system

CQ: chloroquine

CRC: colorectal cancer

CSC: cancer stem cell

CXCR4: C-X-C chemokine receptor type 4

DDS: drug delivery systems

DLS: dynamic light scattering

DNA: deoxyribonucleic acid

DT: diphtheria toxin

E. coli: *Escherichia coli*

EGCG: epigallocatechin gallate

EPR: enhanced permeability and retention effect

FDA: Food and Drug Administration

FdU: Floxuridine

FESEM: field emission scanning electron microscopy

GFP: green fluorescent protein

GRAS: Generally recognised as safe

HA2: hemagglutinin-2

HER2: human epidermal growth factor receptor-type 2

HIV: human immunodeficiency virus

IBs: inclusion bodies

iRFP: infrared fluorescent protein

IT: immunotoxin

K_d: dissociation constant

LPS: lipopolysaccharides

mAb: monoclonal antibody

MALDI: matrix-assisted laser desorption/ionization

MPS: mononuclear phagocytic system

NSCLC: non-small cell lung cancer

PAA: poly (amidoamine)

PE: *Pseudomonas* exotoxin A

PEG: polyethylene glycol

PEI: polyethylenimine

TMV: tobacco mosaic virus

VLP: virus-like particle



INTRODUCTION

INTRODUCTION

1. CANCER TREATMENT AND NANOMEDICINE

Cancer is the second leading cause of death globally. In fact, nearly 1 in 6 deaths is due to cancer nowadays. It has been estimated that in 2018 it will be responsible for 9.6 million deaths (**Figure 1**). Specifically, lung, prostate and colorectal cancer are the most common types of cancer in men, while breast, colorectal and lung cancer are the most common among women¹.

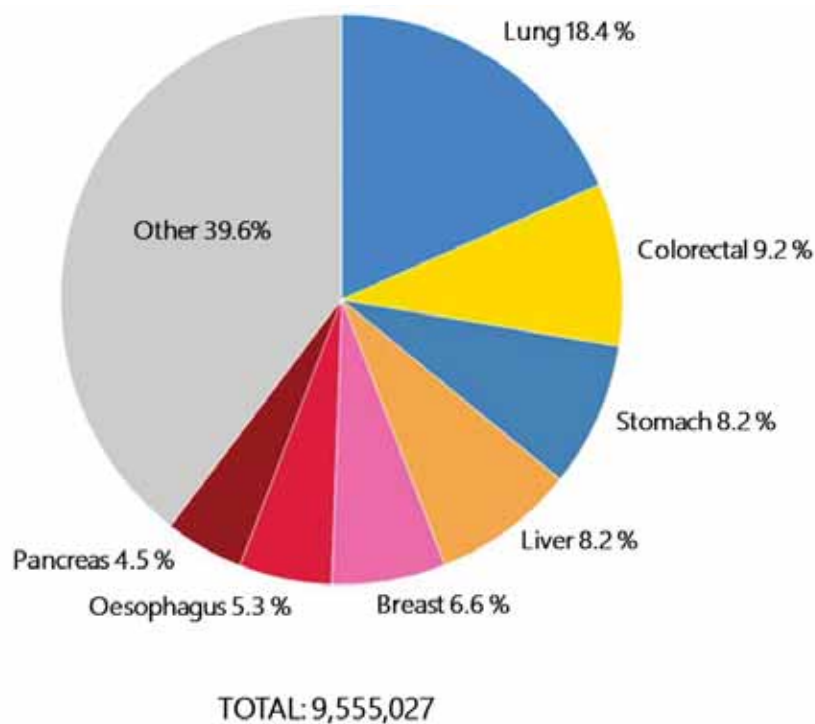


Figure 1. Estimated number of cancer deaths worldwide in 2018 (by cancer type)².

Cancer covers a wide diversity of related diseases, all of which have in common the abnormal non-stopping cell growth in a specific tissue location, forming the tumour³. After diagnoses, usually a combined therapy is required to treat cancer, applying different modalities such as surgery followed by chemotherapy and/or radiotherapy. Unfortunately, chemotherapeutic drugs are non-selective small molecules (<6 nm) that distribute all over the body without discriminating healthy from damaged tissues⁴. This lack of specificity is translated in the appearance of many severe undesirable side effects

such as anaemia, appetite loss, bleeding, constipation, delirium, diarrhoea, oedema, fatigue, fertility issues and hair loss¹. Additionally, the bioavailability of these drugs to tumour tissues is relatively poor. Thus, higher doses are required to reach the desired local drug amount in the tumour tissue, leading to an increased incidence of multiple drug resistance and elevated costs⁵. Consequently, all the intrinsic limitations of conventional cancer therapies and the alarming high number of deaths mentioned above have prompted the development of nanomedicine to increase specificity and improve biodistribution.

Nanomedicine is an emerging field that applies nanotechnology in the pharmaceutical and medical areas^{6,7} through the development of nanoscale-based devices, materials⁸ and compounds for diagnosis and therapy⁹. Regarding this demanding context in oncology, nanomedicine is intensively working on the application of nanotechnologies for the development of more effective and safer cancer treatments in the nanoscale (desirably between 8-100 nm). Since 1950s, drug delivery systems (DDS) have been explored as an alternative platform for the improvement of the current non-efficient marketed drugs¹⁰. Novel DDS, such as nanocarriers, have had a great impact over the years offering targeted versions of the current anticancer drugs performing a controlled release in the target site¹¹.

2. NANOCARRIERS

In nanomedicine, it is being widely studied the use of nanoparticles (ranging from 1 to 100 nm) referred to as nanoscale drug carriers (or nanocarriers). These entities are able to **carry drugs** while protecting them from numerous biological barriers that need to be overcome to finally reach their target tissue. Size, shape, surface charge, porosity, elasticity and stiffness are some of the physical properties that play a decisive role in the nanocarriers' behaviour¹²⁻¹⁶ (**Figure 2**). Moreover, there is a wide versatility regarding chemical composition as both organic (liposomes, polymers, micelles, dendrimers, proteins) and inorganic materials (such as metal or carbon derivatives) are being developed as drug nanocarriers.

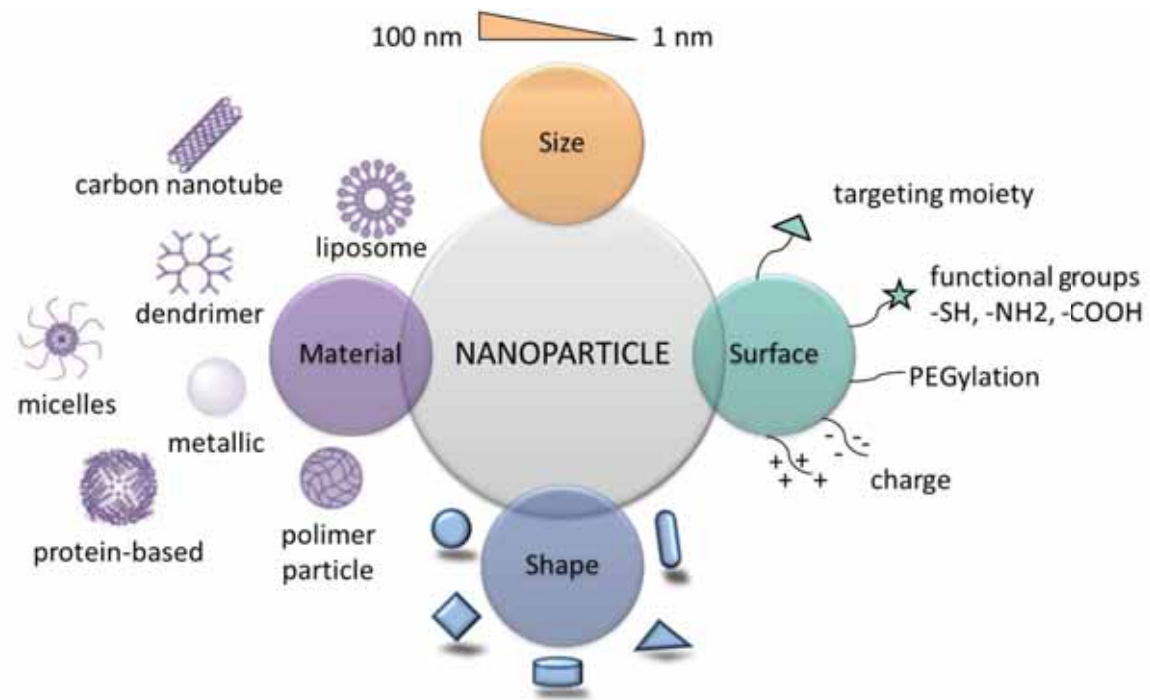


Figure 2. Physicochemical properties that determine the final nanoparticle's behaviour (categorized by size, surface, shape and material). Adapted from¹⁷.

Nanoparticles have demonstrated to be unique and promising carriers for drug delivery as they have a large surface/volume ratio and are small in size. Additionally, they can be designed to protect the drug from degradation, prevent premature interaction with the biological environment and therefore improve the circulation half-life. When the retention in the organism is longer, drug pharmacokinetics and tissue distribution are usually improved too.

PHYSICAL PROPERTIES

Any physical trait of the final nanoparticle, however small it may seem, will have an impact on its efficiency.

Systemic level: **size** is one of the most relevant parameters to be considered when designing a systemically administered nanoparticle. Nanoparticles smaller than ~8 nm undergo renal clearance, whereas large particles (around 100-200 nm) are accumulated in spleen, liver and lungs due to their large fenestrations. **Shape** has also a direct effect in the nanoparticles' half-life in plasma. Spherical-shaped molecules tend to accumulate

in the vessel core, reducing the lateral drift to vessel walls and therefore the cell-binding and uptake. For this reason, it has been suggested the use of non-spherical (discoidal or ellipsoidal) geometries, to prompt margination, oscillatory movements and therefore interaction with the vessel cell wall¹⁸. Additionally, it has been proved that positively **charged** nanoparticles are easily cleared from blood circulation by lung, liver and spleen, while neutral (zwitterionic) or slightly negative nanoparticles show a prolonged circulation time¹⁹. In general, an average size around 10-100 nm, non-spherical geometry and neutrally charged nanoparticles are recommendable to increase blood circulation time, reducing unwanted extravasation and renal clearance (**Table 1**).

Cellular level: once the nanoparticles have travelled through the blood stream, their goal is to reach the target cells, bind to them and internalize. Interestingly, nanoparticles' **size** is again one of the key parameters that influence the total cell uptake, as it has a direct correlation with binding affinity (avidity) and multivalency. Binding affinity is the strength of non-covalent interactions and it is measured using the equilibrium dissociation constant (K_d). On the other hand, multivalency refers to the number of ligands exposed in a single nanoparticle. It has been described that nanoparticles sized around 25-50 nm seem to be ideal for cell-receptor interaction²⁰. Smaller nanoparticles have a reduced surface of interaction and thus, a reduced multivalency. A low ligand density is directly associated with a high K_d , which limits the time of interaction. On the contrary, larger nanoparticles (above 50 nm) present a higher multivalency, which increases the avidity of the interaction (due to a high number of ligand/receptor binding) and limits further interaction with other available receptors (because of a low K_d). Moreover, nanoparticles' **shape** has a direct impact in the cellular uptake. For instance, an experiment revealed that spherical candidates are better than rods²¹, although in particles beyond 100 nm the tendency was opposite, showing a better internalization the rod-shaped candidates. Finally, surface **charge** is another feature that can be tailored to get a better internalization of the nanoparticles at the cellular level. Positively charged nanoparticles show an increased nonspecific uptake, compared to negative nanoparticles, as the cellular membrane is negatively charged because of the presence of glycosaminoglycans.

Table 1. Approximated characteristics (regarding size, shape and charge) for the efficient development of DDS at the systemic and cellular level.

	SYSTEMIC LEVEL	CELLULAR LEVEL
SIZE	10-100 nm	25-50 nm
SHAPE	Non-spherical	Circular
CHARGE	Neutral/slightly negative	Positive

As we can see in **Table 1** each level in the circulation process (systemic or cellular) has its own specificities and requirements regarding nanoparticles' size, shape or charge. It may pose indeed a controversial situation as it would be necessary a dynamic molecule able to adapt to each environment at every stage of the process. In this context, many efforts have been made aiming to overcome opposite needs in a single entity. It has been studied a "charge-conversion" technique, in which nanoparticles' charge is controlled by external stimuli from the microenvironment²². In these experiments, neutrally charged (zwitterionic) nanoparticles become positively charged once they have reached the acidic tumour environment, leading to a better cellular uptake and therefore enhancing their therapeutic effect. Similarly, size-switching systems²³ have been developed to keep large initial sized nanoparticles during blood circulation but becoming smaller after reaching the tumour site to internalize more deeply and exhibit a better efficiency. All these changes in the nanoparticle can be induced by different factors such as the presence of enzymes, light and acidic or hypoxic environment at the tumour tissue.

CHEMICAL COMPOSITION

Nowadays, there is a vast variety of materials that are being used for the development of DDS. They can be mainly classified as: polymeric nanoparticles, micelles, liposomal nanoparticles, inorganic nanoparticles and protein nanoparticles. Currently, predominant FDA-approved nanoparticles developed for therapeutic and imaging purposes are polymeric, liposomal and nanocrystal nanostructures although there is a tendency

towards the increased use of micellar, metallic and protein-based nanoparticles in a near future (Figure 3).

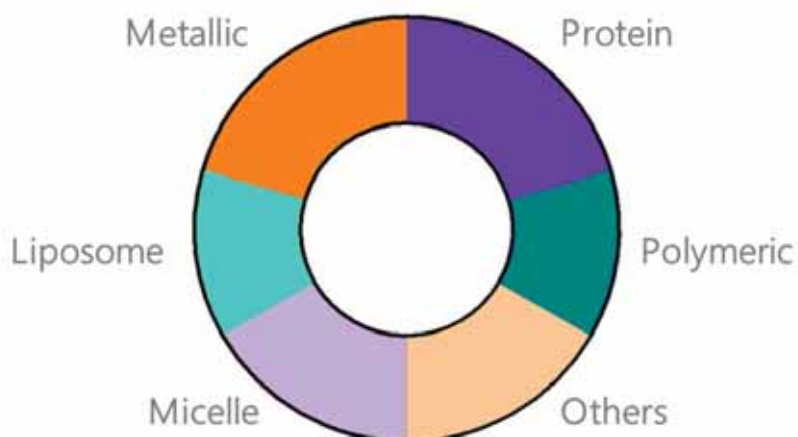


Figure 3. Nanomedicines under clinical trials classified by material type. Adapted from⁶.

Nevertheless, there is a global concern as most of these materials are challenging when moving to preclinical studies²⁴. Despite their potential as DDS, they are not biodegradable and can cause high toxicity or immunogenic reactions. It should be noted that toxic effects are extremely different depending on the nanoparticle's composition. As an example, it has been detected oxidative stress caused by metallic nanoparticles (containing Fe²⁵ or Ce²⁶), whereas induction of inflammatory response has been observed both using micelles and liposomes²⁷. In order to use nanocarriers safely as DDS, it is necessary to reduce their toxicity and improve their biocompatibility. However, DDS are in an early stage and a better understanding of the whole intricate scenario is required. In this regard, proteins are considered biocompatible materials, suitable for human health and disease treatment.

The overall picture of nanoparticles' physicochemical design is not only conditioned by the already mentioned parameters (size, shape, charge or composition). In fact, it is common to observe some discrepancies in this area, supporting the idea that the whole performance is enrolled by many characters and therefore will be also influenced by the tumour type, heterogeneity and microenvironment. For that, aiming to maximize the therapeutic effect it is recommendable to personalize the physicochemical design in a case-by-case basis^{28,29}.

NANOMEDICINE TRENDS AND MARKET

To date, we can divide the evolution of nanocarriers for biomedical applications in three different generations, starting from the 1950s (**Figure 4**). The first generation (1950-1980) nanoparticles were based in the use of novel nanomaterials and basic functionalization to assess their biocompatibility and toxicology. The second generation (1980-2010) was mainly focused on the improved stability and increased half-life circulation through the development of stealth PEGylated vehicles. Moreover, active targeting became a concept of interest to enhance tumour delivery through surface modifications. Finally, the third and current generation (since 2010), still in basic research, relies on the formulation of smart environment-responsive materials³⁰, which are dynamic nanoparticles able to change their inherent properties during the circulation process when exposed to specific conditions (such as low pH or hypoxia)^{10,21}.

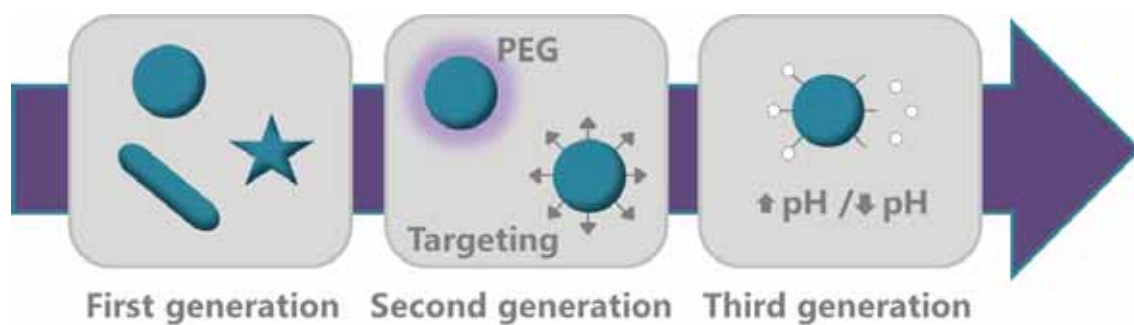


Figure 4. Evolution of nanoparticle design over time regarding the nanomaterials involved and the associated biological challenges. Adapted from²¹.

After decades of studies and publications, therapeutic nanocarriers have evolved from proof-of-concept to marketed products used daily in hospitals. Most FDA-approved ones rely on passive targeting. However, there is a clear tendency towards active targeted candidates to further increase drug accumulation and efficacy at the disease site, while reducing toxicity in off-site organs. In fact, to date only **Denileukin diftitox** (Ontak®) has been FDA approved as an active targeted nanomedicine (excluding antibody-drug conjugates)⁶.

Interestingly, more than 65 % of the investigational applications identified are focused on the treatment of cancer³¹, as there is an alarming need to improve the current inefficient and highly toxic chemotherapies. Additionally, the oncology sector is the predominant therapeutic indication, representing over 35 % of the nanomedical global market (Figure 5).

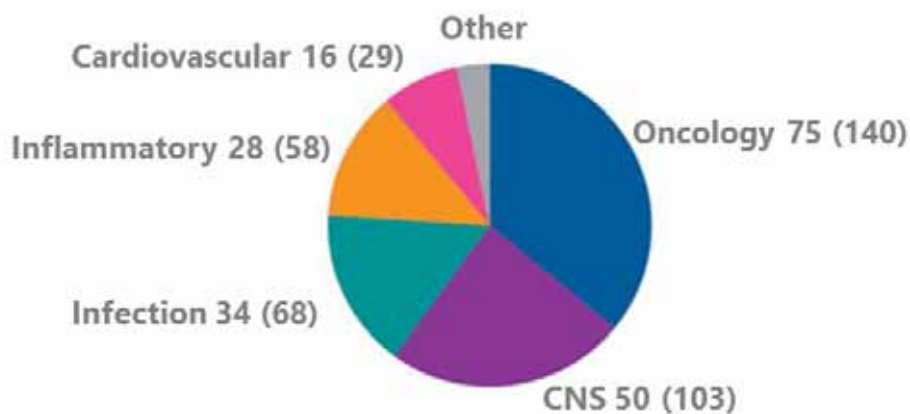


Figure 5. Nanomedical global market in 2014 (in \$ billions) by therapeutic indication. 2019 forecast is indicated in brackets. CNS: Central nervous system. Adapted from³².

In conclusion, as cancer is a leading cause of death worldwide it is the major focus of the nanomedical research effort, to improve the delivery and the therapeutic index of current unspecific anticancer drugs.

3. CELL-TARGETED DRUG DELIVERY

3.1. PASSIVE TARGETING

There is a high demand of drugs that can be delivered to target cancerous cells, thereby reducing adverse side effects while improving therapeutic efficacy. The reason is that when administered systemically, nanoparticles face many biological and physical barriers that hinder its arrival to the target tissue³³ (Figure 7).

The most extensively used strategy for targeting cancer cells is passive targeting, which leads to an unspecific increased accumulation of the drug in the tumour tissue. This phenomenon, which is known as **enhanced permeability and retention effect (EPR)**, takes place in cancer therapeutic strategies because of an increased permeability of blood vessels (with fenestrations of 100-500 nm) and low lymphatic drainage in the tumour site, compared to healthy tissues³⁴ (**Figure 6**). Tumour vessels are irregular in terms of size and shape because of rapid proliferation of the vessel lumen and therefore gaps between endothelial cells are found along the vessel wall³⁵. Additionally, it is described that in the tumour tissue there is an increased fibrosis and extracellular matrix that cause higher fluidic pressure, hampering the extravasation of the nanoparticles from the superficial to the internal parts of the tumour¹⁹.

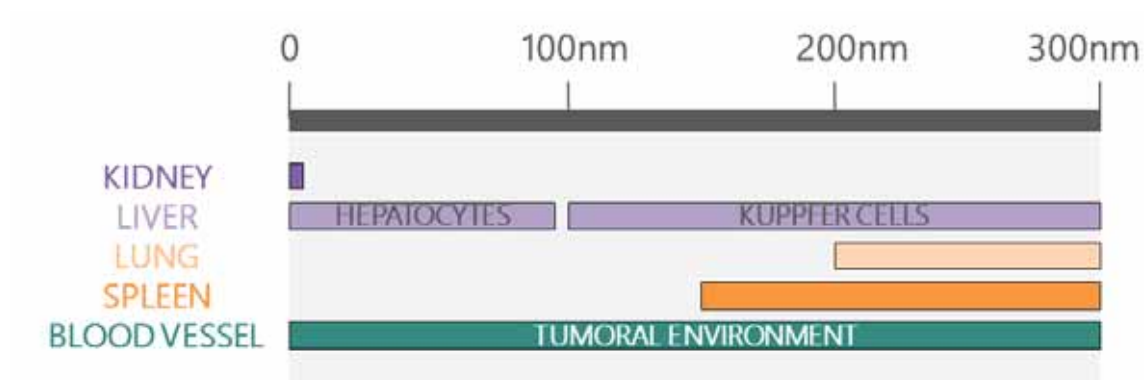


Figure 6. Size-dependent organ accumulation of non-targeted nanoparticle's during the biodistribution process.

Unfortunately, the EPR effect only leads to an increased non-specific accumulation of nanomedicines in the tumour tissue, whereas only a small percentage (less than 1 %) is accumulated intracellularly³⁵. This situation is due to the presence of different physical and biological barriers, which will be described hereafter in sequential order.

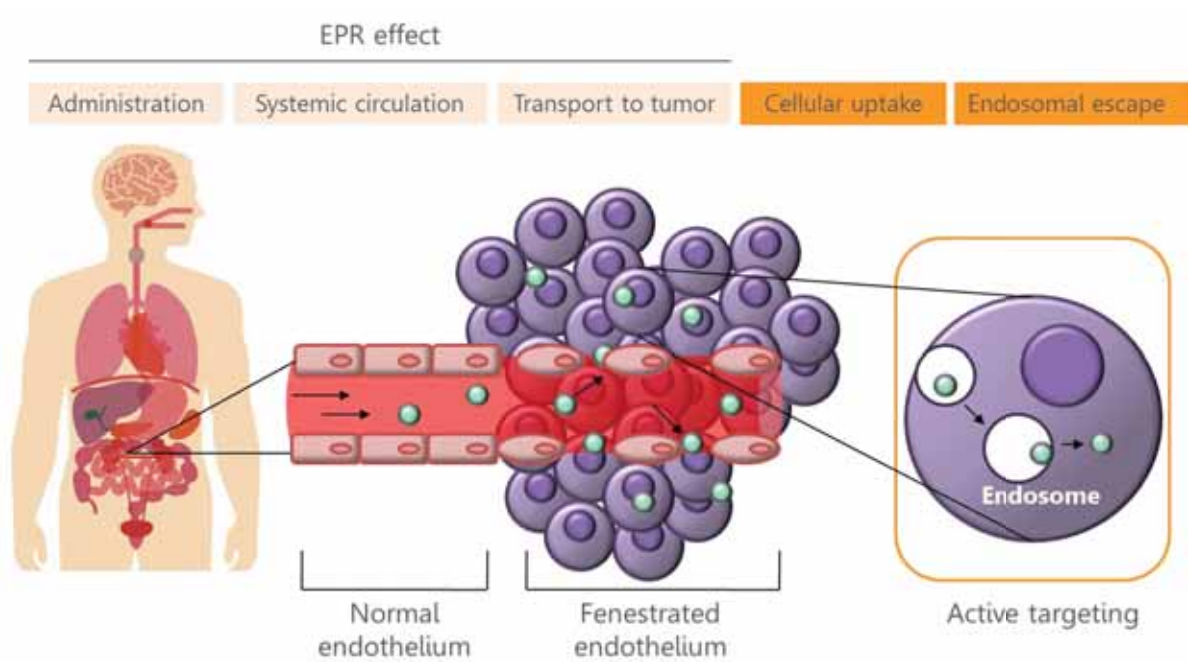


Figure 7. Schematic representation of the expected trajectory followed by nanoparticles due to EPR effect and the hurdles involved upon intravenous administration. Cellular uptake and further intracellular trafficking are almost absent in passively targeted nanoparticles (dark orange).

OVERCOMING BIOLOGICAL BARRIERS

Protein corona

Once nanoparticles are administered and exposed to the biological environment they get immediately in contact with molecules present in the blood stream that form a protein corona around its surface. The coating formed around the nanoparticle (which contains different molecules such as opsonins, immunoglobulins, lipids or serum proteins) has a dramatic impact in the nanoparticle's behaviour (**Figure 8**). First, opsonization increases the recognition and uptake by phagocytic cells, followed by internalization and degradation in lysosomes. Second, it changes nanoparticle's size and shape, hindering its expected biodistribution and pharmacokinetics. Finally, targeted strategies are even more affected, as the protein corona molecules have been proved to mask the ligands present on the surface and it is translated into a decrease in the specificity of the designed nanoparticle^{19,36}. Protein corona formation has been proved in many different nanoparticles formed by inorganic (iron³⁷, gold³⁸ or silica^{39,40}) and organic compounds (such as liposomes⁴¹ or polymers⁴²). However, it should be

highlighted that this process has not been described to affect protein-based nanoparticles up to date.

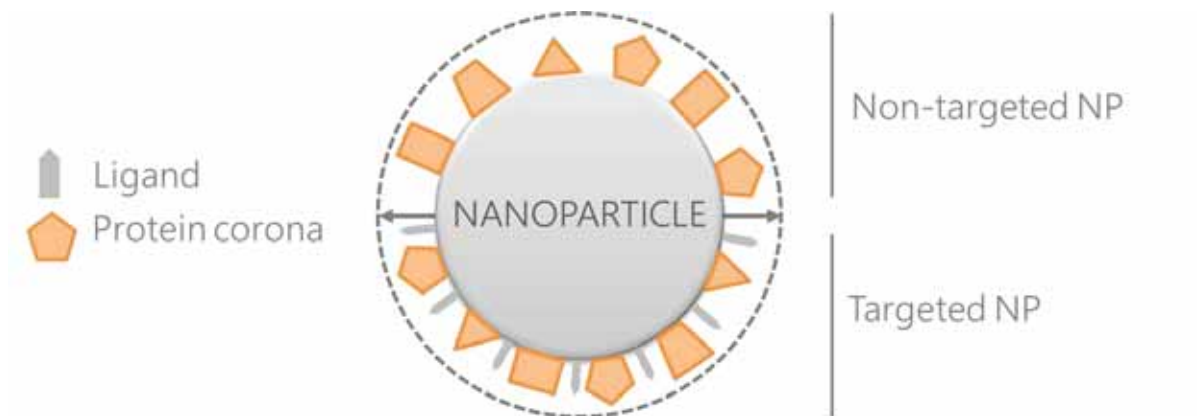


Figure 8. Scheme of protein corona formation (orange) upon nanoparticle systemic administration. Grey arrows indicate the increase in diameter size after corona formation. The final nanoparticle size is represented by a dash line. Adapted from⁴³.

Mononuclear phagocytic system (MPS)

The mononuclear phagocytic system (MPS, also known as reticuloendothelial system) is the part of the immune system responsible for the elimination of macromolecules from circulation. The MPS is composed by phagocytic cells, predominantly monocytes, macrophages (spleen) and Kupffer cells (liver), which perform phagocytosis after the recognition of the opsonins that surround the nanoparticles (**opsonization**)⁷.

This whole scenario has pushed many groups to develop alternatives to avoid or reduce the formation of the protein corona, trying to escape from one of the main barriers (MPS) that compromises the efficiency of nanoparticles (**Figure 9**). One of the most extensively used techniques to overcome this issue is the coating of the surface with compounds such as polyethylene glycol (PEG). This PEGylation interferes with the protein corona formation and with the following activation of phagocytic cells⁴⁴⁻⁴⁷. Another strategy that has been recently developed is the particle-coating biomimetics, which tries to reduce opsonization covering the nanoparticle with leukocyte's⁴⁸ and erythrocyte's⁴⁹⁻⁵¹ membrane. The nanoparticle remains hidden from the MPS, leading to a longer circulation time and subsequent improved cellular uptake. In 2013, a different

camouflaging technique was used, based on the addition of human peptides obtained from CD47 membrane protein, described as “don’t eat me” markers due to their ability to inhibit phagocytic clearance. This peptide specifically binds to phagocytic cells and avoids its degradation⁵².

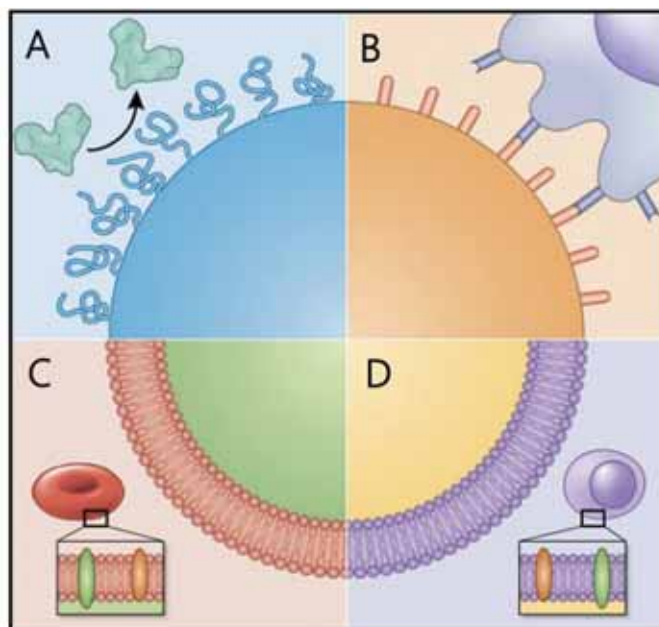


Figure 9. Camouflage strategies developed for the evasion of the MPS effect and increase of the circulation time. A) Surface PEGylation. B) Surface exposure of CD47-derived peptides not recognized by macrophages. C) Red blood cell-membrane coating. D) Leukocyte membrane mimicking. Adapted from¹⁹.

Renal clearance

The kidney is another major organ responsible for the removal of nanoparticles from blood stream. Nanoparticles smaller than ~ 8 nm are filtered and excreted in the urine through the kidney because of filtration slits (around 6-7 nm)⁵³. To get a general idea of the importance of these barriers in cancer treatment, the MPS and the renal clearance system are the main elements responsible for the elimination of most of the administered nanoparticle dose. Even with improvements in biodistribution offered by the EPR effect and PEGylation, around 90 % will inevitably be retained in the reticuloendothelial organs such as the liver and spleen due to clearance by mononuclear phagocytes²¹.

In conclusion, passively targeted delivery presents some issues that need to be improved: (i) further extending blood circulation time, (ii) homing the nanoparticles toward specific

sites for intracellular delivery and (iii) reduction of off-target toxicities. Therefore, efforts are needed to synergize passive targeting with a more dynamic method capable of further improving not only the accumulation at tumour sites but also inside cells⁴.

3.2. ACTIVE TARGETING

On the other hand, active targeting strategies involve the presence of **ligands** in the nanoparticles' surface, which are able to bind specifically to over-expressed receptors or molecules on cancerous organs, tissues, cells or subcellular compartments (also known as tumour markers)⁵⁴. This alternative improves binding and cellular uptake and avoids unspecific interactions with non-target healthy cells (**Figure 10**). Interestingly, an increase in the amount of drug that reaches its target is then translated in a reduction of the dose administered.

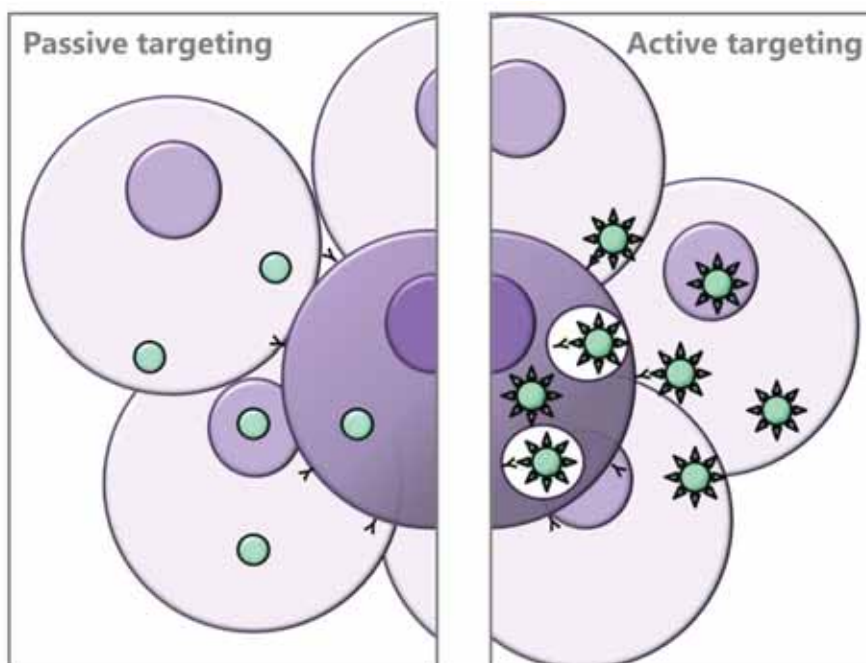


Figure 10. Comparative scheme of passive and active targeting results. Passive targeting (left) is conditioned by the leaky vasculature (EPR effect), which allows nanoparticles to reach the tumour, almost without internalization in tumour cells. Active targeting (right) relies on the use of ligands that bind to overexpressed receptors in the tumour cells. After equivalent administration of a therapeutic nanoparticle, there is a bigger accumulation in tumour tissue and inside the cells in the actively targeted candidate (right).

In oncology, some examples of deeply studied over-expressed receptors in tumour cells are CXCR4 (in more than 20 cancer types), CD44 or HER2 (both in breast cancer)²⁸. Targeting specific cells that over-express certain cell-surface receptors can be achieved by immobilizing a wide diversity of affinity ligands (**Figure 11**) such as antibodies, aptamers, proteins, peptides, nucleic acids, sugars or small molecules to the surface of the nanoparticle^{28,35,55,56}. Surface functionalization will lead then to active targeting which might result in accumulation followed by specific uptake of the nanomedicine into the cells of interest. In consequence, making the right choice is crucial to get an efficient and specific targeting, as each ligand has its own specificities (regarding size, composition and shape) and not all of them will induce necessarily cell internalization (**Figure 11**).

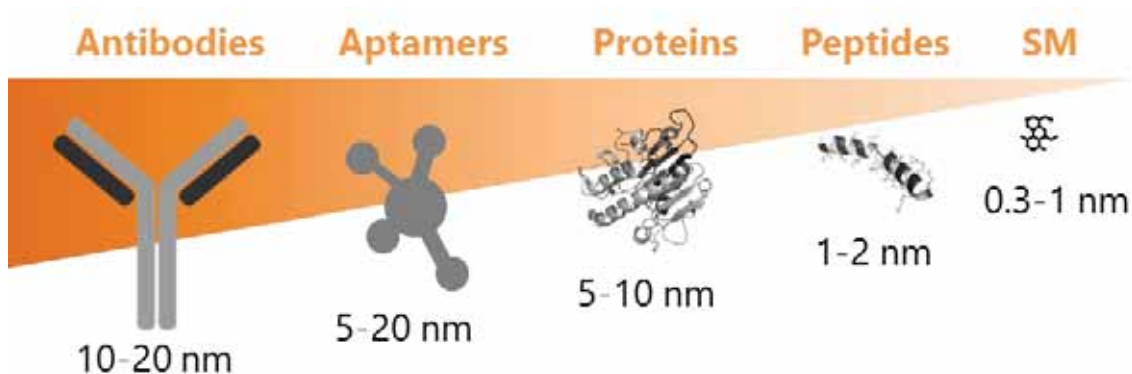


Figure 11. Candidate molecules as ligands for the development of actively targeted nanoparticles, placed in decreasing order regarding their respective size. SM: small molecules. Adapted from⁵⁶.

Antibody drug conjugates (ADCs) are an example of ground breaking actively targeted nanomedicines that combine both targeting and cytotoxic properties^{57,58}. Recombinant monoclonal antibodies (mAbs) are covalently linked to cytotoxic drugs, merging in a single entity the antitumoral activity of a cytotoxic chemical with the high stability and selectivity of mAbs⁵⁹.

In 2000, gemtuzumab ozogamicin was the first FDA-approved ADC, an anti-CD33 monoclonal antibody covalently linked to calicheamicin, indicated for the treatment of acute myeloid leukaemia⁶⁰. Although they seemed promising for their use in cell-targeted delivery of chemotherapies, there are some weaknesses that appeared since then and are being studied for their improvement and success in the clinical⁶¹. Due to

antibody's structure, ADCs are limited as they provide insufficient monovalent or divalent binding to the target cell. This situation is translated in a poor penetrability and therefore high loading capacity is required to reach the therapeutic effect, leading to high toxicities too.

The use of linkers between the drug and the antibody is also a concerning issue⁶². It has been observed a release of the drug counterpart in the blood stream, leading to systemic toxicity and low therapeutic index. This phenomenon is due to extracellular linker instability and degradation before reaching the target cell. An ideal linker would be stable enough during blood circulation while being efficiently cleaved once in the desired target cell⁶³.

ACTIVE TARGETING CHALLENGES

Many parameters need to be considered to optimize targeted delivery such as ligand size, charge, orientation or even density⁶⁴⁻⁶⁷. At first sight, it seems clear that the binding efficiency is directly proportional to the number of ligands present in the nanoparticle surface. Nevertheless, in presence of too many ligands the nanoparticle's size may result affected as well as the access to the receptor for steric reasons, as it has been described in previous studies⁶⁸. Additionally, it is of vital importance to bear in mind that binding affinity and internalization are two independent events and they are not strictly related. It has been demonstrated that a higher binding affinity (with low K_d) is not directly associated with an increased cellular uptake. Therefore, having a good targeting agent is not only about binding to the desired receptor but also inducing cellular uptake.

ENDOSOMAL ESCAPE

Endosomal escape is one of the major concerns when designing actively targeted therapeutic nanoparticles. During endocytosis there is an engulfment of the nanoparticle in membrane-based vesicles, called endosomes. Early endosomes become increasingly

acidic (pH 6.8-6.1) and derive to late endosomes (pH 6.0-4.8). Later, fusion with lysosomal vesicles prompts the degradation of molecules present in the same compartment (due to an extremely acidic environment, around pH 4.5)⁶⁹. For that, before the fusion with the lysosome, endosomal escape must occur to prevent degradation of the cargo to release the nanoparticle to the desired subcellular compartment, whether it is the cytosol, mitochondria or nucleus. For that, a lot of effort is being made to evade this process, trying to find endosomolytic molecules able to release the therapeutic agent to the cytoplasm.

Table 2. Examples of some of the endosomal escape domains in use up to date.

MECHANISM OF ACTION	MOLECULE	SOURCE	REFERENCES
Membrane disruption	Melittin	<i>Apis mellifera</i>	70,71,72
	Exotoxin A	<i>Pseudomonas aeruginosa</i>	73
	Diphtheria toxin	<i>Corynebacterium diphtheriae</i>	74
Membrane fusion	Hemagglutinin (HA2)	Influenza virus	75
	Gp41	HIV	76
	GALA	Synthetic	77
Proton sponge effect	PEI	Chemical	78
	Chloroquine	Chemical	79
	PAA	Chemical	80
	His-rich peptides	Synthetic	81

It has been described that impairment or even loss of efficacy due to endo-lysosomal compartments can be solved through three main mechanisms: membrane disruption, membrane fusion or proton sponge effect (Table 2). First, membrane disruption can be achieved adding antimicrobial peptides such as melittin⁷⁰. Second, endosomal membrane fusion has been observed using viral peptides like influenza virus hemagglutinin-2 peptide (HA2)⁷⁵. Finally, the incorporation of cationic groups (His-rich

tag⁸² or polyethylenimine^{83,84}) prompt the “proton sponge effect”, which causes an influx of water into the acidic endosomes and subsequent membrane rupture.

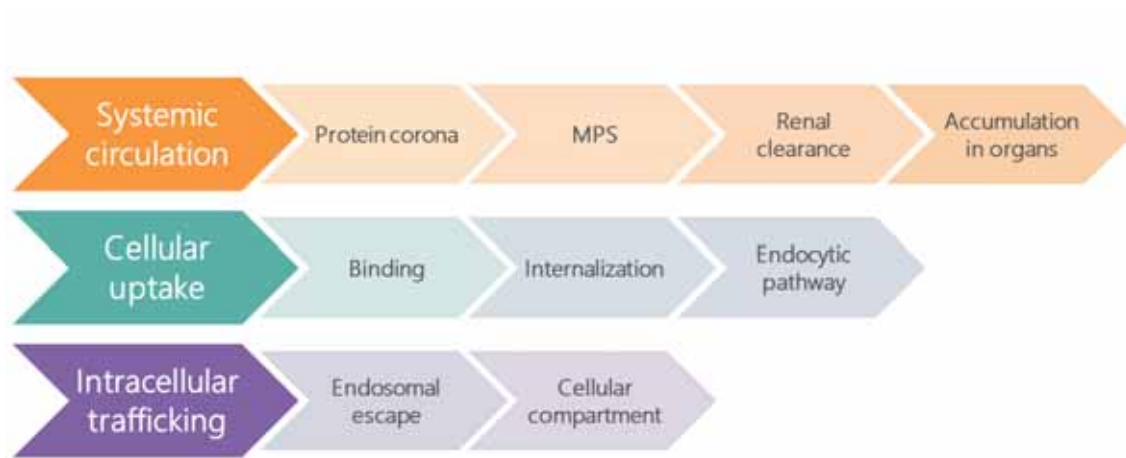


Figure 12. Summary of the main obstacles and processes that actively targeted nanoparticles must overcome during systemic circulation, cellular uptake and intracellular trafficking until reaching the desired cellular compartment. MPS: mononuclear phagocytic system.

3.3. CANCER CELL-TARGETING

Current chemotherapies (sized below the renal clearance threshold) are non-selective, causing indiscriminate cytotoxicity to both cancer and healthy cells. For that, there is an urgent demand in the development of actively targeted alternatives that provide an increased accumulation in tumour tissue without off-target damage, followed by cell-receptor binding and internalization in the tumour cell. Administration of such targeted therapies not only would improve the efficacy in the tumour site but also would reduce the dose required to reach the therapeutic index and consequently, the dosage administered and pertinent expenses. One of the early difficulties that arise when investigating active targeting in cancer is the identification of appropriate tumour cell markers. Usually, cell receptors are present in cancerous cells as well as in healthy cells, hampering the task of working with a marker that is absent in healthy cells and only expressed in tumour cells.

COLORECTAL CANCER

Up to date, colorectal cancer (CRC) is a leading cause of cancer death worldwide (more than 880,000 deaths estimated in 2018) (Figure 1), where more than 70 % is not caused by the primary tumour itself but due to the appearance of metastatic foci. CRC can be divided in different stages (from I to IV) being stage IV the most advanced one, involving the presence of **metastasis**. Unfortunately, a high percentage of newly diagnosed CRCs show already metastasis. Moreover, the 5-year relative survival rate varies from 88.1 % (stage I) to 12.6 % (stage IV) for CRC, meaning that only 12 out of 100 people are still alive at least 5 years after being diagnosed at stage IV⁸⁵.

Cancer stem cells (CSCs) are a subpopulation of cancer cells sharing similar characteristics as normal stem or progenitor cells such as self-renewal ability and multi-lineage differentiation to drive tumor growth and heterogeneity; a subpopulation of CSCs is able to generate long-distance metastasis. Although current therapies can reduce the tumour volume, usually there is a remaining resistant subpopulation of CSCs responsible of subsequent recurrence and metastasis (Figure 13). In fact, chemotherapies reduce the tumour volume, but they enrich the CSC representation in the remaining newly growing tumour. Consequently, there is an urgent need of developing a successful treatment able to eliminate not only the tumour but also the metastatic foci (originated by CSCs).

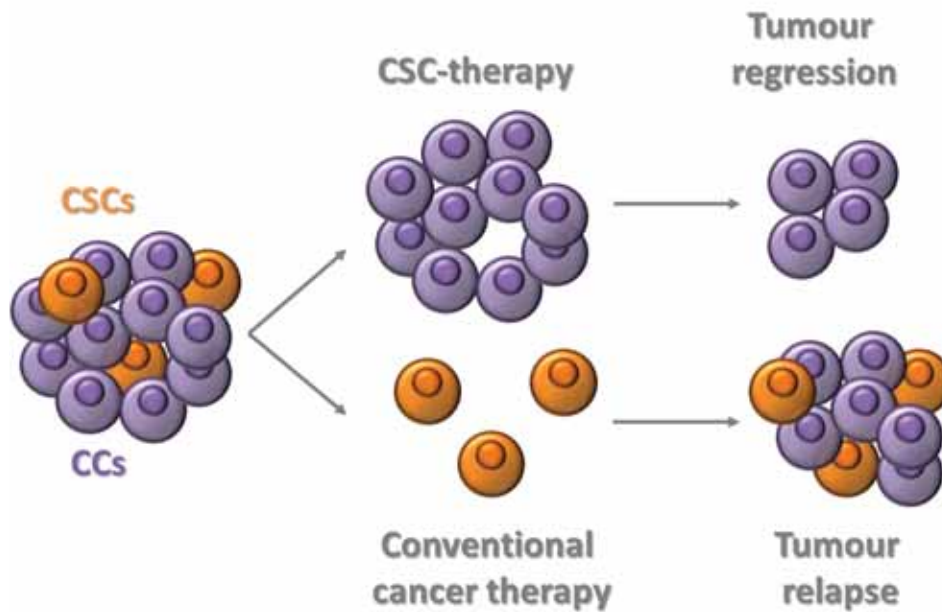


Figure 13. Comparison between the tumour evolution after administration of both conventional or CSC-therapy. CCs: cancer cells, CSCs: cancer stem cells.

The CXCR4 chemokine receptor type 4 (CXCR4) also known as fusin or CD184 is one of the most studied CXCR chemokine receptors due to its role as a coreceptor for HIV entry, described in 1996⁸⁶. It is expressed in different human cells such as lymph nodes or bone marrow⁸⁷ and over-expressed in more than 23 human cancers including CRC. More specifically, it is overexpressed in metastasis-forming CSCs. In CRC cells, the presence of CXCR4 has been associated with tumour growth, invasion, angiogenesis, metastasis, relapse and therapeutic resistance, and therefore it is related to bad prognosis⁸⁸. For all these reasons, CXCR4 is of relevant interest as a prognostic biomarker and for the development of actively targeted nanocarriers against colorectal CSCs. The development of a targeted therapy against colorectal CSCs through CXCR4 as a drug receptor is a great alternative for the improvement of the current non-specific chemotherapies, not only for its specificity but also for its implication in the metastatic process.

4. CARRIER-FREE SELF-ASSEMBLING NANODRUGS

Currently, there is a remarkable trend towards the development of complex and multi-component nanoparticles containing simultaneously organic and inorganic materials. Interestingly, nanoparticles present a large surface/volume ratio, which enables the functionalization of its surface with different agents of interest. Having this idea in mind, there are plenty of possible combinations that can be developed to get an optimized drug-loaded nanocarrier that overcomes the barriers found, for instance, during the administration, blood circulation or tissue targeting processes^{6,89}.

Unfortunately, the arising challenge is the high complexity, which is normally associated with higher costs, chemically heterogenic materials and intricate long-lasting procedures (like drug-conjugation) that complicate the scaling-up process. Although such nanoscale particles may perform improved pharmacokinetics or biodistribution, the amount of total injected material is so large that the truly important molecule which is the drug represents only a 10 % of the total structure^{90,91}. Therefore, a limitation of loading capacity appears when using such nanocarriers, making it more difficult to reach the therapeutic dose. Additionally, the residual non-therapeutic nanomaterial (90 %) that is circulating in the organism could pose a safety issue (**Figure 14**). The excess of inactive nanocarriers that are not properly metabolized or eliminated can cause toxic reactions in the patient. The presence of large amounts of foreign material in the blood stream could lead to the activation of the immune system, increased drug clearance and immunotoxicity. Moreover, the combination of different materials (like metal, carbon or lipids) together in the nanocarrier could exacerbate even more the immunogenic reactions generated. Consequently, it is highly desirable the development of alternative chemically homogeneous nanomaterials that contain the minimal non-functional material.

An analysis was made collecting data from the literature over the last decade regarding the therapeutic nanocarrier's dose found in the tumour tissues after administration in mouse model³⁵. Surprisingly, less than 1 % (median) of the dose administered was located in the solid tumour, meaning that in a hypothetical injected dose of 100

nanoparticles less than 1 reached the tumour tissue (Figure 14). Altogether, these data suggest that there is an imperative need to avoid the use of non-active bulky carriers and simultaneously improve the loading capacity without compromising the patient safety.

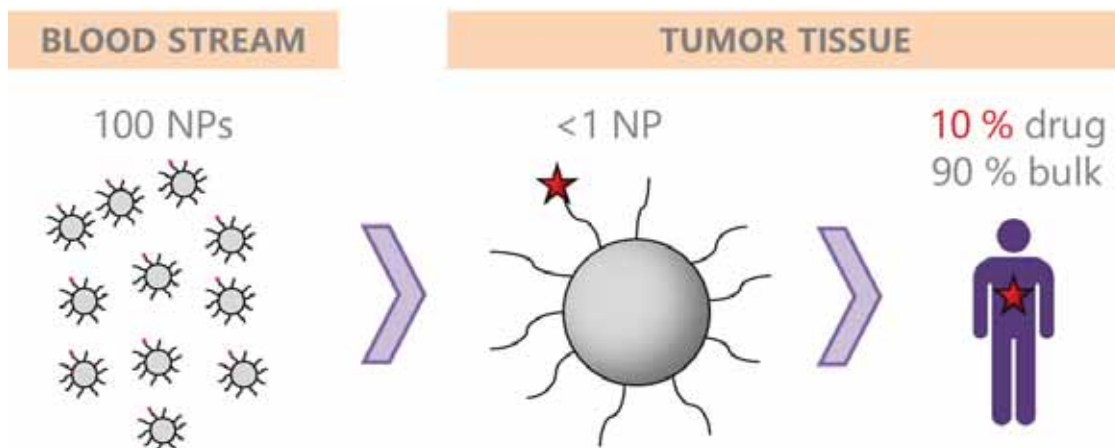


Figure 14. Representation of the nanoparticle dosage loss upon intravenous administration. The drug represents only a 10 % of the total mass reached at the tumour tissue. The residual 90 % corresponds to bulk material with potential toxicity associated.

An interesting alternative to this entangled situation would be the use of self-delivered and self-assembled therapeutic agents (chemotherapeutic, proteins or siRNA) which avoid the need of non-therapeutic materials. There are some examples that have been already developed and contain compounds able to act as a **carrier and therapeutic agent simultaneously** such as PolyMet/siRNA nanoparticles⁹² for the treatment of NSCLC and melanoma, and epigallocatechin gallate (EGCG)^{93,94} for the treatment of breast cancer. Another example of carrier-free self-assembling nanodrugs are the already mentioned ADCs, which consist of monoclonal antibodies (or their fragments) that are linked to cytotoxic drugs. ADCs are promising candidates that are already in the market, mainly for their use in oncology.

In summary, self-delivered therapies (which contain compounds that act both as carrier and drug) appear as greatly improved alternatives to be considered from now on. However, the heterogeneous composition and the time-consuming process formation of these molecules are still unsolved issues that need to be studied in the next years when translating these discoveries to the clinics.

4.1. SINGLE-STEP PRODUCTION OF PROTEIN-BASED NANODRUGS

Cell penetration, endosomal escape, oligomerization, nuclear migration signals or reporter agents (for theragnostic purposes) are some of the additional functions that can improve the final therapeutic effect in the tumour tissue. However, the sequential functionalization process turns out to be a time consuming multistep-based process. In this context, there is a simple and efficient single-step alternative for the formation of homologous instead of heterologous nanoconjugates: **multidomain recombinant protein production**. Proteins are versatile biological materials that can be found extensively in nature. In fact, all the functions mentioned previously (such as cell penetration, endosomal escape or even targeting) can be achieved through fusion proteins that contain peptide domains, each with a specific role. Protein-based nanoparticles can be easily tailored upstream and then produced through recombinant DNA technologies in a simple and fast process, providing as final product homogeneous protein-based nanoparticles versatile and fully functional. Besides, using this procedure, the drug can be added to the whole structure due to the presence of proteins that are inherently cytotoxic or proapoptotic, in nature⁸⁹.

5. RECOMBINANT PROTEINS

Proteins are versatile molecules, which are involved in a plethora of functions in living organisms such as transcription, translation, metabolism or transport^{35,95}. Many are the advantages that make them good biomaterials to work with. They are safe, biocompatible and biodegradable. When needed in big amounts, proteins cannot be obtained from its native source, as they are found in nature at very low concentrations. Alternatively, they can be synthesized using chemical or recombinant approaches. Chemical synthesis involves the use of long multistep-based and expensive procedures whereas recombinant proteins are easily produced using cost-effective methods that rely on recombinant DNA technologies. In the 1980s, the first recombinant protein was FDA-approved for its medical use against diabetes (human insulin, Humulin). Since then, there

has been an inflection point, recombinant proteins have gained a remarkable interest in the biotechnological and biomedical field, as they can be easily scaled up and designed for a wide range of applications.

Currently, there is a wide spectrum of organisms that can be used as recombinant cell factories⁹⁶. Choosing accurately the most appropriate expression system will determine the failure or success in recombinant protein production. Many parameters need to be considered before making the final decision such as protein application, post-translational modifications, yield and costs.

Traditionally, *Escherichia coli* (*E. coli*) has been the pioneering expression system of choice because of its fast growth, simple culture procedures, high yields and low expenses (Table 3). However, like other gram-negative bacteria, *E. coli* contains lipopolysaccharides (LPS), in the outer membrane. LPS (also known as endotoxins) are immunostimulators that cause undesired immunological responses in mammalian hosts that must be further avoided through additional purification procedures. Unfortunately, none of the current methods used to reduce the endotoxin content are efficient enough. For this reason, gram-positive bacteria are an alternative for protein production as they are GRAS (Generally Recognised as Safe) expression systems that do not produce endotoxic compounds⁹⁷. Unlike gram-negative, gram-positive bacteria contain a thick peptidoglycan layer in the cell wall without the presence of LPS. Therefore, gram-positive bacteria such as *Bacillus*, *Corynebacterium* or lactic acid bacteria (like *Lactococcus* or *Lactobacillus*) are regarded as promising candidates when aiming to obtain safe LPS-free recombinant proteins for their use in the biopharmaceutical industry⁹⁸⁻¹⁰².

Table 3. Main advantages and disadvantages of using *E. coli* as a microbial cell factory for the production of soluble recombinant protein. Respective improved alternatives are displayed in orange.

ADVANTAGES	DISADVANTAGES
Wide know-how	Post-translational modifications
Fast growth	(Origami B strain)
Simple genetic manipulation	Lipopolysaccharides
Cost-effective production	(LPS-free strain)
High production yields	Inclusion bodies formation
Scale-up feasibility	(solubilisation process, use of IBs activity)
Safe handling	

Interestingly, to overcome the endotoxin-related limitation of *E. coli*, during the last years a genetically modified endotoxin-free *E. coli* strain has been developed^{101,103}. Specifically, the precursor lipid IV A (contained in LPS) has been modified through the removal of secondary acyl chains, reducing the endotoxic activity about 80 - 95 %. This discovery has widened even more the applications and opportunities of *E. coli*, providing biosafe and cost-effective recombinant proteins, as no endotoxin removal efforts are needed. Nevertheless, there is still a remaining issue when working with eukaryotic proteins that require post-translational modifications as prokaryotic systems are unable to perform them. Alternatively, yeasts^{104,105} (predominantly *Saccharomyces cerevisiae*) and insect cells¹⁰⁶ are promising eukaryotic expression systems. They are able to perform post-translational modifications (such as glycosylation), although they are different to mammalian cells and therefore may be potentially immunogenic¹⁰⁷. On the other hand, mammalian cells^{108,109} benefit from metabolic and protein processing pathways similar to those in human cells, so they (instead of *E. coli*) are a good alternative when producing recombinant human proteins that need post-translational modifications to be correctly folded and functional. However, mammalian cells are more difficult to manipulate and are associated to long-lasting procedures and higher expenses.

In the end, all expression systems have pros and cons and many features need to be considered when deciding the optimal cell factory for each recombinant protein. Thus, to finally succeed in protein recombination production it is necessary to make a balance between the protein's and the expression system's requirements and limitations.

Moreover, when producing recombinant proteins, it is worth considering the generation of inclusion bodies (IBs), which are formed by misfolded protein that tends to aggregate. IBs have been regarded as non-functional waste product for ages, treated as useless material whose formation must be avoided. Interestingly, this conception totally changed after a remarkable work was published in 2005, claiming that IBs are not completely inactive structures and therefore there is a portion of active properly folded protein, which can be used for example as catalysts of bioprocesses¹¹⁰. Since then, hard investigation has been performed to unveil all the potential that this newly discovered active material can possess and the respective applications that can be developed in the biotechnological field¹¹¹⁻¹¹⁵. So far, they seem promising biomaterials for their use in tissue engineering and regenerative medicine^{116,117} and as DDS^{101,102} for the sustained release of soluble targeted protein¹¹⁸.

5.1. PROTEIN ASSEMBLIES

Protein monomers, although described as fully functional structures, are usually organized in higher hierarchical structures, which consist of more than one aminoacidic chain. Self-assembling proteins are able to attach to its counterparts through non-covalent interactions to finally form oligomeric supramolecular structures ranged in the nanoscale (namely protein nanoparticles).

NATURALLY OCCURRING PROTEIN ASSEMBLIES

In **nature** we can find an astonishing number of self-assembling proteins. They can be organized in linear (such as collagen, actin and amyloids) or tubular forms, like tobacco mosaic virus (TMV) or haemolysin. They can also be arranged as rings (like β -clamps, helicases and nucleases) or nanocages (for example ferritin, vaults, chaperons, virus and bacterial compartments)^{95,119} (**Figure 15, left**).

Among natural protein oligomers, virus capsids are one of the most well-known. It has been extensively studied the imitation of such structures for the development of biological nanocages using viral and non-viral proteins. Virus-like particles (VLPs) are multimeric nanostructures formed by viral structural proteins that lack any genetic material, resulting in safe protein-based cages devoid of infectious or replicative activities. Moreover, they can be modified to display peptides or epitopes on the surface in case our goal is to target the nanoparticle or increase its antigenicity, respectively. VLPs have been recently used for the development of vaccines¹²⁰⁻¹²² (for instance, against breast cancer displaying human HER2 on VLPs surface¹²³), drug delivery agents^{124,125} and biosensors¹²⁶, as they are tuneable and promising biological structures. However, for drug delivery purposes virus-associated antigenicity can be a concerning issue. Alternatively, artificial viruses can be formed by non-viral structural proteins that self-assemble as nanocages, allowing the generation of structures with bespoke properties and no related antigenicity¹²⁷.

Natural supramolecular assemblies were extremely interesting at an early stage for their intrinsic oligomeric abilities. In fact, they have been studied in detail for the better understanding of the structure-function relationship. The vast knowledge acquired up to now and the described poor tunability, flexibility and architectonic versatility of natural assemblies has led to the design of **de novo protein assemblies**, which can be controlled to generate endless supramolecular protein assemblies with novel properties and functions.

DE NOVO RATIONAL DESIGN OF PROTEIN ASSEMBLIES

Self-assembling properties are very appealing and have been studied through different techniques. De novo rationally designed protein assemblies have been generated mostly using pre-existing natural oligomeric domains (α -helix or β -strand) and multifunctional modular nanoparticles.

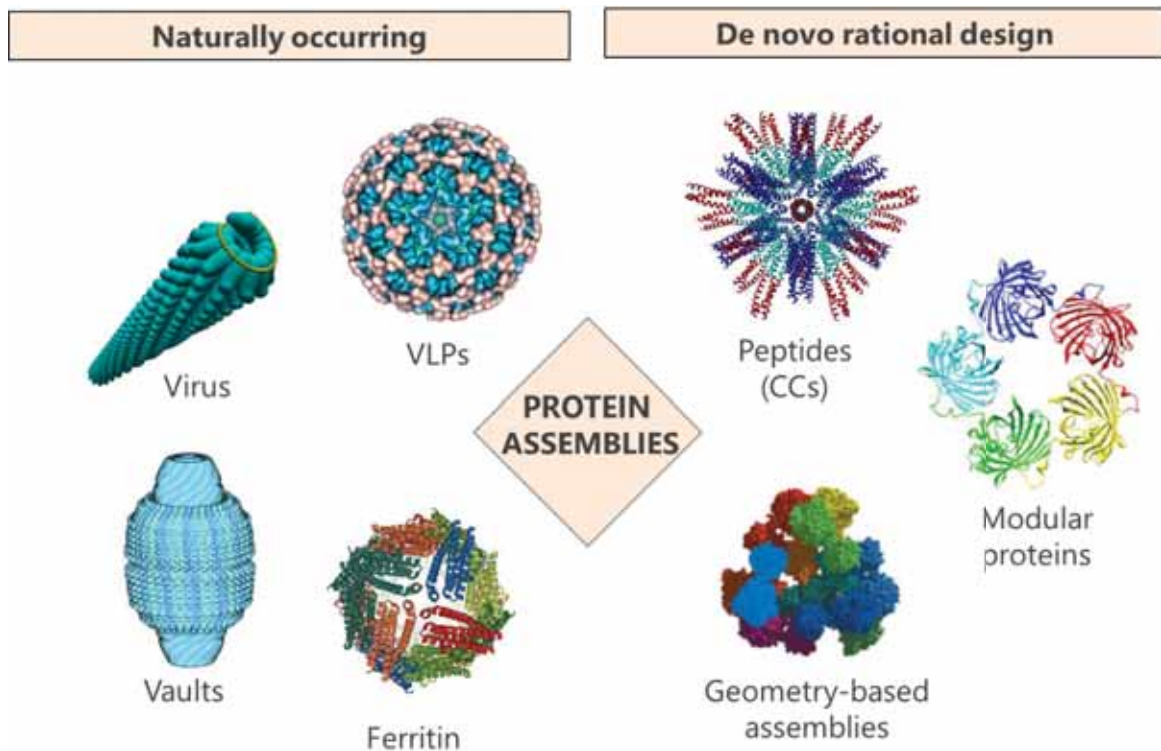


Figure 15. In silico structures of representative protein assemblies naturally occurring (left) or de novo produced through rational design (right). Abbreviations: CC: coiled coil, VLP: virus-like particle.

Natural oligomeric domains (such as α -helices or β -strands) are suitable building blocks for the controlled generation of protein assemblies. β -strands can prompt the formation of amyloid fibrils (stable and highly ordered polypeptide β -sheet aggregates) and gel-like structures. On the other hand, helical coiled coils (CCs) are quaternary structures comprising two or more α -helices supercoiled around each other, resembling the strands of a rope. Such twisted α -helices lead to the formation of CC structures due to the presence of a regular repeating block of seven amino acids. The CC architecture is then simultaneously conditioned by the biophysical nature of the amino acidic chain and the

periodicity of the 7-amino acid block, which can generate diverse structures starting from fibres to tubes, funnels, sheets, spirals or even rings¹²⁸.

Alternatively, natural oligomeric domains (that tend to form dimers or trimers) have been also used for the development of self-assembled structures in a geometry-based manner¹²⁹. This principle relies on the rigid binding between two oligomeric domains that result in a fusion protein (each fusion protein is represented with a different colour in **Figure 15, right**). Each oligomeric domain will interact with identical copies (that have been fused too) forming symmetric nanostructures. Nevertheless, these natural oligomeric domains display moderate functional versatility, and little has been described regarding their applicability in nanomedicine.

In this context, genetic engineering turns out to be an encouraging alternative that has allowed the development of de novo, versatile and **multifunctional modular self-assembled nanoparticles (Figure 16)**. Designing customized proteins that can organize into stable, highly ordered structures is a pursued goal that seems to be feasible nowadays. Moreover, it is particularly appealing because multifunctional self-assembled building blocks are able to mimic virus-like properties and functions, extremely relevant for drug delivery¹³⁰.

5.2. SELF-ASSEMBLING MULTIFUNCTIONAL PROTEINS

Genetic engineering techniques (which rely on the deliberate modification of genetic materials) have allowed to go a step further in the development of fusion proteins, also known as chimeric proteins. Fusion proteins combine diverse non-related effector peptides, each of which has a desired role. All the fused peptides together originate a unique molecule (in a single amino acidic chain), not present in nature, that combines the properties of all the different domains and consequently is able to fulfil all the requirements needed (**Figure 16**). Cell surface ligands, cell penetrating peptides, self-assembling domains or endosomal escape domains are only a few among the long list

of properties that can be added to a chimeric protein so as to improve for example its biodistribution, targeting efficiency and finally therapeutic effect.

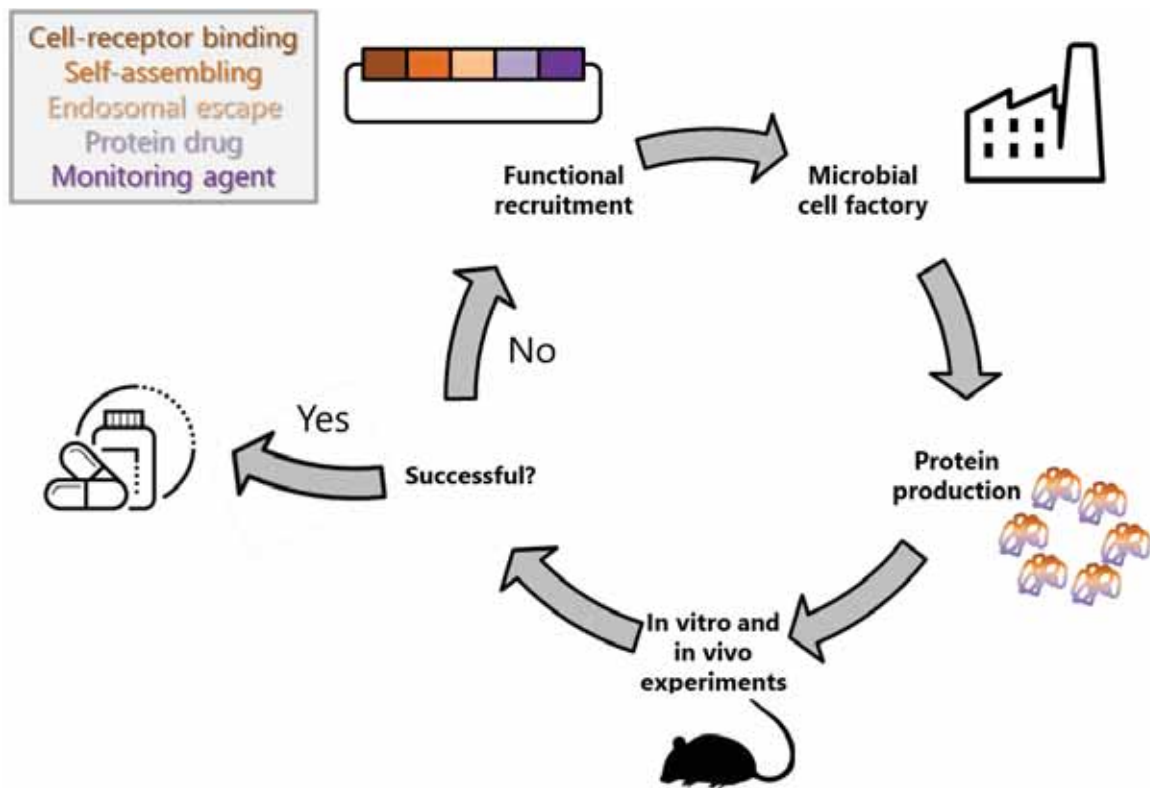


Figure 16. Schematic workflow for the development of recombinant multifunctional self-assembled protein-only nanoparticles.

Etanercept, aflibercept and denileukin diftitox are some of the fusion proteins that have gained regulatory approval for its use in human therapy. Etanercept and aflibercept are fusion proteins that contain Fc region of human IgG1, as it is a stable molecule known for its extended half-life. On the other hand, denileukin diftitox, which is the first marketed fusion protein in 1999, is formed by the catalytic domain of **diphtheria toxin** and the IL-2 as a cell-targeted ligand. The whole structure has been developed for the targeting and treatment of cutaneous T-Cell Lymphoma (CTCL), whose malignant cells over-express the IL-2 receptor⁶.

In conclusion, the use of modular multifunctional proteins would generate infinite possibilities for the development of bespoke nanoparticles that possess all the expected

properties in a single recombinant protein devoid of any additional heterologous compound, which has been previously described as a very appealing concept.

IN-HOUSE NANOARCHITECTONIC PRINCIPLE

In our laboratory there is a remarkable expertise in the design, production and characterization of protein-only nanoparticles (either as soluble or IBs version). Specifically, there is a big interest in the development of soluble self-assembled proteins as nanotherapies.

For that, in our research group it has been described a **nanoarchitectonic principle** that combines non-amyloidogenic **cationic peptides (N-terminus)** and **poly-histidine tags (C-terminus)** in fusion proteins (**Figure 17**). Following this design, protein-only assemblies are formed through non-covalent interactions and generate monodisperse toroidal-shaped (disk-like) nanomaterials. Interestingly, it has been observed that the number of cationic residues present in the N-terminal tag regulates the final nanoparticle size (under a lineal correlation), getting larger nanoparticles with more positively charged N-terminal peptides¹³¹. Besides, it has been proved that the insertion of positively charged residues to non-cationic N-terminal tags enables unassembled monomers to self-organize as protein nanoparticles of around 30 nm¹³².

To date, more than 15 positively charged peptides¹³³⁻¹³⁶ (like R9, T22 and A5G27) have been tested and all of them prompted nanoparticles' formation. Additionally, it has been proved that unrelated core proteins (like GFP, iRFP¹³³ or p53¹³¹) can be added between the cationic peptide and the His-tag and lead to protein oligomerization.

Additionally, the selected cationic N-terminal peptide not only can have a structural role but also can act as a cell-receptor ligand. The possibility to use highly specific ligands has provided us with promising and diverse candidates for cell-targeting purposes (such as drug delivery¹³⁷, tumour imaging¹³³, tissue engineering¹³⁸ and BBB-crossing¹³⁹). On the

other hand, the architectonic C-terminal his-tag is also used for purification purposes through immobilized metal affinity chromatography.

It is worth mentioning that the potential of this nanoarchitectonic principle is due to its **wide applicability**, as it is not restricted to any specific polypeptide. Therefore, any protein of interest can be engineered following this end-terminal tag principle to obtain a self-organized structured version in the nanoscale.

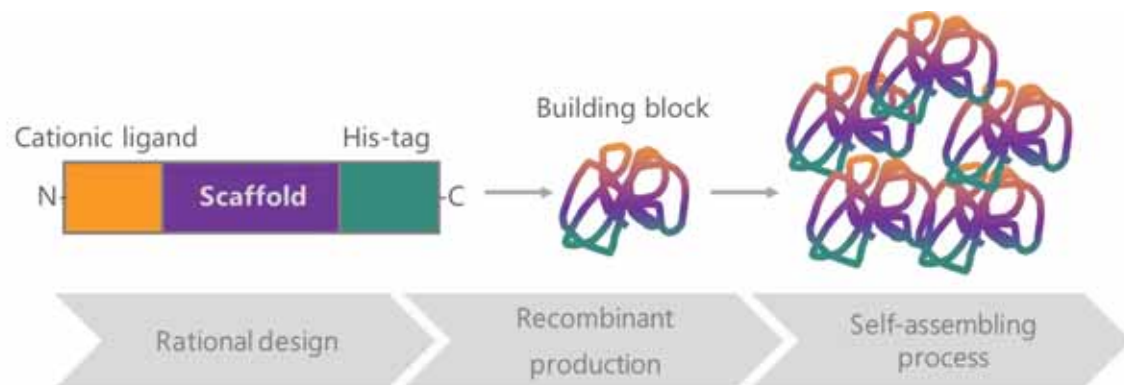


Figure 17. Protein-based nanoarchitectonic principle developed in our group to design multifunctional proteins as highly ordered supramolecular nanostructures.

Specifically, this event offers a promising approach for the customized design and biofabrication of engineered protein-based and highly ordered supramolecular structures as DDS¹³¹.

As a paradigmatic example, the modular **T22-GFP-H6** protein self-assembles as regular toroid nanoparticles of $\sim 12\text{-}13\text{ nm}^{133}$ (**Figure 18**). T22 is an engineered derivative of polyphemusin II whose natural producer is the Atlantic horseshoe crab *Limulus polyphemus*. In this de novo design, T22 was added as a cationic peptide fused to GFP protein and a histidine tag for conformational reasons. Additionally, T22 is an antagonist of CXCR4 receptor, which is overexpressed in metastatic colorectal cancer stem cells. T22-mediated CXCR4 specificity was supported by in vivo experiments in colorectal cancer mouse models after administration of the engineered T22-GFP-H6 fusion protein. Biodistribution experiments revealed that T22-empowered nanoparticles were able to accumulate specifically in primary tumour and metastatic foci¹⁴⁰. The promising results

obtained encouraged us to envisage the further use of T22-GFP-H6 protein-only nanoparticles as potential nanocarriers for drug delivery (i) through conjugation of current chemotherapies^{133,137} or (ii) fusion to intrinsically cytotoxic proteins¹⁴¹.

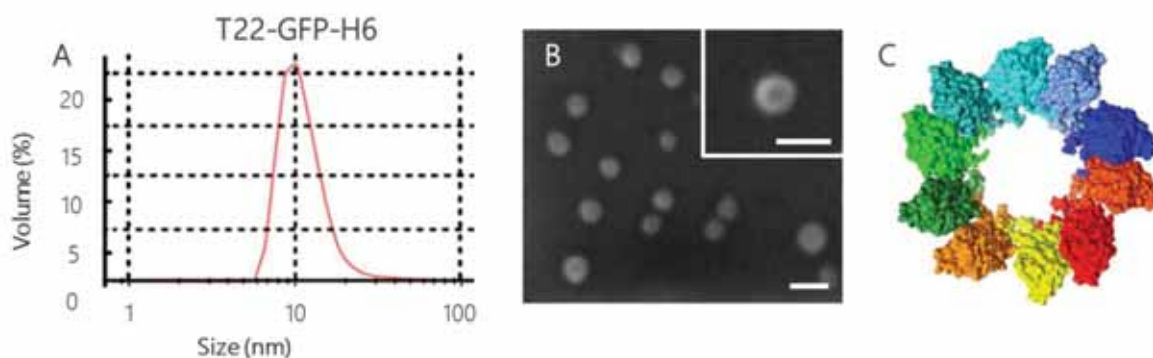


Figure 18. Characterization of T22-GFP-H6 nanoparticles size and structure. A) Dynamic light scattering analysis (DLS) of T22-GFP-H6 nanoparticles. B) Field emission scanning electron microscopy (FESEM) images of T22-GFP-H6 nanoparticles showing cyclic toroidal oligomerization. Bars: 20 nm. C) In silico representation of a T22-GFP-H6 nanoparticle where each building block is illustrated with a different colour (modelled with HADDOCK). Adapted from^{140,142,143}.

6. CYTOTOXIC PROTEINS AS ANTITUMORAL DRUGS

Proteins are involved in many different vital processes; among them **cytotoxicity** has become one of the most appealing ones in the last decades. Many proteins from different sources found in nature are inherently cytotoxic through diverse mechanisms of action (enzymatic inhibition, cell cycle alterations, cellular membrane damage or protein synthesis inhibition). Although extremely different from one to another, animals, plants, insects or even bacteria have been described to produce cytotoxic molecules, mainly for survival reasons. Predation, protection and survival are some of the biological interactions that take place and are involved in the production of such substances in form of toxins or venoms (which are complex combinations of cytotoxic molecules, predominantly proteins and peptides).

In the last decades, cytotoxic proteins have shown to be promising candidates for the development of therapeutic nanomedicines^{144,145}. However, there are some risks

associated when working with such toxic molecules. Chemical conjugation of a toxin to a DDS (apart from posing an additional step in the whole production process) can lead to a limited loading capacity, resulting in an inefficient therapy, unable to reach the therapeutic effect at low doses. Moreover, weak or unstable conjugations can provoke leakage of the toxic moiety during the circulation in the blood stream, causing off-target toxicities to healthy tissues.

Traditionally, toxins have been extracted and purified from their original source (for instance crude venom). However, a few years later it was demonstrated that it was feasible to produce recombinant versions of different toxins and venom proteins while keeping their functionality *in vitro* and *in vivo*. In this context, fusion proteins bearing cytotoxic domains open a plethora of possibilities for the development of homologous protein-based therapeutic nanoparticles. Moreover, if the multifunctional protein not only contains a cytotoxic domain but also a ligand specific of a tumour cell-type, it would generate potent targeted antitumoral candidates. In this regard, the presence of bulk material, drug conjugation procedures, drug leakage or loading capacity will not be concerning issues anymore, as structural and functional entities are found in the same molecule. For these reasons, **recombinant cytotoxic proteins** are becoming widely studied and can indeed be found in the biopharmaceutical market nowadays.

Most of approved cytotoxic proteins are non-natural versions that have been modified somehow for their improved effect *in vivo*. Immunogenicity is usually triggered when the organism is in contact with non-human toxins or monoclonal antibodies that are recognized as foreign. For this reason, toxins are previously de-immunized, to avoid any undesired immunological response after administration¹⁴⁶. This goal can be achieved through point mutations in diverse amino acids that are not present in the active site. Deletions and insertions are also performed in order to remove all the fraction of the toxic protein that is not catalytically active or is responsible for the binding to the natural ligand. Nowadays, during the development of tumour-targeted toxins, the natural binding region is usually replaced through genetic engineering techniques by another sequence previously described as tumour-specific ligand.

CYTOTOXIC PROTEINS FOUND IN NATURE

In nature we can find cytotoxic proteins in a wide diversity of organisms. Human, animal, plant and microbial toxins (**Table 4**) have been extensively studied and applied for the development of therapeutic nanomaterials.

Human proapoptotic factors are extremely appealing as they are not recognized as foreign entities that elicit immunogenic reactions. Therefore, no modifications would be needed when designing a therapeutic recombinant version. Apoptosis is a cell death program that is inhibited through a complex network in tumour cells. The protein family Bcl-2 can be divided in proapoptotic and antiapoptotic proteins¹⁴⁷. Among proapoptotic members, we can find BH3-only proteins (for instance, BID, PUMA, BAD and BIK), that contain Bcl-2 homology (BH) domain BH3 and multidomain proteins (BAX and BAK) with four different BH domains¹⁴⁸. Interestingly, proapoptotic proteins are involved at different levels in the complex apoptotic cascade, to finally cause cellular death by apoptosis. Some of them are able to activate BAX/BAK proteins which are responsible for pore formation in the mitochondrial membrane. Alternatively, other proteins involved (like BAD or BID) are able to bind to anti-apoptotic members, releasing proapoptotic proteins that were previously inhibited.

Animals and insects are considered a rich source of cytotoxic compounds in complex mixtures called venoms. Some of the toxins that can be found in venom mixtures are: chlorotoxin (scorpion), gomesin (spider) and melittin (bee).

On the other hand, plants like *Ricinus communis*, *Saponaria officinalis*, *Abrus precatorius* or *Gelonium multiflorum* have been of great interest for the production of ricin, saporin, abrin and gelonin, respectively¹⁴⁹. All of them are potent ribosome-inactivating proteins (RIPs) that exert potent N-glycosidase activity on the 28S rRNA unit of eukaryotic ribosomes, inhibiting protein synthesis.

Finally, **microorganisms** have been studied as remarkable toxin producers. Pathogenic microorganisms are usually remembered only for their associated detrimental impact

causing plenty of diseases such as infections, gastroenteritis, botulism or diphtheria. However, this conception can be changed trying to benefit from their powerful cytotoxicity. Diphtheria toxin and *Pseudomonas aeruginosa* exotoxin A cause the adenosine diphosphate (ADP)-ribosylation and inactivation of elongation factor 2 (EF-2), which leads to the inhibition of protein synthesis and cell death. Despite their associated high toxicity, they have been smartly engineered for the development of FDA-approved (diphtheria toxin for lymphoma¹⁵⁰ and under development drugs (exotoxin A for mesothelioma and leukaemia¹⁵¹ for the treatment of cancer.

Table 4. Examples of cytotoxic proteins from natural origin that can be used as antitumoral drugs.

CYTOTOXIC PROTEINS	SOURCE	MECHANISM OF ACTION
Proapoptotic proteins		
PUMA	<i>Homo sapiens</i>	Activates BAX and BAK Antiapoptotic protein inactivation
BAD	<i>Homo sapiens</i>	Antiapoptotic protein inactivation
BID	<i>Homo sapiens</i>	
Venoms		
Chlorotoxin	<i>Leiurus quinquestriatus</i> (scorpion)	Chloride channel blocker
Melittin	<i>Apis mellifera</i> (bee)	Surfactant activity
Gomesin	<i>Acanthoscurria gomesiana</i> (spider)	Pore formation
Microbial toxins		
Diphtheria toxin	<i>Corynebacterium diphtheriae</i>	Protein synthesis inhibition (EF-2)
Exotoxin A	<i>Pseudomonas aeruginosa</i>	Protein synthesis inhibition (EF-2)
Adenylate cyclase toxin	<i>Bordetella pertussis</i>	Formation of cation-selective pores
Plant toxins		
Ricin	<i>Ricinus communis</i>	Ribosome-inactivating proteins Protein synthesis inhibition (28S rRNA)
Abrin	<i>Abrus precatorius</i>	
Gelonin	<i>Gelonium multiflorum</i>	

INTRODUCTION

One of the discoveries based on the application of toxic domains are immunotoxins (ITs), which consist of an antibody (or antibody fragment) linked to a toxin. At the early stage of IT development, they were produced through chemical conjugation of the whole antibody and the native toxin. However, this formulation was not efficient enough as tumour and healthy cells were equally damaged (due to the presence of two targeting moieties coming from the antibody and the toxin). To circumvent this issue, the native cell-binding domain of the toxin was removed, and the resulting version of the toxin was attached to the antibody¹⁵². However, ITs were still chemically heterogeneous, large, immunogenic and expensive to produce. For this reason, a lot of modifications have been performed since then aiming to overcome all these difficulties. For instance, through recombinant DNA technologies, proteins were genetically engineered to contain only functional sequences, able to recognize and eliminate tumour cells¹⁵³. Moreover, humanized targeting moieties have been developed to avoid undesired immunogenic reactions. Unfortunately, despite all these improvements, immunogenic reactions and side effects have hindered the leap forward to the clinics.

At this point, it is clear that the use of engineered cytotoxic proteins as antitumoral drugs can mark a crucial turning point in the treatment of cancer. Moreover, produced as fusion proteins in recombinant systems they can be combined with functional domains such as targeting agents or self-assembling domains, allowing the generation of all-in-one, self-delivered antitumoral therapies devoid of heterogenic materials.

7. OVERVIEW

Nowadays, conventional cancer therapies are far from being optimal in terms of efficacy. Current drugs are small chemical entities that equally distribute all over the organism, presenting high systemic toxicity and leading to undesired side effects on healthy tissues. In this context, nanomedicine is an emerging area that offers promising alternatives for the development of improved oncotherapies.

Being extremely versatile materials, recombinant proteins are gaining interest in the biomedical area, with more than 400 recombinant pharmaceuticals approved by medical agencies. Modular and multifunctional protein-based nanoparticles are appealing candidates for drug delivery as they show high stability, biocompatibility and biodegradability in the blood stream. When designing DDS, size is one of the most relevant properties. Particles in the **nanoscale** (desirably around ~8 – 100 nm) benefit from enhanced stability as they escape from renal filtration and thus present extended circulation time and improved biodistribution (compared to smaller chemical drugs). For that, it has been developed in our group a **nanoarchitectonic principle** for the generation of protein supramolecular assemblies ranged in the nanoscale. The principle relies on the use of cationic end-terminal peptides as pleiotropic tags for the oligomerization of monomers into self-assembled nanoparticles. Such modular protein-based nanostructures can be widely used as cell-targeted nanocarriers if the cationic N-terminal peptide is simultaneously a tumour-specific ligand. However, chemical conjugation of nanocarriers to conventional drugs is extremely risky due to the associated drug leakage and subsequent side effects. In this context, the main purpose in this PhD project was to explore the translational applicability of this principle for the development of **all-in-one vehicle-free** protein nanomedicines. This ambitious goal has been addressed through de novo rational design of diverse intrinsically cytotoxic proteins as therapeutic building blocks that combined with endosomal escape domains will produce protein-only tumour-targeted antitumoral drugs.

From now on, encouraged by the promising results discussed in this thesis, we consider it is imperative to keep on studying in detail the potential application of this all-in-one protein-based platform for the treatment of any unrelated diseases.



OBJECTIVES

OBJECTIVES

The protein-based nanoarchitectonic approach described in our group relies on the use of end-terminal cationic peptides and a hexa-histidine tag to induce nanoparticle formation through the self-assembly of multifunctional building blocks, independently of the selected core protein^{131,140}. Additionally, if the cationic peptide is not only a structural moiety but also a ligand, specifically cell-targeted nanocarriers are generated. In this sense, T22-GFP-H6 nanoparticles (targeted to CXCR4 receptor) have performed outstanding results regarding selective biodistribution and accumulation in an orthotopic colorectal cancer mouse model¹³³. The general purpose of this work is to prove the versatility of this architectonic principle through the addition of engineered intrinsically cytotoxic domains. The main aim is to generate in a single entity, all-in-one vehicle-free therapeutic nanomedicines devoid of any bulk material or conjugation process for the treatment of CXCR4⁺ cancers. To this purpose, we planned the following objectives:

- 1) To identify effective therapeutic proteins that fulfill all the regulatory requirements for their use in the clinics.
- 2) To study the incorporation of an endosomal escape promoter, namely fusogenic peptide hemagglutinin-2, for the improved efficiency of internalized T22-empowered protein-only nanoparticles.
- 3) To produce multifunctional self-assembled and self-delivered therapeutic nanoparticles, through the addition of intrinsically cytotoxic toxin-based domains, for the treatment of CXCR4⁺ cancers.
- 4) To generate safe all-in-one vehicle-free cytotoxic protein-based nanocarriers devoid of heterologous non-functional bulk material in a single step process through recombinant DNA technologies.
- 5) To develop smart stimuli-responsive protein-only nanoscale drugs able to discharge accessory protein segments under acidic conditions by adding furin cleavable regions through genetic engineering techniques.



RESULTS

REVIEW 1

Recombinant pharmaceuticals from microbial cells: a 2015 update

Laura Sánchez-García, Lucas Martín, Ramón Manges, Neus Ferrer-Miralles, Esther Vázquez, and Antonio Villaverde

Microbial Cell Factories (2016) 15 (33)

Impact Factor 3.831 BIOTECHNOLOGY & APPLIED MICROBIOLOGY (36/161) Q1

Absence or dysfunction of proteins can lead to the appearance of diseases such as diabetes, growth or clotting disorders. Nowadays the administration of recombinant functional versions of these abnormal or missing proteins is becoming more and more frequent through replacement therapies. The treatment, which might consist in single or repeated doses, aims to reach a functional concentration that complements the lack in the patients' organism.

In this review, our aim is to provide a general overview of the current trends regarding recombinant biopharmaceuticals that are already FDA-approved and under development. Moreover, we have given detailed information about the expression systems used and their properties, followed by the therapeutic areas that benefit the most from recombinant biopharmaceuticals. Nowadays, around 400 recombinant peptides and proteins are found in the market as drugs. Additionally, other 1300 recombinant candidates are ongoing clinical trials. Therefore, there is an expected increase in the total number of marketed recombinant proteins in the next years. Currently, almost 24 % of all marketed protein biopharmaceuticals are indicated for oncology. The potential use of recombinant proteins as drugs is under dramatic expansion. Because of the functional versatility of proteins, it is being observed a tendency towards the development of sophisticated multi-domain proteins able to accomplish all the requirements in a single molecule, instead of plain nature-derived versions. In the 1980s, the first FDA-approved biopharmaceutical Humulin (recombinant human insulin) was produced using *E. coli* as expression system. Since then, although other bacteria, yeasts, insect cells or mammalian cells have been extensively studied, *E. coli* remains one of the most widely used platforms for protein production due to its extensive know-how, high versatility, easy handling and low expenses.

After intensive bibliographic research the published data provides a general picture of the current tendency and the future perspectives in the recombinant biopharmaceutics field. Moreover, this work has provided us with precious information like the promising applicability of recombinant toxins engineered as fusion proteins for their specific delivery towards targeted cancerous cells.

REVIEW

Open Access



Recombinant pharmaceuticals from microbial cells: a 2015 update

Laura Sanchez-Garcia^{1,2,3}, Lucas Martín⁴, Ramon Mangués⁵, Neus Ferrer-Miralles^{1,2,3}, Esther Vázquez^{1,2,3} and Antonio Villaverde^{1,2,3*} 

Abstract

Diabetes, growth or clotting disorders are among the spectrum of human diseases related to protein absence or mal-function. Since these pathologies cannot be yet regularly treated by gene therapy, the administration of functional proteins produced *ex vivo* is required. As both protein extraction from natural producers and chemical synthesis undergo inherent constraints that limit regular large-scale production, recombinant DNA technologies have rapidly become a choice for therapeutic protein production. The spectrum of organisms exploited as recombinant cell factories has expanded from the early predominating *Escherichia coli* to alternative bacteria, yeasts, insect cells and especially mammalian cells, which benefit from metabolic and protein processing pathways similar to those in human cells. Up to date, around 650 protein drugs have been worldwide approved, among which about 400 are obtained by recombinant technologies. Other 1300 recombinant pharmaceuticals are under development, with a clear tendency towards engineered versions with improved performance and new functionalities regarding the conventional, plain protein species. This trend is exemplified by the examination of the contemporary protein-based drugs developed for cancer treatment.

Keywords: Recombinant proteins, Protein drugs, Recombinant DNA, Fusion proteins, Biopharmaceuticals

Background

Human cells produce thousands of proteins that integrated into an extremely complex physiologic network perform precise actions as catalysers, signalling agents or structural components. Then, dysfunction of proteins with abnormal amino acid sequences or the absence of a given protein often results in the development of severe pathologies such as diabetes [1], dwarfism [2], cystic fibrosis [3], thalassaemia [4] or impaired blood clotting [5], among many others [6, 7]. In the absence of standardized gene therapy treatments that would genetically reconstitute functional protein production within the patient, protein deficiencies must be treated by the punctual or repeated clinical administration of the missing protein, so as to reach ordinary functional concentrations. These therapeutic proteins are produced *ex vivo*

mostly in biological systems [8], which must guarantee not only full protein functionalities but also a cost-effective industrial fabrication and the absence of hazardous contaminants. Protein drugs have to necessarily conform to quality constraints stricter than those expected in the production of enzymes for chemical industries, which consequently defines the choice of recombinant hosts, protocols and production strategies. Nowadays, there are over 400 marketed recombinant products (peptides and proteins) and other 1300 are undergoing clinical trials (figures updated on May 2015 [9]).

In this context of expanding protein drug markets, there is a generic consensus about the need to enable drugs for cell- or tissue-targeted delivery to reduce doses, production costs and side effects. While increasing protein stability *in vivo* can be reached by discrete modifications in the amino acid sequence, generating fusions between therapeutic proteins and specific peptide ligands or antibodies that interact with particular cell receptors might allow acquiring specificity in the delivery process.

*Correspondence: Antoni.Villaverde@uab.cat

¹ Institut de Biotecnologia i de Biomedicina, Universitat Autònoma de Barcelona, 08193 Bellaterra, Cerdanyola del Vallès, Spain

Full list of author information is available at the end of the article



© 2016 Sanchez-Garcia et al. This article is distributed under the terms of the Creative Commons Attribution 4.0 International License (<http://creativecommons.org/licenses/by/4.0/>), which permits unrestricted use, distribution, and reproduction in any medium, provided you give appropriate credit to the original author(s) and the source, provide a link to the Creative Commons license, and indicate if changes were made. The Creative Commons Public Domain Dedication waiver (<http://creativecommons.org/publicdomain/zero/1.0/>) applies to the data made available in this article, unless otherwise stated.

In this regard and also pushed by the convenience to combine diagnosis and therapy in theranostic agents [10, 11], contemporary research on protein pharmaceuticals tends towards engineered versions functionally more sophisticated than plain natural polypeptides.

Review

Cell factories

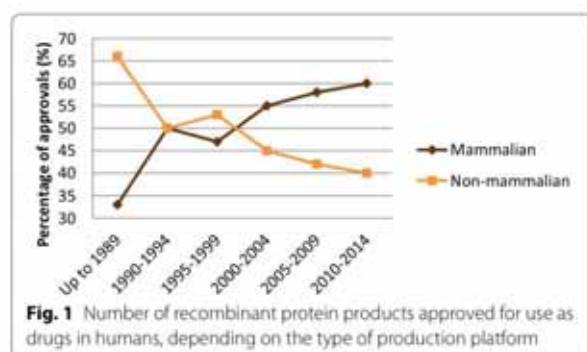
Since early recombinant DNA times, ever-increasing understanding of cell physiology and stress, and of factors involved in heterologous gene expression and protein production empowered the use of different living factories, namely prokaryotic and eukaryotic cells, plants or animals [12, 13]. By using these systems, recombinant production solves source availability problems, is considered a bio-safe and green process and confers the ability to modify amino acid sequences and therefore protein function, to better adjust the product to a desired function [14]. There is a wide and growing spectrum of expression systems that are becoming available for the production of recombinant proteins [15, 16]. *Escherichia coli* was the prevalent platform when the biopharmaceutical sector emerged in the 1980s, and it was followed by the implementation of the yeast *Saccharomyces cerevisiae*. Both systems and the associated genetic methodologies exhibit an unusually high versatility, making them adaptable to different production demands [17]. Despite the exploration of insect cells as initially successful system especially for vaccine-oriented proteins, mammalian cell lines (most notably CHO cells) are nowadays the prevailing animal-derived cell system due to their suitability to produce conveniently glycosylated proteins [18, 19] (Fig. 1). The ability to carry out post translational modifications contrasts with complex nutritional requirements, slow growth and fragility, and relatively high production timing and costs. Thus, among many conventional and emerging cell-based systems for protein production, bacteria, yeast and mammalian cell lines are the most common in biopharma, and both prokaryotic and

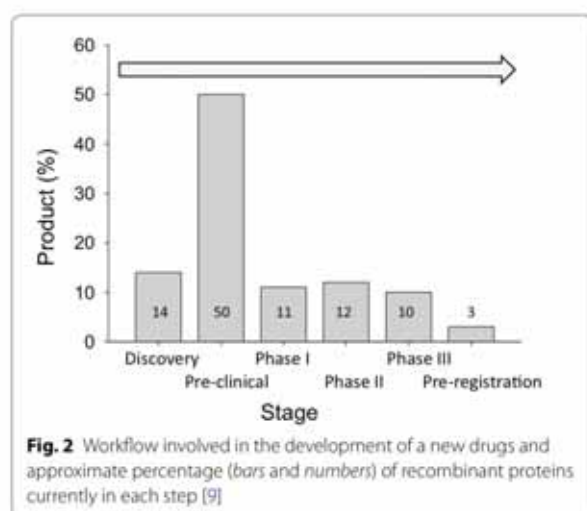
eukaryotic systems are constantly evolving and competing to improve their properties and intensify as platforms of choice for protein drug production [14]. While bacteria has lost its early leading role in the field [19], about 30 % of marketed biopharmaceuticals are still produced in this system [20], as supported by the unusual physiological and genetic manipulability of prokaryotic cells [21].

In fact, the main purpose in the development of new protein production platforms is to enhance drug functionality through reaching successful protein folding and post-translational modifications, while keeping the low complexity and high flexibility associated to prokaryotic cell culture. In this context, Gram-positive bacteria such as *Bacillus megaterium* [22] and *Lactococcus lactis* [23] allow efficient protein secretion in absence of endotoxic cell wall components, while filamentous fungi (such as *Trichoderma reesei*, [24]), moss (*Physcomitrella patens*, [25, 26]) and protozoa (*Leishmania tarentolae*, [27–29]) promote glycosylation patterns similar to those in mammalian proteins but being still cultured through methods simpler than those required by mammalian cells. Extensive descriptions of emerging (bacterial and non-bacterial) platforms specifically addressed to the production of high quality protein drugs can be found elsewhere [15, 16, 21]. The recent development of an endotoxin-free strain of *E. coli* [30] and its application to the fabrication of proteins and protein materials [30–32] paves the road for a cost-efficient and versatile production of proteins intended for biomedical uses by skipping endotoxin removal steps, thus gaining in biosafety and reducing production costs [33]. Hopefully, all these new systems would soon offer improved products in still simple and fully controlled biofabrication approaches.

Trends in protein biopharmaceuticals

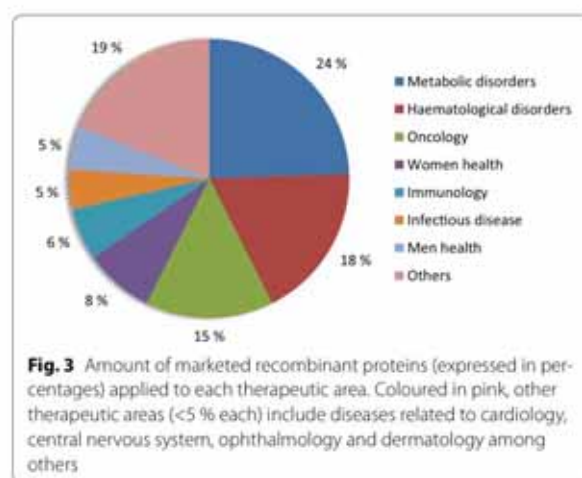
Nearly 400 recombinant protein-based products have been successfully produced and are approved as biopharmaceuticals [9], a term that refers to therapeutic products generated by technologies that involve living organisms [34]. Other 1300 protein candidates are under development, of which around 50 % are in pre-clinical studies and other 33 % in clinical trials [9] (Fig. 2). In this context, an increase in the number of approvals in next years is predictable. Developed by Eli Lilly & Co in the 70's, Humulin, a recombinant human insulin fabricated in the bacterium *E. coli* [35], was the first approved biopharmaceutical (by the FDA) in 1982 [36, 37]. Other natural proteins such as hormones, cytokines and antibodies (Orthoclone OKT3) were among the single nine products approved in 1980s (Table 1). Nowadays, the therapeutic areas that have benefited more from recombinant biopharmaceuticals are metabolic disorders (e.g. diabetes





type 1, type 2, obesity or hypoglycaemia), haematological disorders (e.g. renal anaemia, haemophilia A, bleeding or clotting disorders) and oncology (e.g. melanoma, breast or colorectal cancer), with 24, 18 and 15 % of the approvals respectively (Fig. 3). In this regard, oncology is a clearly expanding market. In the period 2010–2014, 9 out of 54 approved biopharmaceuticals were antitumoral drugs, cancer representing the most common indication within this period. Digging into the molecular bases of biopharmaceuticals, there is a clear trend towards antibody-based products. Over the same period (2010–2014), 17 of the 54 protein drugs approved were monoclonal antibodies (31.5 %), compared with 11 % over 1980–1989 [22]. Furthermore, among the top ten selling protein biopharmaceuticals globally in 2014 (Table 2), six are antibodies or antibody-derived proteins (Humira, Remicade, Rituxan, Enbrel, Avastin, Herceptin; <http://qz.com/349929/best-selling-drugs-in-the-world/>).

Formerly, biopharmaceuticals were recombinant versions of natural proteins, with the same amino acid



sequence as the respective native versions (with only minor modifications, often resulting from the cloning strategy). Since 1990s, a meaningful proportion of the approvals are based on highly modified forms of recombinant proteins. This novel alternative, based on protein or domain fusion and on truncated versions, offers a wide spectrum of possible combinations to obtain novel biopharmaceuticals with different joined activities that are not found together in nature.

Protein drugs for cancer treatment

Oncology is one of the therapeutic indications that dominate the biopharmaceutical market, as cancer is a major cause of morbidity and mortality worldwide. Surgery and radiotherapy are effective in curing cancer at early disease stages; however, they cannot eradicate metastatic disease. The presence of micrometastases or clinically evident metastases at diagnosis requires their use in combination with genotoxic chemotherapy to increase cure rates [38]. Nevertheless, the success of chemotherapy has been hampered because of its lack of selectivity and

Table 1 Recombinant biopharmaceuticals approved in the 1980s

Product	Cell factory	Therapeutic indication	Year
Humulin	<i>E. coli</i>	Diabetes	1982
Protropin	<i>E. coli</i>	hGH deficiency	1985
Roferon A	<i>E. coli</i>	Hairy cell leukaemia	1986
IntronA	<i>E. coli</i>	Cancer, genital warts and hepatitis	1986
Recombivax	<i>S. cerevisiae</i>	Hepatitis B	1986
Orthoclone OKT3	Hybridoma cell line	Reversal of acute kidney and transplant rejection	1986
Humatrope	<i>E. coli</i>	hGH deficiency	1987
Activase	CHO	Acute myocardial infarction	1987
Epogen	CHO	Anaemia	1989

Table 2 Top ten selling protein biopharmaceuticals in 2014

Drug ^a	Active ingredient	Molecule	Sales in billions	Origin
Humira	Adalimumab	Recombinant human monoclonal antibody	12.54	CHO
Sovaldi	Sofosbuvir	Nucleotide analogue polymerase (NS5B) inhibitor	10.28	Chemical
Remicade	Infliximab	Recombinant chimeric, humanized tumor necrosis factor alpha (TNF) monoclonal antibody	9.24	Hybridoma cell line
Rituxan	Rituximab	Recombinant humanized monoclonal antibody	8.68	CHO
Enbrel	Etanercept	Recombinant soluble dimeric fusion protein	8.54	CHO
Lantus	Insulin glargine	Insulin receptor agonist	7.28	<i>E. coli</i>
Avastin	Bevacizumab	Recombinant humanized antibody	6.96	CHO
Herceptin	Trastuzumab	Recombinant humanized monoclonal antibody	6.79	CHO
Advair	Fluticasone propionate and salmeterol xinafoate	Glucocorticoid receptor agonist and β -2 adrenergic receptor agonist	6.43	Chemical
Crestor	Rosuvastatin calcium	Antihyperlipedemic agent	5.87	Synthetic

^a Data according to www.medtrack.com, November 2015

Table 3 Representative examples of supportive protein drugs in cancer

Drug name	Cell factory	Biological role	Mechanism of action	Indications
Filgrastim (Scimax)	<i>E. coli</i>	Cytokine	Stimulates hematopoiesis	Bone marrow transplantation and cancer chemotherapy induced neutropenia
Pegfilgrastim (Neupeg)	<i>E. coli</i>	Cytokine	Stimulates differentiation, proliferation and activation of the neutrophilic granulocytes	Cancer chemotherapy induced neutropenia
Darbepoetin alfa (Aranesp)	CHO cells	Hormone	Stimulates processes of erythropoiesis or red blood cell production	Anemia associated with chronic renal failure, cancer chemotherapy or heart failure. Myelodysplastic syndrome
Lenograstim (CERBIOS)	CHO cells	Cytokine	Stimulates differentiation, proliferation and activation of neutrophilic granulocytes	Neutropenia associated with cytotoxic therapy or bone marrow transplantation
Epoetin alfa (Binocrit)	CHO cells	Hormone	Stimulates production of oxygen carrying red blood cells from the bone marrow	Anemia associated with chronic renal failure and cancer chemotherapy induced anemia

specificity, so that the toxicity to normal tissues limits the dose that could be administered to patients. The development of biopharmaceuticals capable of inhibiting specific molecular targets driving cancer (for instance, monoclonal antibodies anti-Her2—Trastuzumab- or anti-VEGF—Bevacizumab-) goes in this direction [39].

Among marketed protein biopharmaceuticals, almost 24 % (94 products) are used in antitumoral therapies. Most of these products are used for supportive purposes intended to minimize the side effects of chemotherapy, usually neutropenia or anaemia (some representative examples are shown in Table 3). Nineteen out of those 94 products are true antitumoral drugs, 69 % of which are produced in *E. coli* (Fig. 4) and are based on engineered amino acidic sequences, protein fusions and single protein domains (Table 4).

Clearly, modified protein versions are the most abundant in cancer therapies over natural polypeptides. As relevant examples, Ziv aflibercept is a recombinant fusion

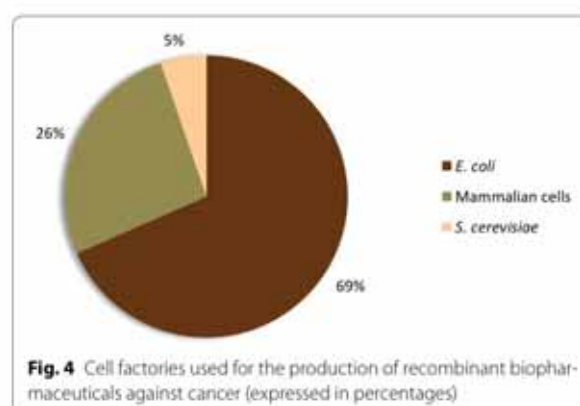


Fig. 4 Cell factories used for the production of recombinant biopharmaceuticals against cancer (expressed in percentages)

protein produced in CHO cells used against colorectal cancer. It consists of portions of each Vascular Endothelial Growth Factor Receptors (VEGFR1 and VEGFR2) fused

Table 4 Anticancer recombinant biopharmaceuticals approved until March 2015

Drug name	Cell factory	Source	Biological role	Indications
Denileukin diftitox	<i>E. coli</i>	Fusion protein	Diphtheria toxin fused to cytokine	Cutaneous T-cell lymphoma
Endostatin	<i>E. coli</i>	Modified	Collagen derivative	Non-small cell lung cancer, metastatic colorectal cancer
Aldesleukin	<i>E. coli</i>	Modified	Cytokine	Metastatic renal cell carcinoma, metastatic melanoma, kidney cancer, angiosarcoma
Interleukin-2	<i>E. coli</i>	Modified	Cytokine	Metastatic melanoma, metastatic renal cell carcinoma
Filgrastim	<i>E. coli</i>	Modified	Cytokine	Acute lymphocytic leukaemia, solid tumour
Interferon alpha-2a	<i>E. coli</i>	Modified	Cytokine	AIDS-related Kaposi's sarcoma, follicular lymphoma, cutaneous T-cell lymphoma, melanoma, chronic myelocytic leukaemia, hairy cell leukaemia, renal cell carcinoma, kidney cancer
Interferon alpha-2b	<i>E. coli</i>	Modified	Cytokine	AIDS-related Kaposi's sarcoma, pancreatic endocrine tumour, melanoma, non-Hodgkin lymphoma, leukaemia, hairy cell leukaemia, renal cell carcinoma, multiple myeloma, CML, follicular lymphoma, melanoma
Interferon alpha-1b	<i>E. coli</i>	Modified	Cytokine	Renal cell carcinoma, hairy cell leukaemia
Interferon gamma-1a	<i>E. coli</i>	Modified	Cytokine	Kidney cancer, sezary syndrome, mycosis fungoides
Tasonermin	<i>E. coli</i>	Natural	Cytokine	Soft tissue sarcoma
Molgramostim	<i>E. coli</i>	Modified	Growth factor	Myelodysplastic syndrome
Nartograstim	<i>E. coli</i>	Modified	Growth factor	Solid tumour
Palifermin	<i>E. coli</i>	Fraction	Growth factor	Metastatic renal cell carcinoma, metastatic melanoma
Sargramostim	<i>S. cerevisiae</i>	Modified	Growth factor	Acute myelocytic leukaemia
Ziv-aflibercept	CHO cells	Fusion protein	Growth factor receptor fused to IgG1	Metastatic colorectal cancer
Thyrotropin alpha	CHO cells	Modified	Hormone	Thyroid cancer
Trastuzumab biosimilar	CHO cells	Modified	Monoclonal antibody	Breast cancer, gastric cancer, metastatic breast cancer
Rituximab biosimilar	CHO cells	Modified	Monoclonal antibody	Non-Hodgkin lymphoma, chronic lymphocytic leukaemia
Interferon alpha	Human lymphoblastoid cells	Modified	Cytokine	AIDS-related Kaposi's sarcoma, multiple myeloma, non-Hodgkin lymphoma, CML, hairy cell leukaemia, renal cell carcinoma

to the constant fraction (Fc) of a human IgG1 immunoglobulin (Fig. 5). This construct acts as a decoy by binding to VEGF-A, VEGF-B and placental growth factor (PlGF), which activate VEGFR. This trap hinders the interaction between the growth factors and the receptors, inhibiting the VEGF pathway which is involved in the angiogenic process [40]. Denileukin diftitox is a recombinant protein composed of two diphtheria toxin fragments (A and B) and a human interleukin-2 (Fig. 5). Diphtheria toxin is a potent exotoxin secreted by *Corynebacterium diphtheriae*.

Due to its peculiar structure, the whole complex, produced in *E. coli*, is capable of delivering a cytotoxic agent directly to a specific target. There are two main active blocks whose function is firstly to selectively deliver the biopharmaceutical (IL-2) and secondly cause cytotoxicity (toxin A and B) [41]. The fusion protein binds to the IL-2 receptor, which is expressed in cancerous cells (cutaneous T cell lymphoma). Once the toxin moiety is internalized, the catalytic domain promotes cell death through protein synthesis inhibition [42].

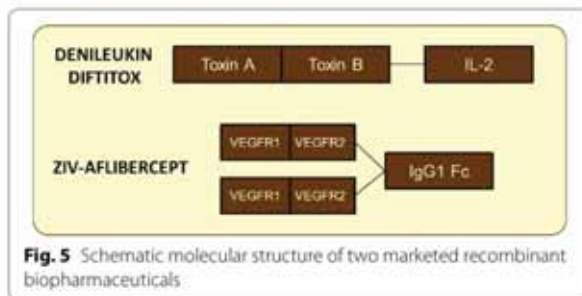


Fig. 5 Schematic molecular structure of two marketed recombinant biopharmaceuticals

As targeted drug delivery for cancer is a most recent and expanding area of research, other non-recombinant, protein-based biopharmaceuticals are also heavily represented. Those mainly include antibody-drug conjugates (ADCs) such as Brentuximab vedotin, Trastuzumab emtansine, or nanoparticle-drug conjugates such as nab-paclitaxel [39, 43]. In these cases, the protein counterpart acts as a targeted vehicle for conventional chemical drugs. Again, this approach pursues the selective drug delivery to specific target cells, aimed to increase antitumoral activity while reducing toxicity on normal cells and the associated side effects.

Products against cancer that provided the highest revenues in 2013 are represented in Fig. 6. Sixty

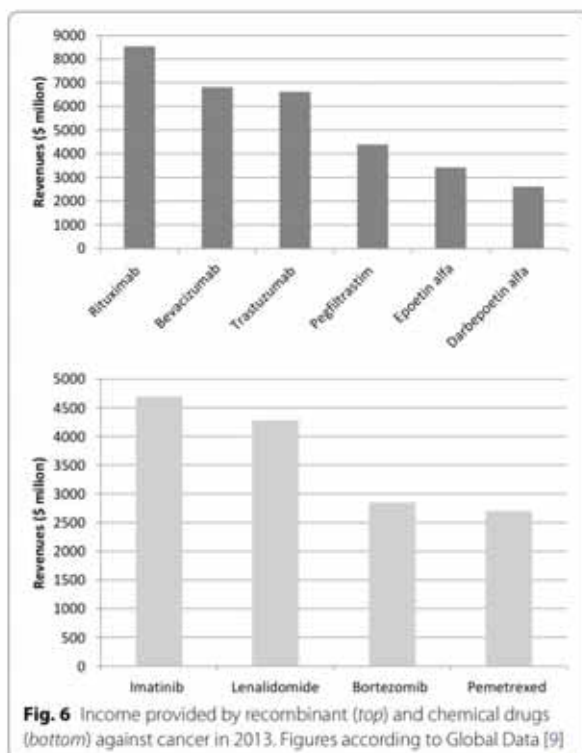


Fig. 6 Income provided by recombinant (top) and chemical drugs (bottom) against cancer in 2013. Figures according to Global Data [9]

percent of those products are recombinant proteins, supporting the idea that recombinant protein production is still a rising and promising platform, offering room for important advances in the biopharmaceutical sector.

Conclusions

In summary, the market and potential for recombinant drugs is expanding by taking advantage of a steady growing spectrum of protein production platforms. Despite the strength of mammalian cell lines as factories, microbial cells and specially *E. coli* are still potent protein factories essentially supported by their versatility and cost-effective cultivation. Recombinant drugs are moving from plain recombinant versions of natural products to more sophisticated protein constructs resulting from a rational design process. Combining protein domains to gain new functionalities is being exploited in drug discovery by exploiting the structural and functional versatility that merge in proteins as extremely versatile macromolecules.

Abbreviations

AIDS: acquired immune deficiency syndrome; ADCs: antibody-drug conjugates; CHO: chinese hamster ovary; CML: chronic myelogenous leukemia; Fc: constant fraction; FDA: food and drug administration; hGH: human growth hormone; IL: interleukin; PlGF: placental growth factor; VEGF: vascular endothelial growth factor; VEGFR: vascular endothelial growth factor receptor.

Authors' contributions

LSG performed most of the bibliographic search and prepared part of the text, tables and figures, under the supervision of NFM and EV. LM and RM contributed with additional information and revised the manuscript. AV coordinated the whole revision, prepared part of the text and figures and the final manuscript version. All authors read and approved the final manuscript.

Author details

¹ Institut de Biotecnologia i de Biomedicina, Universitat Autònoma de Barcelona, 08193 Bellaterra, Cerdanyola del Vallès, Spain. ² Departament de Genètica i de Microbiologia, Universitat Autònoma de Barcelona, 08193 Bellaterra, Cerdanyola del Vallès, Spain. ³ CIBER de Bioingeniería, Biomateriales y Nanomedicina (CIBER-BBN), 08193 Bellaterra, Cerdanyola del Vallès, Spain. ⁴ Technology Transfer Office, Edifici Eureka, Universitat Autònoma de Barcelona, 08193 Bellaterra, Cerdanyola del Vallès, Spain. ⁵ Institut d'Investigacions Biomèdiques Sant Pau, Josep Carreras Research Institute and CIBER-BBN, Hospital de la Santa Creu i Sant Pau, Barcelona, Spain.

Acknowledgements

The authors appreciate the funding for protein drug development received from MINECO (BIO2013-41019-P), AGAUR (2014SGR-132, 2014PROD-00055) CIBER de Bioingeniería, Biomateriales y Nanomedicina (NANOPROTHER), Marató de TV3 foundation (TV32013-132031, TV32013-3930) and ISCIII FIS (PI12/00327, PI15/00272, PI15/00378). LSG received a Lanzadera fellowship from CIBER-BBN, and AV received an ICREA ACADEMIA award.

Competing interests

The authors declare that they have no competing interests.

Received: 3 December 2015 Accepted: 1 February 2016

Published online: 09 February 2016

References

- Vajo Z, Fawcett J, Duckworth WC. Recombinant DNA technology in the treatment of diabetes: insulin analogs. *Endocr Rev*. 2001;22:706–17.
- Takeda A, Cooper K, Bird A, Baxter L, Frampton GK, Gospodarevskaya E, et al. Recombinant human growth hormone for the treatment of growth disorders in children: a systematic review and economic evaluation. *Health Technol Assess*. 2010;14:1–4.
- Cutting GR. Modifier genetics: cystic fibrosis. *Annu Rev Genomics Hum Genet*. 2005;6:237–60.
- Weatherall DJ. Phenotype–genotype relationships in monogenic disease: lessons from the thalassaemias. *Nat Rev Genet*. 2001;2:245–55.
- Powell JS. Lasting power of new clotting proteins. *Hematology Am Soc Hematol Educ Program*. 2014;2014:355–63.
- Hirschhorn JN, Lohmueller K, Byrne E, Hirschhorn K. A comprehensive review of genetic association studies. *Genet Med*. 2002;4:45–61.
- Savic S, McDermott MF. Clinical genetics in 2014: new monogenic diseases span the immunological disease continuum. *Nat Rev Rheumatol*. 2015;11:67–8.
- Assenberg R, Wan PT, Geisse S, Mayr LM. Advances in recombinant protein expression for use in pharmaceutical research. *Curr Opin Struct Biol*. 2013;23:393–402.
- Global Data 2015. <http://www.globaldata.com>. 2015.
- Lammers T, Aime S, Hennink WE, Storm G, Klessling F. Theranostic nanomedicine. *Acc Chem Res*. 2011;44:1029–38.
- Pene F, Courtiere E, Cariou A, Mira JP. Toward theragnostics. *Crit Care Med*. 2009;37:550–8.
- Demain AL, Vaishnav P. Production of recombinant proteins by microbes and higher organisms. *Biotechnol Adv*. 2009;27:297–306.
- Adrio JL, Demain AL. Recombinant organisms for production of industrial products. *Bioeng Bugs*. 2010;1:116–31.
- Walsh G. Biopharmaceutical benchmarks 2014. *Nat Biotechnol*. 2014;32:992–1000.
- Ferrer-Miralles N, Villaverde A. Bacterial cell factories for recombinant protein production; expanding the catalogue. *Microb Cell Fact*. 2013;12:113.
- Corchero JL, Gasser B, Resina D, Smith W, Parrilli E, Vazquez F, et al. Unconventional microbial systems for the cost-efficient production of high-quality protein therapeutics. *Biotechnol Adv*. 2013;31:140–53.
- Ferrer-Miralles N, Domingo-Espin J, Corchero JL, Vazquez E, Villaverde A. Microbial factories for recombinant pharmaceuticals. *Microb Cell Fact*. 2009;8:17.
- Zhu J. Mammalian cell protein expression for biopharmaceutical production. *Biotechnol Adv*. 2012;30:1158–70.
- Baeshen NA, Baeshen MN, Sheikh A, Bora RS, Ahmed M, Ramadan HI, et al. Cell factories for insulin production. *Microb Cell Fact*. 2014;13:141.
- Overton TW. Recombinant protein production in bacterial hosts. *Drug Discov Today*. 2014;19:590–601.
- Chen R. Bacterial expression systems for recombinant protein production: *E. coli* and beyond. *Biotechnol Adv*. 2012;30:1102–7.
- van Dijk JM, Hecker M. *Bacillus subtilis*: from soil bacterium to super-secreting cell factory. *Microb Cell Fact*. 2013;12:3.
- Cano-Garrido O, Rueda FL, Sanchez-Garcia L, Ruiz-Avila L, Bosser R, Villaverde A, et al. Expanding the recombinant protein quality in *Lactococcus lactis*. *Microb Cell Fact*. 2014;13:167.
- Su X, Schmitz G, Zhang M, Mackie RI, Cann IK. Heterologous gene expression in filamentous fungi. *Adv Appl Microbiol*. 2012;81:1–61.
- Decker EL, Reski R. Current achievements in the production of complex biopharmaceuticals with moss bioreactors. *Bioprocess Biosyst Eng*. 2008;31:3–9.
- Decker EL, Reski R. Moss bioreactors producing improved biopharmaceuticals. *Curr Opin Biotechnol*. 2007;18:393–8.
- Basile G, Peticca M. Recombinant protein expression in *Leishmania tarentolae*. *Mol Biotechnol*. 2009;43:273–8.
- Kushnir S, Gase K, Breitling R, Alexandrov K. Development of an inducible protein expression system based on the protozoan host *Leishmania tarentolae*. *Protein Expr Purif*. 2005;42:37–46.
- Breitling R, Klingner S, Callewaert N, Pietrucha R, Geyer A, Ehrlich G, et al. Non-pathogenic trypanosomatid protozoa as a platform for protein expression and production. *Protein Expr Purif*. 2002;25:209–18.
- Mamat U, Wilke K, Bramhill D, Schromm AB, Lindner B, Kohl TA, et al. Detoxifying *Escherichia coli* for endotoxin-free production of recombinant proteins. *Microb Cell Fact*. 2015;14:57.
- Ueda T, Akuta T, Kikuchi-Ueda T, Imaizumi K, Ono Y. Improving the soluble expression and purification of recombinant human stem cell factor (SCF) in endotoxin-free *Escherichia coli* by disulfide shuffling with persulfide. *Protein Expr Purif*. 2016;120:99–105.
- Rueda F, Cano-Garrido O, Mamat U, Wilke K, Seras-Franzoso J, Garcia-Frutos E, et al. Production of functional inclusion bodies in endotoxin-free *Escherichia coli*. *Appl Microbiol Biotechnol*. 2014;98:9229–38.
- Taguchi S, Ooi T, Mizuno K, Matsusaki H. Advances and needs for endotoxin-free production strains. *Appl Microbiol Biotechnol*. 2015;99:9349–60.
- Rader RA. (Re)defining biopharmaceutical. *Nat Biotechnol*. 2008;26:743–51.
- Walsh G. New biopharmaceuticals. *Biopharm Int*. 2012;25:34–8.
- Anonymous. Human insulin receives FDA approval. *FDA Drug Bull*. 1982;12:18–9.
- Johnson IS. Human insulin from recombinant DNA technology. *Science*. 1983;219:632–7.
- Chabner BA, Roberts TG Jr. Timeline: chemotherapy and the war on cancer. *Nat Rev Cancer*. 2005;5:65–72.
- Scott AM, Wolchok JD, Old LJ. Antibody therapy of cancer. *Nat Rev Cancer*. 2012;12:278–87.
- Patel A, Sun W. Ziv-aflibercept in metastatic colorectal cancer. *Biologics*. 2014;8:13–25.
- Manoukian G, Hagemester F. Denileukin difitox: a novel immunotoxin. *Expert Opin Biol Ther*. 2009;9:1445–51.
- Ho VT, Zahrieh D, Hochberg E, Micale E, Levin J, Reynolds C, et al. Safety and efficacy of denileukin difitox in patients with steroid-refractory acute graft-versus-host disease after allogeneic hematopoietic stem cell transplantation. *Blood*. 2004;104:1224–6.
- Lohcharoenkal W, Wang L, Chen YC, Rojanasakul Y. Protein nanoparticles as drug delivery carriers for cancer therapy. *Biomed Res Int*. 2014;2014:180549.

Submit your next manuscript to BioMed Central and we will help you at every step:

- We accept pre-submission inquiries
- Our selector tool helps you to find the most relevant journal
- We provide round the clock customer support
- Convenient online submission
- Thorough peer review
- Inclusion in PubMed and all major indexing services
- Maximum visibility for your research

Submit your manuscript at
www.biomedcentral.com/submit



ARTICLE 1

The fusogenic peptide HA2 impairs selectivity of CXCR4-targeted protein nanoparticles

Laura Sánchez-García, Naroa Serna, Matthias Mattanovich, Petra Cazzanelli, Alejandro Sanchez-Chardi, Oscar Conchillo-Sole, Fran Cortes, Xavier Daura, Ugutz Unzueta, Ramón Mangués, Antonio Villaverde and Esther Vázquez.

Chemical Communications (2017) 53 (33): 4565-4568

Impact factor 6.29 CHEMISTRY, MULTIDISCIPLINARY (28/171) Q1

Nowadays, cell-targeted delivery has raised a huge interest in the development of improved chemotherapies. Peptidic ligands are an example of efficient targeting moieties that can be genetically fused and easily produced through recombinant DNA technologies. However, the entrapment of protein therapeutics in endosomal and subsequent lysosomal compartments leads to harsh proteolysis, which has been reported to be a major reason for impairment or even loss of their efficacy. To circumvent this issue, many endosomolytic peptides have been described to induce efficient cytosolic release of their cargo protein such as hemagglutinin-2 (HA2) from influenza virus.

In this context, we have developed CXCR4-targeted protein nanoparticles (T22-GFP-H6) fused to HA2 peptide in two alternative positions (T22-HA2-GFP-H6 and T22-GFP-HA2-H6) in order to induce their efficient cytosolic release. Both constructs were produced using *E. coli* expression system and further purified and characterized. Cell penetration experiments over CXCR4⁺ cells showed an increased internalization of both HA2-bearing constructs compared to the parental T22-GFP-H6 nanoparticle. However, the improved internalization seems to be unspecific, as it cannot be inhibited by their co-incubation with AMD3100 (a competitor able to block CXCR4 receptor). Additionally, further experiments performed to assess the endosomal escape activity of HA2-containing constructs showed that only T22-GFP-HA2-H6 version was able to efficiently escape from lysosomal compartments.

Taking all this data into consideration, although the genetic incorporation of the endosomal escape peptide HA2 might seem a good alternative, it results inappropriate when working with receptor-specific targeted proteins due to its activity as cell penetrating peptide. Therefore, when choosing an efficient endosomolytic peptide, other mechanisms of action able to induce endosomal escape should be envisaged to bypass receptor specificity alterations.



Cite this: DOI: 10.1039/c6cc09900a

Received 13th December 2016,
Accepted 10th March 2017

DOI: 10.1039/c6cc09900a

rsc.li/chemcomm

The fusogenic peptide HA2 impairs selectivity of CXCR4-targeted protein nanoparticles†

L. Sánchez-García,^{‡,a,g} N. Serna,^{‡,a} M. Mattanovich,^{ab} P. Cazzanelli,^{ab}
A. Sánchez-Chardi,^c O. Conchillo-Solé,^a F. Cortés,^d X. Daura,^{ae} U. Unzueta,^{*f,g}
R. Mangues,^{f,g} A. Villaverde^{*a,g} and E. Vázquez^{a,g}

We demonstrate here that the genetic incorporation of the fusogenic peptide HA2 into a CXCR4-targeted protein nanoparticle dramatically reduces the specificity of the interaction between nanoparticles and cell receptors, a factor to be considered when designing tumour-homing drug vehicles displaying endosomal-escape agents. The loss of specificity is concomitant with enhanced cell penetrability.

Cell-targeted intracellular delivery is a major challenge in innovative medicines, which continuously explore new and more efficient vehicles for conventional and emerging drugs.¹ Targeting can be achieved by the incorporation of ligands for cell receptors into the drug vehicle, which direct specific binding and further endosomal-mediated cell uptake. This is particularly convenient when the vehicle itself is produced in a recombinant form, which allows genetic fusion and biological production of the whole polypeptide.² Unfortunately, endosomal uptake drives the engulfed material to a lysosomal pathway, resulting in acidification and proteolysis. Background endosomal leakage and endosomolytic activities naturally present in the recombinant protein allow a fraction of the complex to reach the cytoplasm. Several natural or modified peptides have been identified as strongly endosomolytic, increasing the fraction of

internalized material that escapes from lysosomal degradation. Among them, the N-terminal peptide HA2 from the influenza virus hemagglutinin has been widely explored in a diversity of protein constructs intended as nanoscale intracellular vehicles. In acidic environments, such as the endosome, the anionic amino acids of HA2 get protonated, an alpha helix is formed and the peptide acts as an amphiphilic anionic stretch that destabilizes the cell membrane.³ HA2 alone,⁴ or in combination with the TAT peptide from the human immunodeficiency virus-1,^{5,6} promotes endosomal release of fusion proteins or nanoscale constructs, which is observed as a promising activity in vehicles for gene therapy and drug delivery.

So far, the potential use of HA2 in combination with specific cell ligands for receptor-mediated cell-targeted delivery has been neglected. However, efficiently combining the selectivity with endosomal escape would represent a step ahead towards the construction of powerful vehicles for targeted drug delivery. Here we have explored this possibility by the incorporation of peptide HA2 into a CXCR4-targeted protein nanoparticle based on a modular, single chain polypeptide (T22-GFP-H6). T22-GFP-H6 self-assembles as toroid nanoparticles of 12 nm, which penetrate CXCR4⁺ cells with high selectivity, in cell culture and *in vivo*.^{7,8} The cationic peptide T22 acts as both a promoter of protein self-assembly⁹ and as a specific ligand of CXCR4,¹⁰ a chemokine receptor whose overexpression is associated with aggressiveness in several types of human cancers.¹¹ In this context, an efficient HA2 version¹² was inserted at two alternative inner positions of T22-GFP-H6 (namely at the amino terminus of the core GFP, or at its carboxy terminus) (Fig. 1A). Both engineered proteins were produced well in *E. coli*, although the lower yield of soluble T22-GFP-HA2-H6 compared to T22-HA2-GFP-H6 resulted in a higher background in mass spectrometry analysis (Fig. 1B). The purity of both products and the predicted molecular mass were however fully assessed by Western blot (Fig. 1B, inset) and using the purification chromatograms (ESI,† Fig. S1). T22-HA2-GFP-H6 and T22-GFP-HA2-H6 proteins spontaneously self-assembled as stable, supramolecular structures with a toroidal shape, with a diameter of 30 nm and 45 nm, respectively, and similar surface

^a Institut de Biotecnologia i de Biomedicina and Departament de Genètica i de Microbiologia, Universitat Autònoma de Barcelona, Bellaterra, 08193 Barcelona, Spain. E-mail: antoni.villaverde@uab.es

^b Department of Biotechnology, University of Natural Resources and Life Sciences (BOKU), Muthgasse 18, 1190 Vienna (BOKU), Austria

^c Servei de Microscòpia, Universitat Autònoma de Barcelona, Bellaterra, 08193 Barcelona, Spain

^d Servei de Cultius Cel·lulars, Producció d'Anticossos i Citometria, (SCAC), Universitat Autònoma de Barcelona, Bellaterra, 08193 Barcelona, Spain

^e Catalan Institution for Research and Advanced Studies (ICREA), 08010 Barcelona, Spain

^f Institut d'Investigacions Biomèdiques Sant Pau and Josep Carreras Research Institute, Hospital de la Santa Creu i Sant Pau, 08025 Barcelona, Spain. E-mail: uunzueta@santpau.cat

^g CIBER de Bioingeniería, Biomateriales y Nanomedicina (CIBER-BBN), Spain

† Electronic supplementary information (ESI) available. See DOI: 10.1039/c6cc09900a

‡ Equally contributed.

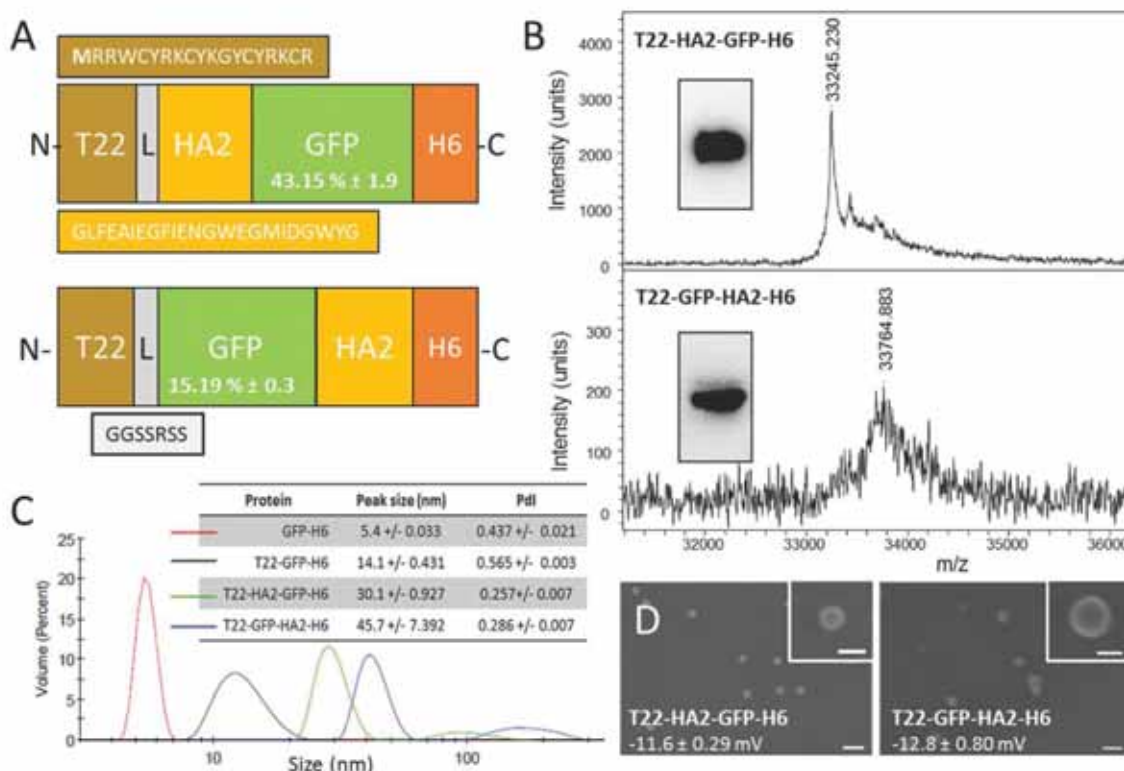


Fig. 1 Production and characterization of HA2-empowered protein nanoparticles. (A) Schematic characterization of protein constructs including a HA2 stretch.¹² The N-terminal methionine, absent in the original sequence of T22, is shown in bold. L is a ligand that offers molecular flexibility. Figures in GFP boxes represent the specific GFP fluorescence compared to the parental T22-GFP-H6. (B) Mass spectroscopy of HA2 proteins upon IMAC purification. Western blot analyses are shown in the inset. (C) DLS size analysis of the protein materials. The unassembled GFP-H6 is shown as reference. In the inset data, the peak size and the polydispersity index (Pdl) are shown. (D) FESEM observations of purified material (size bars are 100 nm, 30 nm in insets). Figures indicate surface charge. Experimental procedures are shown in full in the ESI.†

charge (Fig. 1C and D). The untagged parental GFP-H6 protein version remained unassembled (Fig. 1C). Despite their good stability, T22-GFP-HA2-H6 nanoparticles showed a tendency to form aggregates, as observed from a secondary DLS peak at around 200 nm (Fig. 1C). The insertion of the HA2 peptide rendered constructs with significantly lower fluorescence than T22-GFP-H6, especially in the case of T22-GFP-HA2-H6 (Fig. 1A), indicating a conformational impact of the viral peptide on the building block. However, specific fluorescence was in both cases high enough to monitor protein internalization in cultured CXCR4⁺ HeLa cells.

Cell penetration of both nanoparticles was monitored in the absence and in the presence of a chemical ligand of CXCR4, namely AMD3100, which inhibits binding of T22. As observed (Fig. 2A), the presence of HA2 in the particles enhanced protein penetration in comparison to T22-GFP-H6 nanoparticles, thus confirming the activity of the fusogenic peptide displayed at both accommodation sites. In T22-GFP-HA2-H6, the viral peptide was clearly superior in promoting cell penetration. Even at very low protein concentrations in which the uptake of T22-HA2-GFP-H6 was indistinguishable from that of T22-GFP-H6, its enhancing effect was perceived. Enhanced uptake was not accompanied by cell toxicity (Fig. 2A, inset), an issue that was a

matter of concern because of the hemolytic activities of HA2. These effects were mainly observed in HA2 peptide versions with a free amino terminus,^{12–14} which in the current construct is blocked by T22. On the other hand, the display of HA2 dramatically reduced the specificity of CXCR4-dependent penetration. While AMD3100 inhibited the uptake of T22-GFP-H6 by around 70% it only reduced the penetration of T22-GFP-HA2-H6 by 30% and no inhibition was observed in the case of T22-HA2-GFP-H6 (Fig. 2B). This last protein appears to be internalized in a completely unspecific way (Fig. 2B).

The higher penetrability of HA2-containing nanoparticles respective to the parental T22-GFP-H6 oligomers (Fig. 2A) was supposed to be linked to the enhanced endosomal escape mediated by HA2. To assess this issue, we analyzed the uptake of the HA2-empowered constructs in the presence of chloroquine that inhibits acidification and subsequent lysosomal degradation of the internalized material. This drug equally enhanced the intracellular fluorescence of cells exposed to T22-GFP-H6 and to T22-HA2-GFP-H6 by about 30 fold (Fig. 2C). This indicates that HA2 in T22-HA2-GFP-H6 does not stimulate full endosomal escape of the particles in comparison to the parental T22-GFP-H6. In contrast, chloroquine had much milder enhancing effects on T22-GFP-HA2-H6 (only five-fold increase,

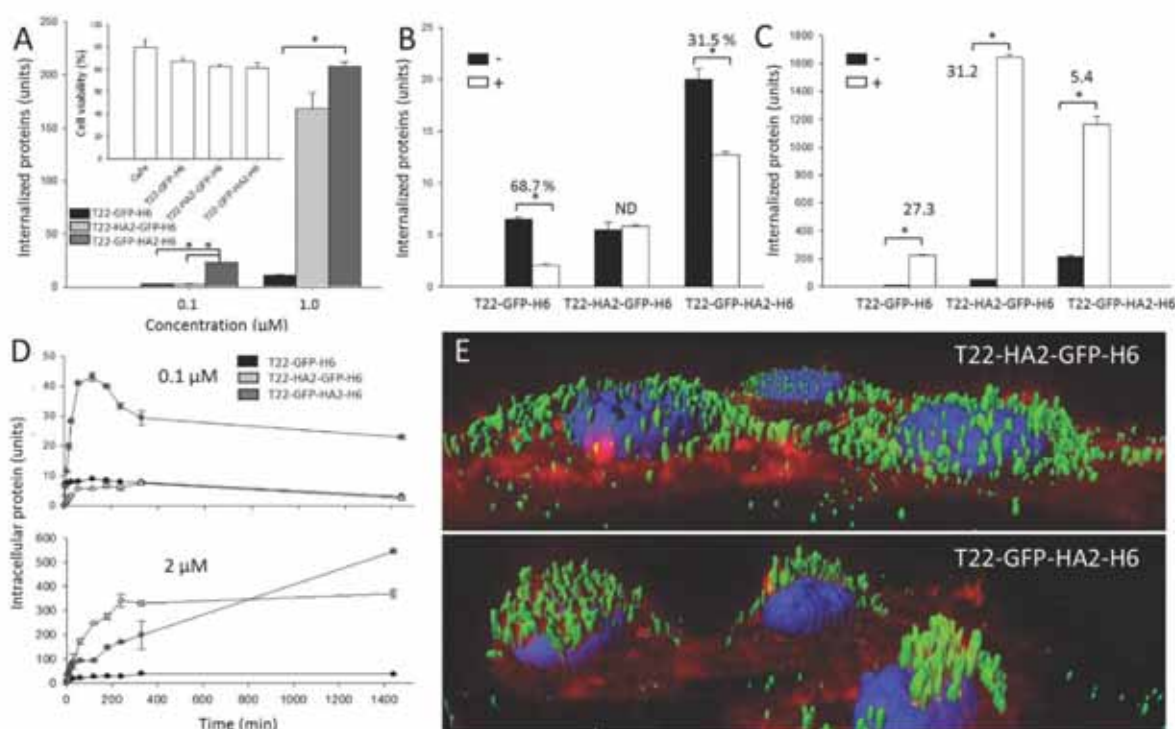


Fig. 2 Functional characterization of HA2-containing nanoparticles. (A) Internalization of T22-GFP-H6 and their HA2-containing derivatives in cultured CXCR4⁺ HeLa cells, after 24 h exposure. Crude fluorescence values were normalized by the specific fluorescence emission of each protein (units) to allow mass-based comparison. In the inset, HeLa cell viability after exposure to 2 μ M of modular proteins for 48 h. (B) Analysis of specific CXCR4-mediated internalization in the absence (–) and in the presence (+) of the CXCR4 ligand AMD3100. Data refer to 1 h after exposure. % of inhibition is indicated in each case, ND means not determinable, as the % was 0. (C) Accumulation of HA2-containing nanoparticles in cultured HeLa cells exposed to 1 μ M of protein during 24 h in the absence (–) or presence (+) of chloroquine. (D) Intracellular accumulation of proteins, added to two alternative concentrations, in exposed CXCR4⁺ HeLa cells. Data are presented as arithmetic mean \pm standard deviation from two independent experiments. (E) Isosurface representation of HeLa cells within a 3D volumetric z axes stack after incubation for 24 h with nanoparticles (at 0.5 μ M). The cell membrane was labeled with CellMask (red signal), cell DNA was labeled with Hoescht 33342 (blue signal) and proteins naturally produced a green signal.

Fig. 2C), proving that the viral peptide shows endosomolytic properties in this construct. In this regard, both HA2-displaying nanoparticles are degraded in cells (Fig. 2D) when added to cell cultures at a concentration of 0.1 μ M, a dose that has been described below the threshold supporting the endosomolytic properties of HA2.¹² However, at 2 μ M, over such a transition value, T22-GFP-HA2-H6 but not T22-HA2-GFP-H6 keeps accumulating in cells during prolonged exposure (Fig. 2D). This is again in the line that this protein, but not the related T22-HA2-GFP-H6 (or in a much more moderate way), is able to escape from lysosomal degradation. The enhanced perinuclear accumulation of T22-GFP-HA2-H6 (Fig. 2E) fully supports this hypothesis.

HA2 destabilizes lipid cell membranes at pH 5–5.5.¹⁵ However, viral strains with HA2 variants show the ability to replicate in target cells at higher pH values.^{16–18} Slight variations in charge distribution at the amino terminus of hemagglutinin and in the isoelectric point of the whole protein allow the fusogenic activities of HA2 at less acidic pH. In this regard, the endosomal escape of modular constructs containing histidine-rich peptides, R9, HA2 and cherry, are disrupted by a nuclear localization signal at the carboxy terminus of HA2.¹² In the constructs generated here both accommodation sites allow a

dramatic enhancement of HA2-mediated cell penetration, although at the expense of a loss of specificity in the interaction with cells. This is particularly deleterious when HA2 is placed in close vicinity to the cationic T22 segment, since T22 is critical for protein–protein contacts.¹⁹ In this case, the construct completely missed the ability to specifically interact with CXCR4⁺ cells, and cell penetration occurs irrespective of endosomal acidification. HA2, in this position, might show enhanced membrane activities influenced by the vicinity of T22. This should produce a differential conformation in the building blocks or the whole nanoparticles already anticipated by differences in the specific fluorescence of the GFP module in both constructs (Fig. 1A). A differential conformational impact of HA2 was confirmed by temperature denaturation followed by Trp emission fluorescence and supported by the molecular modelling of both protein nanoparticles (ESI,† Fig. S2A and B), which resulted in less flexible materials in the case of T22-GFP-HA2-H6. Altogether, while HA2 generically appears as highly appealing for enhancing the integrity of protein-based nanoscale vehicles upon internalization it seems to be poorly appropriate when the efficiency of constructs is based on specific interactions with cell-surface receptors, which might be partially or totally abolished by the viral segment.

The insertion of HA2 in two alternative positions of the tumor-homing nanoparticle T22-GFP-H6 results in a dramatic enhancement of cell penetrability. In the case of T22-GFP-HA2-H6, this is executed through endosomolytic activities and linked to a mild but significant affectation of particle-cell specific interaction. However, regarding T22-HA2-GFP-H6, specificity is completely lost and cell penetration is enhanced in the absence of endosomolytic activity. Taken together, these data indicate that in T22-HA2-GFP-H6, the viral peptide HA2 acts as a cell penetrating peptide rather than as an endosomal escape agent, since it stimulates the penetration of the nanoparticle in a receptor-independent way, probably at the cell surface or at very early endosomal stages. Among the diversity of functional nanoparticles for drug delivery based on biocompatible materials,²⁰ protein nanoparticles offer an unusual structural versatility that allows the precise exploration of functional modular combinations by conventional genetic engineering.

We thank MINECO (BIO2013-41019-P), AGAUR (2014SGR-132) and CIBER de Bioingeniería, Biomateriales y Nanomedicina (project NANOPROTHER) to AV, Marató deTV3 foundation (TV32013-3930) and ISCIII (PI15/00272, co-founding FEDER) to EV and ISCIII (PI15/00378 and PIE15/00028, co-founding FEDER), Marató TV3 (2013-2030) and AGAUR (2014-PROD0005) to RM, for funding our research. Protein production has been partially performed by the ICTS "NANBIOSIS", more specifically by the Protein Production Platform of CIBER-BBN/IBB (<http://www.nanbiosis.es/unit/u1-protein-production-platform-ppp/>). PC and MM thank the Erasmus+ for the financial support during this project. LSG was supported by AGAUR (2016FI_B 00034),

UU received a Sara Borrell postdoctoral fellowship from ISCIII and AV an ICREA ACADEMIA.

References

- 1 R. Duncan and R. Gaspar, *Mol. Pharmaceutics*, 2011, **8**, 2101–2141.
- 2 E. Vazquez, R. Mangues and A. Villaverde, *Nanomedicine*, 2016, **11**, 1333–1336.
- 3 M. Murata, S. Takahashi, S. Kagiwada, A. Suzuki and S. Ohnishi, *Biochemistry*, 1992, **31**, 1986–1992.
- 4 E. Wagner, C. Plank, K. Zatloukal, M. Cotten and M. L. Birnstiel, *Proc. Natl. Acad. Sci. U. S. A.*, 1992, **89**, 7934–7938.
- 5 S. F. Ye, M. M. Tian, T. X. Wang, L. Ren, D. Wang, L. H. Shen and T. Shang, *Nanomedicine*, 2012, **8**, 833–841.
- 6 J. S. Wadia, R. V. Stan and S. F. Dowdy, *Nat. Med.*, 2004, **10**, 310–315.
- 7 M. V. Cespedes, *et al.*, *ACS Nano*, 2014, **8**, 4166–4176.
- 8 M. V. Cespedes, *et al.*, *Nanomedicine*, 2016, **12**, 1987–1996.
- 9 U. Unzueta, *et al.*, *Biomaterials*, 2012, **33**, 8714–8722.
- 10 U. Unzueta, M. V. Cespedes, N. Ferrer-Miralles, I. Casanova, J. Cedano, J. L. Corchero, J. Domingo-Espin, A. Villaverde, R. Mangues and E. Vazquez, *Int. J. Nanomed.*, 2012, **7**, 4533–4544.
- 11 F. Balkwill, *Nat. Rev. Cancer*, 2004, **4**, 540–550.
- 12 J. S. Liou, B. R. Liu, A. L. Martin, Y. W. Huang, H. J. Chiang and H. J. Lee, *Peptides*, 2012, **37**, 273–284.
- 13 I. Neundorff, R. Rennert, J. Hoyer, F. Schramm, K. Lobner, I. Kitanovic and S. Wolf, *Pharmaceuticals*, 2009, **2**, 49–65.
- 14 T. Sugita, T. Yoshikawa, Y. Mukai, N. Yamanada, S. Imai, K. Nagano, Y. Yoshida, H. Shibata, Y. Yoshioka, S. Nakagawa, H. Kamada, S. I. Tsunoda and Y. Tsutsumi, *Br. J. Pharmacol.*, 2008, **153**, 1143–1152.
- 15 J. J. Skehel, K. Cross, D. Steinhauer and D. C. Wiley, *Biochem. Soc. Trans.*, 2001, **29**, 623–626.
- 16 R. S. Daniels, J. C. Downie, A. J. Hay, M. Knossow, J. J. Skehel, M. L. Wang and D. C. Wiley, *Cell*, 1985, **40**, 431–439.
- 17 C. Scholtissek, *Vaccine*, 1985, **3**, 215–218.
- 18 E. E. Ooi, J. S. Chew, J. P. Loh and R. C. Chua, *Virology*, 2006, **3**, 39.
- 19 F. Rueda, *et al.*, *Adv. Mater.*, 2015, **27**, 7816–7822.
- 20 N. Kamaly, B. Yameen, J. Wu and O. C. Farokhzad, *Chem. Rev.*, 2016, **116**, 2602–2663.

The fusogenic peptide HA2 from influenza virus hemagglutinin-2 impairs selectivity of CXCR4-targeted protein nanoparticles

L. Sánchez-García ^{a†}, N. Serna ^{a†}, M. Mattanovich ^{a,b}, P. Cazzanelli ^{a,b}, A. Sánchez-Chardi ^c, O. Conchillo-Solé ^a, F. Cortés ^d, X. Daura ^{a,e}, U. Unzueta ^{f,g,‡}, R. Mangués ^{f,g}, A. Villaverde ^{a,g,‡}, E. Vázquez ^{a,g}

^a *Institut de Biotecnologia i de Biomedicina and Departament de Genètica i de Microbiologia, Universitat Autònoma de Barcelona, Bellaterra, 08193 Barcelona, Spain*

^b *Department of Biotechnology, University of Natural Resources and Life Sciences (BOKU), Muthgasse 18, 1190 Vienna, Austria*

^c *Servei de Microscòpia, Universitat Autònoma de Barcelona, Bellaterra, 08193 Barcelona, Spain*

^d *Servei de Cultius Cel·lulars, Producció d'Anticossos i Citometria, (SCAC), Universitat Autònoma de Barcelona, Bellaterra, 08193 Barcelona, Spain*

^e *Catalan Institution for Research and Advanced Studies (ICREA), 08010 Barcelona, Spain*

^f *Institut d'Investigacions Biomèdiques Sant Pau and Josep Carreras Research Institute, Hospital de la Santa Creu i Sant Pau, 08025 Barcelona, Spain.*

^g *CIBER de Bioingeniería, Biomateriales y Nanomedicina (CIBER-BBN), Spain.*

† Equally contributed.

‡ Corresponding authors.

Experimental procedures

Protein design, production and purification

The pET22b-derivatives encoding proteins T22-HA2-GFP-H6 and T22-GFP-HA2-H6 were designed in house and produced by GeneArt. These plasmids were transformed into the *Escherichia coli* Origami B strain (BL21, OmpT⁻, Lon⁻, TrxB⁻, Gor⁻; Novagen) by conventional heat-shock procedures as described¹. Cells were cultured in Lysogenic Broth (LB) medium² and the gene expression was induced at an OD of ~0.5 by the addition of 0.1 mM and 0.01 mM isopropyl- β -thiogalactopyronaside (IPTG) respectively. Cells were harvested after subsequent overnight culture at 16°C (T22-HA2-GFP-H6) or 20°C (T22-GFP-HA2-H6). After centrifugation at 5,000 g (4 °C, 15 min), the cell pellet was resuspended in Tris buffer (Tris 20 mM, pH 8.0, NaCl 500 mM, imidazole 10 mM) with the addition of ethylenediamine tetra-acetic acid-free protease-inhibitor (Complete EDTA-Free, Roche, Basel, Switzerland). Cells were disrupted by 3 rounds at 1,200 psi in a French Press (Thermo FA-078A) and subsequently purified by IMAC affinity chromatography using HiTrap Chelating HP 1 mL and 5 mL columns (GE Healthcare, Piscataway, NJ, USA) in an ÄKTA purifier (GE Healthcare). The proteins were eluted by a linear gradient of elution buffer (Tris 20 mM, pH 8.0, 500 mM NaCl and 500 mM imidazole) and dialyzed against 166 mM NaHCO₃ buffer (T22-HA2-GFP-H6) or 166 mM NaHCO₃ + 333 mM NaCl buffer (T22-GFP-HA2-H6). Protein amounts were determined by Bradford's assay³.

Protein and nanoparticle characterization

Protein integrity and purity was determined by SDS-PAGE protein electrophoresis and western-blot analysis using an anti-His (Santa Cruz) mouse monoclonal primary antibody (1:500), using a secondary anti-mouse (Santa Cruz) for visualizing (1:1000). The molecular masses of T22-HA2-GFP-H6 and T22-GFP-HA2-H6 proteins were determined by MALDI-TOF mass spectrometry, while the size of the resulting nanoparticles was determined by dynamic light scattering (Zetasizer Nano ZS, Malvern Instruments Limited, Malvern, Worcestershire, UK), performed at 633 nm. Fluorescence of the nanoparticles was determined using a Cary Eclipse Fluorescence Spectrophotometer (Varian, Agilent Technologies, Santa Clara, CA, USA). The nanoparticles were excited at a wavelength of 450 nm and detected at 510 nm.

Field emission scanning electron microscopy (FESEM)

To evaluate the native ultrastructure of the nanoparticles, drops of 3 μ l of each sample were directly deposited on conductive silicon wafers (Ted Pella Inc., Reading, CA, USA) for 1 min, cleared for a few

seconds in deionized water, excess blotted with Whatman filter paper number 1 (GE Healthcare), air dried, and finally observed without coating in a FESEM Merlin (Zeiss, Oberkochen, Germany) operating at 1 kV. Images were acquired with a high resolution in-lens secondary electron detector.

Cell culture

CXCR4⁺ HeLa cells were cultivated in MEM Alpha (Minimum Essential Medium α , Gibco, Rockville, MD, USA) supplemented with 10 % fetal calf serum (Gibco) at 37 °C and 5 % CO₂ in a humidified atmosphere. The media was exchanged for serum-free Optipro medium (Gibco) prior to the addition of nanoparticles. Internalization was analysed by detaching the cells with 1 mg/mL trypsin (for 15 min). This harsh proteolytic treatment has been specifically designed to remove externally attached protein ⁴. Fluorescence emission was determined by a 488 nm laser in a FACS-Canto system (Becton Dickinson, Franklin Lakes, NJ, USA) with a detector D (530/30 nm band pass filter).

For the internalization assay, cells were incubated for 24 h in Optipro medium containing 0.1 μ M and 2 μ M of protein nanoparticles. The uptake kinetics were recorded by exposing the cells to nanoparticles for 5 min, 10 min, 20 min, 30 min, 1 h, 2 h, 3 h, 4 h, 5.5 h and 24 h prior to fluorescence measurement. Fluorescence data recorded by cytometry was corrected by the specific fluorescence of the protein, previously determined by fluorescence spectrophotometry, to render comparative units in terms of protein amount.

In competition assays, cells were incubated with protein nanoparticles in Optipro medium in presence of the specific ligand of CXCR4, AMD3100 (octahydrochloride hydrate). This drug was used at 1 μ M and added 1 h before protein exposure (at 0.1 μ M). For the determination of endosomal escape, cells were incubated in absence and in presence of 100 μ M chloroquine for 4 h before the addition of the protein (at 1 μ M).

Cell viability

Viability of HeLa cells incubated with nanoparticles was determined through a CellTiter-Glo Luminescent Cell Viability Assay (PROMEGA), as described elsewhere [2].

Fluorescence spectroscopy

Conformational variations in the tertiary structure of recombinant proteins were analysed by intrinsic Trp-fluorescence in 0.5 mg/ml protein samples. Temperature-dependent emission was monitored

every 20 °C from 20 to 100 °C at 330 nm, with an excitation wavelength of 280 nm. Scans were taken along the 290-400 nm range after 8 min of temperature equilibration. A total of ten scans were averaged in each plot.

Confocal laser scanning microscopy

For confocal analysis, HeLa cells were grown on Mat-Teck culture dishes (Mat Teck Corp., Ashland, Massachusetts, United States) and nanoparticles were added at 0.5 µM. After 24 h, nuclei were labelled with 5 µg/ml Hoechst 33342 (Molecular Probes, Eugene, Oregon, United States) and the plasma membrane was labelled with 2.5 µg/ml CellMask™ Deep Red (Molecular Probes, Invitrogen, Carlsbad, CA, USA) for 5 min in the dark. Cells were washed in PBS (Sigma-Aldrich Chemie GmbH, Steinheim, Germany). Live cells were recorded with a TCS-SP5 confocal laser scanning microscope (Leica Microsystems, Heidelberg, Germany) using a Plan Apo 63x / 1.4 (oil HC x PL APO lambda blue) objective. Hoechst 33342 DNA labels was excited with a blue diode (405 nm) and detected in the 415-460 nm range. GFP-proteins were excited with an Ar laser (488 nm) and detected in the 525-545 nm range. CellMask was excited with a HeNe laser (633 nm) and detected in the 650-775 nm range. To determine the protein localization inside the cells, stacks of 20 to 30 sections every 0.5 µm along the cell thickness were collected. The projections of the series obtained were generated with Leica LAS AF software, and three-dimensional models were generated using Imaris v. 7.2.1 software (Bitplane; Zürich, Switzerland).

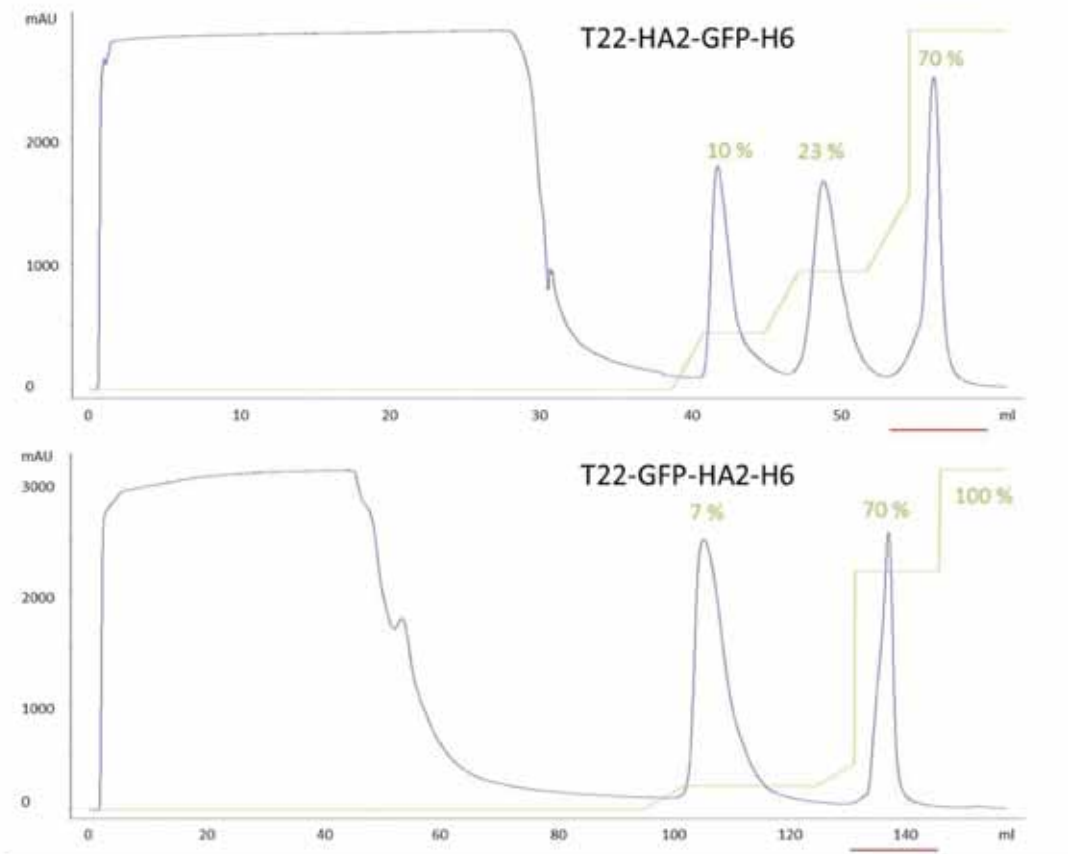
Statistical analysis

All the numerical data (mean values, standard deviations and errors) were calculated using Microsoft Office Excel 2003 (Microsoft) and visualized by Sigmaplot 10.0. One way ANOVA followed by Fisher's least significant difference (LSD) method was used for multiple comparisons. Pairwise comparisons were performed using Student-t test. Statistical differences were assumed at $p < 0.05$.

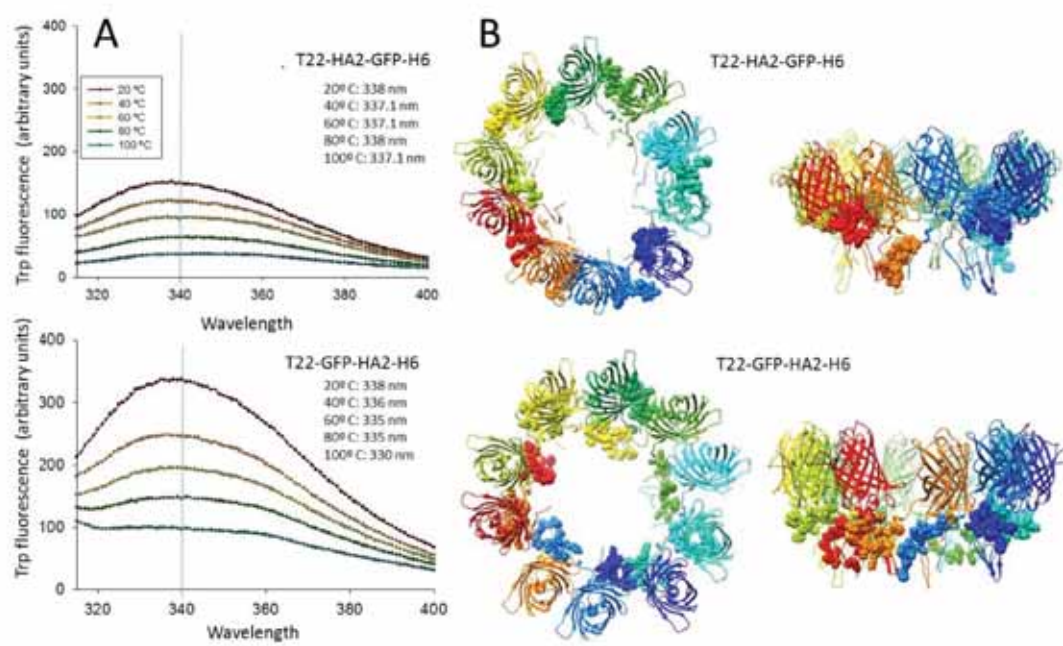
Molecular modelling

Models for T22-HA2-GFP-H6 and T22-GFP-HA2-H6 were build by homology using the Modeller software⁵. Two structures were used as templates, namely T22-GFP-H6 nanoparticles (those in the peak 2 from IMAC purification, 100 % identity,⁶) for the nanoparticle core, and the pdb code 4wa1⁷ including residues from 330 to 352 for the inserted HA2 segment (91.3 % identity). Five hundred

models were generated with very thorough VTFM optimization and MD refinement. Final models were selected based on their DOPE scores ⁸.

Supplementary Figures

Supplementary Figure 1. IMAC chromatograms of HA2-containing nanoparticles. Blue lines correspond to ultraviolet signal expressed as milliAbsorbance Units (mAU). Green lines and numbers indicate the percentage of the elution buffer. Red lines represent the protein fractions that were eluted and collected for further experiments.



Supplementary Figure 2. Conformational and structural analysis of HA2-containing protein nanoparticles. A. Analysis of the tertiary structure of T22-HA2-GFP-H6 and T22-GFP-HA2-H6 nanoparticles by Trp-fluorescence spectroscopy, recorded at different temperatures. The maximum of each spectra is indicated by a blue line. The blueshift from 340 nm to 330 nm shown by T22-GFP-HA2-H6 upon temperature increase (but not by T22-HA2-GFP-H6) indicates a comparatively higher level of compactness of the material. B. Models of T22-HA2-GFP-H6 and T22-GFP-HA2-H6. Nanoparticles in which each monomer is different colored. All atoms in the HA2 segment are represented as spheres while the rest of the protein is shown as ribbons.

References

1. E. F. F. J. Sambrook, T. Maniatis, *Molecular cloning : a laboratory manual* Cold Spring Harbor, N.Y. : Cold Spring Harbor Laboratory Press, 1989.
2. G. Bertani, *Journal of bacteriology*, 2004, **186**, 595-600.
3. M. M. Bradford, *Analytical biochemistry*, 1976, **72**, 248-254.
4. E. Vazquez, N. Ferrer-Miralles and A. Villaverde, *Drug discovery today*, 2008, **13**, 1067-1074.
5. B. Webb and A. Sali, *Current protocols in protein science*, 2016, **86**, 2 9 1-2 9 37.
6. F. Rueda, M. V. Cespedes, O. Conchillo-Sole, A. Sanchez-Chardi, J. Seras-Franzoso, R. Cubarsi, A. Gallardo, M. Pesarrodonna, N. Ferrer-Miralles, X. Daura, E. Vazquez, E. Garcia-Fruitos, R. Mangues, U. Unzueta and A. Villaverde, *Advanced materials*, 2015, **27**, 7816-7822.
7. H. Yang, H. T. Nguyen, P. J. Carney, Z. Guo, J. C. Chang, J. Jones, C. T. Davis, J. M. Villanueva, L. V. Gubareva and J. Stevens, *Journal of virology*, 2015, **89**, 2801-2812.
8. M. Y. Shen and A. Sali, *Protein Sci*, 2006, **15**, 2507-2524.

ARTICLE 2

Self-assembling toxin-based nanoparticles as self-delivered antitumoral drugs

Laura Sánchez-García, Naroa Serna, Patricia Álamo, Rita Sala, María Virtudes
Céspedes, Mònica Roldan, Alejandro Sánchez-Chardi, Ugutz Unzueta, Isolda Casanova,
Ramón Mangués, Esther Vázquez and Antonio Villaverde

Journal of Controlled Release (2018) 274: 81-92

Impact factor 7.877 PHARMACOLOGY & PHARMACY (9/261) D1

Nanoparticle-carried (loaded) cytotoxic drugs are considered promising candidates as they can be widely applied in nanomedicine. However, loading capacity and drug leakage are two main concerns when generating actively targeted cytotoxic nanoparticles that circulate in the blood stream towards its target tissue. For this reason, current trends are focused on the development of self-delivered cytotoxic nanoparticles devoid of any heterologous vehicles, what has been so far an unreached although appealing concept.

In this regard, we worked with two toxic proteins, which are modified versions of diphtheria toxin (from *Corynebacterium diphtheriae*) and exotoxin A (from *Pseudomonas aeruginosa*). These two polypeptides have been engineered for the development of self-delivered, self-assembled and intrinsically cytotoxic nanoparticles devoid of any heterologous carrier. Additionally, they have been fused to the ligand T22 for their specific uptake into CXCR4⁺cancer stem cells. In vivo experiments performed in a colorectal cancer xenograft mouse model, revealed that after systemic administration both therapeutic nanoparticles cause a potent and localized destruction of tumour tissue, followed by tumour reduction. Therefore, the obtained results suggest the adequacy of developing targeted protein-based drugs which act not only as cytotoxic compounds but also as self-assembled and self-delivered entities.

In conclusion, collected data prove that the functional recruitment of modular recombinant proteins and their single-step production through recombinant DNA technologies is a promising alternative for the development of improved inherently cytotoxic molecules devoid of any inactive heterologous carrier.



Contents lists available at ScienceDirect

Journal of Controlled Release

journal homepage: www.elsevier.com/locate/jconrel

Self-assembling toxin-based nanoparticles as self-delivered antitumoral drugs

Laura Sánchez-García^{a,b,c,1}, Naroa Serna^{a,b,c,1}, Patricia Álamo^{c,d,e}, Rita Sala^{c,d},
María Virtudes Céspedes^{c,d}, Mònica Roldan^f, Alejandro Sánchez-Chardi^g, Ugutz Unzueta^{c,d},
Isolda Casanova^{c,d,e}, Ramón Mangues^{c,d,e,*}, Esther Vázquez^{a,b,c}, Antonio Villaverde^{a,b,c,*}

^a Institut de Biotecnologia i de Biomedicina, Universitat Autònoma de Barcelona, Bellaterra, 08193 Barcelona, Spain

^b Departament de Genètica i de Microbiologia, Universitat Autònoma de Barcelona, Bellaterra, 08193 Barcelona, Spain

^c CIBER de Bioingeniería, Biomateriales y Nanomedicina (CIBER-BBN), Spain

^d Institut d'Investigacions Biomèdiques Sant Pau, Hospital de la Santa Creu i Sant Pau, 08025 Barcelona, Spain

^e Josep Carreras Research Institute, Hospital de la Santa Creu i Sant Pau, Barcelona, Spain

^f Unitat de Microscòpia Confocal, Servei d'Anatomia Patològica, Institut Pediàtric de Malalties Rares (IPER), Hospital Sant Joan de Déu, Edifici Consultes Externes, Passeig Sant Joan de Déu, 2, Planta 0, 08950, Esplugues de Llobregat, Barcelona, Spain

^g Servei de Microscòpia, Universitat Autònoma de Barcelona, Bellaterra, 08193 Barcelona, Spain

ARTICLE INFO

Keywords:

Protein materials
Nanoparticles
Drug delivery
Cell-targeting
Recombinant proteins

ABSTRACT

Loading capacity and drug leakage from vehicles during circulation in blood is a major concern when developing nanoparticle-based cell-targeted cytotoxics. To circumvent this potential issue it would be convenient the engineering of drugs as self-delivered nanoscale entities, devoid of any heterologous carriers. In this context, we have here engineered potent protein toxins, namely segments of the diphtheria toxin and the *Pseudomonas aeruginosa* exotoxin as self-assembling, self-delivered therapeutic materials targeted to CXCR4⁺ cancer stem cells. The systemic administration of both nanostructured drugs in a colorectal cancer xenograft mouse model promotes efficient and specific local destruction of target tumor tissues and a significant reduction of the tumor volume. This observation strongly supports the concept of intrinsically functional protein nanoparticles, which having a dual role as drug and carrier, are designed to be administered without the assistance of heterologous vehicles.

1. Introduction

Natural protein toxins are produced by different species of unicellular and pluricellular organisms and are extremely potent functional molecules [1]. Toxins occur alone or as venom components with roles in predation and defense or during tissue colonization in bacterial infections and show a wide spectrum of mechanisms of action that target vital physiological processes. The biological properties of protein toxins can be exploited in a therapeutic context, because they are usually preserved in versions produced by recombinant DNA technologies. This fact allows the industry-oriented, large-scale bioproduction and further formulation of protein toxins as medicines. A few toxin-based drugs have been already approved for use in humans by the medicament agencies, including Captopril for hypertension, Prialt for chronic pain, Integrilin for coronary angioplasty, Byetta for type 2 diabetes, Botox for neuromuscular disorders and Contulakin-G as an analgesic [2–6]. Many

others are currently under development or in clinical trials [7–9]. A major therapeutic value of toxins relies on their ability to kill exposed cells through molecular events that are devoid, in general, of cell type specificity. The high potency exhibited by some toxins enables toxin-mediated cell killing to be explored in oncology to replace or complement conventional chemotherapies [10,11]. However, not only efficient but selective cell killing should be envisaged when developing antitumoral drugs, to minimize the undesired adverse effects and potentially severe toxicity associated to conventional chemotherapies. As an example, in the drug Denileukin difitox, cell targeting is provided by the human interleukin-2. Fused to the fragments A and B of the *Corynebacterium diphtheriae* exotoxin (diphtheria toxin), this cytokine allows binding of the whole fusion to the IL-2 receptor, overexpressed in cutaneous T cell lymphoma cells. Ideally, toxins for use in oncology should be targeted by highly specific ligands of tumoral surface markers [12–15] and administered in stable formulations ensuring

* Corresponding authors.

E-mail addresses: rmangues@santpau.cat (R. Mangues), anton.villaverde@uah.es (A. Villaverde).

¹ Equally contributed.

bioavailability and minimizing renal filtration. This would be achieved by presenting them in sizes over the renal clearance threshold (~8 nm), through the use of nanoscale carriers. Regarding the extremely high potency of toxins, possible drug leakage from the vehicle during blood circulation represents an important risk that limits the development of toxin-based nanoconjugates. In addition, the intrinsic potential toxicity of the nanoparticle used as carrier, is a matter of additional concern at both individual and environmental levels [16,17]. In this regard, the current trends towards developing self-delivery nanoscale drugs devoid of heterologous vehicles [18] might potentially expand the fields or applicability of toxins and other cytotoxic protein drugs in safer ways. However, the first prototypes in this line have resulted in very complex combinations of different types of molecules, that devoid of true nanoscale vehicles, require instead the assistance of accompanying molecular systems to provide the required functions. For instance, self-assembling therapeutic siRNA has been combined with polymeric metformin, condensed with hyaluronic acid and the nanoparticles covered with 1,2-dioleoyl-3-trimethylammonium-propane chloride and cholesterol and functionalized with a sigma receptor ligand [19]. As another recent example, the anticancer agent epigallocatechin gallate was induced to self-assemble in combination with the antitumoral proteins herceptin or interferon alpha-2a (IFN- α 2a), followed by coating with polyethylene glycol [20].

In contrast to the chemical heterogeneity of these constructs, that are observed as representative of vehicle-free nanomedicines [18], the emerging concept of self-delivered nanoscale drugs could be fully achieved by functional recruitment in single molecular species that such as proteins, can oligomerize as chemically homogeneous nanoscale entities with predefined properties [21]. Importantly, nanoscale size in drug formulations is of high clinical relevance as cell penetrability and drug stability are favoured, the enhanced permeability and retention (EPR) effect stimulated and renal clearance largely minimized [18,22]. Recently [23], we have proposed a biological principle to promote self-assembling of fusion proteins as stable protein-only nanoparticles using cationic end-terminal tags. In addition, we have proved that short protein segments, such as pro-apoptotic or antimicrobial peptides, might retain their therapeutic potential when fused to carrier proteins such as GFP and once organized in oligomers [24]. Then, a protein toxin might be genetically instructed, by the addition of architectonic and cell targeting tags, to self-assemble into stable nanoparticles acting as intrinsically functional, cell-targeted protein materials with self-delivery properties. In this context, we have here engineered two potent toxins as CXCR4-targeted self-assembling nanoparticles for the systemic treatment of CXCR4⁺ colorectal cancer. These proteins are the active fragments of the diphtheria toxin and of the *Pseudomonas aeruginosa* exotoxin, that perform ADP-ribosylation of the elongation factor 2 (EF-2), resulting in the irreversible inhibition of protein synthesis and cell death [25,26]. In addition, we designed these drug biomaterials to proteolytically discharge the targeting agent and other non-relevant protein segments upon cell internalization, for the cytotoxic activity being solely executed by the precise protein drug domain.

2. Materials and methods

2.1. Protein design, production, purification and characterization

Synthetic genes encoding the self-assembling modular proteins T22-DITOX-H6 and T22-PE24-H6 respectively were designed in-house (Fig. 1A) and provided by Genentech (ThermoFisher). DITOX contains the translocation and catalytic domains of the diphtheria toxin from *Corynebacterium diphtheriae*. PE24 is based in the de-immunized catalytic domain of *Pseudomonas aeruginosa* exotoxin A in which point mutations that disrupt B and T cell epitopes have been incorporated. Moreover, it has been added a KDEL sequence in the C-terminus of T22-PE24-H6, which enables the binding to KDEL receptors more efficiently at the

Golgi apparatus during subsequent intracellular trafficking [27]. Furin-cleavage sites were inserted between the CXCR4 ligand T22 and the functional toxin (Fig. 1A) to release the amino terminal peptide once internalized into target cells. This has been designed so as the natural version of both toxins act with free amino termini [26,28], and the recombinant versions proved to be active also show this terminal end in absence of additional peptide segments [29,30]. Both gene fusions were inserted into the plasmid pET22b, and the recombinant versions of the vector were transformed by heat shock in *Escherichia coli* Origami B (BL21, OmpT⁻, Lon⁻, TrxB⁻, Gor⁻, Novagen, Darmstadt, Germany). Transformed cells were grown at 37 °C overnight in LB medium supplemented with 100 μ g/ml ampicillin, 12.5 μ g/ml tetracycline and 15 μ g/ml kanamycin. The encoded proteins were produced at 20 °C overnight upon addition of 0.1 and 1 mM IPTG (isopropyl- β -D-thiogalactopyranoside) for T22-DITOX-H6 and T22-PE24-H6 respectively, when the OD₅₅₀ of the cell culture reached around 0.5–0.7. Bacterial cells were centrifuged during 15 min (5000g at 4 °C) and kept at -80 °C until use. Pellets were thaw and resuspended in Wash buffer (20 mM Tris-HCl pH 8.0, 500 mM NaCl, 10 mM imidazole) in presence of protease inhibitors (Complete EDTA-Free, Roche Diagnostics, Indianapolis, IN, USA). Cell disruption was performed by French Press (Thermo FA-078A) at 1200 psi. The lysates were then centrifuged for 45 min (15,000g at 4 °C), and the soluble fraction was filtered using a pore diameter of 0.2 μ m.

Proteins were then purified through the His-tag by Immobilized Metal Affinity Chromatography (IMAC) using a HiTrap Chelating HP 1 ml column (GE Healthcare, Piscataway, NJ, USA) with an AKTA purifier FPLC (GE Healthcare). Elution was achieved using a linear gradient of Elution buffer (20 mM Tris-HCl pH 8.0, 500 mM NaCl and 500 mM imidazole). The eluted fractions were collected, dialyzed against carbonate buffer (166 mM NaCO₃H pH 8) and centrifuged for 15 min (15,000g at 4 °C) to remove insoluble aggregates. The integrity and purity of the proteins was analyzed by mass spectrometry (MALDI-TOF), SDS-PAGE and Western blotting using anti-His monoclonal antibody (Santa Cruz Biotechnology, Santa Cruz, CA, USA). Protein concentration was determined by Bradford's assay. The nomenclature used for the fusion proteins has been established according to their modular organization.

2.2. Furin cleavage design and detection

To promote the intracellular release of ligand-free toxins, two different furin cleavage sites, naturally acting in the respective toxin precursors to activate translocation, were included in T22-DITOX-H6 and T22-PE24-H6 (Fig. 1A). Efficiency of cleavage in the platform was assessed in T22-DITOX-H6, since the expected fragments should exhibit fully distinguishable molecular masses suitable for quantitative analysis. For that, HeLa cell extracts exposed to 1 μ M protein for 24 h were submitted to a Western Blot analysis. After protein incubation, cells were collected, centrifuged, suspended in DPBS and disrupted by sonication. The Western Blot bands were quantified using Image Lab Software version 5.2.1. Two additional modular proteins were also constructed in which these engineered furin cleavage sites were not included, namely T22-DITOX-H6 F⁻ and T22-PE24-H6 F⁻. Their amino acid sequence exactly matched that of the equivalent constructs T22-DITOX-H6 and T22-PE24-H6 at exception of the boldface dark blue peptide (Fig. 1A), corresponding to the protease target site. These non-cleavable constructs were used for a comparative analysis of protein cytotoxicity.

2.3. Fluorescence labelling and dynamic light scattering

T22-DITOX-H6 and T22-PE24-H6 were labelled with ATTO 488 (Sigma Aldrich, Buchs, Switzerland) to track their internalization when performing *in vitro* and *in vivo* experiments. The conjugation was performed at a molar ratio of 1:2 at room temperature in darkness. The

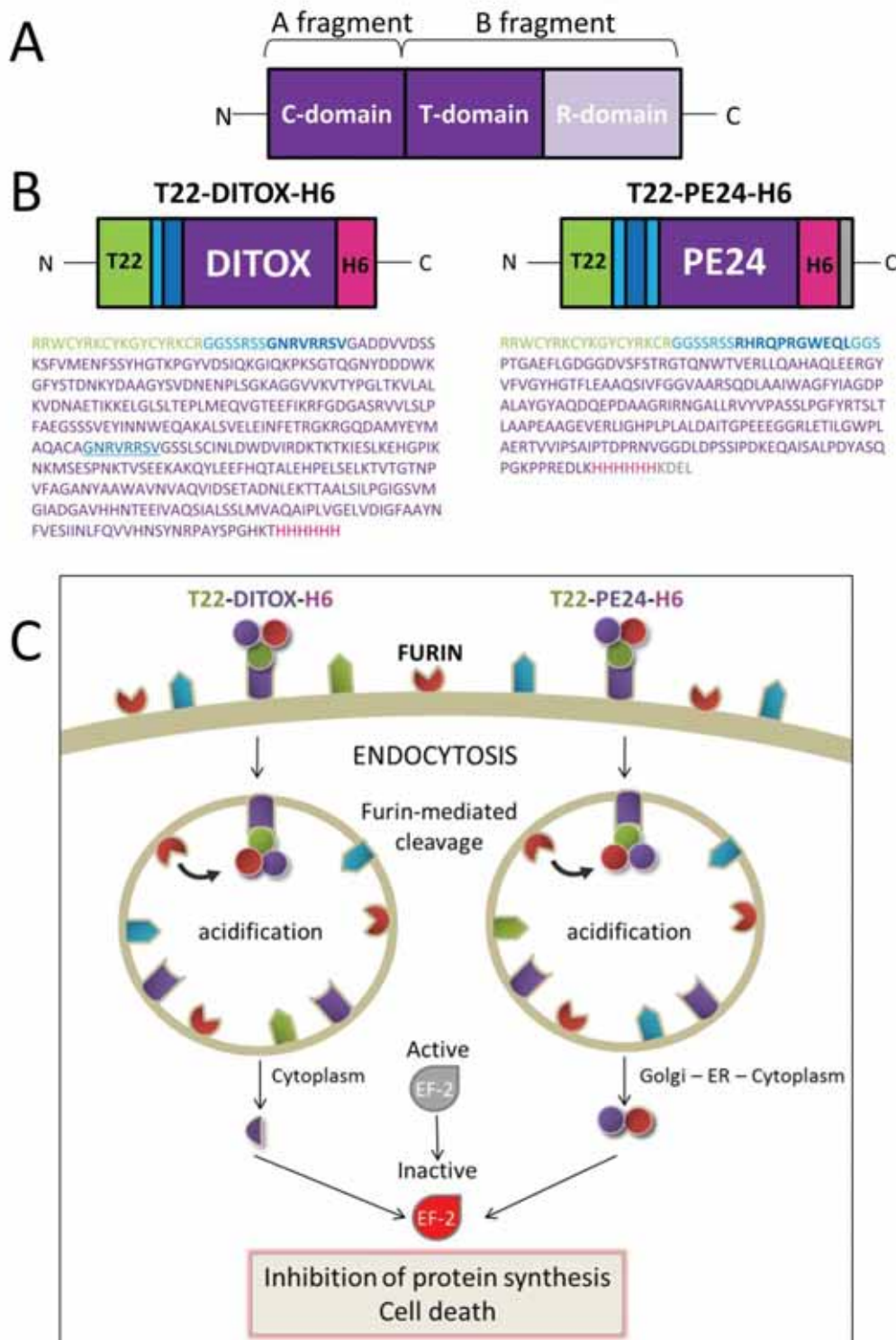


Fig. 1. A. Native structure of A-B toxins such as diphtheria toxin (*Corynebacterium diphtheriae*) or exotoxin A (*Pseudomonas aeruginosa*). The native toxin is divided in two fragments (A and B). Fragment A includes the catalytic domain (C-domain), whereas the fragment B comprises the translocation and the receptor binding domain (T- and R-domain). The selected domains for the construction of the recombinant nanoparticles are coloured in dark purple (T22-PE24-H6 construct does not include the T-domain). B. Modular organization of T22-DITOX-H6 and T22-PE24-H6, in which T22 acts as both CXCR4 ligand and as an architectonic tag. Functional segments are intersected by linker regions (light blue) and furin-cleavage sites (dark blue, boldface). A natural furin-cleavage site also occurs within DITOX (dark blue, underlined), that separates the amino terminal catalytic domain from the carboxy terminal translocation domain. A KDEL peptide has been incorporated neighboring the H6 region in T22-PE24-H6. Box sizes are only indicative. Two additional proteins, namely T22-DITOX-H6 F⁻ and T22-PE24-H6 F⁻ were constructed for comparative purposes, precisely lacking the engineered furin cleavage sites (boldface dark blue regions). C. Expected pathway for the cytotoxicity of T22-DITOX-H6 and T22-PE24-H6 nanoparticles over CXCR4⁺ target cells, upon intracellular furin-mediated release of protein domains useful for biodistribution and cell penetration steps but irrelevant for cell killing. (For interpretation of the references to color in this figure legend, the reader is referred to the web version of this article.)

reaction mixture was gently stirred every 15 min during 1 h, centrifuged for 15 min (15,000g at 4 °C) and dialyzed overnight in the original buffer (166 mM NaCO₃H pH 8) to eliminate free ATTO. Fluorescence of the nanoparticles at 0.1 mg/ml was determined by a Varian Cary Eclipse fluorescence spectrophotometer (Agilent Technologies, Mulgrave, Australia) at 523 nm using an excitation wavelength of 488 nm. For comparative analyses, the intensity of fluorescence was corrected by protein amounts to render specific emission values. Stability of dye conjugation was assessed through the incubation of T22-DITOX-H6* at a final concentration of 0.5 µg/µl in human serum (S2257-5ML, Sigma, St Louis, MO, USA) for 48 h at 37 °C, with gentle agitation. Then, the sample was dialyzed in 300 ml of carbonate buffer (166 mM NaCO₃H, pH 8) for 2 h to remove the free ATTO that might have been released from the nanoparticle. In parallel a positive control was dialyzed containing the same amount of free ATTO. The fluorescence of buffers obtained after the dialysis was measured in the fluorimeter. The volume size distribution of all nanoparticles was determined by dynamic light scattering (DLS) at 633 nm (Zetasizer Nano ZS, Malvern Instruments Limited, Malvern, Worcestershire, UK).

2.4. Ultrastructural characterization

Size and shape of T22-DITOX-H6 and T22-PE24-H6 nanoparticles at nearly native state were evaluated with a field emission scanning electron microscope (FESEM) Zeiss Merlin (Zeiss, Oberkochen, Germany) operating at 1 kV. Drops of 3 µl of each protein sample were directly deposited on silicon wafers (Ted Pella Inc., Reading, CA, USA) for 1 min, excess blotted with Whatman filter paper number 1 (GE Healthcare, Piscataway, NJ, USA), air dried, and observed without coating with a high resolution in-lens secondary electron detector. For each sample, representative images of different fields were captured at magnifications from 120,000 × to 200,000 ×.

2.5. Cell culture and flow cytometry

CXCR4⁺ cervical, colorectal and pancreatic cancer cell lines were used to study the performance of the recombinant proteins *in vitro* (HeLa ATCC-CCL-2, SW1417 ATCC-CCL-238 and Panc-1 ATCC-CCL-1469). HeLa cells were maintained in Eagle's Minimum Essential Medium (Gibco*, Rockville, MD, USA), whereas SW1417 and Panc-1 in Dulbecco's Modified Eagle's Medium (Gibco*). All of them were supplemented with 10% foetal bovine serum (Gibco*) and incubated in a humidified atmosphere at 37 °C and 5% of CO₂ (at 10% for SW1417 cells).

In order to monitor protein internalization, HeLa cells were cultured on 24-well plates at 3 · 10⁴ cells/well for 24 h until reaching 70% confluence. Proteins were incubated for 1 h at different concentrations (100, 500 and 1000 nM) in presence of OptiPRO™ SFM supplemented with L-glutamine. Additionally, specific internalization through CXCR4 receptor was proved adding a specific antagonist, AMD3100 [31,32], which is expected to inhibit the interaction with T22. This chemical inhibitor was added 1 h prior protein incubation at a ratio of 1:10. Furthermore, kinetics of the internalization was performed at a concentration of 1 µM, after different periods of incubation (0, 20, 30, 60, 120, and 240 min). After protein exposure, cells were detached using 1 mg/ml Trypsin-EDTA (Gibco*) for 15 min at 37 °C, a harsh protocol designed to remove externally attached protein [33]. The obtained samples were analyzed by a FACS-Canto system (Becton Dickinson, Franklin Lakes, NJ, USA) using a 15 mW air-cooled argon ion laser at 488 nm excitation. Experiments were performed in duplicate.

2.6. Confocal laser scanning microscopy

For confocal microscopy HeLa cells were grown on Mat-Tek plates (MatTek Corporation, Ashland, MA, USA). Upon exposure to the materials cell nuclei were labelled with 5 µg/ml Hoechst 33342

(ThermoFischer, Waltham, MA, USA) and the plasma membrane with 2.5 µg/ml CellMask™ Deep Red (ThermoFischer) for 10 min at room temperature. Cells were then washed in PBS buffer (Sigma-Aldrich, Steinheim, Germany). The confocal images of the HeLa cells were collected on an inverted TCS SP5 Leica Spectral confocal microscope (Leica Microsystems, Wetzlar, Germany) using 63 × (1.4 NA) oil immersion objective lenses. Excitation was reached via a 405 nm blue diode laser (nucleic acids), 488 nm line of an argon ion laser (nanoparticles) and 633 nm line of a HeNe laser (Cell membrane). Optimized emission detection bandwidths were configured to avoid inter-channel crosstalk and multitrack sequential acquisition setting were used. The confocal pinhole was set to 1 Airy unit and z-stacks acquisition intervals were selected to satisfy Nyquist sampling criteria. Three-dimensional images were processed using the Surpass Module in Imaris X64 v.7.2.1. software (Bitplane, Zürich, Switzerland).

2.7. Cell viability assays

The CellTiter-Glo® Luminescent Cell Viability Assay (Promega, Madison, WI, USA) was used to determine the cytotoxicity of T22-DITOX-H6, T22-PE24-H6, T22-DITOX-H6 F⁻ and T22-PE24-H6 F⁻ nanoparticles on HeLa, SW1417 CXCR4⁺ or SW1417 CXCR4⁻ cell lines. Cells were cultured in opaque-walled 96-well plates at 3500 or 6000 cells/well during 24 h at 37 °C until reaching 70% confluence. All protein incubations were performed in the corresponding medium according to the cell line used. Inhibition of cell death was analyzed by adding AMD3100, a chemical antagonist of CXCR4 [34,35], at a ratio of 1:10, 1 h prior to protein incubation. T22-GFP-H6, a non-functional T22-bearing protein [36] was also used as a competitor of T22-empowered toxins at a final concentration of 2 µM. After protein incubation, a single reagent provided by the manufacturer was added to cultured cells, which prompted lysis and generated a luminescent signal proportional to the amount of ATP present in the sample. The ATP generated is directly related to the quantity of living cells that remain in the well. Then, plates were measured in a conventional luminometer, Victor3 (Perkin Elmer, Waltham, MA, USA). Viability of Panc-1 cells, that overexpress luciferase, was determined with an alternative non fluorescence kit (EZ4U) under the same experimental conditions. The cell viability experiments were performed in triplicate.

2.8. Biodistribution, pharmacokinetics and apoptotic induction analyses in CXCR4⁺ colorectal cancer mouse model after single dose administration of nanoparticles

All *in vivo* experiments were approved by the institutional animal Ethics Committee of Hospital Sant Pau. We used 5 week-old female Swiss Nu/Nu mice, weighing 18–20 g (Charles River, L'Abresle, France), maintained in specific pathogen-free conditions. To generate the subcutaneous (SC) mouse model, we implanted subcutaneously 10 mg of the patient-derived M5 colorectal (CCR) tumor tissue from donor animals in the mouse subcutis. At day 15, when tumors reached approximately 500 mm³, mice received 50 µg single i.v. bolus of T22-DITOX-H6* (n = 3) or 300 µg single i.v. bolus of T22-PE24-H6* (n = 3) in NaCO₃H, pH = 8 buffer. Control animals received the same buffer (n = 3) or 0.25 µg of free ATTO 488 (n = 2). At 5, 24 and 48 h mice were euthanized and subcutaneous tumors and organs (brain, lung, liver, kidney and heart) were collected. Biodistribution of ATTO-labelled nanoparticles in tumor and non-tumor organs was determined by measuring the emitted fluorescence in *ex vivo* tissue sections (3 mm thick) using the IVIS® Spectrum (Perkin Elmer, Santa Clara, CA, USA) platform. The fluorescent signal (FLI), which correlates to the amount of administered protein accumulated in each tissue, was first digitalized, displayed as a pseudocolor overlay, and expressed as radiant efficiency [(p/s/cm²/sr)/µW/cm²]. The FLI values were calculated subtracting FLI signal from experimental mice by FLI auto-fluorescence of control mice. Samples were first fixed with 4% formaldehyde in PBS for

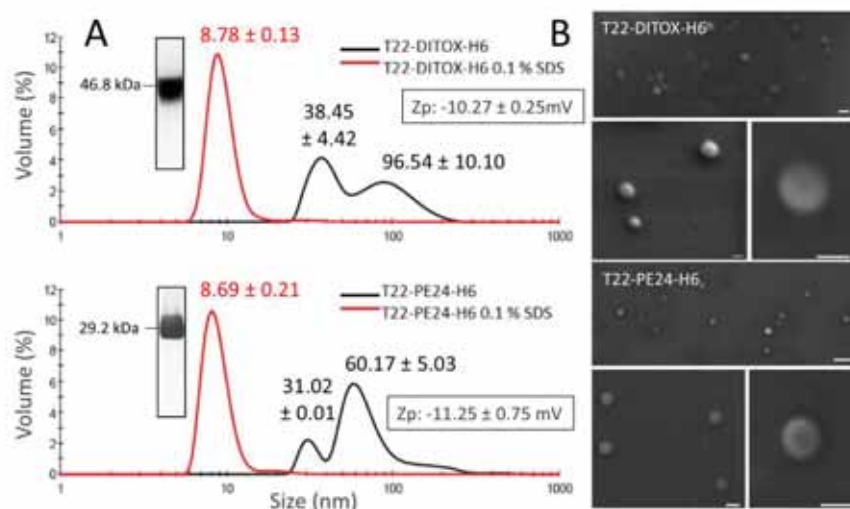


Fig. 2. Nanoarchitecture of toxin-based proteins. A. Size and SDS-mediated disassembling of T22-DITOX-H6 and T22-PE24-H6 nanoparticles determined by DLS. Values of peak sizes (mode) are indicated in bold (in nm, \pm SEM). Z-potential (Z_p) values of the nanoparticles are also indicated. The molecular mass of proteins upon purification is shown by Western Blot upon PAGE-SDS. B. FESEM examination of purified T22-DITOX-H6 and T22-PE24-H6 materials. Bars indicate 50 nm.

24 h to be embedded in paraffin for histopathological evaluation and apoptotic index analyses.

Pharmacokinetic analyses were performed after a 300 μ g single i.v. bolus administration of T22-PE24-H6* in 12 Swiss nude mice, or after a 50 μ g single bolus administration of T22-DITOX-H6* also in 12 animals. We sacrificed three mice per each time point, at 0, 1, 2, 5, 24 and 48 h after the administration and obtained approximately 1 ml of blood EDTA anticoagulated collection tubes. We measured the exact volume of plasma obtained and the fluorescent emission at each time point, and calculated the concentration of nanoparticle as referred to the fluorescence emitted and concentration of the administered dose.

Apoptotic induction analyses were performed in 4 μ m sections of tumors and normal organs (liver, lung, spleen, heart, kidney and brain) stained with hematoxylin and eosin (H&E), which were histopathologically analyzed by two independent observers. Apoptotic induction was evaluated by both, the presence of cell death bodies in H&E stained and Hoechst stained tumor slices. Triton X-100 (0.5%) permeabilized sections were then stained with Hoechst 33258 (Sigma-Aldrich) diluted, 1:5000 in PBS, for 1 h, rinsed with water, mounted and analyzed under fluorescence microscope ($\lambda_{ex} = 334$ nm/ $\lambda_{em} = 465$ nm). The number of apoptotic cell bodies was quantified by recording the number of condensed and/or defragmented nuclei per 10 high-power fields (magnification 400 \times), in blinded samples evaluated by two independent researchers, using CellAB s.

2.9. Antitumor effect in a CXCR4⁺ CRC model after nanoparticle repeated dose administration

To generate the CXCR4⁺ colorectal xenograft mouse models, we used the patient-derived M5 colorectal tumor tissue. Ten mg fragments obtained from donor animals were implanted in the subcutis of Swiss nu/nu mice to generate subcutaneous (SC) tumors as described above ($n = 9$). Once tumors reached approximately 120 mm³, mice were randomized in Control, T22-PE24-H6 and T22-DITOX-H6 groups and received intravenous doses of T22-PE24-H6 or T22-DITOX-H6, both at a repeated dose regime of 10 μ g, 3 times a week, per 8 doses. The control group received buffer using the same administration schedule. Mouse body weight was registered over the experimental period 3 times a week. Seventeen days after the initiation of nanoparticle administration, mice were euthanized and the subcutaneous tumors were taken to measure their final tumor volume and to count the number of apoptotic figures in 5 high-power fields (magnification 400 \times), of H&E stained tumor sections as described above.

2.10. Statistical analysis

The specificity of nanoparticle-promoted cell death and the pairwise data comparisons were checked with a one-way ANOVA and Tukey's tests, respectively. Pairwise divergences of internalization and cell death were evaluated using Student's *t*-tests, whereas Mann-Whitney *U* tests were used to pairwise comparisons of the number of apoptotic bodies. Differences between groups were considered significant at $p < 0.05$ and differences between relevant data are indicated by letters or as \forall for $0.01 < p < 0.05$ and \S for $p < 0.01$ in the Figures. All statistical analyses were performed using SPSS version 11.0 package (IBM, NY, USA), and values were expressed as mean \pm standard error of the mean (SEM).

3. Results

Active fragments of the diphtheria toxin (DITOX) and the *Pseudomonas aeruginosa* exotoxin (PE24) were produced in *Escherichia coli* as the modular fusion proteins T22-DITOX-H6 and T22-PE24-H6 (Fig. 1A, B), intended to induce targeted cell death through the activity of the catalytic fragments of the protein drug (Fig. 1C). The cationic peptide T22, placed at the amino terminus of the whole construct and cooperating with carboxy terminal histidines, promotes both oligomerization into regular nanoparticles [37] and binding to the cell-surface chemokine receptor CXCR4 (overexpressed in many aggressive human cancers [38–41]). In this way, it has been proved efficient in endorsing the endosomal penetration of payload GFP and IRFP into CXCR4⁺ cancer stem cells [23]. Then, T22-DITOX-H6 spontaneously self-assembled into 38 and 90 nm-nanoparticles ($P_{di} = 0.25 \pm 0.01$ nm) and T22-PE24-H6 into ~ 60 nm-nanoparticles ($P_{di} = 0.22 \pm 0.01$, Fig. 2A), always within the size range considered as optimal for efficient cell uptake [22,42,43]. A secondary population of protein material was observed in the case of T22-PE24-H6, being always minority. Nanoparticles were effectively disassembled by 0.1% SDS, resulting in monodisperse building blocks peaking at ~ 6 nm ($P_{di} = 0.60 \pm 0.01$ and 0.30 ± 0.07 respectively), compatible with the expected size of the monomeric protein. However, both protein nanoparticles were fully stable in several physiological buffers in medium term incubation and also when exposed to high salt content buffer (up to 1 M NaCl, not shown), what prompted us expecting high stability *in vivo*. In addition, nanoparticles were found stable after one-year storage at -80 $^{\circ}$ C and upon repeated cycles of freezing and thawing (not shown). The assembled proteins appeared as toroid materials (Fig. 2B), with ultrastructural morphometry (round shape and

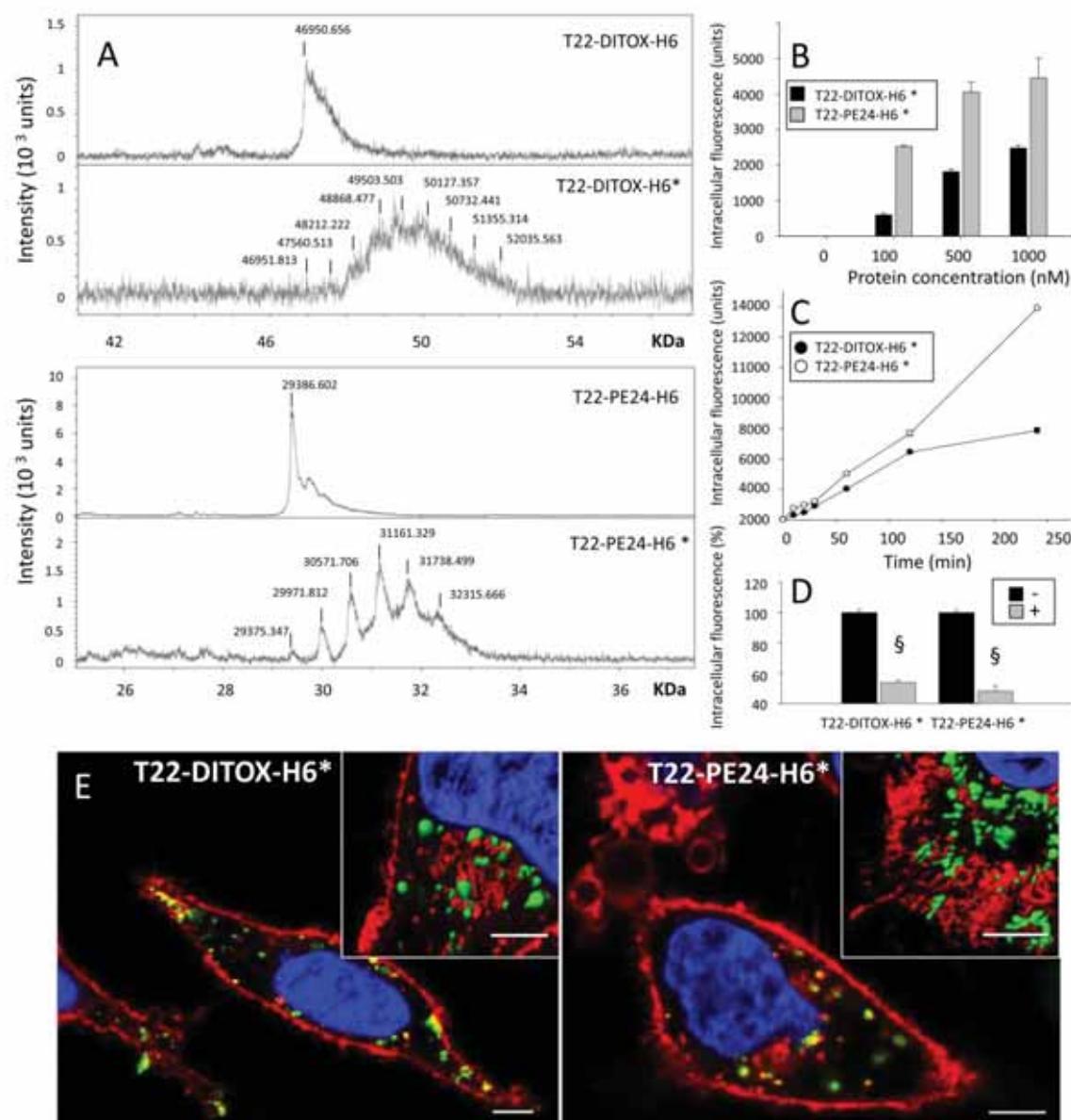


Fig. 3. Internalization of toxin-based nanoparticles in CXCR4⁺ cells. **A.** Mass spectrometry of pure unlabeled and ATTO-labelled (*) T22-DITOX-H6 and T22-PE24-H6 proteins. **B.** Dose-dependent uptake of T22-DITOX-H6* and T22-PE24-H6* nanoparticles in CXCR4⁺ HeLa cells upon 1 h of exposure. **C.** Time course kinetics of cell internalization of T22-DITOX-H6* and T22-PE24-H6* nanoparticles (1 μ M) in CXCR4⁺ HeLa cells. Note the short error bars in the plot. **D.** Protein (100 nM) uptake inhibition by the CXCR4 antagonist AMD3100 (+) upon 1 h of exposure. Significant differences between relevant data pairs are indicated as § for $p < 0.01$. All A, B and C data are presented as mean \pm SEM ($n = 2$). **E.** Confocal microscopy of HeLa cells exposed for 5 h to T22-DITOX-H6* and T22-PE24-H6* nanoparticles (1 μ M). The Cell Mask membrane staining (red) was added together with nanoparticles to observe the endosomal membrane. Nanoparticles are visualized in green and nuclear regions in blue. The yellow spots indicate merging of red and green signals. In the insets, 3D Imaris reconstructions of confocal stacks. Bars indicate 5 μ m. (For interpretation of the references to colour in this figure legend, the reader is referred to the web version of this article.)

clear size populations) that confirmed the size range observed by DLS. The same regular architecture had been previously described for the related T22-GFP-H6 construct, in which the GFP-based sub-units (with a molecular size similar to that of T22-DITOX-H6 and T22-PE24-H6) organized in toroid entities, whose organization has been modelled *in silico* [44] and confirmed by sophisticated analytical methods such as SAXS or high resolution electron microscopy imaging techniques [45].

Purified T22-DITOX-H6 and T22-PE24-H6 nanoparticles were tested for internalization into cultured CXCR4⁺ cells, upon chemically labelling with the fluorescent dye ATTO 488 (tagged with *, Fig. 3A). Both kinds of labelled nanoparticles (Fig. 3A) penetrated target HeLa cells in a dose-dependent manner (Fig. 3B) and accumulated intracellularly

with a kinetics characteristic of receptor-mediated uptake (with a faster slope in the case of T22-PE24-H6*, Fig. 3C). The CXCR4 specificity of the penetration was confirmed through its inhibition by the CXCR4 antagonist AMD3100 [34] (Fig. 3D). Internalized nanoparticles were observed as engulfed into endosomes, especially in cytoplasm areas close to the cell membrane, but they tended to be visualized as membrane-free entities when approaching the perinuclear regions (Fig. 3E), suggesting important endosomal escape. No cell-attached extracellular fluorescence was observed in any case.

Once the internalization was assessed, we tested if the furin cleavage sites introduced in the constructs to release the toxin segments from the building blocks were active in the oligomers. The expected

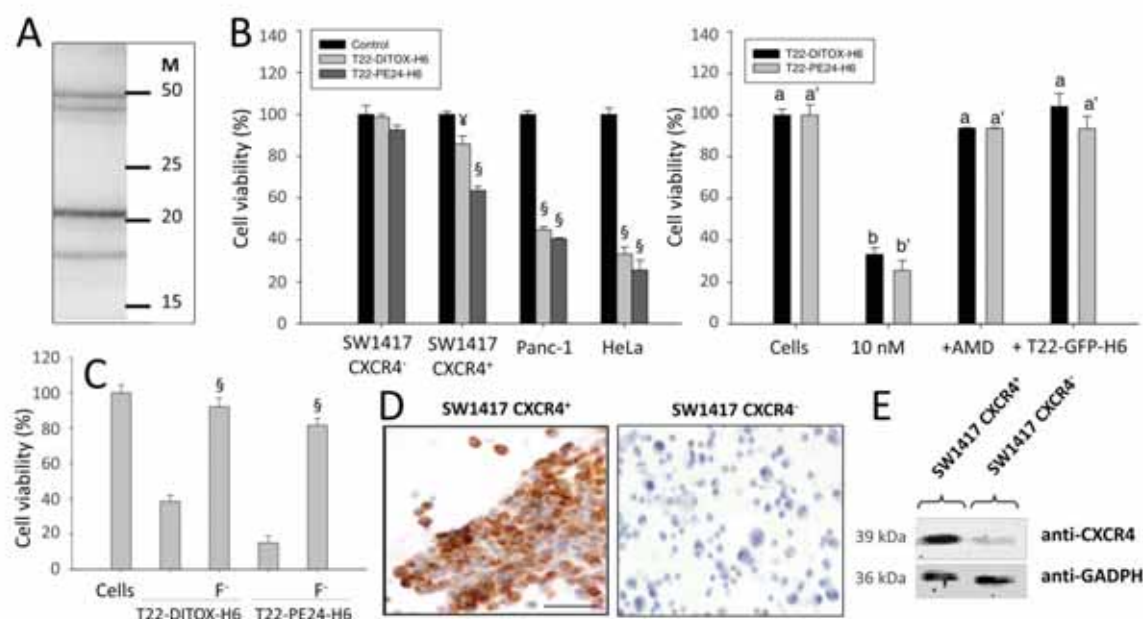


Fig. 4. Specific cytotoxicity of toxin-based nanoparticles in CXCR4⁺ cells. **A.** Detection of intracellular T22-DITOX-H6 by Western blot analysis of HeLa cell extracts, after exposure of the cell cultures to nanoparticles (1 μ M protein) for 24 h. M indicates the migration of molecular weight markers. **B.** Left: Cell death induced by T22-DITOX-H6 and T22-PE24-H6 nanoparticles (10 nM) over a SW1417 CXCR4⁻ cell line and different CXCR4⁺ cell lines (including an isogenic, CXCR4⁺ SW1417 version), 48 h after exposure (72 h for SW1417 cell line). Significant differences between relevant data pairs are indicated as \forall 0.01 < p < 0.05 and \S p < 0.01. Right: Inhibition of HeLa cell death (induced by 10 nM of protein nanoparticles) by either the CXCR4 antagonist AMD3100 or by 2 μ M protein T22-GFP-H6. Significant differences between relevant data are indicated as a change in the letter, from “a” to “b”. All the significant results were p < 0.01. All data are presented as mean \pm SEM (n = 3). **C.** HeLa cell death promoted by T22-DITOX-H6 F⁻ and by T22-PE24-H6 F⁻, compared to the related T22-DITOX-H6 and by T22-PE24-H6 respectively. Cells were exposed to 10 nM of each protein for 48 h. Data and statistics are as in panel B. **D.** Immunocytochemistry staining showing the lack of CXCR4 expression in the isogenic SW1417 CXCR4⁻ cells as compared with the high CXCR4 expression in SW1417 CXCR4⁺ cells. Bar indicates 50 μ m. **E.** Differential CXCR4 protein expression in these cells assessed by an immunoblotting assay. Glyceraldehyde-3-phosphate dehydrogenase (GADPH) was used as protein loading control.

intracellular hydrolysis should enhance the cytotoxic properties of the toxin domains, which would then benefit from lower load of superfluous protein sequences. For that, we explored the sensitivity of the multiple cleavage sites in the construct T22-DITOX-H6 that would offer, upon intracellular digestion, fully distinguishable protein fragments. Unlike the extracellular protein that appears as one single protein species (Figs. 2A and 3A), the His tag immunodetection of the cell-engulfed protein showed the protein as digested by different alternative sites, matching the molecular weight of the expected products for each furin cleavage site. In particular, the release of the T22 peptide through the *de novo* incorporated cleavage site was proved *in vivo* in cell-internalized protein by the shift from the 48.65 kDa full-length protein to the 44.21 kDa fragment, analyzing cell extracts upon exposure to the nanoparticles for 24 h (Fig. 4A). The rest of fragments corresponded to the progressive digestion intermediates that still kept the carboxy terminal tag, by which the protein is immunodetected. The natural cleavage at the internal furin site, which releases the catalytic domain from the translocation domain, is also proved by the occurrence of the major 20.60 kDa segment. Therefore, the catalytic segment alone is expected to occur inside the target cells, among other biologically active versions, at reasonable amounts.

When exploring the cytotoxic effects, both T22-DITOX-H6 and T22-PE24-H6 were effective in killing cultured HeLa cells, with low IC50 values (0.78 nM and 0.99 nM respectively, not shown). The cytotoxic effect was clearly detectable in several CXCR4-expressing cell lines, including SW1417 CXCR4⁺ but not in the isogenic SW1417 CXCR4⁻ line (Fig. 4B, left). Cytotoxicity was mostly abolished by AMD3100 and by the T22-displaying biologically inner protein T22-GFP-H6 (Fig. 4B, right), thus confirming again the specificity of the entrance of the nanoparticles, the intracellular nature of the nanoparticle-mediated toxicity and the expected CXCR4 receptor mediation in cell killing. Besides, it has been observed a reversion effect of T22-DITOX-H6 (90%) when

adding chloroquine, which inhibits endosomal acidification (not shown). This fact confirms that the mechanism of action is pH-dependent as described above (Fig. 1). In this context, we also evaluated the relevance of the removal of accessory protein segments (mediated by furin) on the cytotoxicity of the nanoparticles. For that, versions of T22-DITOX-H6 and T22-PE24-H6 without the engineered cleavage sites (labelled as F⁻) were constructed and tested for biological activity. The comparative analyses of HeLa cell death mediated by these proteins revealed a dramatic drop of cytotoxicity in T22-DITOX-H6 F⁻ and T22-PE24-H6 F⁻ nanoparticles compared to the original materials (Fig. 4C). On the other hand, the differential CXCR4 expression in the isogenic SW1417 cells was fully assessed by immunocytochemistry and Western blot (Fig. 4D,E). Interestingly, the capacity of T22-DITOX-H6 and T22-PE24-H6 to promote cell death was not lost after one-year storage at -80 °C and also upon 4 cycles of freezing and thawing (not shown).

Due to the high CXCR4⁺ specific cytotoxicity observed in cell culture, we next tested the performance of the toxin-based materials *in vivo* using a CXCR4-linked disease model. For that, we explored the biodistribution, antitumor activity and potential side toxicity of both T22-DITOX-H6⁺ and T22-PE24-H6⁺ nanoparticles in a CXCR4 over-expressing subcutaneous colorectal cancer model. As expected, after a single dose *i.v.* administration the protein materials accumulated in tumor in the studied time range (Fig. 5). Other organs such as brain, lung or heart were completely free of fluorescence. However, significant levels of emission associated to both nanoparticles were found in liver and kidney. To discard that significant amounts of ATTO might have been released from the nanoparticles during circulation in blood and generate artefacts in the biodistribution analysis, we evaluated the stability of the dye in T22-DITOX-H6⁺ nanoparticles incubated in commercial serum. At 48 h, only a very minor fraction of fluorescence was released from nanoparticles (5%, Supplementary Fig. 1A). In addition, the administration of free ATTO did not result in detectable

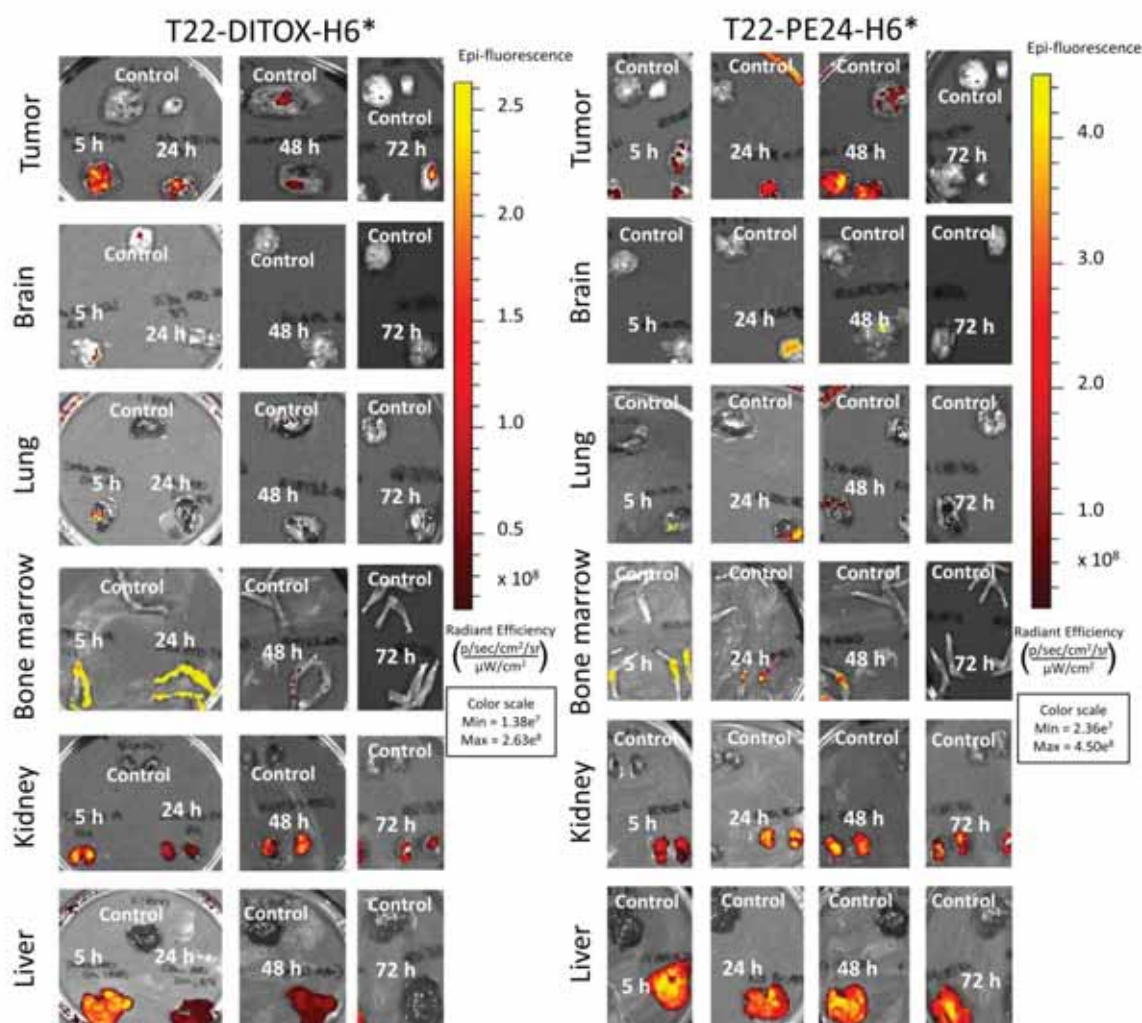


Fig. 5. Biodistribution kinetics of T22-DITOX-H6* and T22-PE24-H6* nanoparticles in a CXCR4⁺ colorectal cancer mouse model. Ex vivo fluorescence emitted by subcutaneous tumor and relevant organs in buffer-administered (control) and T22-DITOX-H6* and T22-PE24-H6*-treated mice at 5, 24, 48 and 72 h after 50 µg or 300 µg single dose i.v. administration. Emission scales are shown as radiant efficiency units (see methods section).

accumulation in tumor (Supplementary Fig. 1B), and the absence of dye signal in major organs was indicative of a fast urine secretion (as expected for a small molecule of 981 Da). These data fully supported the biodistribution of labelled nanoparticles shown in Fig. 5.

The presence of nanoparticles in liver was observed as worthy of a deeper analysis, since hepatic occurrence and damage is a severe concern in conventional and innovative cancer therapies, even in nanoconjugates or antibody-based drugs that show tissue-specific targeting [46–51]. Then, since it would be of crucial interest to discriminate between mere occurrence of fluorescence and toxin-induced damage in these organs, we comparatively investigated cell damage in tumor, liver and kidney. In this regard, we observed a high level of apoptosis induced by both nanoparticles in tumoral tissue, what was especially intense in T22-PE24-H6*-treated animals at 48 h post administration (Fig. 6). In contrast, apoptosis was undetectable in liver or kidney (Fig. 6), and most of the hepatic tissues were histologically normal except for a few and scattered small inflammation foci (Fig. 6) that can be attributed to non-specific extracellular retention of the drug in off-target tissues. This alteration was resolved after 72 h returning to normal histology. Probably, the intracellular activation of the toxins promoted by the furin-mediated release of accessory peptides (Fig. 4) does not occur in hepatic tissue, which does not overexpress CXCR4.

To discard that ATTO might have a positive contribution in the cytotoxicity of the materials in tumor after single dose administration we checked local apoptosis in animals treated with the non-labelled protein versions T22-DITOX-H6 and T22-PE24-H6. This was done at the times, among those tested, showing the highest potency (24 and 48 h respectively). As observed, local apoptosis was still present (Fig. 6) at values even higher than those induced by the labelled protein versions. This result was indicative that the observed antitumoral effect was intrinsically associated to the protein material. Then, data supported the notion that in spite of the occurrence of the protein drug in liver and kidney, this did not translate in a relevant uptake of any of the two nanoparticles in the parenchyma of these tissues. Our observations suggest that both labelled protein drugs underwent transient circulation through the fenestrated hepatic sinusoids and renal glomeruli as reported for other nanoparticles [52]. Moreover, their lack of toxicity in kidney or liver suggest their inability to internalize into the parenchymal cells in these organs because of their negligible CXCR4 expression, in comparison for instance to spleen or bone marrow which despite showing low nanoparticle accumulation express CXCR4 [53]. This is a finding similar to that reported for CXCR4-targeted imaging agents [54]. Then, both T22-DITOX-H6 and T22-PE24-H6 appear to have a therapeutic

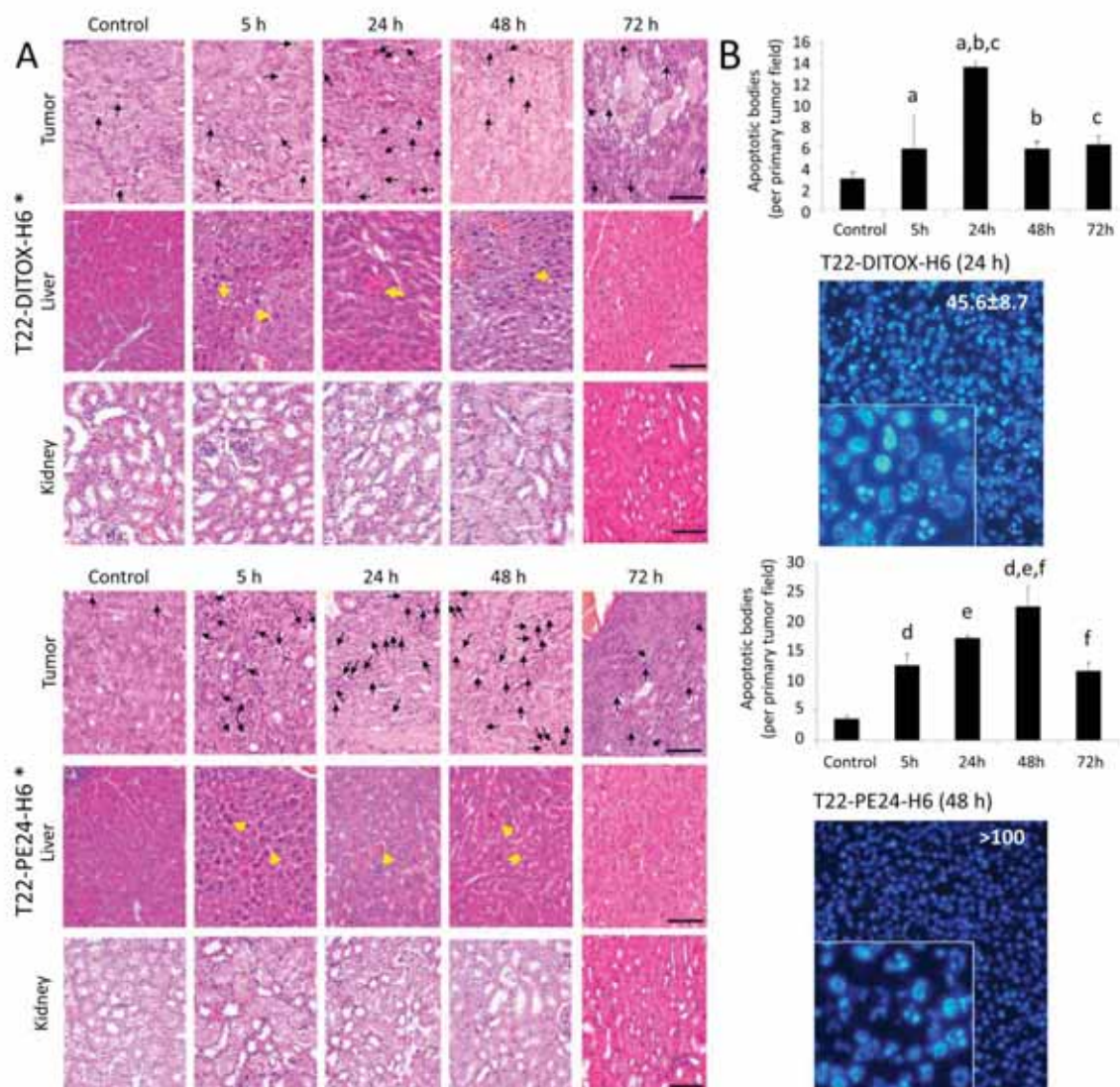


Fig. 6. Local induction of apoptosis in tumor by ATTO-labelled and unlabeled T22-DITOX-H6 (50 μ g) and T22-PE24-H6 (300 μ g) nanoparticles. A. Representative H&E staining of subcutaneous tumors showing apoptotic figures (black arrows). No significant apoptosis was detected in liver tissue at the studied times. Few and small inflammation foci in this organ were observed and are indicated by yellow arrows, which were resolved at 72 h, returning to histologically normal parenchyma. Note the absence of histological alterations in kidneys. Bar: 50 μ m. B. Number of apoptotic cell bodies in H&E tumor slices per ten high-power fields (400 \times magnification) are plotted for each nanoparticle. For the experimental times showing higher number of apoptotic lesions we also show representative Hoechst staining of subcutaneous tumors in animals treated with unlabeled protein versions, at different magnifications. All data are presented as mean \pm SEM (n = 3). Statistical significance: ^ap = 0.008; ^bp = 0.027; ^cp = 0.010; ^{d,e,f}p = 0.001.

index high enough to validate (i) their potential use for the treatment of CXCR4⁺ tumors but more importantly, and (ii) the wide applicability of the transversal concept supporting the self-assembling self-driving protein drugs based on chemically homogenous building blocks.

In order to evaluate further the therapeutic potential of the engineered toxins and the concepts that support the design of toxin-based nanoparticles we also assessed the pharmacokinetics in blood mouse samples after a single dose of 50 μ g for T22-DITOX-H6* or 300 μ g for T22-PE24-H6*. This was done through registering their fluorescence emission at 0, 1, 2, 5, 24 and 48 h after administration. We observed a biphasic decline in plasma concentration from C_{max}, with a fast nanoparticle biodistribution limited to the plasma compartment for both tested proteins (V_d = 3.9 ml T22-PE-H6* and V_d = 3.2 ml for T22-DITOX-H6*). This fast biodistribution was followed by a second and slow elimination phase, with a half-life of t_{1/2} = 30 h for both nanoparticles (Fig. 7A). This kinetic behavior is similar to the one we

previously reported for pharmacologically inactive protein nanoparticles [23], and also similar to that described for antibody-drug conjugates or large nanometric size therapeutic proteins, which show a compartment similar to the unconjugated antibody [55].

In a step further, we assessed the antitumor effect of each nanoparticle in a CXCR4⁺ subcutaneous CRC mouse model after repeated dose administration. After a dosage schedule of 10 μ g of T22-DITOX-H6, three times a week, per 8 doses, we observed at the end of the experiment a 5.8-fold reduction in tumor volume, as compared to buffer-treated mice (p = 0.05). This was associated with a 3.0-fold increase in apoptotic figures in tumor tissue (p < 0.001) (Fig. 7B), with no significant differences in body weight between toxin-treated and control groups (Fig. 7C). Similarly, and after a dosage schedule in mice of 10 μ g of T22-PE24-H6, three times a week, per 8 doses, we observed at the end of the experiment a 2.3-fold reduction in tumor volume, as compared to buffer-treated mice (p = 0.034), associated with a 3.8-fold

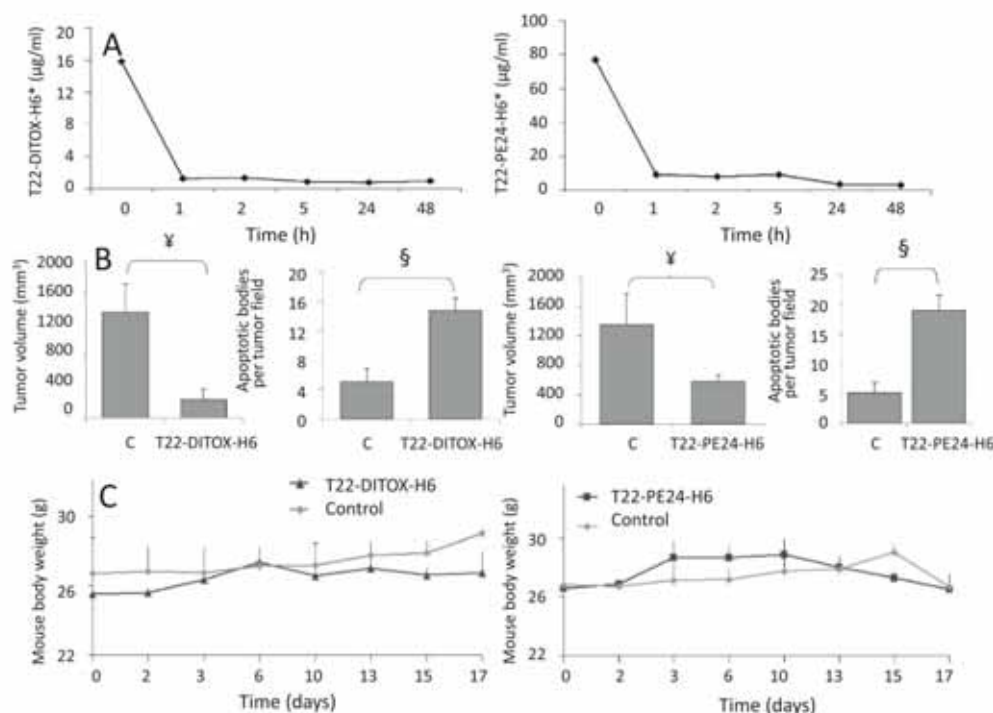


Fig. 7. Pharmacokinetics, antitumor effect and mouse body weight after T22-DITOX-H6 and T22-PE24-H6 administration. **A.** Pharmacokinetics of T22-DITOX-H6* and T22-PE24-H6* after a 50 µg or 300 µg intravenous bolus administration respectively. Fluorescence was recorded in plasma obtained after blood centrifugation at time 0, 1, 2, 5, 24 and 48 h (n = 3 per time point). **B.** Antitumor effect of T22-DITOX-H6 and T22-PE24-H6 measured by the analysis of tumor volume and number of apoptotic bodies at the end of the experiment, after repeated dose administration for each nanoparticle (10 µg, three times a week, × 8 doses). **C.** Evolution of mouse body weight after the described repeated dose regime for the protein nanoparticles. Statistics are ¶ for 0.01 < p < 0.05 and § for p < 0.01. All data are presented as mean ± SEM, n = 3.

increase in the number of apoptotic figures in tumor tissue ($p = 0.001$) (Fig. 7B). Again, no significant differences in body weight between experimental and control groups were observed (Fig. 7C).

4. Discussion

This set of data is in the line of new nanomedical concepts in targeted drug delivery in which the drugs itself act, in addition to their therapeutic functionalities, as self-assembled and self-delivered entities [18]. Conveniently engineered, the protein drugs developed here have been successfully produced and purified in bacteria, and self-organize as toroid nanoparticles of 30–90 nm (Fig. 2). In this form, they penetrate CXCR4⁺ target cells (Fig. 3) and promote receptor specific cell killing both *in vitro* (Fig. 4) and *in vivo* (Fig. 6), resulting in significant programmed cell death induction and in destruction of tumoral tissue after single dose administration (Fig. 6). Moreover, after repeated dose administration the nanostructured toxins increase apoptosis in tumor tissue associated with a significant reduction of tumor volume, with no alteration of mouse body weight (Fig. 7). These data prove the realistic feasibility of the application of these nanostructured toxins in a true therapeutic context. In comparison with similar approaches to generate self-assembling peptidic drugs (as pro-apoptotic and antimicrobial agents) [24,56], the concept explored here (i) does not use supporting irrelevant proteins such as GFP, thus minimizing the amount of bulk inactive material in the drug and enhancing nominal productivity in cell factories and (ii) allows the releasing of the active proteins in the cell cytoplasm by the controlled discharging of accessory protein segments that had been exploited for self-assembling of the building blocks and for the biodistribution and cell-targeted internalization of the nanoparticles. In this regard, the intrinsic cytotoxicity of the protein drugs is dramatically enhanced by the occurrence of the active domain free

from siding accessory peptides (Fig. 4). This is achieved by the appropriate incorporation of intracellular cleavage sites in the fusion protein that allow protein activation once in the right cell compartment and promotes the cytotoxic activity being executed solely by the minimal functional protein domain. As a generic concept, removing the vehicle in cell-targeted nanomedicines [18], would replace the otherwise promoted nanoconjugate strategies [57] through the design of new generations of chemically homogeneous nanoscale drugs. This would not only allow a heavy reduction of fabrication costs, but it will also minimize off-target drug effects, smoother regulatory constraints to drug approval and reduce the concerns about individual and environmental toxicity of inappropriate materials used as carriers. In this regard, other examples of self-assembling, self-delivered drugs are based on the combination of different types of molecules to achieve their function. Note the aggregation of VEGF siRNA, PolyMet (polymeric metformine), polyethylenimine, dicyandiamide, hyaluronic acid, DOTAP, cholesterol, DOTAP and a pegylated targeting ligand [19], or of EGCG, PEG, and herceptin or interferon α -2a [20] in self-delivered materials (summarized in [18]). The exceptional but technologically simple functional recruitment offered by proteins in single polypeptide chains [21] allows not only purifying the drug from recombinant cell factories in a single step by fully standardized recombinant DNA technologies [9], but globally, it also conduces to the simple design of self-assembling nanoparticles that can be easily fabricated in promising endotoxin-free bacterial systems [58,59].

5. Conclusions

We provide here data that fully supports an emerging groundbreaking concept in nanomedicine that is the generation of self-assembled, self-delivered drugs that act in absence of any external vehicle

[18]. The approach presented here, based on modular recombinant proteins, allows the single-step biological production of nanostructured protein materials that exhibit intrinsic therapeutic properties and show an appropriate cell targeting and biodistribution upon systemic administration. This is linked to a specific biological impact (tumor tissue destruction leading to tumor shrinkage) at the local level, because of the cell targeting domains included in the nanoparticle. These functional stretches, useful for biodistribution and during the delivery process, are self-removed from the protein nanoparticles once they have reached the target cell compartment. Then, the cytotoxic protein domain acts very efficiently free from any accessory protein segment. The design of self-organizing, cell-targeted protein drugs at the nanoscale level represents a step forward towards chemically homogeneous nanomedicines that should allow to full discard additional, potentially deleterious carriers.

Supplementary data to this article can be found online at <https://doi.org/10.1016/j.jconrel.2018.01.031>.

Competing interests

LSG, NS, UU, MSC, IC, RM, EV and AV are co-inventors of the patent application EP17169722.0 on the use of self-structured protein drugs.

Acknowledgments

We are indebted to Agencia Estatal de Investigación (AEI) and Fondo Europeo de Desarrollo Regional (FEDER) (grant BIO2016-76063-R, AEL/FEDER, UE), AGAUR (2014SGR-132) and CIBER-BBN (project NANOPROTHER) granted to AV, Marató de TV3 Foundation (TV32013-3930) and ISCIII (PI15/00272 co-founding FEDER) to EV and ISCIII (PI15/00378 and PIE15/00028, co-founding FEDER), Marató de TV3 foundation (TV32013-2030) and AGAUR2014-PROD0005 to RM. Protein production has been partially performed by the ICTS “NANBIOSIS”, more specifically by the Protein Production Platform of CIBER-BBN/IBB (<http://www.nanbiosis.es/unit/u1-protein-production-platform-ppp/>). Biodistribution studies were performed in the NANBIOSIS Nanotoxicology Unit and particle characterization was partially done at the NANBIOSIS Biomaterial Processing and Nanostructuring Unit. We are also indebted to SCAC (UAB) for cell culture facilities and assistance. LSG was supported by AGAUR (2017FI_B100063), NS by a predoctoral fellowship from the Government of Navarra, UU received a Sara Borrell postdoctoral fellowship and MVC is supported by Miguel Servet contract, both from ISCIII and AV an ICREA ACADEMIA award.

References

- [1] J.J. Calvete, L. Sanz, Y. Angulo, B. Lomonte, J.M. Gutierrez, Venoms, venomics, antivenomics, *FEBS Lett.* 583 (2009) 1736–1743.
- [2] C.Y. Koh, R.M. Kini, From snake venom toxins to therapeutics—cardiovascular examples, *Toxicol.* 59 (2012) 497–506.
- [3] P. Russo, A. Del Bufalo, M. Fini, Deep sea as a source of novel-anticancer drugs: update on discovery and preclinical/clinical evaluation in a systems medicine perspective, *EXCLI J.* 14 (2015) 228–236.
- [4] B.G. Livett, K.R. Gayler, Z. Khalil, Drugs from the sea: conopeptides as potential therapeutics, *Curr. Med. Chem.* 11 (2004) 1715–1723.
- [5] M. D'Incalci, M. Simone, M. Tavecchio, G. Damia, A. Garbi, E. Erba, New drugs from the sea, *J. Chemother.* 16 (Suppl. 4) (2004) 86–89.
- [6] J.W. Fox, S.M. Serrano, Approaching the golden age of natural product pharmaceuticals from venom libraries: an overview of toxins and toxin-derivatives currently involved in therapeutic or diagnostic applications, *Curr. Pharm. Des.* 13 (2007) 2927–2934.
- [7] S. Kotova, H.M. Wong, R.B. Cameron, New and emerging therapeutic options for malignant pleural mesothelioma: review of early clinical trials, *Cancer Manag. Res.* 7 (2015) 51–63.
- [8] N.B. Finnerup, N. Attal, S. Haroutounian, E. McNicol, R. Baron, R.H. Dworkin, et al., Pharmacotherapy for neuropathic pain in adults: a systematic review and meta-analysis, *Lancet Neurol.* 14 (2015) 162–173.
- [9] L. Sánchez-García, L. Martín, R. Mangues, N. Ferrer-Miralles, E. Vazquez, A. Villaverde, Recombinant pharmaceuticals from microbial cells: a 2015 update, *Microb. Cell Factories* 15 (2016) 33.

- [10] C. Sarfo-Poku, O. Esham, K.H. Lee, Medical application of scorpion venom to breast cancer: a mini-review, *Toxicol.* 122 (2016) 109–112.
- [11] J. Chalaskul, W.C. Hodgson, S. Kuruppu, N. Prasongsook, Effects of animal venoms and toxins on hallmarks of cancer, *J. Cancer* 7 (2016) 1571–1578.
- [12] C. Zhan, C. Li, X. Wei, W. Lu, W. Lu, Toxins and derivatives in molecular pharmaceuticals: drug delivery and targeted therapy, *Adv. Drug Deliv. Rev.* 90 (2015) 101–118.
- [13] C. Bachran, S.H. Leppla, Tumor targeting and drug delivery by anthrax toxin, *Toxins* 8 (2016).
- [14] Y.M. Li, W.A. Hall, Targeted toxins in brain tumor therapy, *Toxins* 2 (2010) 2645–2662.
- [15] N.G. Rainov, A. Soling, Clinical studies with targeted toxins in malignant glioma, *Rev. Recent Clin. Trials* 1 (2006) 119–131.
- [16] A. Elsassser, C.V. Howard, Toxicology of nanoparticles, *Adv. Drug Deliv. Rev.* 64 (2012) 129–137.
- [17] C. Haynes, Editorial—analytical toxicology of nanoparticles, *Analyst* 139 (2014) 868–869.
- [18] J. Shen, J. Wolfram, M. Ferrari, H. Shen, Taking the vehicle out of drug delivery, *Mater. Today* 20 (2017) 95–97.
- [19] Y. Zhao, W. Wang, S. Guo, Y. Wang, L. Miao, Y. Xiong, et al., PolyMetformin combines carrier and anticancer activities for in vivo siRNA delivery, *Nat. Commun.* 7 (2016) 11822.
- [20] J.E. Chung, S. Tan, S.J. Gao, N. Yongvongsoontorn, S.H. Kim, J.H. Lee, et al., Self-assembled micellar nanocomplexes comprising green tea catechin derivatives and protein drugs for cancer therapy, *Nat. Nanotechnol.* 9 (2014) 907–912.
- [21] E. Vazquez, R. Mangues, A. Villaverde, Functional recruitment for drug delivery through protein-based nanotechnologies, *Nanomedicine* 11 (2016) 1333–1336.
- [22] R. Duncan, R. Gaspar, Nanomedicine(s) under the microscope, *Mol. Pharm.* 8 (2011) 2101–2141.
- [23] M.V. Cespedes, U. Unzueta, W. Tatkiwicz, A. Sanchez-Chardi, O. Conchillo-Sole, P. Alamo, et al., In vivo architectonic stability of fully de novo designed protein-only nanoparticles, *ACS Nano* 8 (2014) 4166–4176.
- [24] N. Serma, M.V. Cespedes, L. Sánchez-García, U. Unzueta, R. Sala, A. Sánchez-Chardi, F. Cortés, N. Ferrer-Miralles, R. Mangues, E. Vázquez, A. Villaverde, Peptide-based nanostructured materials with intrinsic proapoptotic activities in CXCR4⁺ solid tumors, *Adv. Funct. Mater.* 27 (2017) 1700919.
- [25] R.J. Collier, Understanding the mode of action of diphtheria toxin: a perspective on progress during the 20th century, *Toxicol.* 39 (2001) 1793–1803.
- [26] M. Michalska, P. Wolf, Pseudomonas exotoxin A: optimized by evolution for effective killing, *Front. Microbiol.* 6 (2015) 963.
- [27] S. Seetharam, V.K. Chaudhary, D. FitzGerald, I. Pastan, Increased cytotoxic activity of Pseudomonas exotoxin and two chimeric toxins ending in KDE1, *J. Biol. Chem.* 266 (1991) 17376–17381.
- [28] R.K. Holmes, Biology and molecular epidemiology of diphtheria toxin and the tox gene, *J. Infect. Dis.* 181 (Suppl. 1) (2000) S156–67.
- [29] B.Y. Wong, S.A. Gregory, N.H. Dang, Denileukin difitox as novel targeted therapy for lymphoid malignancies, *Cancer Investig.* 25 (2007) 495–501.
- [30] F. Baum, M. Lechmann, B.F. Krippendorff, R. Staack, F. Herting, M. Festag, et al., Characterization of a re-engineered, mesothelin-targeted Pseudomonas exotoxin fusion protein for lung cancer therapy, *Mol. Oncol.* 10 (2016) 1317–1329.
- [31] H.Y. Kim, J.Y. Hwang, S.W. Kim, H.J. Lee, H.J. Yun, S. Kim, et al., The CXCR4 antagonist AMD3100 has dual effects on survival and proliferation of myeloma cells in vitro, *Cancer Res. Treat.* 42 (2010) 225–234.
- [32] J.S. Song, C.M. Kang, H.H. Kang, H.K. Yoon, Y.K. Kim, E.H. Kim, et al., Inhibitory effect of CXCR4 chemokine receptor 4 antagonist AMD3100 on bleomycin induced murine pulmonary fibrosis, *Exp. Mol. Med.* 42 (2010) 465–472.
- [33] J.P. Richard, K. Melikov, E. Vives, C. Ramos, B. Verbeure, M.J. Gait, et al., Cell-penetrating peptides. A reevaluation of the mechanism of cellular uptake, *J. Biol. Chem.* 278 (2003) 585–590.
- [34] J. Kim, K.L. Connelly, E.M. Unterwald, S.M. Rawls, Chemokines and cocaine: CXCR4 receptor antagonist AMD3100 attenuates cocaine place preference and locomotor stimulation in rats, *Brain Behav. Immun.* 62 (2017) 30–34.
- [35] Y.H. Jung, D.Y. Lee, W. Cha, B.H. Kim, M.W. Sung, K.H. Kim, et al., Antitumor effect of CXCR4 antagonist AMD3100 on the tumorigenic cell line of BHP10-3 papillary thyroid cancer cells, *Head Neck* 38 (2016) 1479–1486.
- [36] U. Unzueta, M.V. Cespedes, N. Ferrer-Miralles, I. Casanova, J. Cedano, J.L. Corchero, et al., Intracellular CXCR4(+) cell targeting with T22-empowered protein-only nanoparticles, *Int. J. Nanomedicine* 7 (2012) 4533–4544.
- [37] U. Unzueta, N. Ferrer-Miralles, J. Cedano, X. Zikang, M. Pesarrodona, P. Saccardo, et al., Non-amyloidogenic peptide tags for the regulatable self-assembly of protein-only nanoparticles, *Biomaterials* 33 (2012) 8714–8722.
- [38] T. Koshida, R. Hosotani, Y. Miyamoto, J. Ida, S. Tsuji, S. Nakajima, et al., Expression of stromal cell-derived factor 1 and CXCR4 ligand receptor system in pancreatic cancer: a possible role for tumor progression, *Clin. Cancer Res.* 6 (2000) 3530–3535.
- [39] H. Kulbe, N.R. Levinson, F. Balkwill, J.L. Wilson, The chemokine network in cancer—much more than directing cell movement, *Int. J. Dev. Biol.* 48 (2004) 489–496.
- [40] T. Murakami, A.R. Cardones, S.T. Hwang, Chemokine receptors and melanoma metastasis, *J. Dermatol. Sci.* 36 (2004) 71–78.
- [41] F. Barbieri, A. Bajetto, T. Florio, Role of chemokine network in the development and progression of ovarian cancer: a potential novel pharmacological target, *J. Oncol.* 2010 (2010) 426956.
- [42] A. Albanese, P.S. Tang, W.C. Chan, The effect of nanoparticle size, shape, and surface chemistry on biological systems, *Annu. Rev. Biomed. Eng.* 14 (2012) 1–16.
- [43] B.D. Chithrani, A.A. Ghazani, W.C. Chan, Determining the size and shape

- dependence of gold nanoparticle uptake into mammalian cells, *Nano Lett.* 6 (2006) 662–668.
- [44] F. Rueda, M.V. Cespedes, O. Conchillo-Sole, A. Sanchez-Chardi, J. Seras-Franzoso, R. Cubarsi, et al., Bottom-up instructive quality control in the biofabrication of smart protein materials, *Adv. Mater.* 27 (2015) 7816–7822.
- [45] M. Pesarrodona, E. Crosas, R. Cubarsi, A. Sanchez-Chardi, P. Saccardo, U. Unzueta, et al., Intrinsic functional and architectonic heterogeneity of tumor-targeted protein nanoparticles, *Nanoscale* 9 (2017) 6427–6435.
- [46] B. Vincenzi, G. Armento, M. Spalato Ceruso, G. Catania, M. Lealos, D. Santini, et al., Drug-induced hepatotoxicity in cancer patients - implication for treatment, *Expert Opin. Drug Saf.* 15 (2016) 1219–1238.
- [47] P. Sarges, J.M. Steinberg, J.H. Lewis, Drug-induced liver injury: highlights from a review of the 2015 literature, *Drug Saf.* 39 (2016) 801–821.
- [48] G. Damodar, T. Smitha, S. Gopinath, S. Vijayakumar, Y. Rao, An evaluation of hepatotoxicity in breast cancer patients receiving injection Doxorubicin, *Ann. Med. Health Sci. Res.* 4 (2014) 74–79.
- [49] J. Wang, Y. Wu, M. Dong, X. He, Z. Wang, J. Li, et al., Observation of hepatotoxicity during long-term gefitinib administration in patients with non-small-cell lung cancer, *Anti-Cancer Drugs* 27 (2016) 245–250.
- [50] W. Wang, P. Lie, M. Guo, J. He, Risk of hepatotoxicity in cancer patients treated with immune checkpoint inhibitors: a systematic review and meta-analysis of published data, *Int. J. Cancer* 141 (2017) 1018–1028.
- [51] I.S. Elefthymiou, K.D. Paniazis, A. Iliou, L. Pallis, A. Mariolis, I. Glynou, et al., Tamoxifen induced hepatotoxicity in breast cancer patients with pre-existing liver steatosis: the role of glucose intolerance, *Eur. J. Gastroenterol. Hepatol.* 16 (2004) 593–598.
- [52] N. Bertrand, J.C. Leroux, The journey of a drug-carrier in the body: an anatomophysiological perspective, *J. Control. Release* 161 (2012) 152–163.
- [53] J.B. Regard, I.T. Sato, S.R. Coughlin, Anatomical profiling of G protein-coupled receptor expression, *Cell* 135 (2008) 561–571.
- [54] I.D. Weiss, O. Jacobson, Molecular imaging of chemokine receptor CXCR4, *Theranostics* 3 (2013) 76–84.
- [55] A. Deslándes, Comparative clinical pharmacokinetics of antibody-drug conjugates in first-in-human Phase I studies, *MAbs* 6 (2014) 859–870.
- [56] N. Serna, L. Sanchez-García, A. Sanchez-Chardi, U. Unzueta, M. Roldan, R. Marques, et al., Protein-only, antimicrobial peptide-containing recombinant nanoparticles with inherent built-in antibacterial activity, *Acta Biomater.* 60 (2017) 256–263.
- [57] A.Z. Wang, R. Langer, O.C. Farokhzad, Nanoparticle delivery of cancer drugs, *Annu. Rev. Med.* 63 (2012) 185–198.
- [58] F. Rueda, M.V. Cespedes, A. Sanchez-Chardi, J. Seras-Franzoso, M. Pesarrodona, N. Ferrer-Miralles, et al., Structural and functional features of self-assembling protein nanoparticles produced in endotoxin-free *Escherichia coli*, *Microb. Cell Factories* 15 (2016) 59.
- [59] O. Cano-Garrido, M.V. Cespedes, U. Unzueta, P. Saccardo, M. Roldan, A. Sanchez-Chardi, et al., CXCR4(+)-targeted protein nanoparticles produced in the food-grade bacterium *Lactococcus lactis*, *Nanomedicine* 11 (2016) 2387–2398.

Hereafter the following papers have been placed in the annex section as they are involved in the PhD thesis and are mentioned during the discussion:

- **Annex 1: Review 2**
Protein-based therapeutic killing for cancer therapies
- **Annex 2: Article 3**
Peptide-based nanostructured materials with intrinsic proapoptotic activities in CXCR4⁺ solid tumors
- **Annex 3: Article 4**
Conformational conversion during controlled oligomerization into nonamylogenic protein nanoparticles
- **Annex 4: Article 5**
Selective CXCR4⁺ cancer cell targeting and potent antineoplastic effect by a nanostructured version of recombinant ricin
- **Annex 5: Article 6**
Engineering multifunctional protein nanoparticles by in vitro disassembling and reassembling of heterologous building blocks



DISCUSSION

DISCUSSION

Conventional drug chemotherapies present a lack of specificity leading to off-target toxicities and low therapeutic effect in the tumour. For that, nowadays there is an urgent demand of targeted oncotherapies^{154,155}. A lot of effort is being invested in the development of cell-targeted drugs specifically delivered to over-expressed tumour biomarkers like bFGF for lung cancer¹⁵⁶, CD19 for B-cell malignancies¹⁵⁷, HER2 for breast cancer¹⁵⁸ or CXCR4 for colorectal cancer¹⁵⁹.

In this context, our research group has developed a highly specific vehicle in the nanoscale (T22-GFP-H6) for drug delivery^{133,140}. T22-GFP-H6-FdU nanoconjugates have been generated by covalently binding the targeted protein nanoparticle to FdU (Floxuridine), a polymer of 5-Fluorouracil, a chemical drug commonly used to treat colorectal cancer. Repeated administration of the CXCR4-targeted nanoconjugate resulted in a significant prevention and regression of metastases without associated toxicities¹³⁷.

Not only targeted but also nanoscale drugs are appealing due to their intrinsic physical and biological advantages. Structures ranging nanometer sizes above ~ 8 nm minimize renal clearance, increasing the EPR effect and the circulation time in the blood stream and thus improving the biodistribution profile¹⁶⁰. However, the generation of nanocarriers usually involves the use of inert, bulk material devoid of any therapeutic activity. This non-active material can pose a safety concern if it is not properly metabolized and eliminated from the organism⁹⁰. Furthermore, immune response can be induced by the administration of large amounts of such voluminous nanocarriers causing undesired immunotoxicities. This concerning scenario has prompted the generation of **vehicle-free** entities, using **self-assembling therapeutic agents**^{92,94}, which are able to enhance loading capacity and reduce drug leakage of the nanocarrier, the two main intrinsic limitations in nanoconjugated drugs.

DISCUSSION

In light of the above considerations, as part of my PhD project, in our group we aimed to improve even more the model protein T22-GFP-H6, that resulted so effective when used as a drug vehicle (T22-GFP-H6-FdU nanoconjugate).

First, intrinsically cytotoxic proteins were added as therapeutic agents to the T22-empowered nanoparticles instead of FdU. Therefore, all the functionalities required were in a single polypeptide sequence, without any chemical drug (**T22-CYTOTOXIC DOMAIN-GFP-H6**). For this reason, loading capacity or drug leakage (present in drug-based nanoconjugates) weren't concerning issues anymore, increasing therapeutic efficacy and reducing health risks.

Second, we tried to remove any remaining inactive stretch, replacing GFP by the therapeutic agent itself (**T22-CYTOTOXIC DOMAIN-H6**). Thus, we were keeping the essential segments to achieve a specifically targeted, nanoscale therapy without any unnecessary material.

Before designing de novo cytotoxic protein-based nanoparticles, our aim was to get a global picture of the state of the art in recombinant DNA trends for the treatment of human diseases and elucidate which were the most promising cytotoxic proteins that were explored up to date (**Review 1 and Annex 1**). For that, we did an extensive bibliographic research that is described below.

1. Trends in the development of therapeutic recombinant pharmaceuticals

These days, there is a steadily increasing interest in the generation of recombinant proteins for their use in biomedicine. Currently, there are around **400 marketed recombinant biopharmaceuticals** and 1300 candidates are under development (**Review 1, Figure 2**), all of them aimed to recombinant protein-based therapies. Disorders or diseases that are due to the absence or dysfunction of a specific protein such as diabetes^{161,162} or blood clotting disorders^{163,164} are a suitable target for the use of recombinant proteins, as administration of a given functional protein is required. So far,

natural sources and chemical synthesis present diverse constraints when moving to scale-up processes, such as low yields and long-lasting multistep-based procedures, respectively. At this point, recombinant DNA technology results the most appropriate alternative to produce therapeutic proteins.

In 1980s, the first recombinant protein Humulin (produced in *E. coli*) gained FDA-approval for the treatment of diabetes^{165,166}. Since then, it has been observed a steep rise in the number of protein production platforms, which expand the possibilities for the development of recombinant drugs (Review 1, Table 1). Bacteria¹⁶⁷, yeasts¹⁰⁴, insect cells¹⁰⁶ and mammalian cells¹⁶⁸ have been used in different contexts, regarding the protein specific requirements. Although mammalian cells (which are closer to humans) may seem optimal to produce human proteins, *E. coli* is a more versatile, cost-effective and easy to handle expression system. For this reason, in oncology there is a clear predominance of *E. coli*-produced recombinant pharmaceuticals (69 %) over mammalian cell-derived recombinant therapies (26 %) (Review 1, Figure 4). Cytokines (Aldesleukin, Interleukin-2, Filgrastim) or growth factors (Molgramostim, Nartograstim, Palifermin) are some examples of approved anticancer recombinant biopharmaceuticals produced in *E. coli* (Review 1, Table 4).

Interestingly, the market is leaving behind nature-like plain proteins and evolving towards improved versions that have been modified through insertions, deletions or mutations (Review 1, Table 4). Additionally, fusion of protein-based domains in a rational design basis have been used aiming to expand the functionalities of the current marketed recombinant biopharmaceuticals (for instance Denileukin diftitox¹⁶⁹ and Aflibercept^{170,171}) (Review 1, Figure 5). Fusion proteins offer a long list of possibilities for the generation of tailored biopharmaceuticals with combined versatile functionalities in a single polypeptide, unlike the previously mentioned non-modified plain proteins present in nature.

Specifically, the treatment of cancer, autoimmune or inflammatory diseases, relies on **cell killing activities**. In oncology, there is a long list of chemical compounds (with small molecular weight) that can cause cell toxicity toward cancer cells. However, they also

DISCUSSION

cause undesired toxicities and numerous side effects due to systemic distribution through the organism. Additionally, having a filtration cut-off around ~5-7 nm^{172,173} renal clearance leads to both insufficient half-life and drug amount. Therefore, improvement of the circulation time while increasing selectivity to generate an efficient treatment devoid of any secondary effect in healthy organs is needed.

In this context, it has been widely described the presence of proteins from natural origin that present high **cytotoxic activities**^{89,145,174,175} (**Annex 1**). They can be found in completely different living organisms (animals, plants or microorganisms) in form of proapoptotic proteins, toxins, antimicrobial peptides or venoms. Proteins are versatile and biocompatible materials whose production through recombinant technologies has been proved to be environmentally friendly and reliable for decades. For that, plenty of cytotoxic proteins like BID, PUMA (proapoptotic factors), diphtheria toxin, exotoxin A (microbial toxins), ricin, abrin (plant toxins), chlorotoxin and gomesin (venom components) are nowadays under clinical trials or even approved by the FDA for their use as antitumoral drugs (**Annex 1, Table 2**).

It is worth mentioning that most of these recombinant proteins that are being developed for their use in the clinics are not natural versions. As a matter of fact, they are improved versions that have been previously modified through genetic engineering methodologies. Some of the most common modifications are de-immunization and fusion between protein domains of interest.

First, de-immunization processes are usually performed when working with non-human proteins, which can generate non-desired immunogenic reactions. By removing or replacing some amino acids of the polypeptide it is possible to dramatically reduce the immune response caused by exogenous proteins^{176,177}. An appealing alternative to avoid either immunogenicity or de-immunization processes would be the use of **human proteins**, which will not generate any immune response, such as proapoptotic proteins (**Annex 2**).

Second, fusion proteins rely on a functional recruitment basis, aiming to obtain a modular multifunctional protein able to cover all the necessities in a single polypeptide chain (**Annex 1, Figure 2**). For example, cell-targeting^{178,179} endosomal escape¹⁸⁰⁻¹⁸² or self-assembling domains^{183,184} are widely used for the development of improved pharmaceuticals able to reach a specific cellular marker, avoid endosomal degradation or oligomerize in the nanoscale range, respectively. Immunotoxins are a simple example, which consist of the fusion between an immunoglobulin (targeting domain) and a toxin (cytotoxic domain)¹⁸⁵.

2. Improving efficiency of internalized recombinant protein-only nanoparticles

Cell-targeted intracellular delivery is a continuously increasing field for the improvement of conventional drugs and the development of new ones¹⁶⁰. Recombinant proteins are convenient materials for the development of **cell-targeted therapies** as they can be customized through the fusion of diverse domains of interest, such as ligands. However, the entrapment of protein therapeutics in endo-lysosomal compartments leading to proteolysis has been reported to be a major reason for impairment or even loss of their efficacy (**Article 1**).

In the case of protein-based therapies conjugated to a chemical drug, lysosomal degradation is not a concerning issue as the therapeutic agent (chemical compound) is not susceptible of being degraded in the lysosomes, being able to exert its expected activity despite this phenomenon. Unfortunately, as our aim is to get rid of the chemical partner and develop protein-only therapies, lysosomal degradation is a process that needs to be studied in detail¹⁸⁰, trying to minimize its related deleterious effect.

Consequently, during endocytosis and before the fusion with lysosomes, endosomal escape must occur to prevent degradation and release the therapeutic nanoparticle to the desired subcellular compartment, whether it is the cytosol, mitochondria or nucleus. Thus, as **endosomal escape** is one of the barriers that need to be overcome upon

DISCUSSION

administration, a lot of effort is being made to evade this process. Hopefully, selective and endosomolytic properties together, will give birth to good candidates able to target and increase the amount of proteins that reaches the cytoplasm, promising alternatives for targeted drug delivery.

Interestingly, **viruses** have been evolving during millions of years to overcome degradation once they have internalized in the host cell, for survival reasons¹⁸⁶. For that, they are a suitable source of proteins that can be used to escape from endosomal degradation (for instance, **hemagglutinin peptide HA2** from influenza virus¹⁸⁷). Additionally, a big effort has been made to generate synthetic candidates, developed improving the already discovered natural endosomal escape agents. Apart from natural proteins or peptides, chemical agents have also been described to exert endosomal escape abilities, such as polyethylenimine (PEI) or CQ⁷⁹.

Endosomal escape is achieved predominantly through three different mechanisms of action. First, proton sponge effect can be observed adding his-rich tags or PEI, which cause the internalization of water in endosomes at acidic pH, followed by membrane disruption. Second, pore formation in endosomal membranes, which can be performed by antimicrobial (natural or synthetic) peptides. Third, fusion to lipid membranes has been observed in presence of viral peptides.

Haemagglutinin (HA) is a glycoprotein present on the surface of influenza virus. It is involved in two relevant processes of the viral cell cycle¹⁸⁸. First, it is responsible for the recognition of its host cell, through the binding to sialic acid receptors (mediated by HA1 domain). Once it is internalized through endocytosis, the endosomal compartment is further acidified. At this point, after pH acidification, HA2 domain prompts the endosomal escape through fusion of the host endosomal membrane with the viral membrane, releasing the viral genome inside the host cell. Specifically, the N-terminal sequence of the HA2 subunit consists of an amphiphilic anionic peptide. At acidic pH, there is a conformational change in a helical structure in this peptide, which leads to activate its **fusogenic activity** resulting in destabilization of the endosomal membrane^{188,189}.

The HA2 endosomolytic activity has been tested in different and complex presentations of the peptide. One of them consists of a fusion protein that combines the HA2 peptide with TAT, the cell-penetrating peptide from human immunodeficiency virus (HIV) HA2-TAT¹⁹⁰. Alternatively, HA2 has been fused to diverse functional domains simultaneously (R9-HA2-NLS-mCherry)¹⁹¹: a cell penetrating peptide (R9), a nuclear localization signal (NLS) and a monitoring agent (red fluorescent protein mCherry). Despite the variety of fusion proteins developed up to now, we wondered if it would be possible to obtain actively targeted nanoparticles, combining the HA2 peptide with the CXCR4-specific ligand T22.

In our laboratory, the HA2 peptide¹⁹¹ has been added to T22-GFP-H6 protein in two alternative positions, at the amino and carboxy terminus of the GFP (**T22-HA2-GFP-H6** and **T22-GFP-HA2-GFP**, respectively) ([Article 1, Figure 1A](#)).

T22-GFP-H6 protein self-assembles as protein-only nanoparticles able to **target CXCR4⁺ cells** in vitro and in vivo. However, we have observed that the administered protein is partially degraded in the endosomes (almost 90 %) leading to a loss of efficiency¹⁹². Through HA2 peptide addition, our aim (**FIRST OBJECTIVE**) was to confer endosomolytic activity to T22-GFP-H6 nanoparticles, increasing the amount of protein that succeeds reaching the cell cytoplasm.

Both HA2-bearing versions of T22-GFP-H6 were produced in the prokaryotic expression system *E. coli*, purified by affinity chromatography ([Article 1, Suppl. Figure 1](#)) and followed by further physicochemical characterization. Purity and integrity of both engineered versions was assessed by mass spectrometry (matrix-assisted laser desorption/ionization time-of-flight, MALDI-TOF) and Western Blot ([Article 1, Figure 1B](#)), showing absence of contaminants or proteolysis. Specifically, production yield of the soluble T22-GFP-HA2-H6 was lower than T22-HA2-GFP-H6, which can be observed through MALDI-TOF analysis as a high background signal due to low sample concentration ([Article 1, Figure 1B](#)). Spontaneous self-assembly of both constructs was observed, in form of 30 - 50 nm nanoparticles as observed by DLS ([Article 1, Figure 1C](#)) and FESEM images ([Article 1, Figure 1D](#)). The incorporation of HA2 to T22-GFP-H6

DISCUSSION

protein caused a reduction in fluorescence emission whether it was located at N- or C-terminus, being more affected in T22-GFP-HA2-H6. This result indicates that the newly added peptide sequence had a **conformational impact** in the structure. Recombinant proteins were further tested in vitro to assess their internalization in CXCR4⁺ cells and more importantly their expected endosomolytic effect (**Article 1, Figure 2**). First, internalization experiments were performed in duplicate (in absence and presence of AMD3100, which is a CXCR4 antagonist¹⁹³⁻¹⁹⁵) to test nanoparticles' specificity.

Table 5. Comparative physicochemical properties and cell line performance of the parental T22-GFP-H6 protein (in orange) and the HA2-bearing alternatives.

PROPERTIES	T22-GFP-H6	T22-HA2-GFP-H6	T22-GFP-HA2-H6
Nanoparticle size	14 nm	30 nm	45 nm
Fluorescence	100 %	43 %	15 %
Internalization	Yes (+)	Yes (+++)	Yes (+++)
Specificity	Yes (++)	No	Yes (+)
Endosomal escape	No	No	Yes
Toxicity	No	No	No

The modular protein showed an improved cell internalization in both alternative positions (**Article 1, Figure 2A**). In T22-HA2-GFP-H6, high internalization results are due to a completely loss of cell specificity, as we did not observe a reduction in the internalization when adding the antagonist of CXCR4 (AMD3100). Surprisingly, the second construct T22-GFP-HA2-H6 behaved differently, showing an increase in cell penetration with little affectation in specificity (**Article 1, Figure 2B**).

In order to demonstrate whether the favoured internalization was due to endosomal escape activities or not, in vitro experiments were performed adding chloroquine (CQ) (**Article 1, Figure 2C**). This chemical compound is widely known for preventing endosomal acidification and subsequent protein degradation^{196,197}. Results obtained with T22-HA2-GFP-H6 revealed that cell penetration improvement is not related with any endosomolytic activity. In fact, intracellular fluorescence of both parental T22-GFP-H6 and T22-HA2-GFP-H6 protein with CQ (non-degradative conditions) was around 30-fold higher than the control without CQ. On the contrary, T22-GFP-HA2-H6 signal suffered a

5-fold increase, proving that this construct was able to perform endosomal escape, partially avoiding protein degradation and reaching the cytoplasm.

Moreover, a kinetics experiment was performed at different time points and two different protein concentrations (0.1 and 2 μM) being 0.1 μM under the threshold for endosomolytic properties ([Article 1, Figure 2D](#)). Intracellular accumulation of both proteins at 0.1 μM results in protein degradation, whereas at 2 μM they differ, being T22-HA2-GFP-H6 degraded and T22-GFP-HA2-H6 escaped from the endosomes, supporting the previous data obtained with in vitro CQ experiments. Additionally, confocal microscopy images of protein internalization at 24 h ([Article 1, Figure 2E](#)) showed an increased perinuclear localization of T22-GFP-HA2-H6 protein, compared to T22-HA2-GFP-H6 variant.

Taken together, all the obtained results (summarized in [Table 5](#) for better understanding) indicated that T22-GFP-HA2-H6 nanoparticle was able to induce endosomal escape and reach the cytoplasm. On the other hand, when located at the N-terminus of the core protein (T22-HA2-GFP-H6) the HA2 peptide could be more accurately considered as a cell penetrating peptide.

The addition of HA2 peptide at two different positions had a positive effect increasing cellular internalization, although followed by a detrimental impact in CXCR4 specificity, mostly in the case of T22-HA2-GFP-H6. This phenomenon may be due to the close proximity of HA2 to the ligand T22, which is responsible for specific CXCR4 receptor binding and internalization. Probably, the presence of HA2 in this position had an impact in protein conformation, compromising T22 folding or flexibility. Differences in tertiary structure were confirmed by Trp-fluorescence spectroscopy and modelling of both nanoparticles ([Article 1, Suppl. Figure 2](#)).

The use of the viral fusogenic HA2 peptide should be evaluated individually for each new modular recombinant protein. In the case of T22-GFP-H6 nanoparticles it has been possible to generate a variant (bearing HA2 peptide) with endosomolytic activities, at

expenses of losing selectivity. However, biodistribution experiments are being performed to observe whether selectivity loss in vitro is reproduced in vivo.

All things considered, we have demonstrated that although HA2 fusogenic peptide may seem a good endosomolytic candidate, it might not be optimal particularly when developing cell-targeted drugs, which can be highly affected losing specificity.

3. Generating intrinsically therapeutic protein-only nanoparticles for cancer therapies

Chemically conjugated therapeutic nanoparticles present diverse intrinsic obstacles (such as loading capacity or drug leakage) for the development of efficient and safe nanocarriers for drug delivery⁹⁰. For this reason, our aim was to prove that the nanoarchitectonic principle described in our group (based in the presence of cationic N-terminal and polyhistidine C-terminal tags) could be applied for the development of intrinsically therapeutic protein-only nanoparticles, devoid of any chemical drug (Annex 2).

After doing an extensive bibliographic research (Review 1 and Annex 1) about the use of cytotoxic proteins as therapeutic agents, we found out that proapoptotic factors are particularly valuable, because of their human origin. Being originated in the same organism where they would be administered to, proapoptotic proteins would not induce immunogenic toxicity, commonly observed in heterologous protein drugs. For that, our first choice was in the line of **human origin proapoptotic proteins**, aiming to avoid further immunogenic reactions once administered in patients. Among diverse proapoptotic factors, the BH3 domain of **proapoptotic BAK** (Bcl-2 homologous antagonist killer) was the preferred candidate, as there were successful precedents describing the possibility to produce it in a recombinant fully-active form, using *E. coli* expression system. BAK protein belongs to the Bcl-2 homology family; which induces programmed cell death through caspase-dependent apoptosis. Specifically, it inactivates

antiapoptotic proteins and permeabilizes the mitochondrial membrane, releasing cytochrome C among other factors. For our design, instead of using the whole BAK (which is not properly produced in a recombinant form due to highly hydrophobic nature¹⁹⁸), we used a truncated version that uniquely contains the BH3 domain that keeps proapoptotic properties¹⁹⁹.

For the exploration of the cytotoxic properties of truncated BAK, it was fused to both T22 and H6 for oligomeric purposes. Moreover, they both have a dual role as T22 is a CXCR4-targeting agent and the His-tag was used for purification purposes. Additionally, GFP was added to monitor protein localization (**Annex 2, Figure 1A**). The whole construct (**T22-BAK-GFP-H6**) is envisaged as a potent candidate for theragnostic purposes, combining diagnostic (GFP) and therapeutic properties (BH3-BAK).

The de novo T22-BAK-GFP-H6 multidomain protein was successfully produced in *E. coli* as microbial cell factory and purified using his-tag chromatography with the expected molecular weight (**Annex 2, Figure 1B**). As expected, the rationally designed protein self-assembled as monodisperse nanoparticles of 13.5 nm (**Annex 2, Figure 2C-D**) and presented GFP fluorescence for subsequent imaging quantification.

Regarding in vitro behaviour, different experiments were performed to determine whether generated proapoptotic nanoparticles were able to bind and internalize CXCR4⁺ HeLa (cervix cancer) and SW1417 (colorectal cancer) cells (**Annex 2, Figure 2A**). In fact, in time-dependent experiments (**Annex 2, Figure 2B**) it was observed a receptor dependent penetration of T22-targeted nanoparticles. Interestingly, internalization was reduced in both tested cell lines when pre-treated with AMD3100 (**Annex 2, Figure 2C**). In parallel, T22-BAK-GFP-H6 internalization was demonstrated using confocal microscopy and observing green fluorescent material in perinuclear regions (**Annex 2, Figure 2D-E**). Due to the highly specific penetrability observed in vitro, we decided to perform in vivo experiments using a mouse model of CXCR4⁺ colorectal cancer for biodistribution and therapeutic effect studies in tumour tissues.

DISCUSSION

Systemic administration of T22-BAK-GFP-H6 nanoparticles led to an accumulation of the nanomaterial in tumour tissues, with an accumulation peak at 5 h (ex vivo fluorescence observed) (Annex 2, Figure 3A, B and C). Interestingly, no significant renal accumulation, aggregation in lungs or toxicity was observed in non-tumoral relevant organs (Annex 2, Figure 2D, E and F). Specially, the absence of material in kidney indicates how stable the oligomers are in plasma, as monomeric or disassembled proteins although being targeted to tumour markers, accumulate in kidney¹³³. Moreover, therapeutic experiments demonstrated that T22-BAK-GFP-H6, unlike the non-therapeutic version (T22-GFP-H6) was able to induce in vivo cellular death through caspase-3 activation followed by PARP proteolysis (mediated by caspase-3). Moreover, the presence of apoptotic bodies, necrotic areas in tumour tissues and reduction of mitotic figures was also detected through different techniques (Annex 2, Figure 4).

Translational application

At this point, we wondered if these results were reproducible using any other therapeutic domain, to generate a platform for the generation of intrinsically therapeutic protein nanoparticles. For that, we selected **PUMA**^{200,201} (p53 up-regulated modulator of apoptosis) another human proapoptotic factor. PUMA is a BH3-only proapoptotic protein with a dual role²⁰². First, it interacts with antiapoptotic proteins²⁰³ (Bcl-2 and Bcl-XL) through the BH3 domain. Moreover, it is able to activate BAX and BAK, leading to mitochondrial dysfunction and cell death²⁰⁴. Interestingly, good results were also obtained in this model (Annex 2, Figure 5), being possible to generate T22-PUMA-GFP-H6 nanoparticles, which were efficient in vitro and in vivo, like the previous T22-BAK-GFP-H6 model.

Additionally, promising results obtained encouraged us to try with a completely different cytotoxic protein (not discussed in this thesis), the **antimicrobial peptide GWH1** (Annex 2, Figure 5B), which is a pore-forming agent.

All things considered, we have demonstrated and discussed the feasibility of engineering proapoptotic factors as building blocks for the development of therapeutic, self-assembling protein-only nanoparticles targeted to CXCR4 malignancies (**Annex 2**). It is noteworthy that the studied multifunctional nanoparticles were easily produced in a single step through recombinant DNA technologies devoid of any additional conjugation step or presence of heterologous chemical drugs.

4. Development of smart toxin-based vehicle-free nanoparticles

The results obtained using proapoptotic domains (BAK and PUMA), although being very successful, resulted less potent than we would expect initially (**Annex 2**). One possibility is that mild therapeutic effects are a consequence of the already described lysosomal degradation. As the engineered proapoptotic constructs (T22-BAK-GFP-H6 or T22-PUMA-GFP-H6) do not contain any endosomal escape peptide that can increase the amount of protein able to reach the cytoplasm and therefore reduce the loss of active protein, the therapeutic effect observed can be a result of this phenomenon.

GFP protein is a widely used cell tracking agent, added in our constructs as a scaffold protein too. In this context, being focused on the treatment of malignancies, GFP becomes a dispensable segment in the whole multifunctional domain. Additionally, from a clinical point of view, GFP presence can be a concerning issue regarding immunogenicity and cytotoxicity for the approval of a protein drug by medical regulatory agencies²⁰⁵. Therefore, if we get rid of GFP we would be minimizing even more the complexity, using only crucial stretches for targeting, self-assembling and therapeutic purposes, avoiding any useless inactive material (**THIRD OBJECTIVE**).

For all these reasons, we aimed to go a step further and select other cytotoxic proteins, previously studied through extensive bibliographic research (**Review 1 and Annex 1**) while **removing GFP protein**. Among all cytotoxic domains present in nature, toxins are highly potent candidates that can be applied in a therapeutic context¹⁷⁴. Indeed, they can

be transferred to our system for the development of toxin-based self-assembled and self-delivered protein nanoparticles (**SECOND OBJECTIVE**).

Microbial and plant toxins have been already used for the development of recombinant drugs. The extreme lethality exhibited by toxins makes them particularly good candidates for their use in oncology. However, cancer treatment is not only about killing but also doing it selectively²⁰⁶. For that, it is desirable to use cell targeting moieties that direct the treatment toward a specific tumour marker. In fact, there are interesting examples following this principle that have reached the clinics (Denileukin diftitox, Ontak^{169,207,208}) or are under clinical trials (Exotoxin A^{209,210}). Both examples correspond to modified versions of diphtheria toxin from *Corynebacterium diphtheriae* and exotoxin A from *Pseudomonas aeruginosa*, respectively.

Diphtheria toxin and **exotoxin A** can be divided in three functional domains: catalytic, translocation and receptor-binding domain (**Article 2, Figure 1A**). They perform toxicity through the ADP-ribosylation of eukaryotic elongation factor 2 (eEF-2), causing irreversible synthesis inhibition and cell death (**Article 2, Figure 1C**). Once toxins are internalized through endocytosis, pH acidification promotes **furin-mediated cleavage** between the catalytic and the translocation domains (remaining together due to the presence of disulphide bonds). Moreover, acidic pH induces a change in the conformation of the translocation domain, leading to an insertion through the **endosomal membrane** and release of the catalytic domain to the cytoplasm (where reduction of the disulphide bond separated both domains). Therefore, we could say that both toxins present a native endosomal escape activity that promotes the release from endosomes to the cytoplasmic compartment^{73,74,211}. In the case of exotoxin A, the toxin is trafficked through the Golgi apparatus and endoplasmic reticulum before reaching the cytoplasm. Interestingly, the presence of furin cleavable sites generates a **pH-dependent toxin**, whose activity is only performed when released from any other adjacent segments in the cytoplasmic compartment. Considering the intrinsic properties of both toxins, our aim was to engineer stimuli-responsive (pH-dependent) toxin-based nanoparticles able to discharge the targeting agent upon cell internalization (**FOURTH OBJECTIVE**).

For the design of toxin-based nanoparticles only indispensable active segments were used. Following previous designs, truncated toxins were fused to T22 and his-tag (**T22-DITOX-H6 and T22-PE24-H6**), devoid of GFP protein (**Article 2, Figure 1B**). DITOX refers to the catalytic and translocation domain of diphtheria toxin. However, PE24 contains a de-immunized version of the catalytic domain of *Pseudomonas aeruginosa* exotoxin A. Moreover, a KDEL sequence was added to T22-PE24-H6 to promote a higher binding efficiency to KDEL receptors found in Golgi apparatus during the intracellular stage and further endosomal escape. Additionally, two furin cleavage sites (naturally present in each toxin) were included to promote the intracellular release of ligand-free toxins (**Article 2, Figure 1B**).

Engineered toxins were successfully produced (using *E. coli* as microbial cell factory) and purified. Physicochemical results obtained by mass spectrometry (MALDI-TOF) (**Article 2, Figure 3A**) and Western Blot (**Article 2, Figure 2A**) demonstrated that both eluted samples were extremely pure, and no proteolysis occurred during protein production. As expected, both recombinant proteins formed self-assembled nanoparticles of 30-90 nm (**Article 2, Figure 2**) as determined by DLS and FESEM. Importantly, it has been described that oligomerized T22-DITOX-H6 presents β -structure enrichment compared to the parental monomeric version, followed by an improved thermostability (**Annex 3, Figure 3C-D**), suggesting that self-assembled nanoparticles are favoured with a higher stability when interacting one to each other through non-covalent interactions.

Cytotoxic assays demonstrate that engineered toxins present a selective highly potent therapeutic effect, as they are able to reduce cell viability in diverse CXCR4⁺ cell lines, but not in a CXCR4⁻ (**Article 2, Figure 4B left**). Additionally, therapeutic specificity has been confirmed as AMD3100 and T22-GFP-H6 protein pre-incubation was able to inhibit cytotoxicity (**Article 2, Figure 4B right**).

After succeeding in vitro experiments, we tested the behaviour of T22-empowered toxins in vivo, using a CXCR4⁺ colorectal cancer mouse model. Single-dose experiments were performed to study the apoptotic induction by nanoparticles (**Article 2, Figure 6A**). Obtained results showed a high level of apoptosis in tumour tissues (with a peak at 24 h

DISCUSSION

and 48 h for T22-DITOX-H6 and T22-PE24-H6, respectively) (Article 2, Figure 6B). However, no apoptosis was detected in organs such as liver or kidney. Repeated-dose experiments with T22-DITOX-H6 showed a 5.8-fold reduction in tumour volume, compared to the buffer-treated control group. This result was associated to a 3-fold increase in the number of apoptotic figures in the tumour tissue (Article 2, Figure 7B left). T22-PE24-H6 nanoparticle caused a 2.3-fold reduction in tumour volume, related to a 3.8-fold increase in the apoptotic bodies (Article 2, Figure 7B right). Body weight between treated and non-treated groups showed no significant differences in both toxins (Article 2, Figure 7C).

All in all, the outstanding results obtained in vivo, clearly suggest the feasibility of application of nanostructured toxins in a real therapeutic context. **For the first time, herein we have demonstrated that microbial toxins can be engineered (following the nanoarchitectonic principle described in our group) as building blocks for the development of potent therapeutic, self-delivered protein-only nanomedicines against CXCR4⁺ cancers.**

Comparing these toxin-based candidates with the ones previously developed, based in proapoptotic domains (Annex 2), it has been minimized the amount of irrelevant and inactive bulk material, as GFP protein has been removed without any deleterious effect. We were able to obtain self-assembled nanoparticles bearing only indispensable functional segments to the whole rational design. Therefore, the toxic domain itself has a dual role and act as a therapeutic and scaffold protein simultaneously, devoid of any heterologous carrier.

All things considered, herein we have proved the feasibility of engineering microbial toxins as building blocks for the development of potent therapeutic, self-assembling vehicle-free protein-only nanoparticles devoid of any bulk material.

Going even a step further, we have developed smart stimuli-responsive pH-dependent nanoparticles able to release the catalytic domain from the already used T22 (added for self-assembling, cell-targeting and biodistribution purposes) to increase as much as

possible, the subsequent cytotoxic effect. In this work, we demonstrate a dramatic increase of the toxin activity when it is able to release the N-terminal fragment from adjacent peptides, comparing the same construct without furin cleavage site (F-). Therefore, it is crucial that the toxins developed here keep the N-terminal free of any additional sequence so that they can fully perform their cytotoxic potential (Article 2, Figure 4C).

After de novo rational design of intrinsically cytotoxic nanoparticles through the insertion of furin cleavable sites we have obtained stimuli-responsive nanoparticles able to discharge accessory segments under acidic conditions.

Translational application

So far, it has been possible to engineer microbial toxins as **smart nanoscale vehicle-free entities** for targeted therapies. At that point, we wondered if it was possible to translate the rational design performed (adding cleavage sites and KDEL motifs) to any toxin type trying to improve them to reach the smartest and most potent toxin possible.

In the bibliography it is described that another extremely lethal toxins in nature is **ricin**, produced by the plant *Ricinus communis*^{212,213}. In fact, it has been regarded as a potent drug component mainly in the treatment of leukaemia and lymphoma (Annex 1, Table 2). Being such a promising candidate, ricin-derived **T22-mRTA-H6** protein was designed (Annex 4, Figure 1A) following the nanoarchitectonic principle that induces the formation of nanostructured nanoparticles¹³³. Protein production was performed using *E. coli* as expression system. Subsequently, protein purification was conducted using His-based affinity chromatography. A single protein size of 35.91 kDa was detected through Western Blot (Annex 4, Figure 1B) and confirmed by MALDI-TOF. Moreover, protein assembly was observed as 11 nm-sized nanostructures by DLS and FESEM (Annex 4, Figure 1C-D). Nanoscale sizes are highly relevant (as previously mentioned in the introduction) for the improvement of cellular penetrability, stability, EPR effect and reduction of renal clearance. mRTA domain corresponds to a modified (N132A) version

DISCUSSION

of ricin A chain, for the reduction of previously observed vascular leak syndrome associated to ricin administration^{212,213}. Moreover, through rational design, two additional fragments were added. **Furin cleavage site** was added for the release of accessory sequences that can interfere in the final cytotoxic activity of ricin catalytic domain, whereas **KDEL motif** was incorporated for endosomal escape purposes. The combination of the different motifs mentioned with the toxin, dramatically improves (100-fold) the previously described cytotoxic effect ($IC_{50} = 1 \times 10^{-6}$ M in HeLa cells)²¹⁴ (**Annex 4, Figure 2A**). Additionally, non-cytotoxic activity in CXCR4⁻ cell lines supports efficient therapeutic selectivity of the nanostructured toxin.

As expected, the therapeutic activity was also preserved *in vivo*, when using a disseminated AML (acute myeloid leukaemia) mouse model (**Annex 4, Figure 5**). After systemic administration, there was a dramatic reduction of leukemic cells (in affected organs such as backbone, hindlimbs, liver or spleen (**Annex 4, Figure 5B**)). Moreover, histopathology experiments after administration reveal that no toxicity is observed in off-target organs (**Annex 4, Figure 6**).

Altogether, we have succeeded developing an extremely potent and highly selective toxin that is assembled in nanoscale entities devoid of any vehicle that may compromise biocompatibility once administered to the patient.

Proof of concept

The present approximation, represented by diverse tumour targeted microbial and plant toxins, relies on the generation of smart self-assembling, self-delivered therapies formed by homogeneous materials devoid of any non-functional bulk vehicle. Moreover, they are not static but dynamic entities able to discharge an accessory segment of the protein that has been already used to avoid any further negative impact in the therapeutic protein (**Table 6**). In other words, we obtain in a single-step process an all-in-one bespoke therapeutic nanoparticle with all the functionalities needed. Being such a

versatile and potent principle, it should be transversally explored for the increased number of human diseases treatable with recombinant pharmaceuticals.

Table 6. Advantages of smart toxin-based nanostructured antitumoral drugs compared to drug-conjugated nanoparticles.

PROPERTIES	ASSOCIATED ADVANTAGES
Chemically homogeneous	Single-step process, reduced costs
Self-delivered	Reduced off-target effects
Vehicle-free	Minimized bulk material and risks
Intrinsically therapeutic	No conjugation or loading limitations
Self-assembled	Less renal filtration, successful biodistribution
Discharge of accessory segments	High efficiency
No leakage	Reduced toxicities and safety concern

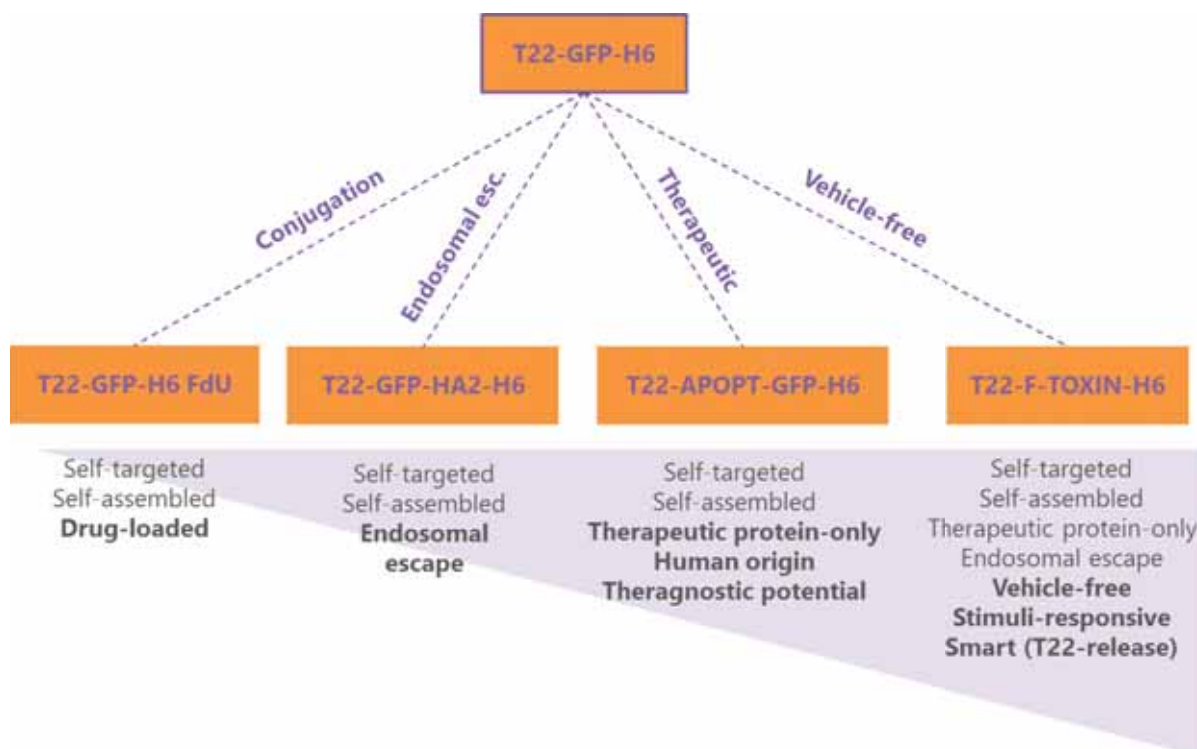


Figure 19. Summary of the recombinant proteins discussed in this PhD thesis (presented in sequential order). Novel properties achieved in each de novo design are in bold.

All the results discussed in this thesis have encouraged us to patent the use of all-in-one protein-only drugs as self-delivered, self-assembled nanoparticles with intrinsic therapeutic activities (**PATENT EP17169722**) (**Annex 6**).

5. Future perspectives

Recombinant protein-only nanoparticles formed by N-terminal cationic peptides and C-terminal His-tag are highly biocompatible materials that present functional and structural versatility. Herein, T22-empowered nanoparticles have been generated bearing different functional domains. Endosomal escape agents and cytotoxic stretches like proapoptotic domains, microbial toxins and plant toxins have been successfully produced as homomeric CXCR4-targeted self-assembled nanoparticles.

Recently, it has been described in our group a novel in vitro procedure that reversibly **disassembles protein homomeric oligomers** and controls their subsequent re-assembling, to form **heteromeric nanoparticles** (**Annex 5**). A combination of imidazole and salt was able to disrupt building blocks' electrostatic interactions and prompt oligomers' disassembling in a reversible manner (as removal of the previously added agents through dialysis recovered nanoparticle formation). Specifically, **T22-GFP-H6** and **T22-BFP-H6** (blue fluorescent protein) nanoparticles (**Annex 5, Figure 1A-B**) were disassembled and reassembled to finally obtain hybrid T22-GFP-H6/T22-BFP-H6 nanoparticles, containing both building blocks in a single heteromeric self-assembled entity as verified by FRET (**Annex 5, Figure 3A-B top**). The formation of **hybrid nanoparticles** dramatically enlarges the tunability and manipulability of protein-based materials for their use in nanomedicine.

In the context of cell-targeted delivery, this technique results extremely promising as it also enables the development of **dual targeted therapies**²¹⁵ (bispecific or biparatopic), combining different ligands (**Annex 5, Figure 3A-B bottom**). The selected ligands could bind to different epitopes of the same receptor (biparatopic vehicles, **Figure 20, bottom**) or to different cell-markers (bispecific vehicles), like natural viruses do during infection

processes. HIV infects host cells through dual targeting using gp120 and gp40, which recognize CXCR4 and CCR5, respectively²¹⁶. In CXCR4-targeted therapies, designing biparatopic nanoparticles would be a promising alternative for the improved delivery and selectivity towards CXCR4⁺ cells using T22 and another ligand specific for CXCR4 receptor.

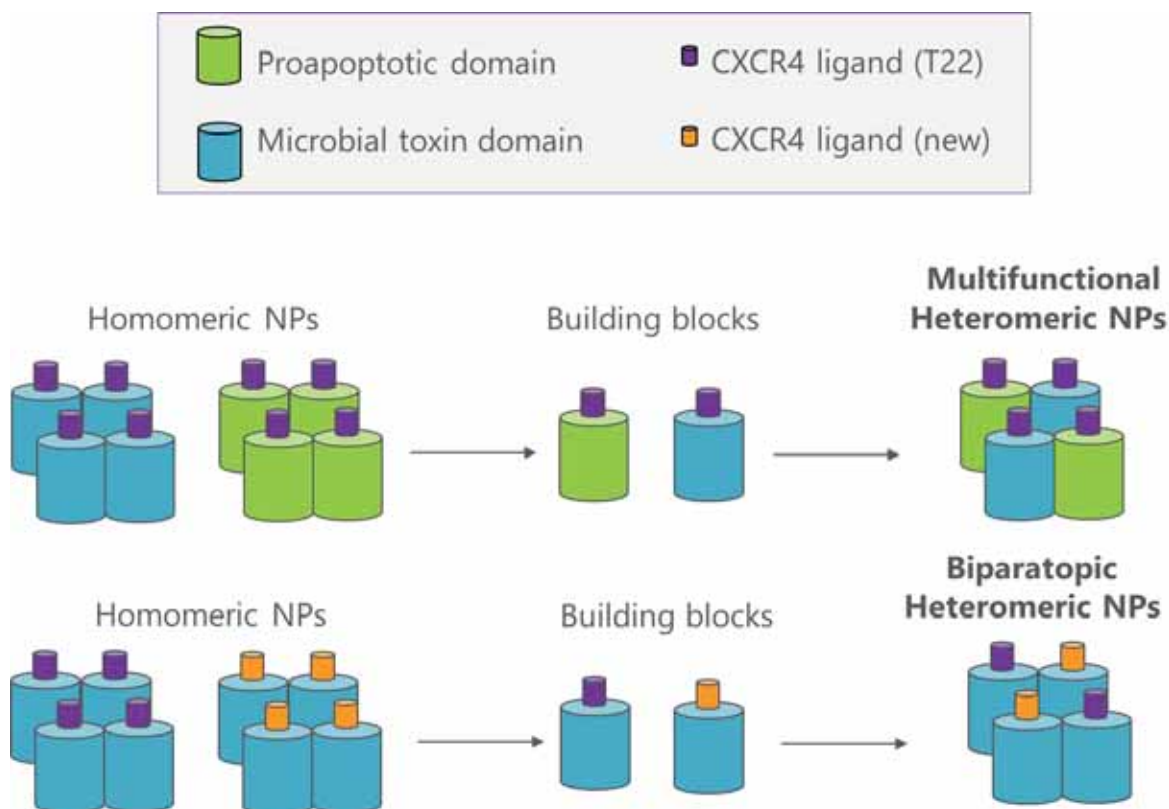


Figure 20. Design of heteromeric protein nanoparticles. Protein homomeric nanoparticles are reversibly disassembled into building blocks and further oligomerized mixing two different subpopulations. Schematic representation of hybrid therapeutic nanoparticles formation, bearing proapoptotic and toxic domains are represented (top). Schematic representation of hybrid CXCR4-targeted nanoparticles formation adding different ligands that recognize diverse epitopes in the same receptor (bottom). Adapted from [Annex 5](#).

On the other hand, diverse biological activities could be incorporated to hybrid nanoparticles (following the T22-GFP-H6/T22-BFP-H6 model). In the discussion, intrinsically therapeutic proteins have been successfully produced as potent homomeric self-assembled nanoparticles (BAK, PUMA, DITOX, PE24 and mRTA). The combination of these cytotoxic building blocks could lead to the clinical use of combined potent therapies that having a synergistic effect would increase the therapeutic efficacy while using lower doses in the clinics ([Figure 20, top](#)).



CONCLUSIONS

CONCLUSIONS

- Nowadays, there is an increasing interest in the generation of recombinant proteins for clinical use. Approximately, 400 marketed recombinant biopharmaceuticals have been FDA-approved and 1300 candidates are under development.
- In oncology, there is a clear predominance of *E. coli*-produced recombinant pharmaceuticals over mammalian cell-derived recombinant therapies.
- The incorporation of HA2 fusogenic peptide in T22-empowered nanoparticles highly increases cell internalization in vitro, although at expense of a loss of receptor-specificity. For that, experiments are in progress to determine whether such impairment is translated into an inefficient biodistribution in vivo.
- Genetically engineered cytotoxic proteins from different sources (proapoptotic factors, microbial and plant toxins) have been successfully produced as self-assembled, self-delivered protein-only nanoparticles while keeping their intrinsic therapeutic activities.
- It has been demonstrated that the nanoarchitectonic principle described in our group could be translated to unrelated intrinsically therapeutic protein-only nanoparticles, devoid of any conjugated chemical drug. Therefore, it is a suitable platform for the generation of cell-targeted intrinsically therapeutic protein nanoparticles.
- Engineered toxin-based protein assemblies have been successfully produced as chemically homogeneous all-in-one vehicle-free targeted nanomedicines devoid of any voluminous and heterologous material (like GFP). Moreover, they performed outstanding biodistribution and antitumoral effects, observed through tumour volume reduction and absence of off-target toxicity in CXCR4⁺ colorectal cancer mouse models.

CONCLUSIONS

- The incorporation of furin cleavable sites through de novo rational design has enabled the formation of smart stimuli-responsive (pH-dependent) toxin-based nanoparticles able to discharge accessory segments under acidic conditions. Specifically, it has been translated to microbial and plant toxins, proving its flexibility, independently of the cytotoxic domain's origin.
- The generation of smart all-in-one vehicle-free protein nanomedicines is such a versatile and potent principle that results in a promising proof of concept that should be transversally explored for the increased number of diseases treatable with recombinant pharmaceuticals.



ANNEXES

ANNEX 1: REVIEW 2

Protein-based therapeutic killing for cancer therapies

Naroa Serna, **Laura Sánchez-García**, Ugutz Unzueta, Raquel Díaz, Esther Vázquez,
Ramón Manges and Antonio Villaverde

Trends in Biotechnology (2018) 36: 318-335

Impact factor 13.578 BIOTECHNOLOGY & APPLIED MICROBIOLOGY (3/161) D1

Review

Protein-Based Therapeutic Killing for Cancer Therapies

Naroa Serna,^{1,2,3} Laura Sánchez-García,^{1,2,3} Ugutz Unzueta,^{3,4} Raquel Díaz,^{1,2,3} Esther Vázquez,^{1,2,3} Ramón Mangués,^{3,4,*} and Antonio Villaverde^{1,2,3,*}

The treatment of some high-incidence human diseases is based on therapeutic cell killing. In cancer this is mainly achieved by chemical drugs that are systemically administered to reach effective toxic doses. As an innovative alternative, cytotoxic proteins identified in nature can be adapted as precise therapeutic agents. For example, individual toxins and venom components, proapoptotic factors, and antimicrobial peptides from bacteria, animals, plants, and humans have been engineered as highly potent drugs. In addition to the intrinsic cytotoxic activities of these constructs, their biological fabrication by DNA recombination allows the recruitment, in single pharmacological entities, of diverse functions of clinical interest such as specific cell-surface receptor binding, self-activation, and self-assembling as nanoparticulate materials, with wide applicability in cell-targeted oncotherapy and theragnosis.

Antitumor Drugs: Molecular Size, Circulation, and Specificity

Regenerative medicine aims at favoring cell adhesion, viability, and spread under adverse physiological conditions. By contrast, therapies of cancer and of inflammatory or autoimmune diseases (such as Crohn's disease, lupus erythematosus, and multiple sclerosis) are based on effective cell killing. In oncotherapy, the destruction of differentiated cancer cells decelerates tumor growth, while efficient killing of **cancer stem cells** (CSCs, see Glossary; still to be fully accomplished in a clinical context) is expected to control recurrence and metastasis, the primary causes of patient death [1]. Conventional cancer treatments are based on a wide spectrum of systemically administered small molecular weight chemicals (alkylating agents, anthracyclines, microtubule inhibitors, antimetabolites, platinum-based agents, topoisomerase inhibitors, tyrosine kinase inhibitors, and histone deacetylase inhibitors, among others). In the absence of targeting, hepatic and renal damage, and undesired toxicity over other healthy organs, results in numerous life-threatening side effects (Figure 1) including bone marrow toxicity (anemia, thrombocytopenia, and neutropenia), nausea, vomiting, cardiotoxicity, and immunosuppression leading to enhanced susceptibility to infectious diseases. Because systemic toxicity restricts the doses to be administered, drugs do not reach the local concentration necessary for fully effective activity [2]. Insufficient therapeutic effect is also related to the small molecular size of antitumor drugs. Drugs that are below the renal filtration cut-off (estimated to be between 5 and 7 nm [3,4]) are cleared by the kidneys, minimizing their amount in blood and their circulation time (Figure 1). Conjugation to **polyethylene glycol** (PEG) increases drug hydrophilicity, impairs uptake by reticuloendothelial cells, minimizes clearance by neutralizing antibodies, and reduces renal filtration, globally enhancing the therapeutic effect [5]. However, because PEGylation does not add any targeting ability, it does not represent a significant improvement regarding side toxicities. Moreover, reduced circulation time and the absence of selective cell killing in conventional chemotherapeutics have pushed the field towards exploring

Highlights

Targeting cytotoxic drugs in oncology is essential because side toxicities limit reaching effective local doses.

Functionalization of nanoscale drug vehicles has so far achieved a moderate targeting effect. The nanoscale size of drug preparations favors enhanced permeability and retention (EPR) and reduces renal filtration.

Proteins are used as inert nanoscale carriers and as functional targeting agents in the form of antibodies or ligands that bind to tumor cell-surface markers.

Many protein species exhibit potent cytotoxic activities that have been exploited to develop new antitumor drugs.

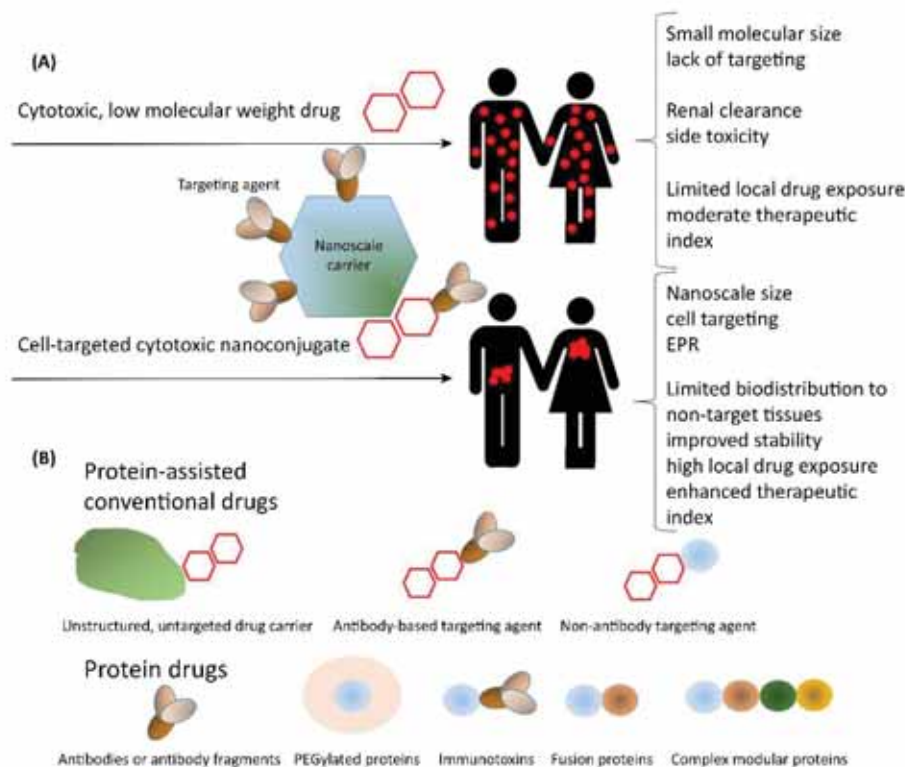
Protein engineering and recombinant DNA technologies allow cytotoxic proteins to be empowered with accessory domains for oligomerization, targeting, endosomal escape, and self-activation. Therefore, the production of self-assembling, self-delivered protein drugs for oncology is becoming feasible.

¹Institut de Biotecnologia i de Biomedicina, Universitat Autònoma de Barcelona, 08193 Cerdanyola del Vallès, Spain

²Departament de Genètica i de Microbiologia, Universitat Autònoma de Barcelona, 08193 Cerdanyola del Vallès, Spain

³Centro de Investigación Biomédica en Red (CIBER) de Bioingeniería, Biomateriales y Nanomedicina, 08193 Cerdanyola del Vallès, Spain

⁴Institut d'Investigacions Biomèdiques Sant Pau and Josep Carreras



Research Institute, Hospital de la Santa Creu i Sant Pau, 08025 Barcelona, Spain

*Correspondence: rmangues@santpau.cat (R. Mangués) and Antoni.Villaverde@uab.cat (A. Villaverde).

Trends in Biotechnology

Figure 1. Spectrum of Current Antitumoral Drugs and their Relevant Features. (A) The chemotherapy of cancer is commonly approached by the use of low molecular weight chemicals (red symbols and dots) that display generic cytotoxicity to both tumor and healthy cells. Their low molecular size (usually <5 nm, permitting renal clearance) and lack of selectivity confer them with an undesirable biodistribution. This is associated with severe side effects and suboptimal drug concentrations in tumor tissues. Pharmacological linkage of these chemicals to nanoscale carriers (bottom, blue) and their functionalization with targeting agents (purple) can minimize renal clearance of the nanoconjugates and increase local drug levels. Connecting the drug to carrier nanoparticles or to targeting agents are mechanistically independent strategies which do not need to be necessarily coupled. As an example, antibody–drug conjugates (ADCs; Box 2) consist of chemical drugs that are directly linked to antibodies against tumor cell-surface targets. (B) Diverse roles of proteins in oncotherapy formulations, either as drug-assisting agents (providing nanoscale size and stability or targeting) or as drugs themselves with intrinsic cytotoxic activities. Depending on the designed functionalities, the protein drugs can be presented in alternative constructions or formulations. Abbreviations: EPR, enhanced permeability and retention; PEGylation, linkage to polyethylene glycol.

nanoscale drug carriers [6], which are nanosized particles to which the drug is associated to form a drug nanoconjugate [7,8]. These vehicles, because of their size scale [9], are thought to play a dual role in (i) allowing the effective anchoring of sufficient ligands of tumor surface markers for cell targeting, and (ii) enlarging the size of the conjugate to over the renal cut-off value, thereby minimizing renal filtration [10] (Figure 1).

Cell-Targeted and Untargeted Nanocarriers

Regarding cell-targeted drug delivery, different types of targeting moieties induce selective accumulation in target tissues by exploiting cell-surface molecules that are overexpressed in some cancer cell lineages (Box 1). Binding to these molecules usually promotes receptor-mediated endosomal uptake of the ligands and linked payloads. Internalization is favored by

Box 1. Cell-Surface Molecular Targets in Cancer

Tumor cells overexpress on their surface different types of molecules (membrane receptors or markers), mainly proteins, that can serve as targets for drug anchorage and specific cell penetration through functionalization with specific ligands [13]. Earlier attempts to target cytotoxic drugs to cancer cells were aimed to fast-dividing tumor cells, leaving tumor-initiating cells unattended. This might result in consequent relapse a few months later because these therapies increase the percentage of CSCs that repopulate the tumor mass and that also account for metastases and resistance to treatment. Therefore, current research on cancer surface markers is mainly focused on CSCs. CSCs are defined by a combination of membrane markers or receptors that are common to different tumors, such as CD44, CD133, CD24, ESA, CXCR4, $\alpha_2\beta_1$, and the multidrug resistance MDR1 and ABCB2 [101,102]. Some of them are particularly associated with specific types of cancer in rapidly expanding catalogues that include CD44, CD24, and ALDH1 with breast cancer [103], CXCR4, LGR5, CLDN1, LY6G6D/F, and TLR4 with colorectal cancer [104–106], CD151 with ovarian cancer [107] and Sox2, Oct4, and CD90 with lung cancer [108]. Because these markers are also expressed by progenitor non-tumor cells [109], the potential risk of side effects is not completely excluded. Therefore, it is a challenge to identify truly selective CSC markers that are sufficiently overexpressed versus progenitor cells to allow safe expansion of the therapeutic window [106]. The development of multispecific or multiparatopic drugs or nanoconjugates should pave the way for more specific delivery into tumor CSCs.

multivalent display of ligands on nanoscale entities, that promotes multiple cell anchorage and favors endosome formation [11]. Aptamers, **monoclonal antibodies** (mAbs), antibody derivatives or mimetics, and receptor specific peptidic ligands [12] have been explored as targeting agents [13]. Avidity (the strength with which a non-covalent attachment to a target molecule occurs) and selectivity (the ability to recognize a very specific target cell or receptor among other cell types or receptor molecules) can be further enhanced by the use of multiparatopic [14] or multispecific [15] agents that bind to different epitopes of a given cell-surface marker or to several markers, respectively, by the recruitment of diverse ligands in the conjugate.

When drugs are required to be relatively large [9], incorporating molecular carriers that are too big might lead to aggregation in the lung and undesired clearance by macrophages of the mononuclear phagocyte system acting in the liver (Kupffer cells) or spleen. This can be avoided by keeping the conjugate size above 7 nm but below 100 nm (in the size range of most viruses) [11]. The nanoscale character of drug-carrier nanoconjugates offers additional advantages such as **enhanced permeability and retention** (EPR) and improved drug stability *in vivo* [10]. The transcellular pores and fenestrae in the tumor vasculature are estimated to measure up to 500 nm [16], allowing the passage of materials up to this size. Targeting agents are usually attached to the carrier (Figure 1). Of course, targeting can be directly conferred to the drug without any carrier by direct chemical coupling between the chemical and a cell-surface receptor ligand. The chemical linker must remain stable during the extracellular phases of the delivery process [17], keep the drug functional, and maintain the proper biodistribution conferred by the targeting agent [18]. **Antibody-drug conjugates** (ADCs, Box 2), using mAbs as drivers, are the best representatives of this category of complexes. The antibody counterpart passively confers a nanoscale size (mostly <10 nm), but usually only monovalent or divalent binding to the target cell.

Many categories of materials (dendrimers, metals, polymers, carbon nanotubes, and proteins, among others) are being explored as partners in drug nanoconjugates. Because most are highly stable and poorly biocompatible, there are reasonable concerns about their intrinsic toxicity, challenging both patient and environment safety [6]. In this context, proteins, as biocompatible macromolecular materials, are especially appealing as drug partners. Protein production in cell factories is undertaken by fully scalable, environmentally friendly, and reliably tested procedures. Since the approval of insulin by the US **Food and Drug Administration** (FDA) in the early 1980s, recombinant DNA technologies for protein engineering and production have been extensively developed [19]. Most protein-drug conjugation methods are based

Glossary**Anticancer peptides (ACPs):**

AMPs that bind to negatively charged molecules on the cancer cell membranes and selectively induce tumor apoptosis or necrosis.

Anti-drug antibodies (ADAs):

these are generated during the immune response against an antigen present in a protein therapeutic after its administration to an organism.

Antibody-drug conjugate (ADC): a chemically coupled complex between a drug and a targeting antibody that offers cell selectivity in the delivery process.

Antimicrobial peptide (AMP): often referred as host defense peptides, they are important players in the innate immune response.

Cancer stem cell (CSC): cancer cells with capacity for self-renewal and differentiation into diverse cell types occurring in tumors. The subset of CSCs differ from more differentiated tumor cells in their unique capacity to initiate and repopulate a tumor.

Diphtheria toxin (DT): an exotoxin secreted by the pathogenic bacterium *Corynebacterium diphtheriae*, the etiological agent of diphtheria.

Enhanced permeability and retention (EPR): local drug retention resulting from the highly permeable tumor vasculature combined with poor lymphatic drainage.

Epidermal growth factor receptor (EGFR): a transmembrane protein that acts as a receptor for specific ligands, such as EGF and transforming growth factor- β , that bind to the receptor to activate cell signaling.

Fab fragment: the antigen-binding fragment of an antibody.

Food and Drug Administration (FDA): the US federal agency responsible for protecting public health by ensuring the safety and efficacy of drugs and biopharmaceuticals.

Fv fragment: the variable region of an antibody; comprises the variable loops of the light and heavy chains that are responsible for antigen binding.

Major histocompatibility complex (MHC): a set of proteins displayed on the surface of cells that recognize foreign antigens to trigger their

Box 2. The Antibody–Drug Conjugate Concept – Successes and Limitations

ADCs represent the earliest and simplest strategy to increase drug aggressivity and selectivity against tumor cells. The first approved ADCs were gemtuzumab ozogamicin (Mylotarg) in 2000, indicated for acute myeloid leukemia, and ibritumomab tiuxetan (Zevalin) and tositumomab (Bexar) in 2002 and 2003, respectively, both indicated for non-Hodgkin lymphoma. In ADCs, mAbs directed against cell-surface markers (Box 1) are used as delivery agents for targeted systemic transport of chemically coupled cytotoxic drugs, ideally inactive in the linked state. Microtubule inhibitors including maytansinoids (DM1/DM4) and auristatins (in form of **monomethyl auristatin E/F**: MMAE, MMAF) rapidly kill proliferating cells and are the most commonly used drugs in ADCs. Cytotoxicity is achieved by receptor-mediated internalization and drug release from lysosomal compartments. Several generations of new ADCs have been developed with increasing efficacies and clinical successes. Humanizing the mAb [110], improving linkers for maximal extracellular stability and intracellular drug release [111], and maximizing the molar ratio between drug and mAb [112] have resulted in improved immunoconjugates. However, they only marginally meet the expected clinical standards regarding efficiency and lack of side toxicity. Frequent life-threatening toxicities are reported for ADCs [113], mainly due to highly potent payload drugs (required because only <1% of the injected ADC dose reaches the tumor [114,115]). The most common adverse effects of ADCs include MMAE-mediated bone marrow suppression leading to neutropenia, infections, and sepsis, and DM4-induced ocular toxicity. MMAF-based conjugates induce thrombocytopenia and ocular toxicity whereas DM1 causes gastrointestinal toxicity, thrombocytopenia, and neutropenia [113]. More than 70 ADCs are currently in clinical development, whereas 20 have been discontinued. As a paradigm of ADC development, gemtuzumab ozogamicin delivers calicheamicin γ 1 (one of the most cytotoxic antitumor drugs so far identified) to CD33-expressing cells through a humanized mAb to which the drug is linked by cleavable bonds. The use of gemtuzumab was discontinued in 2010 because of a lack of improved efficacy regarding free drug and significant side effects including severe myelosuppression, type III hypersensitivity, vein occlusion, and death. Only two ADCs are currently on the market, Adcetris® (brentuximab vedotin, targeting monomethyl auristatin E to CD30⁺ cells and indicated for anaplastic large cell lymphoma and Hodgkin lymphoma) and Kadcyla® (trastuzumab emtansine, targeting emtansine to HER2⁺ cells and indicated for breast cancer). Both are under strict pharmacovigilance. Slightly differently from ADCs, immunocytokine conjugates do not internalize into cells but instead localize their antitumor effect by stimulating the immune system. This is an active area of research with many new compounds entering clinical trials, such as A-dmDT390-bisFv(UCHT1), moxetumumab pasudotox, LMB-2 [anti-Tac(Fv)-P38], and RG7787 [SS1(dsFv)-PE38]. Taking a fully different perspective, mAbs have been also explored for tumor delivery of more complex antitumor entities. Among them, the CD20-targeted delivery of *Salmonella* bacterial cells expressing prodrug-converting enzymes [116] is particularly interesting in the context of prodrug technologies that pursue the enzyme-mediated local (cell-targeted) activation of the drug cytotoxicity [117].

on lysine-amine and cysteine-thiol coupling by amine-activated ester/carboxylic acid and thiol-maleimide chemistries, respectively. The use of non-natural amino acids (oxime ligation, azide-alkyne cyclization) or enzyme-assisted ligation (sortase A, transglutaminase, glycan remodeling) [20,21] is also common. A paradigm of how proteins are incorporated as partners of small molecular drugs to enhance size and stability is abraxane (Nab-paclitaxel) that was first FDA-approved for breast cancer in 2005. Abraxane is a nanostructured complex (sized 130 nm [22]) formed by non-covalent hydrophobic interaction and high-pressure homogenization of human albumin and paclitaxel. This results in a nanoparticle colloidal suspension [23] for use in metastatic breast, pancreatic, and non-small lung cancers. Similar approaches are represented by Nab-rapamycin, that incorporates rapamycin to albumin and is undergoing clinical trials for refractory bladder cancer, and by xyotax (paclitaxel-polyglumex), a nanometric polymer of polyglutamate conjugated to paclitaxel, in clinical trials for the treatment of ovarian or head and neck carcinomas and glioblastoma.

Cytotoxic Proteins

Many proteins from diverse natural sources exhibit potent cytotoxic activities toward mammalian cells, through deleterious enzymatic activities or by precise interventions in the cell cycle. Snakes are a rich source of cytotoxic proteins for oncology and cardiovascular disorders [24]; marine snails, of ion channel blockers [25]; scorpions, of neurotoxins, antitumor agents, and ion channel blockers [26]; and spiders for painkillers, inflammation, and cardiovascular disorders [27]. Furthermore, plants [28] and bacteria [29] have provided a diversity of protein-based antitumor agents. Botox (Allergan), the *Clostridium botulinum* neurotoxin A (also marketed as

processing and the activation of an immune response. They are classified into class I and II. MHC class II proteins are expressed on dendritic cells, macrophages, and B cells.

Monoclonal antibody (mAb): an antibody produced by the controlled culture of a clone of antibody-producing immune cells.

Monomethyl auristatin E (MMAE): a synthetic derivative of dolastatin, a peptapeptide inhibitor of tubulin polymerization with potent antimetastatic activity that was isolated from a species of sea hare.

Monomethyl auristatin F (MMAF): a synthetic derivative of dolastatin, an inhibitor of tubulin polymerization with lower antitumor activity than MMAE.

Platelet-derived growth factor receptor (PDGFR): a cell surface receptor that binds to and is activated for cell signaling by the family of PDGF polypeptides.

Polyethylene glycol (PEG): a polymer of ethylene oxide that, once bound to nanoparticles, inhibits their clearance by the immune system.

***Pseudomonas aeruginosa* exotoxin A (PE):** a bacterial secreted protein that inhibits the elongation factor-2 in protein synthesis.

Ribosome-inactivating protein (RIP): a bacterial or a plant protein toxin that arrests protein synthesis in eukaryotic cells by acting on the ribosome.

scFv fragment: single-chain variable region fragment; a fusion between the variable regions of the heavy and light chains of an antibody that is produced as a recombinant protein.

Therapeutic index (TI): an indicator of drug toxicity versus therapeutic efficacy. TI is determined in animal models as the lethal drug dose for 50% of the treated individuals (LD_{50}) divided by the minimum effective dose, also for 50% of the individuals (ED_{50}).

Vascular endothelial growth factor (VEGF): a hypoxia-induced secreted protein that stimulates the formation of blood vessels in normal tissues and in tumors.

Vascular endothelial growth factor receptor (VEGFR): a cell-surface receptor that is bound and

Dysport, Ipsen; and Xeomin, Merz Pharma) blocks the neuronal release of acetylcholine, resulting in muscular paralysis [30]. As a paradigm of the wide applicability of toxic proteins, the FDA has approved this bacterial toxin to treat chronic migraines, abnormally intense sweating, strabismus, overactive bladder, and muscle spasms, among other therapeutic applications (apart from the better-known cosmetic use in wrinkle reduction). In this context, venom components and toxins, **antimicrobial peptides** (AMPs), and proapoptotic factors emerge as powerful therapeutic candidates. In addition, antibodies directed to particular cell-surface targets, apart from being used as tools for selective delivery, might initiate themselves deadly signaling cascades by acting as indirect cytotoxic drugs. Many natural or modified forms of these proteins are in clinical trials or are already FDA-approved for oncotherapy (Table 1). Furthermore, the flexibility of proteins as tunable macromolecules allows their functional and structural tuning to reach the desired nano-scale size and targeting [31], that might be achieved in modular, multidomain proteins by the appropriate combination of functional stretches [32,33].

activated by its ligand VEGF for cell signaling.

Venoms

Venoms are complex combinations of toxins which are highly bioactive (cytotoxic) molecules that are generally peptides and proteins [34]. They act on exposed cells by diverse mechanisms that include cell-cycle alterations, induction of apoptosis and necrosis [35], cell membrane depolarization [26], cell growth inhibition, cellular membrane disruption, or JAK2/STAT3 down-regulation [36]. Numerous venom protein toxins have been produced in recombinant forms (Table 2), revealing a similar modular architecture [37] that offers additional versatility in the engineering of these agents as multifunctional drugs (Figure 2).

Plant Toxins

Individual toxins are found in plants, amphibians, and microorganisms. Plant toxins are extremely potent molecules. Many of them (such as ricin, saporin, abrin, trichosanthin, bouganin, and gelonin) fall into the category of **ribosome-inactivating proteins** (RIPs), *N*-glycosidases that depurinate a single adenine residue in the 23S/25S/28S rRNA stem-loop, blocking protein translation and leading to cell death. Some RIP plant toxins such as trichosanthin exhibit an inherent preferential activity for cancer cells that blocks the PKC/MAPK signaling pathway and induces apoptosis [38]. Trichosanthin and related toxins are particularly interesting because they also inhibit HIV-1 multiplication owing to their capacity to cleave supercoiled double-stranded DNA into linear and nicked circular DNA [39,40].

Microbial and Animal Toxins

Microbial toxins have been also adapted as drugs. Deltoidin diftotox (Ontak[®]) is an engineered, FDA-approved drug based on the *Corynebacterium diphtheriae* toxin (**diphtheria toxin**, DT) fused to interleukin-2 that targets the toxin to leukemia and lymphoma cells that display IL-2 receptors [41]. *Pseudomonas aeruginosa* exotoxin A (PE) has been also produced through recombinant methodologies in different versions which are in clinical trials to treat mesothelioma and leukemia [42,43]. Among animal toxins, melittin, a 26 amino acid peptide, is the main component of bee (*Apis mellifera*) venom and shows high membranolytic activity [35]. Chlorotoxin is a scorpion peptide (from *Leiurus quinquestriatus*) that can bind selectively to cancer cells via matrix metalloproteinase 2 (MMP-2) and annexin 2 expressed by several malignancies [44].

Antimicrobial Peptides

AMPs are short polypeptides (2–9 kDa) that, in the innate immune system of higher organisms, act as a first line of defense against microbial infections. AMPs show avidity for negatively charged cell membranes and promote cell lysis through pore formation [45]. Some AMPs,

Table 1. Representative Examples of Cytotoxic Antitumor Drugs Involving Proteins and Their Main Side Effects*

Drug	Marketed/in trials	Structure/target molecule	Pharmacological indication	Adverse effects	Refs
Chemical drugs					
Protein-stabilized nanoparticles					
Paclitaxel polyglumex	Xyotax	Paclitaxel-poly-L-glutamic acid macromolecular nanoparticle conjugate	Advanced non-small cell lung cancer, recurrent ovarian or colorectal cancer	Neurological toxicity (severe neuropathy), hematological toxicity	[81]
Nab-paclitaxel	Abraxane	Albumin-bound paclitaxel nanoparticle formulation	Metastatic breast cancer, advanced non-small cell lung cancer, pancreatic carcinoma	Electrocardiogram abnormality, peripheral sensory neuropathy, dehydration, nausea	[82]
Protein drugs					
mAbs					
Trastuzumab	Herceptin	Binds to the extracellular domain of HER2 to inhibit the growth of HER2 ⁺ tumors	Metastatic HER2 ⁺ breast cancer, metastatic HER2 ⁺ gastric cancer	Cardiomyopathy, heart failure, infusion reactions (dyspnea, hypoxia, interstitial pneumonitis), nephrotic syndrome	www.upToDate.com/online/
Cetuximab	Erbix	Binds to EGFR, HER1, and c-ErbB-1, inhibiting EGF binding, leading to tumor cell apoptosis and inhibition of tumor growth	K-Ras wild-type metastatic colorectal cancer, head and neck cancer, squamous cell carcinoma	Cardiopulmonary arrest, acneiform rash, hypomagnesemia, infusion reactions, hypotension, loss of consciousness, shock, myocardial infarction, interstitial lung disease	www.upToDate.com/online/
Bevacizumab	Avastin	Binds to VEGF-A, preventing its association with endothelial receptors Fl-1 and KDR to block endothelial proliferation, inhibiting angiogenesis and tumor growth	Metastatic cervical, colorectal, or renal cell carcinomas, glioblastoma, non-small cell lung cancer, epithelial ovarian cancer	Gastrointestinal fistula and perforation, heart failure, hemorrhage, hypertension, infusion reactions, necrotizing fasciitis	www.upToDate.com/online/
Olisatumab	Lartuvo	Binds to PDGFR- α , preventing PDGF-AA, PDGF-BB, and PDGF-CC binding to block growth and angiogenesis in sarcomas	Soft tissue sarcoma	Nausea, vomiting, diarrhea, hematopoietic toxicity, infusion reaction, hypotension, anaphylactic shock, cardiac arrest	www.upToDate.com/online/
Ipilimumab	Yervoy	Binds to CTLA-4 on cytotoxic T cells, enhancing T cell immune responses against tumors	Unresectable or metastatic melanoma, adjuvant treatment of cutaneous melanoma	Life-threatening immune-mediated dermatitis, colitis and neuropathies, endocrine disorders,	www.upToDate.com/online/

Table 1. (continued)

Drug	Marketed/in trials	Structure/target molecule	Pharmacological indication	Adverse effects	Trials
Nivolumab	Opdivo	Binds to the PD-1 receptor, blocking PD-L1 and PD-L2 binding and restoring antitumor T cell immune response	Metastatic colorectal, head and neck, squamous, non-small cell lung, renal cell, and urothelial carcinomas, Hodgkin lymphoma, and metastatic melanoma	Hepatotoxicity, ophthalmic toxicity Adrenal insufficiency, immune-mediated rash, type 1 diabetes, encephalitis, colitis, thyroiditis, nephritis, hepatitis, pneumonitis, hypophysitis, infusion reactions	www.updatelabs.com/online/
Multispecific antibodies					
Catumaxomab	Removab	Trifunctional bispecific (EPCAM and CD3) mAb binding tumor, T cells, and Fc region to activate immunity	Malignant ascites due to epithelial carcinomas	Lymphopenia, abdominal pain, nausea, vomiting, diarrhea, pyrexia, fatigue, chills, pain	[83]
Bintumomab	Blincyto	Bispecific mAb that binds to CD19 on B cells and CD3 on T cells	Relapsed or refractory B cell precursor acute lymphoblastic leukemia	Cytokine release syndrome, neurological toxicity	[84]
Cergutuzumab amunlekin	In clinical trials	IL-2 variant (IL2v) moiety, bivalent carcinoembryonic antigen (CEA) mAb	Locally advanced and/or metastatic carcinoembryonic antigen-positive solid tumors	Fever, chills, flu-like symptoms, nausea, diarrhea, hypotension	[85]
PEGylated proteins					
Pegaspargase	Onaspar	PEGylated bacterial asparaginase	Acute lymphoblastic leukemia, extranodal natural killer/T cell lymphoma	Delayed hypersensitivity reactions, neurotoxicity, hepatotoxicity	[86]
Peginterferon	PegINTRON	PEGylated Interferon	Melanoma	Neuropsychiatric disorders, bone marrow suppression, autoimmune disease, acute hypersensitivity	NIH database https://clinicaltrials.gov/ct2/show/study/NCT00238329
Immunotoxins					
A-dimDT390-bisFv(UCHT1)	In clinical trials	Anti-CD3-gamma-epsilon Fv fragments-modified form of DT	Cutaneous T cell lymphoma	Fever, chills, edema, hypalbuminemia, hypotension, transaminitis	[87]
Moxetumumab pseudotox	In clinical trials	Anti-CD22 mAb-modified PE fragment	Relapsed and refractory hairy cell leukemia, acute lymphoblastic leukemia	Hypalbuminemia, aminotransferase elevations, edema, headache, hypotension, nausea, fatigue	[88]

Table 1. (continued)

Drug	Marketed/in trials	Structure/target molecule	Pharmacological indication	Adverse effects	Trials
LMB-2 (anti-TacFv-F38)	In clinical trials	Anti- α subunit IL-2R (CD25) mAb-modified PE fragment	Hairy cell leukemia, cutaneous T cell lymphoma, chronic lymphocytic leukemia	Reversible cardiomyopathy, transaminase elevations, fever	https://clinicaltrials.gov/ct2/show/study/NCT00321555
RG7787 SS1(osFv)-PE38	In clinical trials	Mesothelin-binding SS1 Ab-modified PE fragment	Mesothelioma, triple-negative breast cancer, gastric cancer	Edema, hypalbuminemia, fatigue, vascular leak syndrome	https://clinicaltrials.gov/ct2/show/study/NCT00024887
Fusion proteins					
Aliberscept	Zaltrap	VEGFR1 and 2 fragments-Fc human IgG1 fusion protein	Metastatic colorectal cancer	Hemorrhage, gastrointestinal perforation, hypersension, infection	[87]
Etanerscept	Ertoral	Tumor necrosis factor receptor-Fc human IgG1 fusion protein	Lymphoma and other malignancies	Tuberculosis, fungal or viral infections, injection site reaction	https://clinicaltrials.gov/ct2/show/study/NCT00201682
EphB4-HSA	In clinical trials	EphB4 extracellular domain fused to human serum albumin acting as decoy receptor	Advanced urothelial, head and neck, non-small cell lung carcinomas and melanoma	Stevens-Johnson syndrome, toxic epidermal necrolysis, peripheral edema, hematotoxicity	https://clinicaltrials.gov/ct2/show/study/NCT01642342 and NCT0271756
Denileukin difitox	Ontak	Interleukin 2-DT fragments A and B fusion protein	Cutaneous T cell lymphoma	Influsion reactions, hepatotoxicity, visual loss, vascular leak syndrome	[88]
OXS-1550 (DT2219ARL)	In clinical trials	Bispecific scFv anti-CD19 and anti-CD22 mAb-modified form of DT fusion protein	Relapsed/refractory B cell lymphoma or leukemia	Peripheral edema and hypalbuminemia	https://clinicaltrials.gov/ct2/show/study/NCT02370160

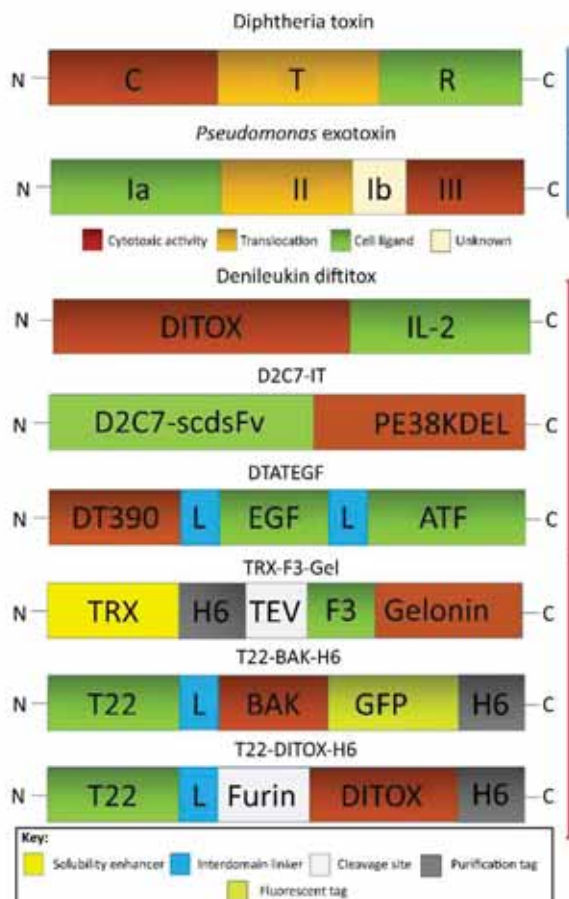
*The list is not exhaustive but includes the most explored/used agents.

Table 2. Representative Examples of Main Cytotoxic Proteins Explored as Antitumor Drugs Produced as Recombinant Versions in Bacterial Cell Factories

Protein	Source	Mechanism of action	Therapeutic application	Recombinant protein (producing organism)	Cancer tested	Refs
Proapoptotic						
BID	Homo sapiens	Activator; interacts with high affinity to all antiapoptotic proteins and directly activates BAX and BAD	Proapoptotic	<i>E. coli</i> RosettaBlue (DE3), <i>E. coli</i> M15, <i>E. coli</i> BL21 (DE3)	Breast, ovarian, and prostate cancer	[65]
PUMA	Homo sapiens	Activator; interacts with high affinity to all antiapoptotic proteins and directly activates BAX and BAK	Proapoptotic	<i>E. coli</i> BL21 and <i>E. coli</i> origins B	Colon cancer	[60]
BAD	Homo sapiens	Sensitizer; interacts with antiapoptotic proteins. High affinity for BCL-2 and BCL-XL	Proapoptotic	<i>E. coli</i> BL21	Glioma, leukemia, and gastrointestinal carcinoma	[63]
Blk	Homo sapiens	Sensitizer; interacts with antiapoptotic proteins. High affinity for BCL-W and BCL-XL	Proapoptotic	<i>E. coli</i> BL21 and <i>E. coli</i> DH5 α	Colon adenocarcinoma	[68]
BAK/BH3	Homo sapiens	Antagonizes antiapoptotic protein function	Proapoptotic	<i>E. coli</i> origins B	Cervical and colon cancer	[60]
Toxin or venom component						
Diphtheria toxin (DT)	<i>Corynebacterium diphtheriae</i> (bacterium)	Inhibition of EF-2 and therefore protein synthesis	Proapoptotic	<i>E. coli</i> BL21 (DE3)	Neuroblastoma, breast cancer, and colon cancer	[69]
Exotoxin A (PE)	<i>Pseudomonas aeruginosa</i> (bacterium)	Inhibition of EF-2 and therefore protein synthesis	Proapoptotic	<i>E. coli</i> BL21 (DE3)	Burkitt's lymphoma	[90]
Chlorotoxin	<i>Leiurus quinquestratus</i> (scorpion)	Chloride channel blocker	Targeting and slightly apoptotic	<i>E. coli</i> BL21 Star™ (DE3)	Glioma	[91]
Melittin	<i>Apis mellifera</i> (bee)	Surfactant activity	Cytotoxicity	<i>E. coli</i> Rosetta	Glioma	[92]
Gomesin	<i>Acanthoscuria gomesiana</i> (spider)	Pore formation	Proapoptotic	<i>E. coli</i> BL21 (DE3)	Epidermoid carcinoma, cervical adenocarcinoma, and breast adenocarcinoma	[93]
Agi-hp1n	<i>Gloydius tsaiys Pallas</i> (snake)	induces apoptosis or necrosis but the mechanism remains to be explored	Anti-metastasis	<i>E. coli</i> BL21 (DE3) and DH5 α	Liver cancer	[94]

Table 2. (continued)

Protein	Source	Mechanism of action	Therapeutic application	Recombinant protein (producing organism)	Cancer tested	Refs
Colombistatins 2, 3, and 4	<i>Bothrops colombei</i> (snake)	Inhibit ristocetin, ADP, collagen	Potent anti-platelet aggregation activity	<i>E. coli</i> BL21 star	Human skin melanoma	[35]
Ricin	<i>Ricinus communis</i> (plant)	Protein synthesis inhibition by the cleavage of a single adenine residue in 28S ribosomal RNA	Anti-proliferative activity	<i>E. coli</i> strain MV1190	Leukemia and lymphoma	[36]
Abrin	<i>Abrus precatorius</i> (plant)	Protein synthesis inhibition by the cleavage of a single adenine residue in the 28S ribosomal RNA	Cell growth inhibition	<i>E. coli</i> BL21(DE3) and Rosetta strains	Melanoma and colon cancer	[97]
Gelonin	<i>Gelonium multiflorum</i> (plant)	Protein synthesis inhibition by the cleavage of a single adenine residue in the 28S ribosomal RNA	Anti-proliferative activity	<i>E. coli</i> BL21 (DE3) and TOP10 strains	Leukemia, glioblastoma, cervical, prostate, and ovarian cancer	[98]



Trends in Biotechnology

Figure 2. Modular Organization of Natural and Representative Engineered Toxins. Natural toxins (blue set) usually show a modular architecture, illustrated here by diphtheria toxin (DT) and *P. aeruginosa* exotoxin A (PE). Engineered versions (red set) have been adapted by modular protein engineering for functional recruitment as antitumor drugs. Denileukin difitox is an immunotoxin that delivers DT (lacking the receptor-binding domain, DITOX) and targets the IL-2 receptor [88]. D2C7-IT is an immunotoxin fusion consisting of single-chain variable-region antibody fragments (**scFv fragments**) of the mAb D2C7 (D2C7-scFv). It targets both the wild-type form (EGFRwt) and the in-frame deletion mutant form (EGFR Δ) of epidermal growth factor receptor (EGFR), and is fused to domains II and III of PE (PE38KDEL) [D2C7-(scFv)-PE38KDEL] [99]. DTATEGF is a bispecific immunotoxin based on a DT version (DT390) that binds to both the EGF receptor (EGFR) and the urokinase-type plasminogen activator receptor (uPAR) [100]. In TRX-F3-Gel the active N-terminal segment of the plant toxin gelonin is targeted by F3, a ligand of nucleolin that is overexpressed by several tumor cell lineages. The thioredoxin (TRX) H6 segment, that is used to enhance solubility and for purification upon recombinant production, is removed *in vitro* by Tev protease [96]. In T22-BAK-H6 the human proapoptotic BAK is targeted by T22, a ligand of the cell-surface tumor marker CXCR4. The construct self-assembles as toroid nanoparticles through the combined presence of T22 and H6 (H6 also acts as a purification tag, and GFP allows visualization of the material) [80]. In T22-DITOX-H6 the C and T domains of DT are presented in a similar way. The inserted furin cleavage site complements the internal site located between the C and T domains. In the endosome, the minimal cytotoxic segment of the construct, namely the C domain, is released upon endosomal acidification. Box sizes are merely illustrative and do not reflect actual proportions.

called **anticancer peptides** (ACPs), selectively bind to cancer cells, inducing tumor apoptosis or necrosis [46,47]. Some ACPs also inhibit tumor angiogenesis [48] and show immunomodulatory activities [49]. Most ACPs are of human or animal origin, but others have been isolated from peptide libraries or have been generated by *de novo* design.

Proapoptotic Proteins

The apoptotic cell death program serves as a natural barrier to tumor development through the extrinsic apoptosis pathway, that is activated by extracellular proapoptotic stimuli, and via the intrinsic pathway, that is mainly controlled by the BCL-2 family of proteins consisting of antiapoptotic and proapoptotic members [50]. Proapoptotic proteins can be categorized into BH3-only proteins (BIM, BID, PUMA, NOXA, BAD, BIK, and HRK) that contain only one BCL-2 homology (BH) domain (BH3), and into multidomain proteins (BAX and BAK) with four BH regions (BH1, BH2, BH3, and BH4) [51]. BH3-only proteins are divided into activators and sensitizers [52]. Activators convert inactive BAX/BAK monomers into pore-forming proteins that assemble into oligomeric complexes in the mitochondrial outer membrane. Sensitizers displace activator BH3 proteins from binding to antiapoptotic members, leaving them free to bind to and activate BAX/BAK [53]. The clinical value of proapoptotic proteins (and many AMPs as well) as drugs in oncology is enriched because of the human origin of these proteins, which administration would not promote the immunotoxicity that is usually associated with heterologous protein drugs.

mAbs

mAbs are not only used as drivers in targeted drug delivery but they can also induce antitumor effects by direct interaction with the target protein [54]. Therefore, they represent the largest group of approved therapeutic proteins in oncology [55]. Most inhibit target receptors involved in tumor epithelial cell growth [such as HER2, **epidermal growth factor receptor** (EGFR) and **platelet-derived growth factor receptor α** (PDGFR- α)], but others inhibit tumor growth indirectly by targeting ligands or receptors involved in tumor angiogenesis, such as **vascular endothelial growth factor A** (VEGF-A) or **vascular endothelial growth factor receptor 2** (VEGFR-2). In addition, the fastest-developing mAb drugs target cancer and immune cell (e.g., T cell) molecules (CTLA-4, PD-1, PD-L1) to reactivate antitumor immune cell function (Table 1). In comparison to untargeted chemotherapy, mAbs display a longer half-life, increased selectivity, and reduced off-target effects. However, their limited extravasation and tumor access promote the development of tumor resistance and dose-limiting toxicities [56].

Engineering Cytotoxic Proteins as Drugs

Most cytotoxic proteins that are approved or under clinical development are not natural but are modified versions with improved functionalities. Toxins and mAbs of non-human origin are generically immunotoxic and require deimmunization-oriented engineering. By contrast, nano-scale organization through multimeric self-assembling, ideally conferring multivalent cell targeting (necessary for non-antibody protein drugs), requires functional recruitment by the fusion of additional protein stretches to the active drug domain (Figure 2). Therefore, protein-based cytotoxic drugs usually have a modular architecture, a concept clearly illustrated by immunotoxins that are simple modular fusions of a toxin (for cytotoxicity) and an antibody or antibody fragment (**Fab fragment**) (for cell targeting).

Deimmunization

Drugs based on non-human proteins contain antigenic peptides that are presented by **major histocompatibility complex** (MHC) II molecules on antigen-presenting cells in a process that activates T cells and stimulates B cells to generate **anti-drug antibodies** (ADAs). In addition, B

cells can be directly activated by multivalent ligands and B cell receptor crosslinking by foreign epitopes [57], which leads to ADA-mediated immune responses during drug treatment upon re-exposure. This event, occasionally inconsequential, may instead neutralize drug effectiveness or cause serious clinical adverse effects which may terminate drug development or lead it to be withdrawn from the market. In this context, hypersensitivity reactions have been reported [58], including acute infusion reactions occurring shortly upon re-exposure (e.g., denileukin difitox, brentuximab vedotin, trastuzumab emtansine), hypersensitivity to unrelated allergens, or the development of autoimmune diseases and flu-like reactions (cergutuzumab, amunaleukin, blinatumomab) associated with cytokine release (Table 1). Less often, therapeutic proteins may be immunosuppressive, leading to frequent and often severe adverse effects such as relapsed bacterial, viral, or fungal infections (e.g., Y90-ibritumomab tiuxetan, etanercept, aflibercept, sitimagene cerdenovec, and talimogene laherparepvec) and complications such as virus-induced neoplasias.

Early immunotoxins (i.e., immune-targeted toxins, see below) lacked a sufficient therapeutic window because of dose-limiting toxicity that induced the life-threatening vascular leak syndrome (edema, weight gain, hypoalbuminemia, and orthostatic hypotension) [59]. Precise protein engineering has been applied to reduce the immunogenicity of PE and DT catalytic fragments to be incorporated to immunotoxins. The portions of these toxins that are not essential for cytotoxic activity or processing have been deleted from the sequence, reducing the molecular weight of the cytotoxic drug component [58]. Moreover, immunotoxicity has been minimized by eliminating antigenic T and B cell epitopes, which limits the immunogenicity of the toxin and reduces the off-target effects that prevent repeated treatment cycles. Deimmunization of a PE fragment (PE38) was achieved by introducing mutations in B or T cell epitopes without compromising antitumor potency, and by deletion of the PE domain II which prevented the induction of vascular leak syndrome [60]. A truncated DT (DT390) has also been deimmunized by point mutations of surface-exposed highly hydrophilic amino acids (R, K, D, E, and Q) to eliminate B cell epitopes without losing antitumor activity [61]. Third-generation immunotoxins consisting of a humanized targeting moiety (e.g., a mAb, **Fv fragment**, or Fab) fused to a deimmunized cytotoxic domain of the toxin are currently entering clinical trials. mAbs tend to offer a higher **therapeutic index** (TI) than small-molecule drugs, namely a wider margin between effective and toxic doses. However, their protein nature and relatively large size may stimulate the immune system, leading to various adverse effects (Table 1). Murine mAbs induce the formation of human anti-mouse antibodies in patients, but protein engineering efforts to humanize them have significantly reduced their immunogenicity [58].

Simple Fusion Technologies

Immunotoxins (Table 1) are composed of catalytic fragments of highly cytotoxic plant or bacterial toxins bound to highly selective targeting mAbs, Fv, or Fab fragments. They kill dividing and non-dividing cells by inhibition of protein synthesis, a unique mechanism of action that is synergistic in combination with genotoxic chemotherapy provided that they show non-overlapping toxicities [62].

An immunotoxin containing the DT A and B fragments fused to human IL-2 was marketed in 2001 as denileukin difitox. It showed activity against several hematological malignancies, particularly cutaneous T cell lymphoma (CTCL). However, the induction of vascular leak syndrome has limited its use. Two additional immunotoxins are currently in clinical assays. A-dmDT390-bisFv(UCHT1) is a fusion protein of DT bound to the Fv fragment of CD3 that targets T cells and is active against CTCL [63], and DT2219ARL consists of a DT fragment bound to Fv fragments of CD19 and CD22 that are active against B lineage leukemia or

lymphoma. In addition, an immunotoxin consisting of PE38 fused to an anti-Tac subunit of IL-2R [LMB-2; anti-Tac(Fv)-PE38] is currently in clinical trials, and shows activity in several hematological neoplasias. RG7787 is composed of an Fab version of the SS1 antibody bound to a modified and less-immunogenic PE fragment. Because it is active in animal models of mesotheliomas without significant adverse effects, it is expected to enter clinical trials soon. Moxetumomab pasudotox is an anti-CD22 Fv fused to PE38 that is being evaluated for the treatment of CD22⁺ B cell malignancies (e.g., hairy cell leukemia, acute lymphoblastic leukemia) which show high response rates [60]. Antibody and antibody fragments have been also used for the targeting of non-toxin cytotoxic proteins such as proapoptotic factors. An example is e23sFv-TD-tBID, which exploits a single-chain anti-HER2 antibody fragment to target the proapoptotic BCL-2 family member BID [64].

From a different approach, simple fusion technologies facilitate selective binding and/or cellular penetration of protein drugs by non-antibody protein agents such as cell-penetrating peptides (CPPs). Proapoptotic peptides fused to the transactivator of transcription (TAT) of human immunodeficiency virus (TAT-BID) [65], Antennapedia homeoprotein (Ant-BAKBH3) [66], or the receptor-binding domain of DT (Bad-BTTR) [67] immediately activate untargeted apoptosis. Other driving peptides used as fusions are gonadotropin-releasing hormone (GnRH, in the form of GnRH-BIK, GnRH-BAK, and GnRH-BAX) [68] and the human granulocyte-macrophage colony-stimulating factor (as hGM-CSF-BAD) [69]. Similar approaches applied to AMPs promote their internalization and mitochondrion-dependent apoptosis in the micromolar range. For example, the natural magainin II (MG2) fused to the CPP penetratin shows an IC₅₀ in the micromolar range [70]. Even more appealingly, MG2 linked to bombesin recognizes a variety of human cancer cells and it shows specific and higher cytolytic effects compared to magainin alone in mice bearing MCF-7 breast tumor grafts [71]. Moreover, the *de novo* designed antimicrobial peptide KLAKLAK fused to a protein transduction domain (PTD) specifically kills endothelial cells [72], and the same peptide fused to HER2-targeting/neutralizing domain targets specifically HER2-overexpressing cells *in vitro* and *in vivo* [73].

More sophisticated versions of fusion technologies generate modular recombinant proteins with diverse functionalities through domains collected from different origins (Figure 2). Functional recruitment enhances the precision in the protein drug delivery process, enabling the polypeptide to perform accurate extra- and intracellular activities. Most of these constructions are produced in very simple microbial cell factories (Table 2) according to generic protein production technologies.

Modular Design of Smart Cytotoxic Proteins

Innovative antitumor drugs still show severe side effects despite these engineering efforts (Table 1), and have therefore driven further drug development based on safer principles. The two-partner fusion strategies discussed above (and also most of the modular approaches) enhance specificity but with still inappropriate nanoscale size and usually with mono- or divalent presentation of the targeting agent. Conventional nanoscale carriers used in nanomedicine, however, impose an undesirable burden of potentially toxic bulk material that prompts urgent exploration of vehicle-free nanostructured drugs able to self-assemble [10]. In this emerging concept, self-assembling protein domains [74] can be used in modular constructs that self-organize as vehicle-free multifunctional protein drugs. For instance, some cationic peptides that are potent ligands of tumor markers promote oligomerization of fusion proteins when combined with polyhistidines. As a paradigmatic example, the peptide T22, a ligand of CXCR4 (overexpressed in >20 human cancers), has been incorporated to histidine-tagged GFP constructions, and makes them self-organize into regular nanoparticles of 12–60 nm that feature

Trends in Biotechnology

CellPress
REVIEWS

multivalent display of this peptide [75,76]. Upon injection, these materials accumulate in tumor tissues in absence of renal filtration [3]. The same principle has been applied to protein-only blood–brain barrier (BBB)-crossing nanoparticles [77] and to CD44-targeted nanoparticles for imaging or drug delivery in breast cancer [78]. The modular architecture of these fusions allows the incorporation of additional functional domains such as fusogenic peptides for enhanced endosomal escape [79]. By exploiting this principle, proapoptotic peptides, AMPs, and microbial toxins have been instructed to self-assemble as cell-targeted nanoparticles ([80] and our unpublished data).

These strategies, together with the accumulated information on cytotoxic proteins, targeting agents, recombinant antibodies, and other functional domains discussed above, should allow fast emergence of truly vehicle-free [10] and cell-targeted cytotoxic nanomedicines that, based on functional recruitment, would necessarily involve multifunctional proteins as core components.

Concluding Remarks and Future Perspectives

Unquestionably, targeting cytotoxic agents in cancer therapies is urgently needed. A plethora of approaches in this regard, using nanotechnological principles, have so far offered improved but still only moderately effective drugs mainly because of associated side toxicities. Empirical observations but also emerging bioengineering concepts point to the design of protein-based cytotoxic drugs as promising alternatives. Proteins are extremely versatile macromolecules produced in recombinant cell factories by cost-effective and fully scalable methods based on recombinant DNA technologies that have been developed and optimized for almost 40 years. In contrast to other biological macromolecules, nanostructured materials, and chemicals, proteins can simultaneously execute, in single-chain polypeptides, all the functions required in oncotherapy (see Outstanding Questions). These activities include efficient cell targeting, potent cytotoxicity, self-assembly to achieve the optimal nanoscale size, and regular oligomerization for multiple and ordered display of cell ligands. The incorporation of functional cassettes by simple fusion approaches allows affinity tags to be recruited for one-step purification from cell factories, endosomolytic agents, protease target sites, and intracellular trafficking domains, among others. Anticipated bottlenecks in the use of these biopharmaceuticals have been already observed and minimized during the development of the >400 protein drugs that are approved for human use. Protein engineering offers valuable approaches for significant deimmunization or ablation of residual drug interactivity with non-target organs (that might lead, for instance, to hepatic toxicity). In this context, an increasing number of protein-only prototypes have already confirmed the possibility of recruiting high functional complexity in simple and safe biological entities. This is in contrast to chemically heterogeneous nanoconjugates in which these functions are provided by the conjugation of different types of molecules, mostly produced by non-biological processes. The expanding catalogues of functional modules (venoms, toxins, proapoptotic factors, AMPs, and others) and cancer-relevant ligands, together with emerging nanobiotechnological principles, are expected to result in a new generation of antitumor drugs that – solely formed from recombinant proteins – might be competitive in the biopharma market for safer, highly efficient, and more precise cancer therapies.

Disclaimer Statement

A.V., E.V., N.S., L.S.G., U.U., and R.M. are coinventors of a patent covering the use of self-assembling, nanostructured cytotoxic proteins.

Outstanding Questions

Can cytotoxic proteins be engineered to fully eliminate their side toxicities through precise protein engineering or humanization?

Are ligands of CSC-specific markers sufficiently potent to allow a significant local accumulation of associated drugs in cancer tissues?

Would protein engineering provide satisfactory tools for competitive large-scale recombinant production of effective protein-only cytotoxic drugs?

Would self-assembling, cell-targeted, and self-delivered protein drugs be a realistic alternative or a synergistic complement to current cancer therapies based on untargeted chemical drugs?

Acknowledgments

We are indebted to grants from the Ministerio de Economía, Industria y Competitividad (MINECO; grant BIO2013-41019-P), the Agencia Estatal de Investigación (AEI), and the Fondo Europeo de Desarrollo Regional (FEDER) (grant BIO2016-76063-R, AEI/FEDER, UE), the Agència de Gestió d'Ajuts Universitaris i de Recerca (AGAUR; 2014SGR-132), and CIBER-BBN (project NANOPROTHER) to A.V.; the Marató de TV3 foundation (TV32013-3930) and the Instituto de Salud Carlos III (ISCIII; PI15/00272 co-funding with FEDER) to E.V.; and ISCIII (PI15/00378 and PIE15/00028, co-funding with FEDER), Marató TV3 (TV32013-2030), AGAUR (2014-SGR-01041, 2014-PRCO0005) and CIBER-BBN (NanoMets 3) to R.M. in support of our research on cell-targeted antitumor drugs. L.S.-G. was supported by AGAUR (2017FL_B100063), N.S. by a predoctoral fellowship from the Gobierno de Navarra, R.D.O. by an overseas predoctoral fellowship from Conacyt (Gobierno de México, 2016), U.U. received a Sara Borrell postdoctoral fellowship from ISCIII, and A.V. an Institució Catalana de Investigació y Estudios Avanzados (ICREA) ACADEMIA award.

Appendix A Supplementary data

Supplementary data associated with this article can be found, in the online version, at <https://doi.org/10.1016/j.tibtech.2017.11.007>.

References

- Miller, K.D. et al. (2016) Cancer treatment and survivorship statistics, 2016. *CA Cancer J. Clin.* 66, 271–289
- Vilaverde, A. et al. (2016) Targeting in cancer therapies. *Med. Sci.* 4, 6
- Céspedes, M.V. et al. (2014) In vivo architectonic stability of fully de novo designed protein-only nanoparticles. *ACS Nano* 8, 4166–4176
- Choi, H.S. et al. (2007) Renal clearance of quantum dots. *Nat. Biotechnol.* 25, 1165–1170
- Mahra, P., N.B. and Dey, R.K. (2016) PEGylation in anti-cancer therapy: an overview. *Asian J. Pharm. Sci.* 11, 337–348
- Lee, M.S. et al. (2017) Nanoparticle-delivered chemotherapy: old drugs in new packages. *Oncology* 31, 198–206
- Perez-Herrero, E. and Fernandez-Medarde, A. (2015) Advanced targeted therapies in cancer: drug nanocarriers, the future of chemotherapy. *Eur. J. Pharm. Biopharm.* 93, 52–79
- Pradkeep, P. et al. (2017) Targeted nanotechnologies for cancer intervention: a patent review (2010–2016). *Expert Opin. Ther. Pat.* 27, 1005–1019
- MÄhrhøj, B. (2013) Nanosize drug delivery system. *Curr. Pharm. Biotechnol.* 14, 1221
- Shin, J. et al. (2017) Taking the vehicle out of drug delivery. *Mater. Today* 20, 95–97
- Unzueta, U. et al. (2015) Towards protein-based viral mimetics for cancer therapies. *Trends Biotechnol.* 33, 253–256
- Chou, L.Y. et al. (2011) Strategies for the intracellular delivery of nanoparticles. *Chem. Soc. Rev.* 40, 233–245
- Yao, V.J. et al. (2016) Ligand-targeted theranostic nanomedicines against cancer. *J. Control. Release* 240, 267–286
- Li, J.Y. et al. (2016) A biparastopic HER2-targeting antibody–drug conjugate induces tumor regression in primary models refractory to or ineligible for HER2-targeted therapy. *Cancer cell* 29, 117–129
- Brinkmann, U. and Kontemann, R.E. (2017) The making of bispecific antibodies. *mAbs* 9, 182–212
- Setyawati, M.J. et al. (2015) Understanding and exploiting nanoparticles' intimacy with the blood vessel and blood. *Chem. Soc. Rev.* 44, 8174–8199
- Polakis, P. (2016) Antibody drug conjugates for cancer therapy. *Pharmacol. Rev.* 68, 3–19
- Chari, R.V. et al. (2014) Antibody–drug conjugates: an emerging concept in cancer therapy. *Angew. Chem.* 53, 3796–3827
- Sanchez-Garcia, L. et al. (2016) Recombinant pharmaceuticals from microbial cells: a 2015 update. *Microb. Cell Fact.* 15, 33
- Beck, A. et al. (2017) Strategies and challenges for the next generation of antibody–drug conjugates. *Nat. Rev. Drug Discov.* 16, 315–337
- Teuchkarna, K. and An, Z. (2016) Antibody–drug conjugates: recent advances in conjugation and linker chemistries. *Protein Cell* Published online October 14, 2016. <http://dx.doi.org/10.1007/s13238-016-0323-0>
- Gradishar, W.J. (2006) Albumin-bound paclitaxel: a next-generation taxane. *Expert Opin. Pharmacother.* 7, 1041–1053
- Sofias, A.M. et al. (2017) The battle of 'nano' paclitaxel. *Adv. Drug Deliv. Rev.*
- Wisheed, H. et al. (2017) Snake venom: from deadly toxins to life-saving therapeutics. *Curr. Med. Chem.* 24, 1874–1891
- Prashanth, J.R. et al. (2014) Cone snail venom: from novel biology to novel therapeutics. *Future Med. Chem.* 6, 1659–1675
- Ortiz, E. et al. (2015) Scorpion venom components as potential candidates for drug development. *Toxicol.* 93, 125–135
- Pineda, S.S. et al. (2014) Spider venom: implications for drug discovery. *Future Med. Chem.* 6, 1699–1714
- Bolognesi, A. et al. (2016) Ribosome-inactivating proteins from plants: a historical overview. *Molecules* 21, 1827
- Mitchell, P. and Gress, T.M. (2004) Bacteria and bacterial toxins as therapeutic agents for solid tumors. *Curr. Cancer Drug Targets* 4, 689–702
- Dressler, D. (2016) Botulinum toxin drugs: brief history and outlook. *J. Neural Transm.* 123, 277–279
- Corchero, J.L. et al. (2014) Recombinant protein materials for bioengineering and nanomedicine. *Nanomedicine* 9, 2617–2628
- Vazquez, E. et al. (2009) Modular protein engineering in emerging cancer therapies. *Curr. Pharm. Des.* 15, 893–916
- Vazquez, E. et al. (2016) Functional recruitment for drug delivery through protein-based nanotechnologies. *Nanomedicine* 11, 1333–1336
- Calvete, J.J. et al. (2017) Protein-species quantitative venomomics: looking through a crystal ball. *J. Venom. Anim. Toxins Incl. Trop. Dis.* 23, 27
- Gajski, G. and Garaj-Vrhovac, V. (2013) Melittin: a lytic peptide with anticancer properties. *Environ. Toxicol. Pharmacol.* 36, 697–705
- Mara, S.K. et al. (2015) Defined nanoscale chemistry influences delivery of peptide-toxins for cancer therapy. *PLoS One* 10, e0125908
- Casewell, N.R. et al. (2013) Complex cocktails: the evolutionary novelty of venoms. *Trends Ecol. Evol.* 28, 219–229

38. Miao, J. et al. (2015) Trichostatin suppresses the proliferation of glioma cells by inhibiting LGR5 expression and the Wnt/beta-catenin signaling pathway. *Oncol. Rep.* 34, 2645–2652
39. Zheng, Y.T. et al. (2000) Anti-HIV-1 activity of trichostatin, a novel ribosome-inactivating protein. *Acta Pharmacol. Sin.* 21, 179–182
40. Li, M.X. et al. (1991) Trichostatin, a potent HIV-1 inhibitor, can cleave supercoiled DNA in vitro. *Nucleic Acids Res.* 19, 6309–6312
41. Manoukian, G. and Hagemeister, F. (2009) Denileukin difitox: a novel immunotoxin. *Expert Opin. Biol. Ther.* 9, 1445–1451
42. Hassan, R. et al. (2014) Phase 1 study of the antimesothelin immunotoxin SS1P in combination with pemetrexed and cisplatin for front-line therapy of pleural mesothelioma and correlation of tumor response with serum mesothelin, mesotheliocyte potentiating factor, and cancer antigen 125. *Cancer* 120, 3311–3319
43. Kräftman, R.J. and Pastan, I. (2015) Immunocytotoxicity in the management of hairy cell leukemia. *Best Pract. Res. Clin. Haematol.* 28, 236–245
44. Dardévil, L. et al. (2015) Chlorotoxin: a helpful natural scorpion peptide to diagnose glioma and fight tumor invasion. *Toxins* 7, 1079–1101
45. Mahlapuu, M. et al. (2016) Antimicrobial peptides: an emerging category of therapeutic agents. *Front. Cell. Infect. Microbiol.* 6, 194
46. Felcio, M.R. et al. (2017) Peptides with dual antimicrobial and anticancer activities. *Front. Chem.* 5, 5
47. Deslouches, B. and Di, Y.P. (2017) Antimicrobial peptides with selective antitumor mechanisms: prospect for anticancer applications. *Oncotarget* 8, 46635–46651
48. Wong, J.H. et al. (2013) Cathelicidins: peptides with antimicrobial, immunomodulatory, anti-inflammatory, angiogenic, anticancer and pro-cancer activities. *Curr. Protein Pept. Sci.* 14, 504–514
49. Hickey, A.L. et al. (2013) Immune modulation by multifaceted cationic host defense (antimicrobial) peptides. *Nat. Chem. Biol.* 9, 761–768
50. Gross, A. (2016) BCL-2 family proteins as regulators of mitochondrial metabolism. *Biochim. Biophys. Acta* 1857, 1243–1246
51. Edlich, F. (2017) BCL-2 proteins and apoptosis: recent insights and unknowns. *Biochem. Biophys. Res. Commun.* Published online July 1, 2017. <http://dx.doi.org/10.1016/j.bbrc.2017.06.190>
52. Glab, J.A. et al. (2017) BH3-only proteins: the thorny end of the ER stress response. *Cell Death Dis.* 8, e2889
53. Shamas-Din, A. et al. (2013) Mechanisms of action of Bcl-2 family proteins. *Cold Spring Harb. Perspect. Biol.* 5, a008714
54. Monarity, A. et al. (2016) Current targeted therapies in the treatment of advanced colorectal cancer: a review. *Thor. Adv. Med. Oncol.* 8, 276–293
55. Ecker, D.M. et al. (2015) The therapeutic monoclonal antibody market. *mAbs* 7, 9–14
56. Dy, G.K. and Adjei, A.A. (2013) Understanding, recognizing, and managing toxicities of targeted anticancer therapies. *CA Cancer J. Clin.* 63, 249–279
57. Yin, L. et al. (2015) Therapeutic outcomes, assessments, risk factors and mitigation efforts of immunogenicity of therapeutic protein products. *Cell. Immunol.* 295, 118–126
58. Grinberg, Y. and Benhar, I. (2017) Addressing the immunogenicity of the cargo and of the targeting antibodies with a focus on demumunized bacterial toxins and on antibody-targeted human effector proteins. *Biomedicines* 5, 28
59. Blythman, H.E. et al. (1981) Immunotoxins: hybrid molecules of monoclonal antibodies and a toxin subunit specifically kill tumour cells. *Nature* 290, 145–146
60. Mazor, R. et al. (2016) Immunogenicity of therapeutic recombinant immunotoxins. *Immunol. Rev.* 270, 152–164
61. Schmolz, J.U. et al. (2015) Mutagenic demumunization of diphtheria toxin for use in biologic drug development. *Toxins* 7, 4067–4082
62. Alewine, C. et al. (2015) Advances in anticancer immunotoxin therapy. *Oncologist* 20, 176–185
63. Frankel, A.E. et al. (2015) Resimma, an anti-CD3epsilon recombinant immunotoxin, induces durable remissions in patients with cutaneous T-cell lymphoma. *Haematologica* 100, 794–800
64. Shan, L.Q. et al. (2008) scFv-mediated delivery of truncated BID suppresses HER2-positive osteosarcoma growth and metastasis. *Cancer Biol. Ther.* 7, 1717–1722
65. Orzechowska, E.J. et al. (2014) Controlled delivery of BID protein fused with TAT peptide sensitizes cancer cells to apoptosis. *BMC Cancer* 14, 771
66. Holinger, E.P. et al. (1999) Bak BH3 peptides antagonize Bcl-xL function and induce apoptosis through cytochrome c-independent activation of caspases. *J. Biol. Chem.* 274, 13298–13304
67. Ichinose, M. et al. (2002) Extracellular Bad fused to toxin transport domains induces apoptosis. *Cancer Res.* 62, 1433–1438
68. Azar, Y. and Lorberboun-Galski, H. (2000) CnFh-Bak/Baw/Bak chimeric proteins target and kill adenocarcinoma cells: the general use of pro-apoptotic proteins of the Bcl-2 family as novel killing components of targeting chimeric proteins. *Apoptosis* 5, 531–542
69. Arignani, A. and Youle, R.J. (2006) A chimeric protein induces tumor cell apoptosis by delivering the human Bcl-2 family BH3-only protein Bax. *Biochemistry* 44, 4074–4082
70. Liu, S. et al. (2013) Penetratin-mediated delivery enhances the antitumor activity of the cationic antimicrobial peptide Magainin II. *Cancer Biother. Radiopharm.* 28, 289–297
71. Liu, S. et al. (2011) Enhancement of cytotoxicity of antimicrobial peptide magainin II in tumor cells by bombesin-targeted delivery. *Acta Pharmacol. Sin.* 32, 79–88
72. Mai, J.C. et al. (2001) A proapoptotic peptide for the treatment of solid tumors. *Cancer Res.* 61, 7709–7712
73. Meschenmoser, K. et al. (2013) Targeting cancer with a bifunctional peptide: in vitro and in vivo results. *In Vivo* 27, 431–442
74. Ferrer-Miralles, N. et al. (2015) Engineering protein self-assembly in protein-based nanomedicines for drug delivery and gene therapy. *Crit. Rev. Biotechnol.* 35, 209–221
75. Rueda, F. et al. (2015) Bottom-up instructive quality control in the biolabification of smart protein materials. *Adv. Mater.* 27, 7816–7822
76. Pisarodona, M. et al. (2017) Intrinsic functional and architectural heterogeneity of tumor-targeted protein nanoparticles. *Nanoscale* 9, 6427–6436
77. Serna, N. et al. (2016) Rational engineering of single-chain polypeptides into protein-only, BBB-targeted nanoparticles. *Nanomedicine* 12, 1241–1251
78. Pisarodona, M. et al. (2014) Intracellular targeting of CD44⁺ cells with self-assembling, protein only nanoparticles. *Int. J. Pharm.* 473, 296–295
79. Sanchez-Garcia, L. et al. (2017) The fusogenic peptide HA2 impairs selectivity of CXCR4-targeted protein nanoparticles. *Chem. Commun.* 53, 4565–4568
80. Serna, N. et al. (2017) Peptide-based nanostructured materials with intrinsic proapoptotic activities in CXCR4⁺ solid tumors. *Adv. Funct. Mater.* 27, 1700919
81. Northfelt, D.W. et al. (2014) Phase 2 trial of paclitaxel polyglumex with capecitabine for metastatic breast cancer. *Am. J. Clin. Oncol.* 37, 167–171
82. Muranaka, T. et al. (2017) Comparison of efficacy and toxicity of FOLFIRINOX and gemcitabine with nab-paclitaxel in unresectable pancreatic cancer. *J. Gastrointest. Oncol.* 8, 566–571
83. Pilanc, K.N. et al. (2016) Dramatic response to catumaxomab treatment for malign ascites related to renal cell carcinoma with sarcomatoid differentiation. *Am. J. Ther.* 23, e1078–e1081

84. von Stackelberg, A. et al. (2016) Phase I/Phase II study of binatumomab in pediatric patients with relapsed/refractory acute lymphoblastic leukemia. *J. Clin. Oncol.* 34, 4381–4389
85. Klein, C. et al. (2017) Cerguhuzumab: a CEA-targeted IL-2 variant-based immunocytokine for combination cancer immunotherapy: overcoming limitations of aldesleukin and conventional IL-2-based immunocytokines. *Oncotarget* 8, e1277306
86. Wei, W. et al. (2017) Effectiveness of pegaspargase, gemtastine, and oxaliplatin (P-GEMOX) chemotherapy combined with radiotherapy in newly diagnosed, stage IE to IIE, nasal-type, extranodal natural killer/T-cell lymphoma. *Hematology* 22, 320–329
87. Scartozzi, M. et al. (2016) Aflibercept, a new way to Target angiogenesis in the second line treatment of metastatic colorectal cancer (mCRC). *Target. Oncol.* 11, 489–500
88. Olsen, E. et al. (2001) Pivotal phase III trial of two dose levels of denileukin difitox for the treatment of cutaneous T-cell lymphoma. *J. Clin. Oncol.* 19, 378–388
89. Choudhary, S. et al. (2016) Targeting c-kit receptor in neuroblastomas and colorectal cancers using stem cell factor (SCF)-based recombinant bacterial toxins. *Appl. Microbiol. Biotechnol.* 100, 263–277
90. Della Cristina, P. et al. (2015) Systematic comparison of single-chain Fv antibody-fusion toxin constructs containing *Pseudomonas* exotoxin A or saporin produced in different microbial expression systems. *Microb. Cell Fact.* 14, 19
91. Wang, X.M. et al. (2013) Recombinant expression and downstream processing of the disulfide-rich tumor-targeting peptide chlorotoxin. *Exp. Ther. Med.* 6, 1049–1053
92. Buhman, J.S. et al. (2013) Active, soluble recombinant melittin purified by extracting insoluble lysate of *Escherichia coli* without denaturation. *Biotechnol. Prog.* 29, 1150–1157
93. Kuzmin, D.V. et al. (2017) Comparative in vitro study on cytotoxicity of recombinant beta-hairpin peptides. *Chem. Biol. Drug Des.* Published online August 16, 2017. <http://dx.doi.org/10.1111/cbdd.13081>
94. Sun, K. et al. (2017) Expression, purification and characterization of a novel recombinant SVTLE, r-αgk1p1n-2, from *Glycydium haysi* Pallas venom gland in *Escherichia coli*. *Protein Expr. Purif.* 136, 7–13
95. Suntravat, M. et al. (2016) Expression, purification, and analysis of three recombinant ECD disintegrins (γ-cobolbatins) from P-II class snake venom metalloproteinases affecting platelet aggregation and SK-MEL-28 cell adhesion. *Toxicol.* 122, 43–49
96. Moshiri, M. et al. (2016) Ricin toxicity: clinical and molecular aspects. *Rep. Biochem. Mol. Biol.* 4, 60–95
97. Gadadhar, S. and Karande, A.A. (2013) Abrin immunotoxin-targeted cytotoxicity and intracellular trafficking pathway. *PLoS One* 8, e68304
98. Ham, S.H. et al. (2017) Molecular tumor targeting of gelonin by fusion with F3 peptide. *Acta Pharmacol. Sin.* 38, 897–906
99. Chandramohan, V. et al. (2013) Construction of an immunotoxin, D2C7-(scd5Fv)-PE38KDEL, targeting EGFRwt and EGFRvIII for brain tumor therapy. *Clin. Cancer Res.* 19, 4717–4727
100. Huang, J. et al. (2012) Intracerebral infusion of the bispecific targeted toxin DTATEGF in a mouse xenograft model of a human metastatic non-small cell lung cancer. *J. Neurooncol.* 109, 229–238
101. Leon, G. et al. (2016) Cancer stem cells in drug resistant lung cancer: targeting cell surface markers and signaling pathways. *Pharmacol. Ther.* 158, 71–90
102. Akban-Birgin, S. et al. (2015) Cancer stem cells, cancer-initiating cells and methods for their detection. *Drug Discov. Today* 21, 836–842
103. Ricardo, S. et al. (2011) Breast cancer stem cell markers CD44, CD24 and ALDH1: expression distribution within intrinsic molecular subtype. *J. Clin. Pathol.* 64, 937–946
104. Sewda, K. et al. (2016) Cell-surface markers for colon adenoma and adenocarcinoma. *Oncotarget* 7, 17773–17789
105. Hirsch, D. and Reid, T. (2016) Targeting colorectal cancer (stem-like) cells using LGR5 directed antibody drug conjugates. *Ann. Transl. Med.* 4, 508
106. Cospedes, M.V. et al. (2016) Cancer-specific uptake of a liganded protein nanocarrier targeting aggressive CXCR4⁺ colorectal cancer models. *Nanomedicine* 12, 1987–1996
107. Madrano, M. et al. (2017) Interrogation of functional cell-surface markers identifies CD151 dependency in high-grade serous ovarian cancer. *Cell Rep.* 18, 2343–2358
108. Yan, X. et al. (2013) Identification of CD90 as a marker for lung cancer stem cells in A549 and H460 cell lines. *Oncol. Rep.* 30, 2733–2740
109. Kim, W.T. and Ryu, C.J. (2017) Cancer stem cell surface markers on normal stem cells. *EMB Rep.* 50, 285–298
110. Safdari, Y. et al. (2013) Antibody humanization methods – a review and update. *Biotechnol. Genet. Eng. Rev.* 28, 175–186
111. Pilow, T.H. (2017) Novel linkers and connections for antibody–drug conjugates to treat cancer and infectious disease. *Pharm. Pat. Anal.* 5, 25–33
112. Hamblett, K.J. et al. (2004) Effects of drug loading on the antitumor activity of a monoclonal antibody drug conjugate. *Clin. Cancer Res.* 10, 7063–7070
113. Donaghy, H. (2016) Effects of antibody, drug and linker on the preclinical and clinical toxicities of antibody–drug conjugates. *mAbs* 8, 659–671
114. Stefan Wilhelm, A.J.T. et al. (2016) Analysis of nanoparticle delivery to tumours. *Nat. Rev. Mater.* 1, 16014
115. Duncan, R. and Gaspar, R. (2011) Nanomedicines under the microscope. *Mol. Pharm.* 8, 2101–2141
116. Massa, P.E. et al. (2013) *Salmonella* engineered to express CD20-targeting antibodies and a drug-converting enzyme can eradicate human lymphomas. *Blood* 122, 705–714
117. Giang, I. et al. (2014) Prodrug applications for targeted cancer therapy. *AAPS J.* 16, 899–913

ANNEX 2: ARTICLE 3

Peptide-based nanostructured materials with intrinsic proapoptotic activities in CXCR4⁺ solid tumors

Naroa Serna, María Virtudes Céspedes, **Laura Sánchez-García**, Ugutz Unzueta, Rita Sala, Alejandro Sánchez-Chardi, Francisco Cortés, Neus Ferrer-Miralles, Ramón Manges, Esther Vázquez, and Antonio Villaverde

Advanced Functional Materials (2017) 27: 1700919

Impact factor 13.325 MATERIALS SCIENCE, MULTIDISCIPLINARY 13/285 D1

Peptide-Based Nanostructured Materials with Intrinsic Proapoptotic Activities in CXCR4⁺ Solid Tumors

Naroa Serna, María Virtudes Céspedes, Laura Sánchez-García, Ugutz Unzueta, Rita Sala, Alejandro Sánchez-Chardi, Francisco Cortés, Neus Ferrer-Miralles, Ramón Mangues,* Esther Vázquez, and Antonio Villaverde*

Protein materials are gaining interest in nanomedicine because of the unique combination of regulatable function and structure. A main application of protein nanoparticles is as vehicles for cell-targeted drug delivery in the form of nanoconjugates, in which a conventional or innovative drug is associated to a carrier protein. Here, a new nanomedical approach based on self-assembling protein nanoparticles is developed in which a chemically homogeneous protein material acts, simultaneously, as vehicle and drug. For that, three proapoptotic peptidic factors are engineered to self-assemble as protein-only, fully stable nanoparticles that escape renal clearance, for the multivalent display of a CXCR4 ligand and the intracellular delivery into CXCR4⁺ colorectal cancer models. These materials, produced and purified in a single step from bacterial cells, show an excellent biodistribution upon systemic administration and local antitumoral effects. The design and generation of intrinsically therapeutic protein-based materials offer unexpected opportunities in targeted drug delivery based on fully biocompatible, tailor-made constructs.

1. Introduction

The systemic administration of drugs in form of nanoconjugates benefits from enhanced drug stability when compared to free molecules.^[1] Valuable additional properties such as cell-targeting might also be merged into a given hybrid composite through the chemical incorporation of functional groups in nanoscale vehicles, taking profit from the high surface/volume

ratio of nanomaterials.^[2] When administered systemically, the resulting drug-loaded conjugates sizing between ~8 and 100 nm escape from renal filtration in absence of aggregation in lung or other highly vascularized organs.^[3] This fact, combined with appropriate physicochemical properties of the material might result in extended circulation time and prolonged drug exposure to target organs, thus enhancing the therapeutic impact and benefits for the patient. Among the diversity of materials under investigation as drug carriers, including metals, ceramics, polymers, and carbon nanotubes, proteins offer unique properties regarding biocompatibility and degradability, that in the context of rising nanotoxicological concerns,^[4] make them especially appealing. As the engineering of protein self-assembling into nano-

structured materials is rapidly progressing^[5] and the control over the final geometry and physicochemical properties becomes tighter,^[6] protein materials are gaining functional and structural versatility as vehicles from chemically coupled drugs. However, many protein species are, themselves, efficient drugs usable in human therapy, as attested by more than 400 protein-based products approved by main medicines agencies.^[7] Therefore, it would be interesting to test if recombinant

N. Serna, L. Sánchez-García, Dr. N. Ferrer-Miralles, Dr. E. Vázquez, Prof. A. Villaverde
Institut de Biotecnologia i de Biomedicina
Universitat Autònoma de Barcelona
Bellaterra 08193, Barcelona, Spain
E-mail: antoni.villaverde@uab.cat

N. Serna, L. Sánchez-García, Dr. N. Ferrer-Miralles, Dr. E. Vázquez, Prof. A. Villaverde
Departament de Genètica i de Microbiologia
Universitat Autònoma de Barcelona
Bellaterra 08193, Barcelona, Spain


N. Serna, Dr. M. V. Céspedes, L. Sánchez-García, Dr. U. Unzueta, R. Sala, Dr. N. Ferrer-Miralles, Prof. R. Mangues, Dr. E. Vázquez, Prof. A. Villaverde
CIBER de Bioingeniería
Biomateriales y Nanomedicina (CIBER-BBN)
Bellaterra 08193, Barcelona, Spain
E-mail: RMangues@santpau.cat

DOI: 10.1002/adfm.201700919

Dr. M. V. Céspedes, Dr. U. Unzueta, R. Sala, Prof. R. Mangues
Biomedical Research Institute Sant Pau (IIB-Sant Pau)
and Josep Carreras Research Institute
Hospital de la Santa Creu i Sant Pau
08025 Barcelona, Spain

Dr. A. Sánchez-Chardi
Servei de Microscòpia
Universitat Autònoma de Barcelona
Bellaterra 08193, Barcelona, Spain

F. Cortés
Servei de Cultius Cel·lulars
Producció d'Anticossos i Citometria
Universitat Autònoma de Barcelona
Bellaterra 08193, Barcelona, Spain

 The ORCID identification number(s) for the author(s) of this article can be found under <https://doi.org/10.1002/adfm.201700919>.

protein drugs might be engineered as self-organizing building blocks of functional nanoparticles, which in this form, would exhibit intrinsic therapeutic activities. This might allow excluding the need of further activation and drug conjugation, as the nanomaterial itself would act as a nanoscale drug (desirably between 8 and 100 nm). In this way, chemically homogenous protein nanoparticles with intrinsic therapeutic activities (like the current plain protein species used in human medicine, -e.g., hormones, growth factors, vaccines, etc.) could be biologically produced in a single step as nanoscale assembled oligomers. Acting the material itself as a drug, the possibility of drug leakage during circulation would be largely minimized, especially for proteolytically stable polypeptides. Because of the easy protein engineering, building blocks might also contain functional peptides such as cell-targeting agents, endosomolytic agents or nuclear localization signals, in the form of fused stretches with modular organization. To explore this innovative concept, we have applied a nanoarchitectonic principle based on the addition, to a core protein, of a cationic N-terminal domain plus a C-terminal polyhistidine.^[8] It is known that these end-terminal tags and the resulting charge distribution in the whole fusion promote self-assembling and oligomerization of monomeric proteins as robust toroid nanoparticles, stable in plasma^[9] and with high cellular penetrability if empowered with cell-targeting peptides.^[10] By using this strategy, we have demonstrated here the possibility to generate multifunctional nanoscale materials that being chemically homogenous, act simultaneously as drugs and targeting agents. This proof-of-concept opens a plethora a new therapeutic opportunities based on protein-only supramolecular materials with intrinsic functionalities. These entities can be easily produced by the same biological procedures used during more than 30 years for conventional, unassembled protein pharmaceuticals.

2. Results and Discussion

It is known that cationic and histidine-rich end-terminal promote self-assembling and oligomerization of monomeric proteins as robust toroid nanoparticles, stable in plasma and with high cellular penetrability if empowered with cell-targeting peptides.^[9] We tested if this principle could be applied to therapeutic proteins by engineering the functional BH3 domain of the proapoptotic Bcl-2 homologous antagonist killer (BAK) protein. We aimed to convert it in the building block of self-assembling protein-only nanoparticles with intrinsic antitumoral activities. BAK is a well-known pro-apoptotic factor belonging to the Bcl-2 protein family that triggers programmed cell death by caspase-dependent apoptotic pathway through inactivating antiapoptotic proteins, permeabilizing the mitochondrial membrane, and consequently, releasing cytochrome C and other mitochondrial cell death factors.^[11,12] Although the full length BAK is reluctant to biological fabrication (because of its highly hydrophobic nature linked to the transmembrane region), truncated forms containing the functional BH3 domain exert proapoptotic activities.^[13] Of course, whether BH3 BAK would be still functional as assembled into cell-targeted nanoparticles could not be predicted in advance.

To explore this possibility, we fused the cationic peptide T22, a potent CXCR4-ligand that targets metastatic CXCR4⁺ colorectal cancer stem cells in vivo,^[9] to the BAK BH3 domain, for the construction of a BAK-based building block (Figure 1A). The green fluorescent protein (GFP) was incorporated to the fusion platform to conveniently monitor the localization of the material and to explore the potential use of the material in diagnosis as well as in therapy (or for theragnosis).^[14] The chimeric protein was biofabricated in *Escherichia coli* (*E. coli*) and purified by conventional procedures in form of a unique and stable molecular species with the expected mass (Figure 1B). As expected, the protein spontaneously assembled into discrete, monodisperse materials of about 13.5 nm in diameter, which upon treatment with sodium dodecyl sulfate (SDS) disassembled into building blocks of >7 nm (Figure 1C). T22-BAK-GFP-H6 monomers were slightly larger than BAK-GFP-H6 protein (<7 nm), that remained unassembled because of the absence of the cationic T22. Disassembling was not observed upon 5 h incubation in Optipro complex culture medium (not shown), indicative of stability of nanoparticles in complex physiological media. Also, T22-BAK-GFP-H6 nanoparticles were fluorescent, exhibiting a specific green fluorescence emission of 306.7 ± 7.8 units μg^{-1} , appropriate for quantitative imaging. High-resolution scanning electron microscopy revealed these materials as planar objects with regular morphology (Figure 1D). Regarding functional analyses, we first determined the ability of protein nanoparticles to bind and penetrate, in a receptor-dependent way, CXCR4⁺ cells. Indeed, the assembled T22-BAK-GFP-H6 protein efficiently penetrated CXCR4⁺ HeLa and SW1417 cells (Figure 2A). The kinetics of accumulation was compatible with receptor-mediated endocytosis (Figure 2B), while the uptake was CXCR4-dependent, as the inhibitor of T22-CXCR4 interaction, AMD3100,^[15] dramatically reduced the intracellular fluorescence in both cell lines upon exposure. The control T22-devoid construct failed to enter cells (Figure 2C). The efficient penetration of T22-BAK-GFP-H6 was confirmed by the generic occurrence of fluorescence in most exposed cells (Figure 2D), and by the intracellular accumulation of the material in the perinuclear region (Figure 2E). T22-BAK-GFP-H6 was intrinsically nontoxic, as the viability of CXCR4⁺ cells, into which the materials do not penetrate, remained unaltered after prolonged exposure (Figure 2B, inset).

Given the high CXCR4-linked cell penetrability of T22-BAK-GFP-H6 nanoparticles we tested the new material in a mouse model of CXCR4⁺ colorectal cancer, regarding biodistribution and capacity of the material to induce selective apoptosis in tumoral tissues. The systemic administration of T22-BAK-GFP-H6 nanoparticles through the tail vein resulted in a transient accumulation of the material in tumor, peaking at 5 h as determined by ex vivo fluorescence images and by IHC (Figure 3A–C). Other relevant organs such as kidney showed only residual fluorescence emission levels (Figure 3D), confirming not only the desired localization of the materials but also the absence of significant renal accumulation, aggregation in lung or detectable toxicity in the time-course (Figure 3D,E). In particular, the absence of protein in kidney (Figure 3D,F) was fully indicative of a high stability of the oligomers in plasma, as monomeric or disassembled proteins, even when targeted to specific tumoral markers by tumor-homing peptides,

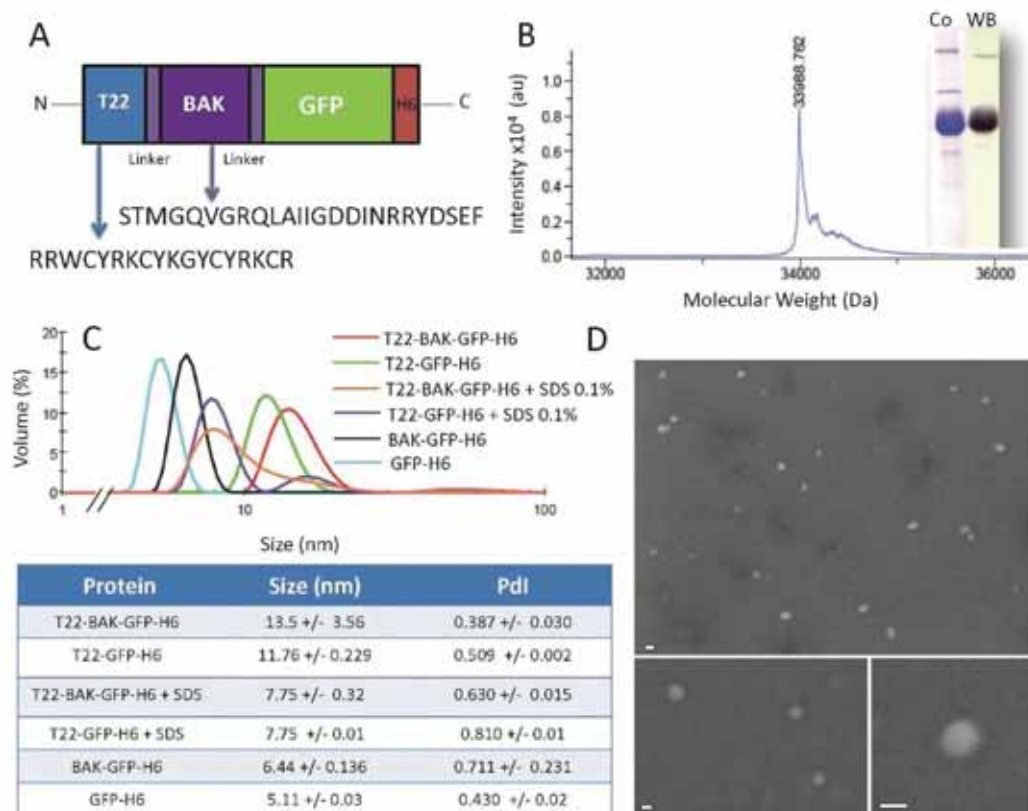


Figure 1. Design and biochemical characterization of T22-BAK-GFP-H6 nanoparticles. A) Schematic representation of the CXCR4-binding T22-BAK-GFP-H6 building block indicating its modular composition. The amino acid sequences of the CXCR4 peptide ligand T22 and the therapeutic BH3 domain of BAK protein are shown. Lengths of the modules are approximate. The linker sequence is GGSSRSSS. B) Mass spectrometry of the purified T22-BAK-GFP-H6 fusion indicating the experimental molecular weight (33 988.762 Da). Protein integrity is also shown through Coomassie blue-stained sodium dodecyl sulfate polyacrylamide gel electrophoresis gels (Co) and by H6 immunodetection in Western blot (WB). C) Hydrodynamic size distribution of T22-empowered nanoparticles in their native state and upon SDS-mediated disassembling. The parental BAK-GFP-H6 and GFP-H6 proteins that do not assemble and the related T22-GFP-H6 particles (and SDS-mediated disassembled monomers) are included here for size comparison. All proteins were in solution in their respective storage buffers. D) FESEM images of randomly selected fields showing the ultrastructural morphology of T22-BAK-GFP-H6 nanoparticles. Bars indicate 20 nm.

accumulate in kidney.^[9] At 24 but not at 48 h, the tumor still showed detectable fluorescence (Figure 3B), indicating prolonged permanence of nanoparticles in the target organ.

As compared to the parental T22-GFP-H6 or the untargeted BAK-GFP-H6 protein, T22-BAK-GFP-H6 induced a significantly decrease of mitotic figures (Figure 4A), that must be consequently attributed to the targeted penetration of functional BAK. This was associated with caspase-3 activation, proteolysis of PARP, occurrence of apoptotic bodies and increased necrotic areas in tumor tissues shortly (2 h) after the administration of the treatment in mice (Figure 4B–F). Tumor cell apoptosis peaked at 5 h and it was maintained for at least 48 h (Figure 4A). By contrast, the nontargeted BAK-GFP-H6 protein yielded only a negligible level of caspase-3 activation or apoptosis in tumors, since it did not differ from the background in buffer-treated tumors (Figure 4F). Histological alterations were not observed in any of the explored nontarget organs (Figure 3E). These observations proved not only the molecular availability of the BAK BH3 domain when delivered as regular

nanoparticles but, as envisaged, that T22-BAK-GFP-H6 nanoparticles exhibited intrinsic biological activity.

At this stage, we wondered how much generic applicability the platform based on therapeutic protein-only nanoparticles would have. In principle, any recombinant protein should be suitable for being empowered as building blocks of functional nanoparticles. In this context, we tested the formation of functional nanoscale materials based on the p53-upregulated modulator of apoptosis PUMA^[16] and the antimicrobial peptide GWH1,^[17] both also inducing apoptosis upon internalization in cancer cells. Under the same modular scheme than T22-BAK-GFP-H6, T22-PUMA-GFP-H6 (Figure 5A), and T22-GWH1-GFP-H6 (Figure 5B) form nanoparticles of 20 and 24 nm, respectively, that as in the case of BAK-based construct retain the GFP fluorescence (not shown). When administered in vivo, both nanoparticles accumulate in tumor (Figure 5C,D), with a minor occurrence of T22-GWH1-GFP-H6 in kidney. This is again indicative of the stability of the oligomers in plasma as materials over 8 nm in size, what prevents renal filtration.^[9]

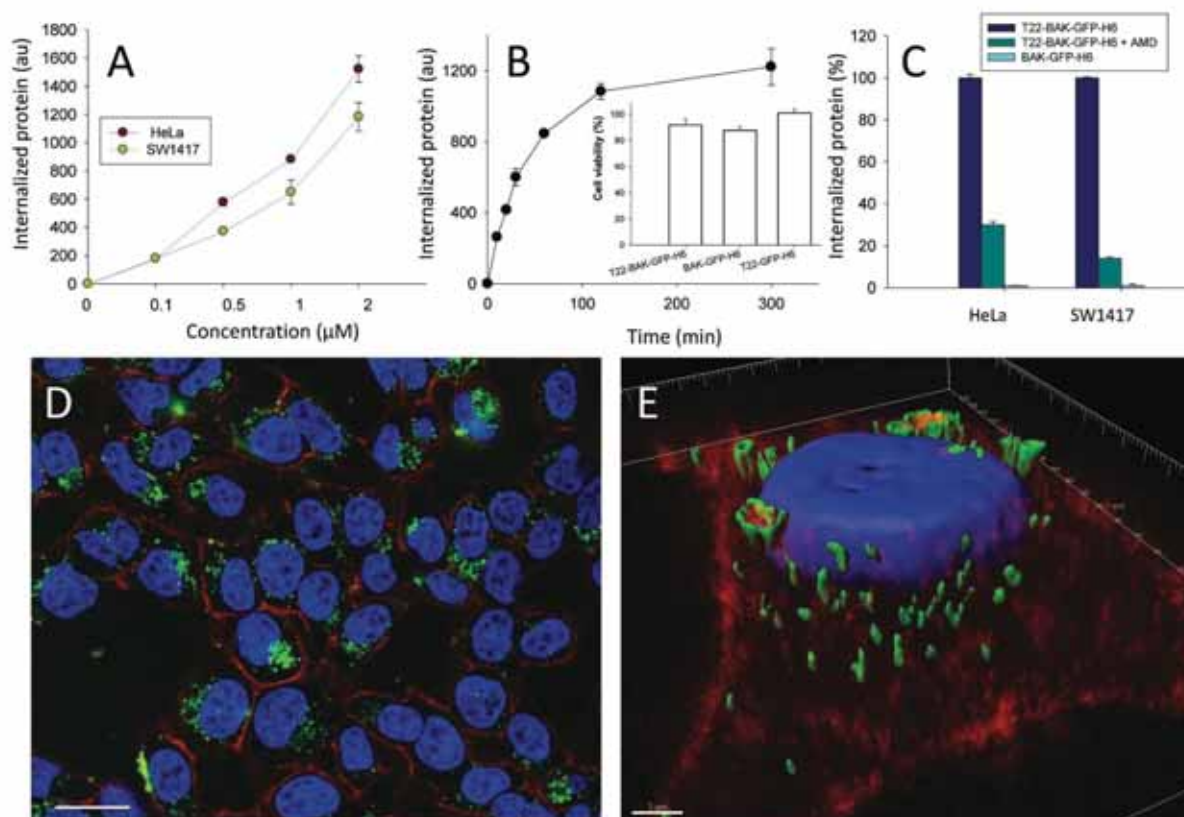


Figure 2. Cell penetrability of T22-BAK-GFP-H6 nanoparticles. A) Internalization of T22-BAK-GFP-H6 nanoparticles in cultured CXCR4⁺ HeLa and SW1417 cells after 24 h exposure. The intensity of intracellular fluorescence is corrected by specific fluorescence, resulting into arbitrary units (au) that are representative of protein amounts. B) Time-dependent intracellular accumulation of nanoparticles (2×10^{-6} M) T22-BAK-GFP-H6 nanoparticles by HeLa cells. Inset: viability of CXCR4⁺ SW1417 cells upon exposure to 2×10^{-6} M T22-BAK-GFP-H6 nanoparticles for 48 h. C) Specificity of CXCR4-mediated internalization of T22-BAK-GFP-H6 nanoparticles determined by the use of the CXCR4⁺ inhibitor AMD3100. D) Intracellular localization of T22-BAK-GFP-H6 nanoparticles upon 24 h of exposure to HeLa cells, observed by confocal sections. Nanoparticles are seen in green since they are naturally fluorescent, while nuclei are labeled in blue and cell membranes in red. Bar indicates 25 μ m. E) Details of targeted cells during the uptake of nanoparticles in a 3D confocal reconstruction. Bar indicates 3 μ m.

Both type of nanoparticles significantly reduced the mitotic rates and even with some variability, the drug materials tended to induce cell death and promote selective necrosis in tumoral tissues, this effect being significant in the case of the PUMA-based material (Figure SE,F).

Taking all these data together, we have here demonstrated that three different proapoptotic proteins, engineered to self-assemble as nanoscale protein materials, act themselves as chemically homogenous drugs that do not need further activation or functionalization upon production. In this nanoscale form and upon specific receptor-mediated internalization, the core protein stretches of these therapeutic materials, namely, BH3 BAK, PUMA, and GWH1 are available for functionality. It is known that BH3 BAK binds antiapoptotic proteins,^[12] inhibits them and alters the balance between proapoptotic and antiapoptotic proteins. This, in turn, induces caspase activation and PARP proteolysis without loss of mitochondrial membrane potential or detectable translocation of cytochrome c from mitochondria to cytosol.^[18] In this regard, we have indeed confirmed the absence of cytochrome C activation in target tissues

(not shown) upon nanoparticle administration. The global effect could be initiated by the interaction between the exposed BH3 motifs in the nanoparticle and the antiapoptotic protein Bcl-XL, which would displace BAK from the BAK/Bcl-XL heterodimers, leading to the oligomerization and retrotranslocation of the free proapoptotic BAK protein to the OMM and apoptosis initiation.^[19] This argument is supported by previous *in vitro* work demonstrating that BAK overexpression^[20] or exogenous BH3 BAK peptides antagonize the Bcl-XL function, triggering fast caspase-3 dependent apoptosis in tumor cells.^[13] By contrast, the induction of intrinsic (mitochondrial-mediated) apoptosis by genotoxic drugs (e.g., in chemotherapy) requires at least 24 h to be completed,^[21,22] because of the time interval required upon DNA damage check point activation to reach the cellular decision between DNA repair and induction of cell death.^[23]

Similarly, PUMA is a (Bcl-2 homology 3) BH3-only protein that triggers cell death by interacting with pro and antiapoptotic proteins of the Bcl-2 family.^[24] This protein directly activates BAX and BAK,^[24,25] and it also binds to pro-survival proteins

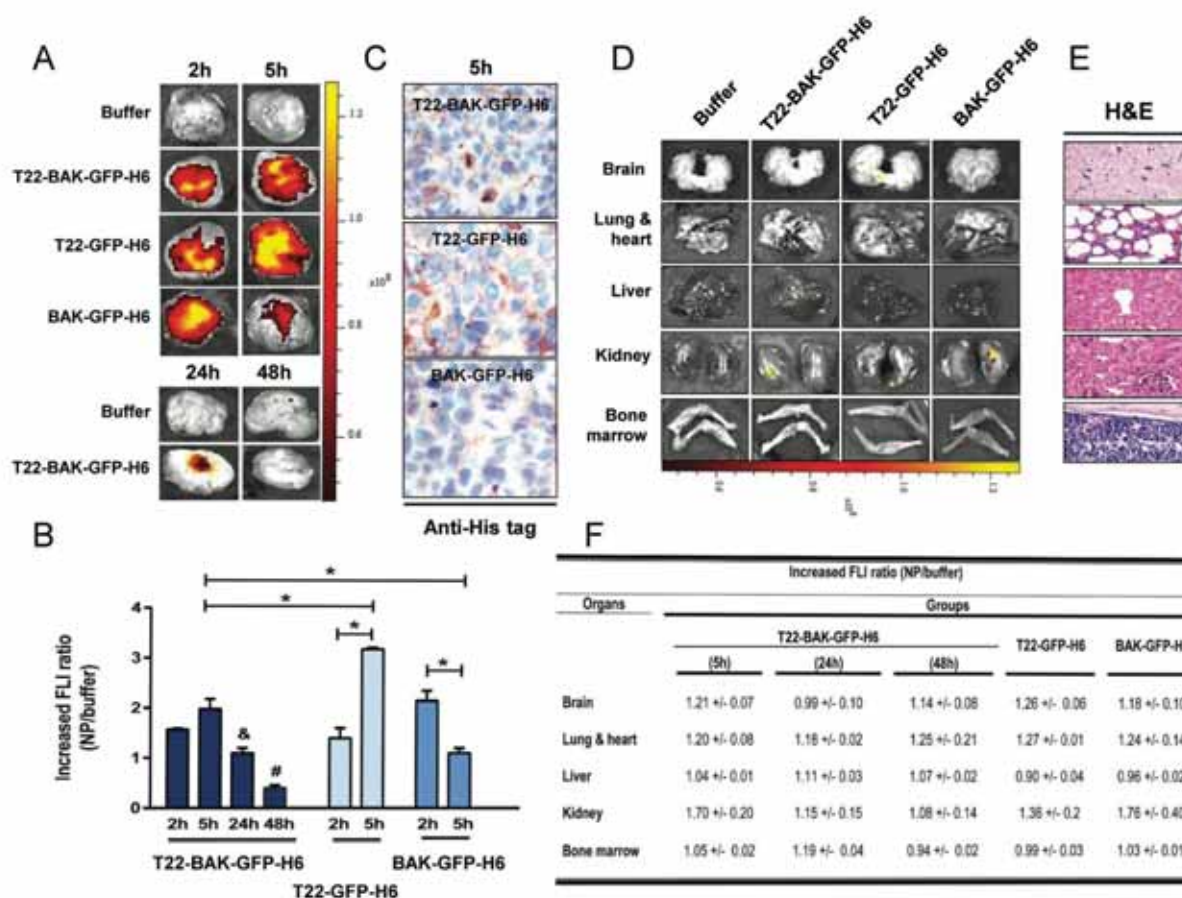


Figure 3. Accumulation and organ biodistribution of T22-GFP-H6 and T22-BAK-GFP-H6 nanoparticles and unassembled BAK-GFP-H6 protein in CXCR4⁺ colorectal tumors. A) Representative ex vivo tumor fluorescence images (FLI) at 2, 5, 24, and 48 h after iv administration of 330 μg dose of each protein. B) GFP fluorescence quantitation in tumors at 2, 5, 24, and 48 h using the IVIS spectrum system. The FLI ratio was calculated dividing the GFP signal from the protein-treated mice by the autofluorescence signal of buffer-treated mice at each organs. & and # $p < 0.05$ bars indicate statistically significant compared to the rest of T22-BAK-GFP-H6-treated groups. * $p < 0.05$ bars indicate a statistically significant between the designated groups. C) Immunohistochemistry against the His-tag domain of the nanoparticles in the tumors at 5 h. D) Representative ex vivo images of the material accumulated in mouse brain, lung, heart, liver, kidney, and bone marrow tissues after treatment. Note the absence or residual fluorescence in these organs compared to tumors. E) Representative H&E staining showed no altered architecture in any organ. F) Quantitation of GFP fluorescence signal in brain, lung and heart, liver, kidney, and bone marrow tissues expressed as fluorescent ratio. This was calculated by dividing the fluorescence of each organ in protein-treated mice by the autofluorescence measured in buffer-treated mice of the respective organ of the time-course experiment. The fluorescence of all protein doses (334 μg each) was recorded by IVIS (total radiant efficiency) just before administration (T22-GFP-H6: 8.4×10^{11} [p s^{-1}]/ $\mu\text{W cm}^{-2}$); T22-BAK-GFP-H6: 8.1×10^{11} [p s^{-1}]/ $\mu\text{W cm}^{-2}$); BAK-GFP-H6: 8.5×10^{11} [p s^{-1}]/ $\mu\text{W cm}^{-2}$) and the final generated data were corrected by specific fluorescence to allow precise comparison between materials and time points. Data expressed as mean \pm SE. Abbreviations: H&E, hematoxylin and eosin staining; iv: intravenous; FLI: fluorescent imaging; NP: nanoparticle.

(Bcl-2 and Bcl-XL) through the BH3 domain^[26] acting as a decoy and preventing their binding and therefore the inhibition of BAX and BAK. On the other hand, GWH1 exerts its cytolytic activity by folding into an amphipathic helix,^[17] which is probably conserved in T22-GWH1-GFP-H6. Although showing a milder effect than the other tested constructs, GWH1 in form of nanomaterial is supposed to exert cell lytic effects by two sequential events consisting on binding to cell membranes followed by permeabilization.

In the context of the pushing needs of cell-targeting and of biocompatible materials as nanoscale drug vehicles, engineering therapeutic proteins into protein-only nanoparticles with

intrinsic therapeutic activity represents a totally new concept of immediate transversal applicability. In contrast to conventional heterogeneous nanoconjugates, in which nonprotein carriers are chemically functionalized for drug loading,^[27] self-assembling protein drugs are produced in form of nanoparticles in a single step by biological fabrication.^[28] This approach allows avoiding the risk of drug leakage during circulation and prevents any potential toxicity associated to some of the materials used as nanoscale drug vehicles. Protein plasticity further allows the generation of modular constructs in which diverse functions such as cell targeting and even fluorescence emission can be combined with the therapeutic protein itself, without increasing

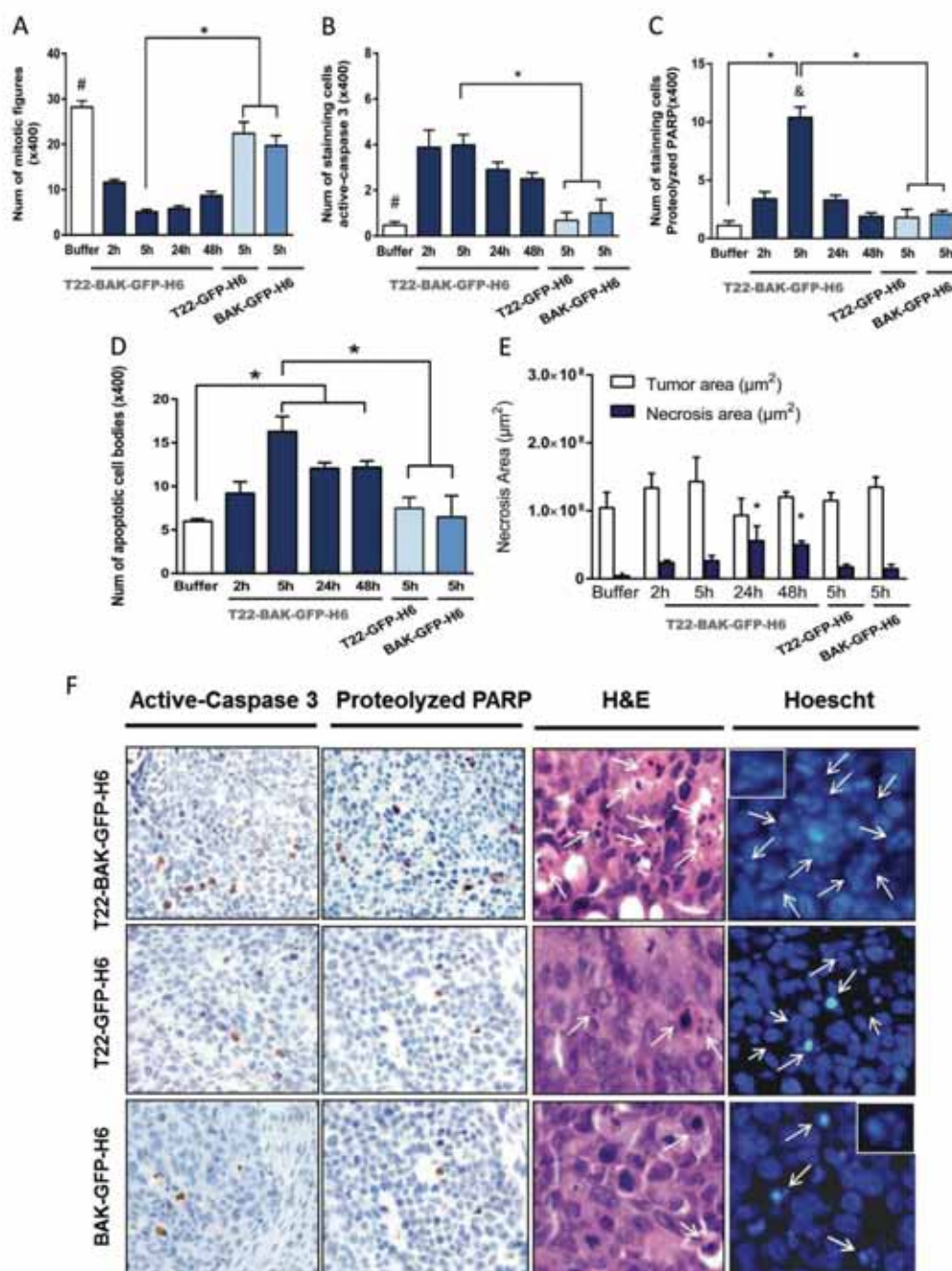


Figure 4. Reduced proliferation index, caspase-3 activation, proteolyzed PARP, apoptosis induction, and necrotic rates in tumors bearing mice at 2, 5, 24, and 48 h after administration of T22-BAK-GFP-H6 compared to buffer and T22-GFP-H6 and BAK-GFP-H6 control counterparts. Quantitation in tumors of the number of mitotic figures (mitotic activity index) by A) H&E staining and both, B) cleaved (active) caspase-3 and C) proteolyzed PARP positive tumor cells by IHC. #, & $p < 0.05$ bars indicate statistically significant compared to T22-BAK-GFP-H6-treated groups at each time; * $p < 0.05$ bars indicate statistically significant between the designated groups. D) Counts of apoptotic figures detected by nuclear condensation after Hoechst staining. * $p < 0.05$ bars indicate statistically significant between the designated groups. E) Measurements of total and necrotic area (μm^2) in low-power field magnification tumor slices using the Cell D software. * $p < 0.05$ bars indicate statistically significant between 2 and 5 h treated groups. F) Representative microphotographs of active caspase-3 and proteolyzed PARP positive cells (stained tumor cells), and cell dead bodies by both, H&E, and Hoechst staining (white arrows) 5 h after treatment with T22-BAK-GFP-H6 and control counterpart nanoparticles ($\times 400$ magnification; inserts at $\times 1000$ magnification). All quantified values in panels (A–D) were obtained by counting 10 high-power field ($\times 400$) per sample. Data were expressed as mean \pm SE. All statistical analyses were performed applying the Mann Whitney U-test. Abbreviations: H&E, hematoxylin and eosin staining.

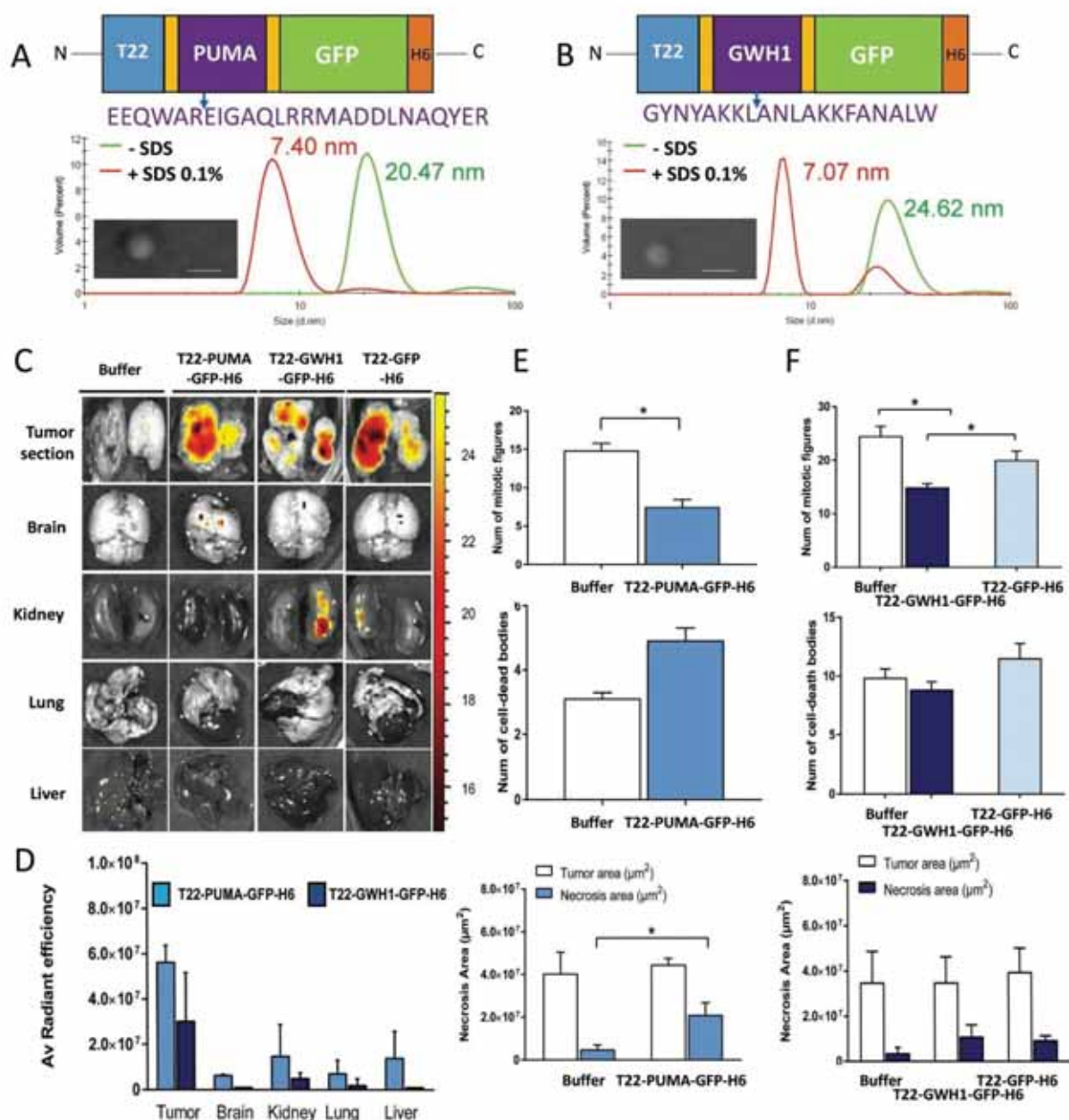


Figure 5. Physical and biological characterization of T22-PUMA-GFP-H6 and T22-GWH1-GFP-H6 nanoparticles. Schematic representation of the building blocks based on A) PUMA and on B) GWH1. The amino acid sequences of the therapeutic protein stretches are indicated while the rest of the constructs are as in Figure 1. The DLS plots of the nanoparticles (green) and of the disassembled building blocks (red) are depicted, sided by the value of the peaks in nm. Representative FESEM images of isolated nanoparticles are also shown. Bars indicate 40 nm. C) Representative ex vivo tumor fluorescence images (FLI) and normal organs (brain, kidney, lung, heart, and liver tissues) after iv administration of 330 µg dose of each nanoparticle at 5 h. D) Quantitation of fluorescence signal (radiant efficiency) in the respective organs. E,F) Quantitation of the number of mitotic figures, (H&E staining), the number of apoptotic figures detected by nuclear condensation after Hoechst staining and necrosis area (H&E staining) in tumors at 5 after the administration of T22-PUMA-GFP-H6 or T22-GWH1-GFP-H6 compared to T22-GFP-H6 control counterpart. All quantitations were done as indicated in Figure 4. The fluorescence of protein doses recorded by IVIS just before the administration were 8.9×10^{11} [p s^{-1}]/[$\mu\text{W cm}^{-2}$] (T22-PUMA-GFP-H6) and 7.4×10^{11} [p s^{-1}]/[$\mu\text{W cm}^{-2}$] (T22-GWH1-GFP-H6), respectively, and generated data were adjusted for comparisons as indicated in Figure 3.

the complexity of the production process (that remains restricted to a single recombinant polypeptide). The self-assembling platform based on cationic end-terminal peptides is universal and

performs irrespective of the nature of the core polypeptide,^[29] allowing its application in a theoretically unlimited catalogue of therapeutic proteins. If having a human origin, the resulting

constructs should not pose immunogenicity limitations in repeated administrations, which are only observed in the case of live-lasting chronic diseases that require live-lasting repeated doses (such as rare diseases). For that, and although GFP has been successfully incorporated in the prototypes presented here as a convenient reporter for cell internalization and systemic biodistribution, GFP-free human proteins would be highly desirable as final drugs. Also, the convenient size of the constructs between ≈ 8 and 100 nm prevents renal filtration and aggregation and favors cell internalization, what is also enhanced by the multivalent display of the homing peptide.^[6]

The presented approach, illustrated here with three structurally unrelated tumor-targeted proapoptotic factors in a colorectal cancer model, shall be transversally explored for the further development of self-assembling, self-delivered homogeneous materials for the increasing number of human pathologies recognized as systemically treatable with protein drugs.

3. Experimental Section

Protein Design, Production, and Purification: The engineered fusion proteins were named according to their modular organization (Figures 1 and 5). Synthetic genes were designed in house and obtained from GeneArt inserted into the prokaryotic expression pET-22b vector. The encoded proteins were produced in plasmid-bearing *E. coli* Origami B (BL21, OmpT⁻, Lon⁻, TrxB⁻, Gor⁻, Novagen) cells, cultured in 2 L-shaker flasks with 500 mL of LB medium with 100 $\mu\text{g mL}^{-1}$ ampicillin, 15 $\mu\text{g mL}^{-1}$ kanamycin, and 12.5 $\mu\text{g mL}^{-1}$ tetracycline at 37 °C. Recombinant gene expression was induced at an OD₅₅₀ around 0.5–0.7 upon the addition of 0.1 $\times 10^{-3}$ M isopropyl- β -D-thiogalactopyranoside and then, bacterial cells were kept growing 3 h at 37 °C for T22-BAK-GFP-H6 production and overnight at 20 °C for T22-GFP-H6, T22-CWH1-GFP-H6, and T22-PUMA-GFP-H6 production. Bacterial cells were then harvested by centrifugation at 5000 g for 15 min at 4 °C and resuspended in wash buffer (20 $\times 10^{-3}$ M Tris-HCl, 500 $\times 10^{-3}$ M NaCl, 10 $\times 10^{-3}$ M imidazol, pH 8.0) in the presence of EDTA-free protease inhibitor (Complete EDTA-Free; Roche, Basel, Switzerland). Cells were disrupted at 1200 psi in a French Press (Thermo FA-078A) and lysates were centrifuged for 45 min (15 000 g at 4 °C). All proteins were purified by His-tag affinity chromatography using HiTrap Chelating HP 1 mL columns (GE Healthcare, Piscataway, NJ, USA) by AKTA purifier FPLC (GE Healthcare). After filtering the soluble fraction, samples were loaded onto the column and washed with 10 column volumes of wash buffer. Elution was achieved by a linear gradient of 20 $\times 10^{-3}$ M Tris-HCl, 500 $\times 10^{-3}$ M NaCl, 500 $\times 10^{-3}$ M imidazole, pH 8.0, and purified fractions were collected and analyzed by SDS-PAGE and Western Blotting with anti-His monoclonal antibody (Santa Cruz Biotechnology, Heidelberg, Germany) to observe the protein of interest. Proteins were dialyzed overnight at 4 °C, against sodium bicarbonate buffer with salt (166 $\times 10^{-3}$ M NaHCO₃, pH 7.4 + 333 $\times 10^{-3}$ M NaCl). These buffers were the final solvents for further experiments. Protein integrity and purity were checked by mass spectrometry (MALDI-TOF) and quantified by Bradford's assay.

Fluorescence Determination, Dynamic Light Scattering (DLS), and Field Emission Scanning Electron Microscopy (FESEM): The fluorescence of the fusion proteins was determined in a Varian Cary Eclipse fluorescence spectrophotometer (Agilent Technologies, Palo Alto, CA, USA) at 510 nm using an excitation wavelength of 450 nm. Volume size distribution of nanoparticles and monomeric GFP protein fusions were determined by DLS at 633 nm (Zetasizer Nano ZS, Malvern Instruments Limited, Malvern, UK). For fluorescence determination, protein samples were diluted in the corresponding storage buffer to 0.5 mg mL⁻¹, in 100 μL final volume. For DLS analyses, proteins (stored at -80 °C) were thawed and 50 μL of each sample was used. FESEM qualitative analyses were performed with Zeiss Merlin (Zeiss, Oberkochen, Germany) field

emission scanning electron microscope operating at 1 kV and equipped with a high resolution in-lens secondary electron detector. Microdrops of diluted purified proteins were deposited onto silicon wafer surfaces (Ted Pella, Reading, CA, USA), air-dried, and immediately observed.

Cell Culture and Flow Cytometry: The CXCR4⁺ HeLa cell line (ATCC-CCL-2) was cultured in Eagle's minimum essential medium (Gibco, Rockville, MD, USA) supplemented with 10% fetal calf serum (Gibco), and incubated at 37 °C and 5% CO₂ in a humidified atmosphere. Meanwhile SW1417 cell line was maintained in Dulbecco's modified Eagle's medium (Gibco GlutaMAX, Thermo Fisher Scientific, Waltham, MA, USA) supplemented with 10% fetal calf serum (Gibco), and incubated at 37 °C and 10% CO₂ in a humidified atmosphere. HeLa and SW1417 cell lines were cultured on 24-well plate at 3×10^4 and 12×10^4 cells per well respectively for 24 h until reaching 70% confluence. Nanoparticles and monomeric proteins were added at different concentrations (ranging from 0.1 $\times 10^{-6}$ to 2 $\times 10^{-6}$ M) to the cell culture in the presence of Optipro medium (Gibco) 24 h before the flow cytometry analysis. Cell samples were analyzed on a FACSCanto system (Becton Dickinson, Franklin Lakes, NJ, USA) using a 15 W air-cooled argon-ion laser at 488 nm excitation. GFP fluorescence emission was measured with a detector D (530/30 nm band pass filter) after an adapted treatment with 1 mg mL⁻¹ trypsin (Gibco) for 15 min that ensures the removal of externally attached protein.^[30] Specific internalization of nanoparticles was measured using AMD3100/CXCR4⁺ inhibitor (octahydrochloride hydrate, Sigma-Aldrich, Steinheim, Germany). For this experiment, T22-BAK-GFP-H6 was labeled with ATTO488 (41698, Sigma-Aldrich) during 1 h in darkness at room temperature to obtain a more fluorescent protein. T22-BAK-GFP-H6-ATTO488 was added at 25 $\times 10^{-9}$ M during 1 h of incubation in presence of AMD3100 at 1:10 ratio.

Confocal Microscopy: HeLa cells were grown on Mat-Tek culture dishes (MatTek Corporation, Ashland, MA, USA). Medium was removed and cells were washed with DPBS, Optipro medium supplemented with L-glutamine and proteins were added 24 h before staining at 2 $\times 10^{-6}$ M. Nuclei were labeled with 0.2 $\mu\text{g mL}^{-1}$ Hoechst 33342 (Molecular Probes, Eugene, OR, USA) and the plasma membranes with 2.5 $\mu\text{g mL}^{-1}$ CellMask Deep Red (Molecular Probes) in darkness for 10 min. Live cells were recorded by TCS-SP5 confocal laser scanning microscopy (Leica Microsystems, Heidelberg, Germany) using a Plan Apo 63 \times /1.4 (oil HC \times PL APO lambda blue) objective. To determine the location of particles inside the cell, stacks of 10–20 sections were collected at 0.5 μm Z-intervals with a pinhole setting of 1 Airy unit. Images were processed and the 3D reconstruction was generated using Imapris version 7.2.1.0 software (Bitplane, Zürich, Switzerland).

Biodistribution: Five-week-old female Swiss nu/nu mice weighing between 18 and 20 g (Charles River, L'Abresille, France) and maintained in specific-pathogen-free (SPF) conditions, were used for in vivo studies. All the in vivo procedures were approved by the Hospital de Sant Pau Animal Ethics Committee and performed according to European Council directives. To generate the subcutaneous mouse model, 10 mg of SP5 CCR tumor tissue was obtained from donor animals and implanted subcutaneously in the subcutis of swiss nu/nu mice. When tumors reached 500 mm³ approximately, mice were randomly allocated and administered with T22-BAK-GFP-H6, BAK-GFP-H6, and T22-GFP-H6 nanoparticles at 330 μg per mouse dose.

Short (2 and 5 h) and long times (24 and 48 h) were assayed to explore the biological effects of the administered nanoparticles. For that, mice were euthanized and tumor and brain, pancreas, lung and heart, kidney, liver, and bone marrow were collected and examined separately for ex vivo GFP fluorescence in an IVIS Spectrum equipment (PerkinElmer Inc, Waltham, MA, USA). The fluorescent signal (FLI) was first digitalized, displayed as a pseudocolor overlay, and expressed as radiant efficiency. The FLI ratio was calculated dividing the FLI signal from the protein-treated mice by the FLI autofluorescent signal of control mice. Finally, all organs were collected and fixed with 4% formaldehyde in phosphate-buffered solution for 24 h. These samples were then embedded in paraffin for histological and immunohistochemical analyses as well as for determination of mitotic and apoptotic index and necrosis evaluation.

Histopathology and Immunohistochemistry Analyses: 4 μm thick sections were stained with hematoxylin and eosin (H&E), and a complete histopathological analysis was performed by two independent observers. The presence and location of the His tag in the protein materials and of the proteolyzed Poly (ADP-Ribose) polymerase (PARP) and the active cleaved-Caspase 3 protein in tissue sections were assessed by immunohistochemistry using the DAKO immunosystem equipment and standard protocols. A primary antibody against the His tag (1:1000; MBL International, Woburn, MA, USA), anti-PARP p85 fragment pAb (1:300; Promega, Madison, WI, USA) or antiactive caspase 3 antibody (1:300, BD PharMingen, San Diego, CA, USA) were incubated for 25 min after incubation with the secondary antibody in tumor tissues at 2, 5, 24, and 48 h. The number of stained cells was quantified by two independent blinded counters who recorded the number of positive cells per 10 high-power fields (magnification 400 \times). Representative pictures were taken using CellAB software (Olympus Soft Imaging v 3.3, Nagano, Japan).

Assessment of Mitotic, Apoptotic, Necrotic Rates: Tumor slices were also processed to assess proliferation capacity by counting the number of mitotic figures per ten high-power fields (magnification $\times 400$) in H&E stained tumors. Apoptotic induction was evaluated by the presence of cell death bodies in H&E and also by Hoechst staining in tumor slices. Hoechst 33258 (Sigma-Aldrich, Steinheim, Germany) staining was performed in Triton X-100 (0.5%) permeabilized sections. Slides were then stained with Hoechst 33258 (1:5000 in PBS) for 1 h, rinsed with water, mounted, and analyzed under fluorescence microscope ($\lambda_{\text{ex}} = 334 \text{ nm}$, $\lambda_{\text{em}} = 465 \text{ nm}$). The number of apoptotic bodies was quantified by two independent blinded recording the number of condensed and/or defragmented nuclei per 10 high-power fields (magnification 400 \times). Necrosis area in tumors was quantified using CellAB software at 15 \times magnification and representative pictures were taken using the same CellAB software at 400 \times magnification.

Acknowledgements

N.S. and M.V.C. contributed equally to this work. The authors are indebted to MINECO (BIO2013-41019-P), AGAUR (2014SGR-132), and CIBER de Bioingeniería, Biomateriales y Nanomedicina (Project NANOPROTHER) to A.V., Marató de TV3 foundation (TV32013-3930) and FIS (PI15/00272, cofunding ISCIII and FEDER) to E.V., and ISCIII (PI15/00378 and PIE15/00028, cofunding FEDER), Marató TV3 (2013-2030), and AGAUR2014-PROD0005 to R.M. for funding the research on protein-based therapeutics. Protein production was performed in part by the ICTS "NANBIOSIS," more specifically by the Protein Production Platform of CIBER in Bioengineering, Biomaterials & Nanomedicine (CIBER-BBN)/IBB, at the UAB SepBioES scientific-technical service (<http://www.nanbiosis.es/unit/u1-protein-production-platform-ppp/>). All in vivo experiments were performed by the ICTS "NANBIOSIS," more specifically by the CIBER-BBN's Nanotoxicology Unit Platform. A.V. received an ICREA ACADEMIA award. M.V.C. was supported by a Miguel Servet contract and U.U. received a Sara Borrell postdoctoral fellowship, both from ISCIII, while L.S.-G. was supported by AGAUR (FI-DGR).

Conflict of Interest

MVC, UU, RM, EV and AV are co-inventors in a patent on the uses of T22 as a tumor-targeting agent (WO2012095527).

Keywords

advanced therapies, nanoparticles, protein materials, self-assembly, therapeutic proteins

Received: February 18, 2017

Revised: May 8, 2017

Published online: July 4, 2017

- [1] R. Duncan, R. Gaspar, *Mol. Pharm.* **2011**, *8*, 2101.
- [2] D. Peer, J. M. Karp, S. Hong, O. C. Farokhzad, R. Margalit, R. Langer, *Nat. Nanotechnol.* **2007**, *2*, 751.
- [3] B. Feng, J. L. LaPerle, G. Chang, M. V. Varma, *Expert Opin. Drug Metab. Toxicol.* **2010**, *6*, 939.
- [4] N. Sanvicens, M. P. Marco, *Trends Biotechnol.* **2008**, *26*, 425.
- [5] N. Ferrer-Mirallès, E. Rodríguez-Carmona, J. L. Corchero, E. García-Fruitos, E. Vázquez, A. Villaverde, *Crit. Rev. Biotechnol.* **2015**, *35*, 209.
- [6] U. Unzueta, M. V. Cespedes, E. Vázquez, N. Ferrer-Mirallès, R. Mangués, A. Villaverde, *Trends Biotechnol.* **2015**, *33*, 253.
- [7] L. Sánchez-García, L. Martín, R. Mangués, N. Ferrer-Mirallès, E. Vázquez, A. Villaverde, *Microb. Cell Fact.* **2016**, *15*, 33.
- [8] N. Serna, M. V. Cespedes, P. Saccardo, Z. Xu, U. Unzueta, P. Alamo, M. Pesarrodona, A. Sánchez-Chardi, M. Roldán, R. Mangués, E. Vázquez, A. Villaverde, N. Ferrer-Mirallès, *Nanomedicine* **2016**, *12*, 1241.
- [9] M. V. Cespedes, U. Unzueta, W. Tatkiwicz, A. Sánchez-Chardi, O. Conchillo-Sole, P. Alamo, Z. Xu, I. Casanova, J. L. Corchero, M. Pesarrodona, J. Cedano, X. Daura, I. Ratera, J. Veciana, N. Ferrer-Mirallès, E. Vázquez, A. Villaverde, R. Mangués, *ACS Nano* **2014**, *8*, 4166.
- [10] Z. K. Xu, U. Unzueta, M. Roldán, R. Mangués, A. Sánchez-Chardi, N. Ferrer-Mirallès, A. Villaverde, E. Vázquez, *Mater. Lett.* **2015**, *154*, 140.
- [11] F. Llambi, T. Moldoveanu, S. W. Tait, L. Bouchier-Hayes, J. Temirov, L. L. McCormick, C. P. Dillon, D. R. Green, *Mol. Cell* **2011**, *44*, 517.
- [12] D. Westphal, G. Dewson, P. E. Czabotar, R. M. Kluck, *Biochim. Biophys. Acta* **2011**, *1813*, 521.
- [13] E. P. Holinger, T. Chittenden, R. J. Lutz, *J. Biol. Chem.* **1999**, *274*, 13298.
- [14] J. H. Ryu, H. Koo, I. C. Sun, S. H. Yuk, K. Choi, K. Kim, I. C. Kwon, *Adv. Drug Delivery Rev.* **2012**, *64*, 1447.
- [15] U. Unzueta, M. V. Cespedes, N. Ferrer-Mirallès, I. Casanova, J. Cedano, J. L. Corchero, J. Domingo-Espin, A. Villaverde, R. Mangués, E. Vázquez, *Int. J. Nanomed.* **2012**, *7*, 4533.
- [16] Y. Zhang, D. Xing, L. Liu, *Mol. Biol. Cell* **2009**, *20*, 3077.
- [17] Y.-L. Sophia Chen, J.-H. Li, Ch.-Y. Yu, Ch.-J. Lin, P.-H. Chiu, P.-W. Chen, Ch.-Ch. Lin, W.-J. Chen, *Peptides* **2012**, *36*, 257.
- [18] E. P. Holinger, T. Chittenden, R. J. Lutz, *J. Biol. Chem.* **1999**, *274*, 13298.
- [19] F. Todt, Z. Cakir, F. Reichenbach, F. Emschermann, J. Lauterwasser, A. Kaiser, G. Ichim, S. W. Tait, S. Frank, H. F. Langer, F. Edlich, *EMBO J.* **2015**, *34*, 67.
- [20] Q. S. Tong, L. D. Zheng, L. Wang, J. Liu, W. Qian, *BMC Cancer* **2004**, *4*, 33.
- [21] C. Gajate, F. An, F. Mollinedo, *J. Biol. Chem.* **2002**, *277*, 41580.
- [22] D. T. Stefanou, A. Bamias, H. Episkopou, S. A. Kyrtopoulos, M. Likka, T. Kalampokas, S. Photiou, N. Gavalas, P. P. Sfakakis, M. A. Dimopoulos, V. L. Souliotis, *PLoS One* **2015**, *10*, e0117654.
- [23] T. Rich, R. L. Allen, A. H. Wyllie, *Nature* **2000**, *407*, 777.
- [24] E. H. Shroff, C. M. Snyder, G. R. Budinger, M. Jain, T. L. Chew, S. Khuon, H. Perlman, N. S. Chandel, *PLoS One* **2009**, *4*, e5646.
- [25] H. C. Chen, M. Kanai, A. Inoue-Yamauchi, H. C. Tu, Y. Huang, D. Ren, H. Kim, S. Takeda, D. E. Reyna, P. M. Chan, Y. T. Ganesan, C. P. Liao, E. Gavathiotis, J. J. Hsieh, E. H. Cheng, *Nat. Cell Biol.* **2015**, *17*, 1270.
- [26] J. Yu, L. Zhang, P. M. Hwang, K. M. Kinzler, B. Vogelstein, *Mol. Cell* **2001**, *7*, 673.
- [27] E. Vázquez, R. Mangués, A. Villaverde, *Nanomedicine* **2016**, *11*, 1333.
- [28] E. Vázquez, A. Villaverde, *Nanomedicine* **2013**, *8*, 1895.
- [29] U. Unzueta, N. Ferrer-Mirallès, J. Cedano, X. Zikung, M. Pesarrodona, P. Saccardo, E. García-Fruitos, J. Domingo-Espin, P. Kumar, K. C. Gupta, R. Mangués, A. Villaverde, E. Vázquez, *Bio-materials* **2012**, *33*, 8714.
- [30] J. P. Richard, K. Melikov, E. Vives, C. Ramos, B. Verbeure, M. J. Gait, L. V. Chernomordik, B. Lebleu, *J. Biol. Chem.* **2003**, *278*, 585.

ANNEX 3: ARTICLE 4

**Conformational conversion during controlled oligomerization into
nonamylogenic protein nanoparticles**

Julieta M. Sanchez, **Laura Sánchez-García**, Mireia Pesarrodoná, Naroa Serna, Alejandro Sánchez-Chardi, Ugutz, Unzueta, Ramón Mangués, Esther Vázquez and Antonio Villaverde

Biomacromolecules (2018) 19: 3788-3797
Impact factor 5.738 POLYMER SCIENCE (6/87) D1



Conformational Conversion during Controlled Oligomerization into Nonamylogenic Protein Nanoparticles

Julieta M. Sánchez,^{‡,§} Laura Sánchez-García,^{§,||} Mireia Pesarrodona,^{†,§,||,▽} Naroa Serna,^{†,§,||} Alejandro Sánchez-Chardi,[‡] Ugutz Unzueta,^{†,§,||,¶} Ramón Mangués,^{||,¶} Esther Vázquez,^{*,†,§,||} and Antonio Villaverde^{*,†,§,||}

[‡]Institut de Biotecnologia i de Biomedicina, Universitat Autònoma de Barcelona, Bellaterra 08193 Barcelona, Spain

[§]Universidad Nacional de Córdoba, Facultad de Ciencias Exactas, Físicas y Naturales, ICTA and Departamento de Química, Cátedra de Química Biológica, Córdoba, Argentina, CONICET, Instituto de Investigaciones Biológicas y Tecnológicas (IIBYT), Córdoba, Argentina, Av. Velez Sarsfield 1611, X5016GCA Córdoba, Argentina

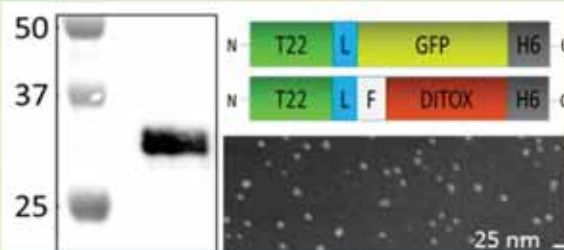
[¶]Departament de Genètica i de Microbiologia, Universitat Autònoma de Barcelona, Bellaterra, 08193 Barcelona, Spain

^{||}CIBER de Bioingeniería, Biomateriales y Nanomedicina (CIBER-BBN), Bellaterra, 08193 Barcelona, Spain

[‡]Servei de Microscòpia, Universitat Autònoma de Barcelona, Bellaterra, 08193 Barcelona, Spain

^{*}Biomedical Research Institute Sant Pau (IIB-Sant Pau) and Josep Carreras Research Institute, Hospital de la Santa Creu i Sant Pau, 08025 Barcelona, Spain

ABSTRACT: Protein materials are rapidly gaining interest in materials sciences and nanomedicine because of their intrinsic biocompatibility and full biodegradability. The controlled construction of supramolecular entities relies on the controlled oligomerization of individual polypeptides, achievable through different strategies. Because of the potential toxicity of amyloids, those based on alternative molecular organizations are particularly appealing, but the structural bases on nonamylogenic oligomerization remain poorly studied. We have applied spectrofluorimetry and spectropolarimetry to identify the conformational conversion during the oligomerization of His-tagged cationic stretches into regular nanoparticles ranging around 11 nm, useful for tumor-targeted drug delivery. We demonstrate that the novel conformation acquired by the proteins, as building blocks of these supramolecular assemblies, shows different extents of compactness and results in a beta structure enrichment that enhances their structural stability. The conformational profiling presented here offers clear clues for understanding and tailoring the process of nanoparticle formation through the use of cationic and histidine rich stretches in the context of protein materials usable in advanced nanomedical strategies.



INTRODUCTION

Protein materials are gaining interest in materials sciences and in nanomedicine because of the intrinsic biocompatibility and nonrecalcitrant nature of polypeptides that makes their use in drug delivery or regenerative medicine safer than other micro- or nanoscale composites.¹ Additionally, biologically and environmentally friendly fabrication of proteins in recombinant organisms² and the possibility to modulate their structure and function through genetic engineering³ allow the generation of tailored functional or multifunctional materials,⁴ with unique characteristics such as a plasticity unreachable by metals, polymers, ceramics, or other nanostructured materials. The construction of protein-based materials relies on the controlled oligomerization of individual polypeptides, which act as building blocks of complex supramolecular arrangements. This is achieved by the engineering of natural oligomerization domains, by domain-swapping, or through the regulation of protein–protein contacts by a diversity of strategies,^{1b,2b}

among which one of the best exploited is controlled amyloid fibril formation.^{1a,5} The structural conversion from isolated protein monomers to components of larger amyloid structures has been studied and reviewed in detail,⁶ and the analysis of the conformational changes along the process allows designing new categories of building blocks for novel tailored materials⁷ with potentially improved properties and functionalities.^{1a,6a,8}

Among nonfibril protein materials, isometric nanoparticles (NPs) resulting from protein self-assembling are of special interest in cell-targeted delivery of protein and nonprotein drugs.⁹ In this context, cationic protein segments such as polyarginines, as short peptides¹⁰ or as N-terminal protein fusions,¹¹ promote self-assembling.¹² Supported by this

Received: June 13, 2018

Revised: July 23, 2018

Published: July 27, 2018

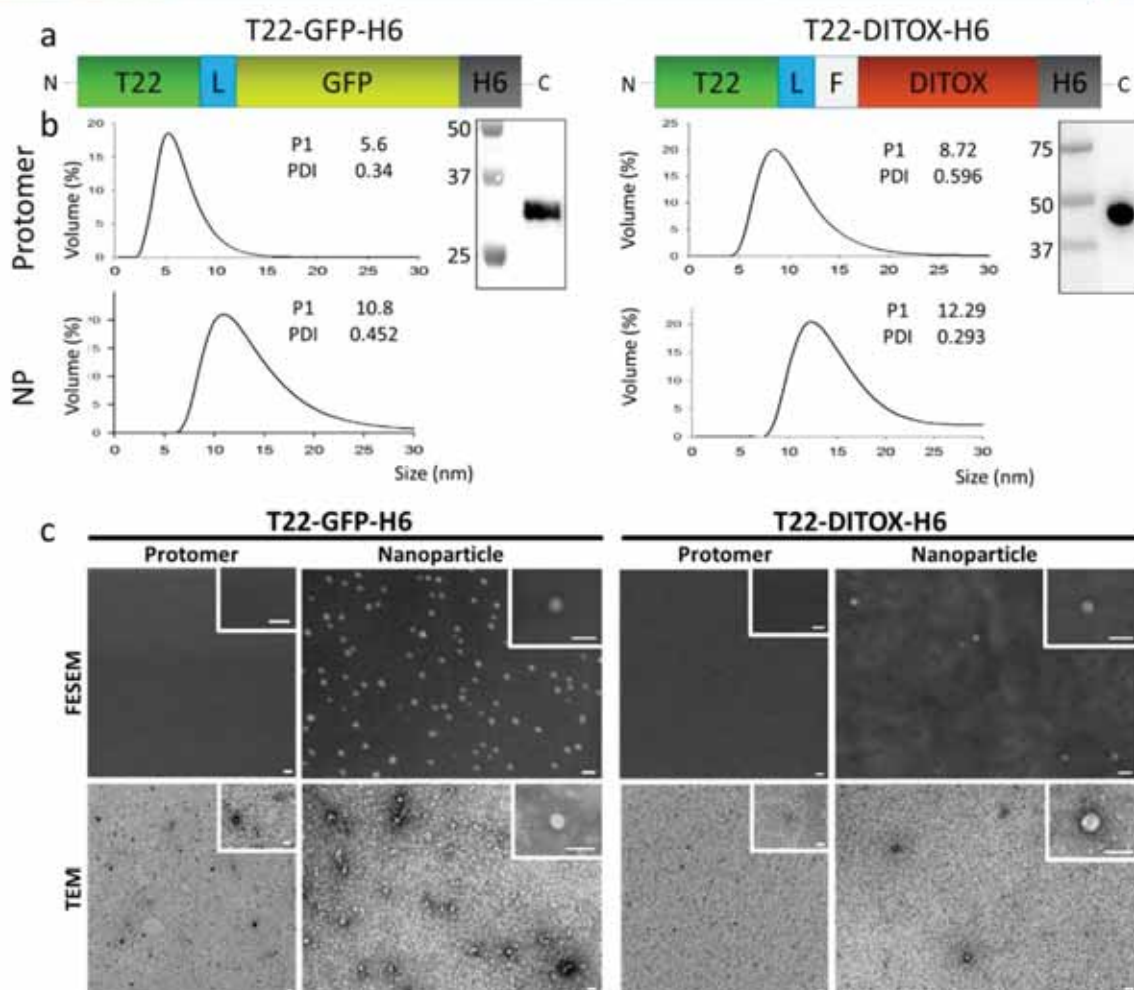


Figure 1. (a) Modular organization of T22-GFP-H6 and T22-DITOX-H6. L corresponds to a peptidic linker that confers molecular flexibility, and F corresponds to a furin cleavage site. Box sizes are only indicative. Additional details of the constructions are given elsewhere.^{19,22} (b) DLS measurements of disassembled (top) and assembled (bottom) proteins. Numbers indicate mean peak size and polydispersity index (PDI), in nanometers. In the inset, Western blot analyses of purified proteins. Numbers indicate the molecular mass or markers (in kDa). (c) FESEM and TEM images of protomers and NPs. Bar size is 25 nm.

principle, T22-GFP-H6 and related fusion proteins are fluorescent building blocks that self-assemble as cyclic homomeric NPs of 10–20 nm¹¹ through the combination of electrostatic, hydrogen bond, and van der Waals forces, as determined from protein modeling.¹³ These materials are formed by around 10 monomers that organize in a single molecular layer as a nanoscale disk.^{13b,14} A major driver of the assembling process is the N-terminal domain, namely, the peptide T22. This cationic protein segment is an engineered version of polyphemusin II from Atlantic horseshoe crab *Limulus polyphemus*, which is a well-known antagonist of the cell surface cytokine receptor CXCR4 chemokine receptor type 4 (CXCR4).¹⁵ CXCR4 is used by the human immunodeficiency virus to initiate cell infection,¹⁶ but, in addition, it is an important stem-cell marker in several common human cancers,¹⁷ including metastatic colorectal cancer.¹⁸ T22 specifically and efficiently binds to and penetrates CXCR4⁺ cells via CXCR4-specific endocytosis, both in vitro and in vivo.¹⁹ T22-mediated uptake of materials is dramatically

favored when the ligand is presented in an oligomeric form,²⁰ probably because of the cooperative multimeric cell binding through simultaneous receptor–ligand interactions.^{9a} Therefore, whereas CXCR4 and its specific ligand T22 have proved clinical relevance regarding cell-targeted antitumoral drug delivery,^{9b} the structural basis of T22-mediated NP formation is not known. In this context, we have taken here diverse biophysical approaches, mainly spectrofluorimetry and spectropolarimetry, to explore how these T22-empowered polypeptides acquire conformation compatibility with their assembly as CXCR4⁺ tumor-targeted NPs. For that, T22-GFP-H6, usable as an antitumoral drug carrier,^{13a} and its derivative T22-DITOX-H6 have been used as models. T22-DITOX-H6 contains, instead of GFP, the active domain of the potent diphtheria toxin,²¹ as the resulting material is a self-assembled, self-delivered NP with intrinsic and cell-targeted antitumoral activity.²² Devoid of any heterologous carrier, T22-DITOX-H6 NPs fulfill the emerging medical concept of vehicle-free nanoscale drugs.²³

MATERIALS AND METHODS

Protein Production and Purification. T22-GFP-H6 is a modular recombinant protein that contains the potent CXCR4 ligand T22 and that spontaneously self-assembles upon bacteria production and protein purification as green fluorescent NPs.^{12,15,19a} T22-DITOX-H6 is a fully engineered derivative of the previous protein, also showing self-assembling properties, that delivers the unfused functional form of a diphtheria toxin fragment into target cells (Figure 1a), as has recently been described.²³ Both proteins were produced in recombinant *Escherichia coli* Origami B (BL21, Omp[−], Lon[−], TrxB[−], Gor[−], Novagen, Darmstadt, Germany) cultures from the engineered plasmid pET22b. Cells were grown at 37 °C in LB medium supplemented with 100 µg/mL ampicillin, 12.5 µg/mL tetracycline, and 15 µg/mL kanamycin. When the OD₅₅₀ of the cultures reached around 0.5 to 0.7, 0.1 mM IPTG (isopropyl-β-D-thiogalactopyranoside) was added and incubated overnight at 20 °C (for T22-GFP-H6 and T22-DITOX-H6 production). Then, cells were collected by centrifugation for 15 min (5000g at 4 °C). Cell disruption was performed in a French press (Thermo FA-078A) at 1200 psi. The lysates were then centrifuged for 45 min (15 000g at 4 °C), and the soluble fraction was filtered using a pore diameter of 0.2 µm. Proteins were then purified by their H6 region by immobilized metal affinity chromatography (IMAC) using a HiTrap Chelating HP 1 mL column (GE Healthcare, Piscataway, NJ) with an AKTA purifier FPLC (GE Healthcare). Elution was achieved by elution buffer (20 mM Tris-HCl, pH 8; 500 mM NaCl; 500 mM imidazole), and proteins were then dialyzed against carbonate buffer with salt (166 mM NaCO₃H, pH 8; 333 mM NaCl). Protein concentration was obtained by the Bradford's assay. Protein production has been partially performed by the ICTS "NANBIOSIS", more specifically by the Protein Production Platform of CIBER-BBN/IBB (<http://www.nanbiosis.es/unit/u1-protein-production-platform-ppp/>).

Preparation of Nanoparticles and Unassembled Subunits. Upon purification, the T22-derived protein NPs occur as an unbalanced mixture of NPs and unassembled protomers¹⁴ that are separated by size-exclusion chromatography through a HiLoad Superdex 16/600 200 pg column at 1 mL/min flow rate, as described elsewhere.¹⁴ Such alternative protein versions are, in general, stable in these respective forms,^{13a} allowing their further experimental analysis in such forms. This stability is probably due to subtle electrostatic or conformational variability, although assembling and disassembling can be effectively promoted by the manipulation of buffer conditions such as the ionic strength.²⁴ The starting materials usable for subsequent experiments are described in Figure 1.

Determination of Intrinsic Fluorescence. Fluorescence spectra were recorded in a Cary Eclipse spectrofluorimeter (Agilent Technologies, Mulgrave, Australia). A quartz cell with 10 mm path length and a thermostated holder were used. The excitation and emission slits were set at 5 nm. Excitation wavelength (λ_{ex}) was set at 295 nm. Emission spectra were acquired within a range from 310 to 550 nm. The protein concentration was 0.25 mg/mL in carbonate buffer with salt. To evaluate conformational difference between protomer and NP, we decided to apply the center of spectral mass (CSM) for comparison. CSM is a weighted average of the fluorescence spectrum peak. Also, it is related to the relative exposure of the Trp to the protein environment. The maximum red shift in the CSM of the Trp is compatible with a large solvent accessibility.²⁵

The CSM was calculated for each of the fluorescence emission spectra²⁶ according to eq 1, where I_i is the fluorescence intensity measured at the wavelength λ_i .

$$\lambda = \frac{\sum \lambda_i \cdot I_i}{\sum I_i} \quad (1)$$

Determination of GFP Chromophore Fluorescence. The chromophore fluorescence dependence on the temperature was also evaluated. Fluorescence spectra were recorded in a Cary Eclipse spectrofluorimeter (Agilent Technologies). A quartz cell with 10 mm path length and a thermostated holder were used. The excitation slits set at 2.5 nm and emission slits were set at 5 nm. λ_{ex} was set at 488

nm. Emission spectra were acquired within a range from 500 to 650 nm. T22-GFP-H6 concentration was 0.25 mg/mL in carbonate buffer with salt.

Fluorescence Resonance Energy Transfer with T22-GFP-H6. The unique GFP tryptophan (Trp) is located 1.3 to 1.5 nm away from the chromophore. So, an efficient energy transfer from Trp to the chromophore should be possible. Fluorescence resonance energy transfer (FRET) analysis was developed by exciting the GFP sample at $\lambda_{ex} = 295$ nm and reading the fluorescence emission at 513 nm. Emission spectra were acquired within a range of 500 to 650 nm. The protein concentration used was 0.25 mg/mL in carbonate buffer with salt.

Dynamic Light Scattering. The volume size distribution of NPs was determined at 0.25 mg/mL in carbonate buffer with salt by dynamic light scattering (DLS) at 633 nm (Zetasizer Nano ZS, Malvern Instruments Limited, Malvern, U.K.). Samples were maintained at the indicated temperature for 5 min before the measurement. The heating rate for thermal profiles was set at 1 °C/min.

Electron Microscopy (EM). The ultrastructural morphometry (size and shape) of unassembled protomers and NPs was determined at nearly native state both by deposition on silicon wafers with field-emission scanning electron microscopy (FESEM) and by negative staining with transmission electron microscopy (TEM). Drops of 3 µL of NPs and unassembled versions of T22-GFP-H6 and T22-DITOX-H6 at 0.25 mg/mL in carbonate buffer with salt were directly deposited on silicon wafers (Ted Pella, Reading, CA) for 1 min, and the excess of liquid was blotted with Whatman filter paper number 1 (GE Healthcare), air-dried for few minutes, and immediately observed without coating with a FESEM Zeiss Merlin (Zeiss, Oberkochen, Germany) operating at 1 kV equipped with a high-resolution in-lens secondary electron detector. Drops of 3 µL of the same four samples were directly deposited on 200-mesh carbon-coated copper grids (Electron Microscopy Sciences, Hatfield, PA) for 30 s, and the excess was blotted with Whatman filter paper, contrasted with 3 µL of 1% uranyl acetate (Polysciences, Warrington, PA) for 1 min, blotted again, and observed in a TEM JEOL 1400 (Jeol, Tokyo, Japan) operating at 80 kV equipped with a Gatan Orius SC200 CCD camera (Gatan, Abingdon, U.K.). For each sample and technique, representative images of different fields were captured at high magnifications (from 100 000× to 500 000×).

Circular Dichroism. Measurements were made with a JASCO J-715 spectropolarimeter (JASCO, Oklahoma City, OK) with a thermostated device by a Peltier system. Spectropolarimeter using a 1 mm path length quartz cell. Each spectrum was an average of six scans. The protein concentration was adjusted to 0.25 mg/mL in carbonate buffer with salt. Scan speed was set at 50 nm/min with a 1 s response time. Molar ellipticity was calculated according to eq 2.

$$[\theta]_l^{MRW} = \frac{MRW \times \theta}{l \times c} \quad (2)$$

where MRW is the mean residue molecular weight calculated from the protein sequence, θ is the measured ellipticity (in degrees) at a given wavelength, l is the path length in millimeters, and c is the protein concentration in g/mL. Measurements were carried out in the 200–260 nm region. Molar ellipticity units were deg cm² dmol^{−1} residue^{−1}. For the thermal studies, the heating rate was set at 1 °C/min.

RESULTS

T22-GFP-H6 and its derivative T22-DITOX-H6 (Figure 1a) have been produced in recombinant bacteria as single molecular species (Figure 1b) and obtained as either unassembled protomers or assembled NPs (Figure 1b,c), with sizes and molecular architecture described elsewhere.^{13b,22} This fact allows the comparative analysis of the conformation acquired by these proteins in each supramolecular form. For that, intrinsic fluorescence spectrum and circular dichroism

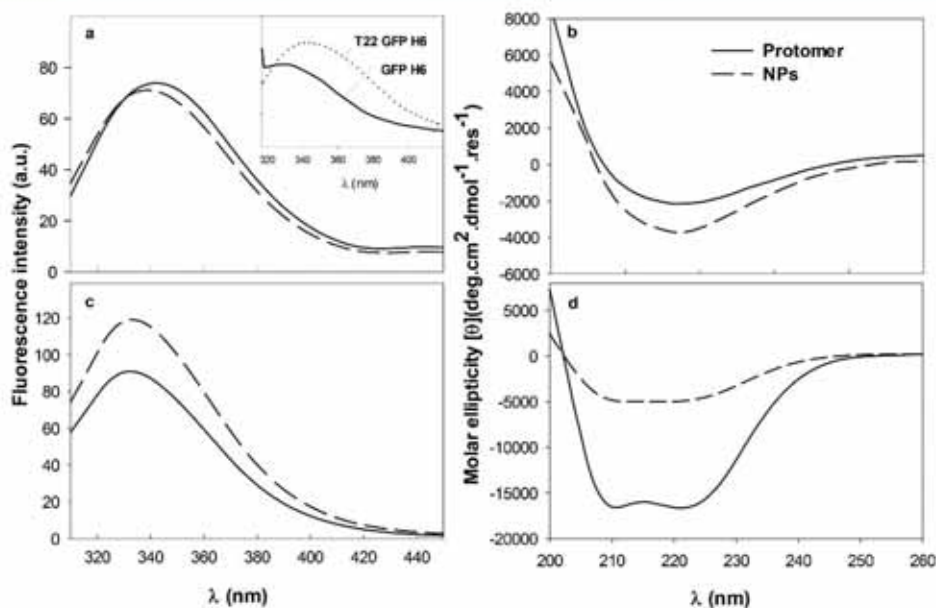


Figure 2. Protein spectroscopy obtained at 25 °C for the protomer (whole line) and the NP (dashed line) versions. (a) T22-GFP-H6 Trp fluorescence spectra. (b) T22-GFP-H6 CD spectra. (c) T22-DITOX-H6 fluorescence spectra. (d) T22-DITOX-H6 CD spectra.

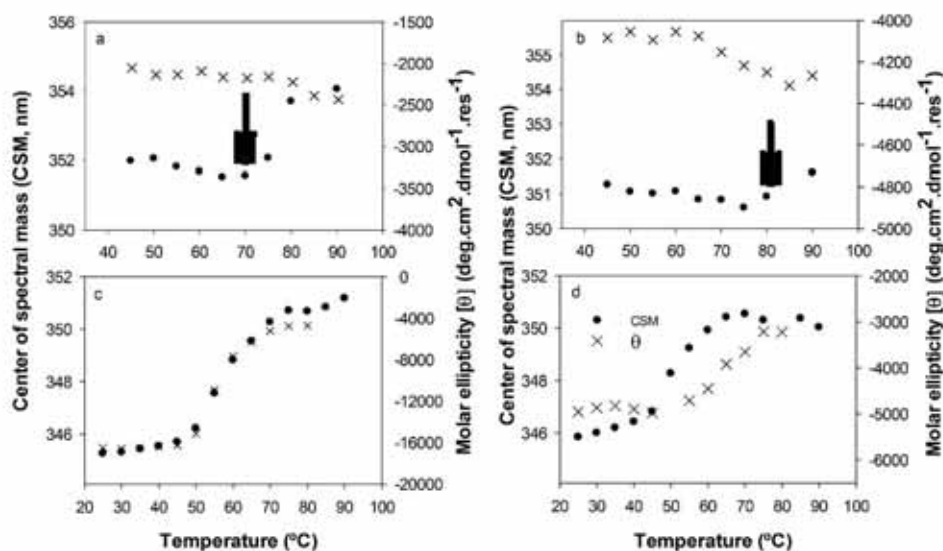


Figure 3. Protein thermal unfolding measured by the center of spectral mass of the Trp fluorescence spectrum CSM (black symbols) and by far-UV CD molar ellipticity values (× symbols) at (a,b) 218 and (c,d) 222 nm. (a,b) T22-GFP-H6 protomer and NPs, respectively. (c,d) T22-DITOX-H6 protomer and NPs, respectively.

spectrum of each protein versions were determined to identify possible structural changes as the monomer undergoes conversion into NPs. In tryptophan (Trp)-containing proteins, the amino acid fluorescence dominates the emission spectrum upon excitation at 295 nm, and it results in being sensitive to the molecular environment.²⁶ This property is related to the protein globular conformation. Initially, the T22-GFP-H6 Trp fluorescence spectrum was performed (Figure 2a). GFP contains only one Trp located 1.3 to 1.5 nm away from the chromophore, and efficient energy transfer from Trp to the green chromophore should be possible. This fact explains the low-intensity values for Trp fluorescence emission in GFP-

H6.²⁷ Besides, T22 contains only one Trp residue located after two arginines from the amino terminal sequence. Therefore, the higher accessibility to the molecular environment reflected a more hydrated or polar environment for Trp from T22. The inset from Figure 2a proved that in this protein the Trp fluorescence signal comes mainly from the cationic peptide instead of GFP domain. Because T22 seems to be more exposed to the medium,^{13b} no visible differences could be detected between both protein formats. However, subtle changes in the fluorescence signal were observed, and T22-GFP-H6 NPs exhibited a discrete displacement of the CSM toward minor values with respect to the protomer. In such NP

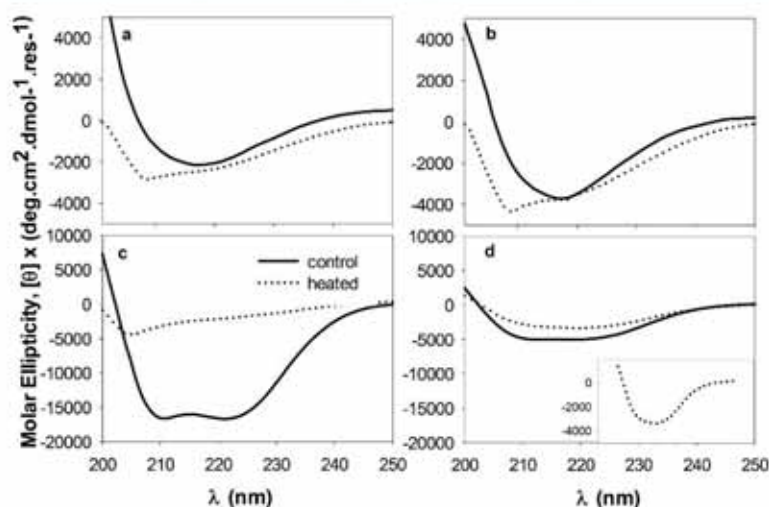


Figure 4. Far-UV CD spectra of T22-GFP-H6 building blocks (a) and NPs (b) and T22-DITOX-H6 building blocks (c) and NPs (d) before (whole line) and after (dashed line) the thermal treatment up to 90 °C for T22-GFP-H6 versions and up to 70 °C for T22-DITOX-H6. The inset details the spectrum of heated T22-DITOX-H6 NPs.

version, new intra- or intermolecular interaction of T22 within the protein assembly appeared (Figure 2a). On the contrary, CD studies demonstrated the highly β -sheet secondary structure of T22-GFP-H6, with a spectrum minimum at 217 nm (Figure 2b, whole line). The oligomeric form of T22-GFP-H6 exhibited an inconspicuous increase in beta structure extent with respect to the protomer (Figure 2b, dashed line). The minimum increase was only 2000 molar ellipticity units (from -2000 to -4000).

On the contrary, T22-DITOX-H6 contains five Trp residues, what makes this construct suitable for intrinsic fluorescence analysis. The fluorescence spectrum analysis of this protein obtained at 25 °C turned out a CSM value of 345.2 nm and a maximal wavelength, λ_{max} , of 330 nm (Figure 2c, whole line). These data were compatible with Trp residues localized in a nonpolar environment. It is interesting to compare this CSM value of 345.2 nm with CMS of 352 nm obtained with the T22-GFP-H6 protomer. As mentioned above, the fluorescence signal of the GFP moiety comes from the Trp highly accessible to a polar environment. Within the NPs, the Trp residues of T22-DITOX-H6 sensed a less hydrophobic environment (CMS = 345.9) while λ_{max} moved from 332 to 334 nm (Figure 2c, dashed line or Figure 3c,d, black points from 25 to 40 °C). Although these last results are not drastically different, a remarkable contrast in the far UV CD signal emerged between T22-DITOX-H6 as a protomer and as a NP (Figure 2d). The protomer exhibited highly alpha structure (two spectrum minima at 211 and 222 nm) as previously reported for the catalytic domain of diphtheria toxin.²⁸ In the assembled form, the alpha structure content seemed to fade away concomitant with the appearance of beta conformation as the two minima become less noticeable (Figure 2d, dashed line). Besides, the secondary structure content analyzed by JASCO spectra-manager analysis software showed an increase in beta structure of 23% (RMS:25%) as the protomer takes part of NPs. In these cases, the spectra wavelength range was 190 to 260 nm.

The unfolding of each protein version was studied by the analysis of the tertiary (center of spectral mass (CSM)) and the secondary (the molar ellipticity value at the spectrum

minimum point) structure as the temperature increased. When proteins unfolded, Trp residues moved to a highly hydrated environment and consequently the CSM value grew (Figure 3). On the contrary, the secondary structure faded away versus temperature and an increase in the molar ellipticity was recorded (Figure 3, \times symbols). The unfolding temperature (T_m) is the " \times " value that corresponds to the inflection point in the curve (Figure 3). In this context, the heating of unassembled T22-GFP-H6 caused a modest increase in the CSM value at 70 °C (Figure 3a), indicating that the protein transitioned to a more loosely packed structure. Moreover, in T22-GFP-H6 NPs, this event was negligible (Figure 3b). In both versions of T22-GFP-H6, the molar ellipticity seemed to be unaltered while heating (Figure 3a,b, \times symbols). Despite that, no visible secondary structure appeared in the CD spectra of T22-GFP-H6 after heating the protein to 90 °C (Figure 4a,b). This indicated that at 90 °C the secondary structure of both formats of T22-GFP-H6 vanished, but it cannot be demonstrated by the thermal profile of the CD value at 222 nm analyses.

In the thermal unfolding of the T22-DITOX-H6 building block, a typical two-state thermal transition was observed. The unfolding temperature (T_m) is 57 °C (Figure 3c). Because fluorescence studies are related to the tertiary structure and far-UV CD deals with the secondary structure of proteins, the overlaid experimental curves confirmed that T22-DITOX-H6 protomer unfolds as a cooperative unit. In contrast, T22-DITOX-H6, assembled as NPs, revealed a more complex thermal unfolding profile. In contrast with what happens with the subunit, the oligomeric protein first loses its tertiary conformation (Figure 3d), and this event occurs at a lower temperature than in the case of protomers ($T_m = 52$ °C). However, the secondary structure was preserved at higher temperatures with respect to the protomer ($T_m = 64$ °C) (Figure 3d). This complex thermal unfolding was previously described for other oligomeric proteins.²⁹ Besides, the data in Figure 4d demonstrate that after heating to 70 °C T22-DITOX-H6 preserved its secondary structure in NPs (see the inset). The molar ellipticity value exhibited by the protomer jumps around 14 000 units from low to high temperatures

(from $-18\,000$ to -4000 ellipticity), while the change in molar ellipticity of NPs during the whole heating range is just 2000 units (from -4800 to -3200). Therefore, we confirm that oligomerization confers secondary structure thermal stability to T22-DITOX-H6, although it is still unclear with the situation of T22-GFP-H6 upon heating. To go further into the analyses of NP integrity, we evaluated the hydrodynamic size of the NPs and the possible disassembly associated with temperature increase.

DLS analyses confirmed the oligomeric nature of the NP samples at 25 °C. T22-GFP-H6 protomer showed a size of 5.6 nm (pdi = 0.342), while the NPs measured 12.3 nm (pdi = 0.452) (Figure 5a,c, whole line). Contrary to what is expected

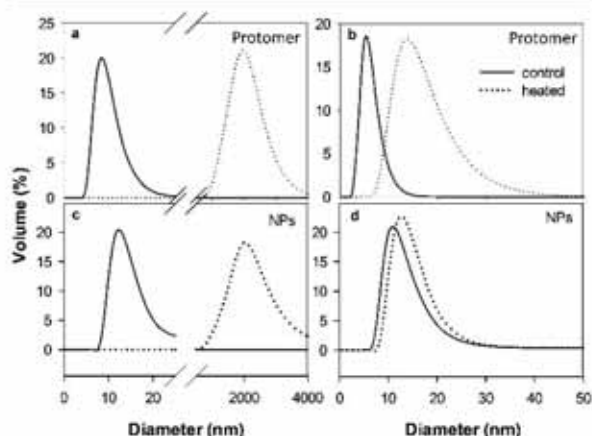


Figure 5. Relative frequency distribution of diameters (volume-weighted distribution) determined by DLS. (a) T22-GFP-H6 protomers, (b) T22-DITOX-H6 protomers, (c) T22-GFP-H6 NPs, and (d) T22-DITOX-H6 NPs. The whole line represents the measurement at 25 °C and the dashed line represents the measurement at 70 (for T22-DITOX-H6) or 85 °C (for T22-GFP-H6).

when the protein was heated to 85 °C, the building block acquired on average an oligomeric size of 13.5 nm (pdi = 0.178), equally from that presented by the heated NPs (13.5 nm (pdi = 0.159)). Therefore, the disassembling of NPs as temperature increased was ruled out. It is noteworthy that, in fact, the heated samples displayed higher particle size, a phenomenon that could be related to the highly hydrated or unfolding nature of T22-GFP-H6. The reason for acquiring a similar particle size would need further investigation, but it could be related to the appearance of an oligomeric transition state during unfolding in the NPs as in the protomer. The unassembled T22-DITOX-H6 exhibited a molecular size of 8.72 nm (pdi = 0.596) at 25 °C (Figure 5b, whole line), and the NP size was on average 12.3 nm (pdi = 0.293) (Figure 5d, whole line). When both samples were heated to 70 °C, the proteins were completely aggregated (Figure 5d, dashed line). These last DLS size measurements of protomers and NPs were ~ 1990 nm (pdi = 0.25), far from the detection limit of the equipment. Despite the NP coagulation state, they seemed to retain secondary structure, as demonstrated by data in Figure 3d (dashed line or inset). In addition, data in the inset of Figure 4d also supported the preservation of secondary structure while heating.

Later, we take advantage of the internal FRET phenomenon that occurs within the protein. Interestingly, the fluorescence of the green chromophore excited at 488 nm (λ_{ex}) was practically the same within both versions (Figure 6a). On the

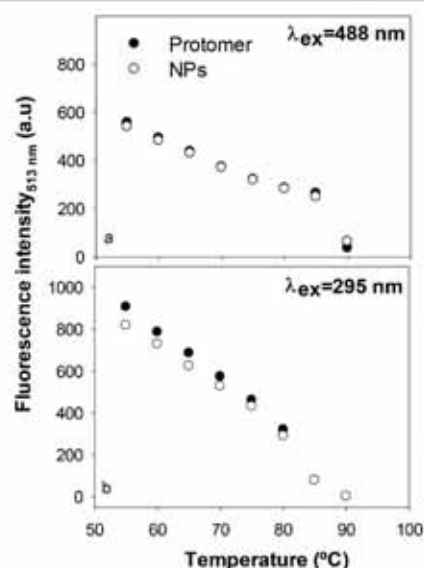


Figure 6. T22-GFP-H6 chromophore fluorescence intensity (at 513 nm) decrease versus temperature measured at two different λ_{ex} /wavelengths (a) $\lambda_{ex} = 488$ nm and (b) $\lambda_{ex} = 295$ nm.

contrary, we evaluated the internal FRET as described in the Materials and Methods. Surprisingly, the fluorescence decay occurs with different slopes, depending on the supramolecular state of T22-GFP-H6 up to 80 °C (Figure 6b) ($\text{slope}_{\text{Protomer}} = -23 \pm 0.5$ and $\text{slope}_{\text{NPs}} = -20 \pm 0.7$). Beyond this temperature, both protein versions exhibited the same fluorescence intensity, suggesting that up to 80 °C there is subtle remoteness between the fluorophores concomitant with distinct structural features within NPs. Above 80 °C, similar protein structure exhibited similar fluorescence values (Figure 6a) and similar sizes (Figure 5 a,c)

In an attempt to assess that the subtle structural qualities of NPs with respect to T22-GFP-H6 protomer modulate the thermal stability up to 80 °C, we studied the thermal reversibility of the internal FRET upon heating. The obtained data demonstrated that upon cooling from 80 °C, the protein within the NPs recovered 62% of the initial fluorescence at 40 °C (Figure 7a,b).

On the contrary, the heating of the protein samples to 90 °C demonstrated that the recovery of fluorescence values after cooling to 40 °C was negligible for both protein versions (Figure 7c,d). Then, we can conclude that a subtle structural difference appears in both T22-GFP-H6 versions that is maintained until the protein sample is heated to 80 °C.

DISCUSSION

Peptide and protein self-assembling is a complex thermodynamic process³⁰ whose control, even partial, might allow the generation of promising protein-based materials with a spectrum of biomedical applications, especially in drug delivery.^{2a,b,4,8,31} Several types of protein NPs for industrial or biomedical applications have been generated by exploiting

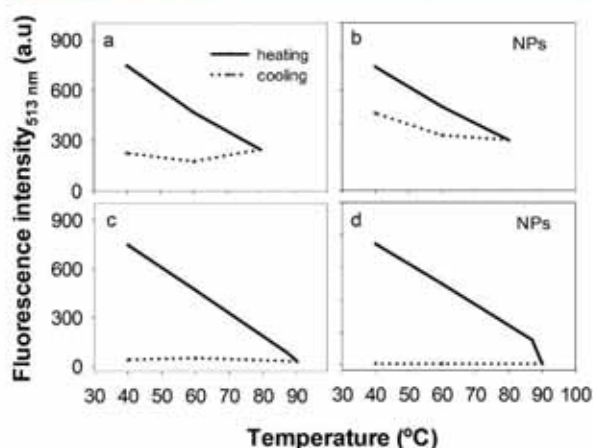


Figure 7. T22-GFP-H6 chromophore fluorescence intensity (at 513 nm, $\lambda_{ex} = 295$ nm) as heating-cooling cycle. (a,b) Heating to 80 °C and cooling to 40 °C. (c,d) Heating to 90 °C and cooling to 40 °C.

the hydrophobic interactions between short amylogenic peptides³² or the structural plasticity of transmembrane proteins,³³ among others. In the context of the emerging interest of artificial viruses as drug delivery agents,^{9a,34} antimicrobial peptides^{9b,35} and a diversity of proteins and protein segments^{11b,36} have been genetically instructed to self-assemble as mimetics of viral capsids for cell-targeted drug or gene delivery. Such materials are structurally distinguishable from those based on amyloid fibrils,^{1a,d,5} which are being developed as well using different nanoscale architectonic principles.

A category of GFP-based oligomeric NPs (T22-GFP-H6) and a potent self-targeted, self-delivered, nanostructured protein drug (T22-DITOX-H6, Figure 1), fully representative of the vehicle-free emerging concept in nanomedicine,²³ have been explored here regarding the conformational changes undergone during oligomerization. These NPs organize as symmetric toroid architectures^{13b} whose assembly appears to be initiated by electrostatic cross-molecular contacts¹² and supported by a diversity of noncovalent interactions between building blocks (including hydrogen bond and van der Waals interactions).^{13a} The C-terminal histidine-rich domain has a prevalent role in the oligomerization process because imidazole is a potent disruptor of the material once formed.²⁴ The resulting nanoscale materials are highly soluble, do not form fibrils, and show a moderate content of cross-molecular β -sheet conformation compared with amyloid aggregates of the same protein species,^{13b,36} supportive of a nonamylogenic character. These types of protein-only constructs are supported by a modular multidomain architecture, and they are especially appealing regarding the design of innovative tumor-targeted cancer medicines, where T22-DITOX-H6 is a paradigmatic representative. Produced by biological fabrication in a single step, they self-deliver therapeutic proteins with cytotoxic activities, such as human pro-apoptotic factors, toxins, or venom components, in a nanostructured way and with a high level of selectivity for specific tumor markers.^{9b,37} The use of human proteins or deimmunized toxin versions as the main component of these novel drugs, in constructs that do not contain heterologous protein segments (or as minor components), is expected to minimize or eliminate the risk of immune reactions that might be associated with the

repeated administration of nonhuman polypeptides as therapeutics.³⁸

In general, how proteins adopt their conformation during controlled self-assembling to form nonamyloid materials is a neglected issue but is of pivotal relevance in the context of the growing interest in protein-based functional materials.^{2a,b,4,6a,8} In the oligomeric state, the GFP-based T22-GFP-H6 construct presents a shift on λ_{max} values and an increase in the CD signal (Figure 2a,b, respectively). T22-GFP-H6 contains two Trp residues (one within GFP and the other within T22). Their emission (expressed as CSM value) senses a higher hydrophobic environment compared with this phenomenon in the subunit (Figure 2a). Besides, an important proportion of the fluorescence comes from T22 (Figure 2a, inset). These results, concomitant with an increase in the beta structure content in the NP forms (Figure 2b), are in agreement with the concept that the structural conformation is explained by the appearance of the intermolecular interactions in the NPs. Nevertheless, the expansion of the structural information obtained by internal FRET experiments proves that subtle structural rearrangements emerge in GFP moieties of the protein once assembled in NPs. Overall, the described structural features are related to a resilient conformation (Figure 6a,b) of the NPs until 80 °C with respect to their unassembled, individual building blocks. After a thermal heating to 85 °C/90 °C, an unfolded structure is achieved (Figure 4a,b). Surprisingly, both protomers and NPs reached the same oligomer size (Figure 4b,d), suggesting that particular oligomeric forms could also represent an intermediate transition state in the thermal unfolding of the unassembled version.

Finally, DITOX-based NPs present a notably distinct conformation with respect to the subunit version. As NPs, the fusion protein exhibits lesser alpha content and higher beta structure than the protomer version (Figures 2d and 3 d). This result is concomitant with those obtained with fluorescence analyses, like the modest increase in the CSM values in NPs with respect to the subunits (Figure 2c,d) that could be related to the increase in the functionality of DITOX-based NPs. Interestingly, the secondary structure of the NP version remains practically changeless up to 70 °C, and the protein gets aggregated in stable and well-formed NPs (Figures 4d and 5d).

All of these data, apart from the explanation of the conformational transition of protein building blocks into nonamyloid protein NPs, suggest a higher structural stability of the proteins once assembled compared with the unassembled versions. In fact, this NP thermodynamic stability could represent a kinetically trapped state of the proteins, as demonstrated in our previous analyses^{12,24} and still under study. Such notably high stability of the oligomers had been already observed *in vivo*, where a proper tissue targeting and excellent tumor biodistribution are achieved by T22-empowered NPs but not by the equivalent unassembled protein versions.^{13a} The data presented here strongly push toward the use of oligomeric versions of cell-targeted drugs or vehicles versus the monomeric or dimeric versions employed in immunotoxins, antibody-drug nanoconjugates, and other innovative drugs.^{9b} Structurally, protein-based oligomers might offer all of the conditions for the optimal mimicking of protein-based natural nanoscale agents so that such viruses are ideal regarding tissue penetrability, multivalent ligand presentation, and intracellular cell delivery.^{9a,39}

■ CONCLUSIONS

The results presented in this study demonstrate the novel conformation and structure acquired by T22-empowered polypeptides as building blocks of regular homo-oligomers, which is compatible with their functionality as CXCR4⁺ tumor-targeted NPs. While the internal compactness of the polypeptide is dependent on the specific amino acid sequence located between the cationic and histidine-rich terminal peptides (see the differences between GFP and DITOX), oligomerization occurs concomitantly to an increase in beta structure, which seems to be associated with a thermal stabilization of the protein in the complex. Whether this enhanced structural stability is connected to an improved functional stability, thus supporting the high in vivo performance of these NPs, needs to be further investigated. This structural profiling adds clues for the further design of self-assembling protein NPs that, like T22-DITOX-H6, base both architecture and therapeutic activity on the conformation of the assembled protein.

■ AUTHOR INFORMATION

Corresponding Authors

*E.V.: E-mail: Esther.vazquez@uab.es.

*A.V.: E-mail: Antoni.villaverde@uab.es.

ORCID

Antonio Villaverde: 0000-0002-2615-4521

Present Address

▽M.P.: Institute for Research in Biomedicine (IRB Barcelona), The Barcelona Institute of Science and Technology, Barcelona 08028, Spain.

Author Contributions

The manuscript was written through contributions of all authors. All authors have given approval to the final version of the manuscript.

Notes

The authors declare the following competing financial interest(s): L.S.-G., N.S., U.U., R.M., E.V., and A.V. have authored a patent on the use of self-assembling, tumor-targeted cytotoxic proteins.

■ ACKNOWLEDGMENTS

Protein production and DLS have been partially performed by the ICTS "NANBIOSIS", more specifically by the Protein Production Platform of CIBER-BBN/IBB (<http://www.nanbiosis.es/unit/u1-protein-production-platform-ppp/>) and the Biomaterial Processing and Nanostructuring Unit (<http://www.nanbiosis.es/portfolio/u6-biomaterial-processing-and-nanostructuring-unit/>). J.M.S. is a Career Investigator from CONICET (Government of Argentina), L.S.-G. was supported by a predoctoral fellowship from AGAUR (2017FI_B100063), N.S. was supported by a predoctoral fellowship from the Government of Navarra, and U.U. received a Sara Borrell postdoctoral fellowship from AGAUR. A.V. received an ICREA ACADEMIA award. This study has been funded by the Agencia Estatal de Investigación (AEI) and Fondo Europeo de Desarrollo Regional (FEDER) (grant BIO2016-76063-R, AEI/FEDER, UE), AGAUR (2017SGR-229), and CIBER-BBN (project VENOM4-CANCER) granted to A.V., ISCIII (PI15/00272 cofunding FEDER) to E.V., and ISCIII (PI15/00378 and PIE15/00028, cofunding FEDER) to R.M.

■ REFERENCES

- (1) (a) Li, D.; Jones, E. M.; Sawaya, M. R.; Furukawa, H.; Luo, F.; Ivanova, M.; Sievers, S. A.; Wang, W. Y.; Yaghi, O. M.; Liu, C.; Eisenberg, D. S. Structure-Based Design of Functional Amyloid Materials. *J. Am. Chem. Soc.* **2014**, *136* (52), 18044–18051. (b) Ferrer-Miralles, N.; Rodriguez-Carmona, E.; Corchero, J. L.; Garcia-Fruitos, E.; Vazquez, E.; Villaverde, A. Engineering protein self-assembling in protein-based nanomedicines for drug delivery and gene therapy. *Crit. Rev. Biotechnol.* **2015**, *35* (2), 209–21. (c) Loo, Y.; Goktas, M.; Tekinay, A. B.; Guler, M. O.; Hauser, C. A.; Mitraki, A. Self-Assembled Proteins and Peptides as Scaffolds for Tissue Regeneration. *Adv. Healthcare Mater.* **2015**, *4* (16), 2557–86. (d) Kumar, V. A.; Wang, B. K.; Kanahara, S. M. Rational design of fiber forming supramolecular structures. *Exp. Biol. Med.* **2016**, *241* (9), 899–908. (e) Yeates, T. O.; Liu, Y.; Laniado, J. The design of symmetric protein nanomaterials comes of age in theory and practice. *Curr. Opin. Struct. Biol.* **2016**, *39*, 134–143.
- (2) (a) Sutherland, T. D.; Rapson, T. D.; Huson, M. G.; Church, J. S. Recombinant Structural Proteins and Their Use in Future Materials. *Subcell. Biochem.* **2017**, *82*, 491–526. (b) Kobayashi, N.; Arai, R. Design and construction of self-assembling supramolecular protein complexes using artificial and fusion proteins as nanoscale building blocks. *Curr. Opin. Biotechnol.* **2017**, *46*, 57–65. (c) Corchero, J. L.; Vazquez, E.; Garcia-Fruitos, E.; Ferrer-Miralles, N.; Villaverde, A. Recombinant protein materials for bioengineering and nanomedicine. *Nanomedicine* **2014**, *9* (18), 2817–28.
- (3) Sanchez-Garcia, L.; Martin, L.; Mangués, R.; Ferrer-Miralles, N.; Vazquez, E.; Villaverde, A. Recombinant pharmaceuticals from microbial cells: a 2015 update. *Microb. Cell Fact.* **2016**, *15*, 33.
- (4) Sutherland, T. D.; Huson, M. G.; Rapson, T. D. Rational design of new materials using recombinant structural proteins: Current state and future challenges. *J. Struct. Biol.* **2018**, *201* (1), 76–83.
- (5) Knowles, T. P. J.; Mezzenga, R. Amyloid Fibrils as Building Blocks for Natural and Artificial Functional Materials. *Adv. Mater.* **2016**, *28* (31), 6546–6561.
- (6) (a) Wei, G.; Su, Z.; Reynolds, N. P.; Arosio, P.; Hamley, I. W.; Gazit, E.; Mezzenga, R. Self-assembling peptide and protein amyloids: from structure to tailored function in nanotechnology. *Chem. Soc. Rev.* **2017**, *46* (15), 4661–4708. (b) Wendell, D. W.; Patti, J.; Montemagno, C. D. Using biological inspiration to engineer functional nanostructured materials. *Small* **2006**, *2* (11), 1324–9.
- (7) Dai, B.; Li, D.; Xi, W.; Luo, F.; Zhang, X.; Zou, M.; Cao, M.; Hu, J.; Wang, W.; Wei, G.; Zhang, Y.; Liu, C. Tunable assembly of amyloid-forming peptides into nanosheets as a retrovirus carrier. *Proc. Natl. Acad. Sci. U. S. A.* **2015**, *112* (10), 2996–3001.
- (8) Guttenplan, A. P. M.; Young, L. J.; Matak-Vinkovic, D.; Kaminski, C. F.; Knowles, T. P. J.; Itzhaki, L. S. Nanoscale click-reactive scaffolds from peptide self-assembly. *J. Nanobiotechnol.* **2017**, *15* (1), 70.
- (9) (a) Unzueta, U.; Cespedes, M. V.; Vazquez, E.; Ferrer-Miralles, N.; Mangués, R.; Villaverde, A. Towards protein-based viral mimetics for cancer therapies. *Trends Biotechnol.* **2015**, *33* (5), 253–8. (b) Serna, N.; Sanchez-Garcia, L.; Unzueta, U.; Diaz, R.; Vazquez, E.; Mangués, R.; Villaverde, A. Protein-Based Therapeutic Killing for Cancer Therapies. *Trends Biotechnol.* **2018**, *36* (3), 318–335.
- (10) (a) Holowka, E. P.; Sun, V. Z.; Kamei, D. T.; Deming, T. J. Polyarginine segments in block copolypeptides drive both vesicular assembly and intracellular delivery. *Nat. Mater.* **2007**, *6* (1), 52–7. (b) Liu, L.; Xu, K.; Wang, H.; Jeremy Tan, P. K.; Fan, W.; Venkatraman, S. S.; Li, L.; Yang, Y. Y. Self-assembled cationic peptide nanoparticles as an efficient antimicrobial agent. *Nat. Nanotechnol.* **2009**, *4* (7), 457–63.
- (11) Vazquez, E.; Roldan, M.; Diez-Gil, C.; Unzueta, U.; Domingo-Espin, J.; Cedano, J.; Conchillo, O.; Ratera, I.; Veciana, J.; Daura, X.; Ferrer-Miralles, N.; Villaverde, A. Protein nanodisk assembling and intracellular trafficking powered by an arginine-rich (R9) peptide. *Nanomedicine* **2010**, *5* (2), 259–68.
- (12) Unzueta, U.; Ferrer-Miralles, N.; Cedano, J.; Zikung, X.; Pesarrodonna, M.; Saccardo, P.; Garcia-Fruitos, E.; Domingo-Espin, J.

Kumar, P.; Gupta, K. C.; Mangues, R.; Villaverde, A.; Vazquez, E. Non-amyloidogenic peptide tags for the regulatable self-assembly of protein-only nanoparticles. *Biomaterials* **2012**, *33* (33), 8714–22.

(13) (a) Cespedes, M. V.; Unzueta, U.; Tatkiewicz, W.; Sanchez-Chardi, A.; Conchillo-Sole, O.; Alamo, P.; Xu, Z.; Casanova, I.; Corchero, J. L.; Pesarrodona, M.; Cedano, J.; Daura, X.; Ratera, I.; Veciana, J.; Ferrer-Mirallès, N.; Vazquez, E.; Villaverde, A.; Mangues, R. In vivo architectonic stability of fully de novo designed protein-only nanoparticles. *ACS Nano* **2014**, *8* (5), 4166–76. (b) Rueda, F.; Cespedes, M. V.; Conchillo-Sole, O.; Sanchez-Chardi, A.; Seras-Franzoso, J.; Cubarsi, R.; Gallardo, A.; Pesarrodona, M.; Ferrer-Mirallès, N.; Daura, X.; Vazquez, E.; Garcia-Fruitos, E.; Mangues, R.; Unzueta, U.; Villaverde, A. Bottom-Up Instructive Quality Control in the Biofabrication of Smart Protein Materials. *Adv. Mater.* **2015**, *27* (47), 7816–22.

(14) Pesarrodona, M.; Crosas, E.; Cubarsi, R.; Sanchez-Chardi, A.; Saccardo, P.; Unzueta, U.; Rueda, F.; Sanchez-Garcia, L.; Serna, N.; Mangues, R.; Ferrer-Mirallès, N.; Vazquez, E.; Villaverde, A. Intrinsic functional and architectonic heterogeneity of tumor-targeted protein nanoparticles. *Nanoscale* **2017**, *9* (19), 6427–35.

(15) Murakami, T.; Maki, W.; Cardones, A. R.; Fang, H.; Tun Kyi, A.; Nestle, F. O.; Hwang, S. T. Expression of CXCR4 chemokine receptor-4 enhances the pulmonary metastatic potential of murine B16 melanoma cells. *Cancer Res.* **2002**, *62* (24), 7328–34.

(16) Wilen, C. B.; Tilton, J. C.; Doms, R. W. Molecular mechanisms of HIV entry. *Adv. Exp. Med. Biol.* **2012**, *726*, 223–42.

(17) (a) Klönisch, T.; Wiehac, E.; Hombach-Klonisch, S.; Ande, S. R.; Wesselborg, S.; Schulze-Osthoff, K.; Los, M. Cancer stem cell markers in common cancers - therapeutic implications. *Trends Mol. Med.* **2008**, *14* (10), 450–60. (b) Sun, X.; Cheng, G.; Hao, M.; Zheng, J.; Zhou, X.; Zhang, J.; Taichman, R. S.; Pienta, K. J.; Wang, J. CXCL12/CXCR4/CXCR7 chemokine axis and cancer progression. *Cancer Metastasis Rev.* **2010**, *29* (4), 709–22.

(18) (a) Kim, J.; Mori, T.; Chen, S. L.; Amersi, F. F.; Martinez, S. R.; Kuo, C.; Turner, R. R.; Ye, X.; Bilchik, A. J.; Morton, D. L.; Hoon, D. S. Chemokine receptor CXCR4 expression in patients with melanoma and colorectal cancer liver metastases and the association with disease outcome. *Ann. Surg.* **2006**, *244* (1), 113–20. (b) Liang, Z.; Yoon, Y.; Votaw, J.; Goodman, M. M.; Williams, L.; Shim, H. Silencing of CXCR4 blocks breast cancer metastasis. *Cancer Res.* **2005**, *65* (3), 967–71.

(19) (a) Unzueta, U.; Cespedes, M. V.; Ferrer-Mirallès, N.; Casanova, I.; Cedano, J.; Corchero, J. L.; Domingo-Espin, J.; Villaverde, A.; Mangues, R.; Vazquez, E. Intracellular CXCR4(+) cell targeting with T22-empowered protein-only nanoparticles. *Int. J. Nanomed.* **2012**, *7*, 4533–44. (b) Cespedes, M. V.; Unzueta, U.; Alamo, P.; Gallardo, A.; Sala, R.; Casanova, I.; Pavon, M. A.; Mangues, M. A.; Trias, M.; Lopez-Pousa, A.; Villaverde, A.; Vazquez, E.; Mangues, R. Cancer-specific uptake of a liganded protein nanocarrier targeting aggressive CXCR4+ colorectal cancer models. *Nanomedicine* **2016**, *12* (7), 1987–1996.

(20) Xu, Z.; Unzueta, U.; Roldán, M.; Mangues, R.; Sánchez-Chardi, A.; Ferrer-Mirallès, N.; Villaverde, A.; Vázquez, E. Formulating tumor-homing peptides as regular nanoparticles enhances receptor-mediated cell penetrability. *Mater. Lett.* **2015**, *154*, 140–143.

(21) Akbari, B.; Farajnia, S.; Ahdi Khosroshahi, S.; Safari, F.; Yousefi, M.; Dariushnejad, H.; Rahbarnia, L. Immunotoxins in cancer therapy: Review and update. *Int. Rev. Immunol.* **2017**, *36*, 207–219.

(22) Sanchez-García, L.; Serna, N.; Alamo, P.; Sala, R.; Cespedes, M. V.; Roldán, M.; Sanchez-Chardi, A.; Unzueta, U.; Casanova, I.; Mangues, R.; Vazquez, E.; Villaverde, A. Self-assembling toxin-based nanoparticles as self-delivered antitumoral drugs. *J. Controlled Release* **2018**, *274*, 81–92.

(23) Shen, J.; Wolfram, J.; Ferrari, M.; Shen, H. Taking the vehicle out of drug delivery. *Mater. Today* **2017**, *20* (3), 95–97.

(24) Unzueta, U.; Serna, N.; Sanchez-Garcia, L.; Roldán, M.; Sanchez-Chardi, A.; Mangues, R.; Villaverde, A.; Vazquez, E. Engineering multifunctional protein nanoparticles by in vitro

disassembling and reassembling of heterologous building blocks. *Nanotechnology* **2017**, *28* (50), 505102.

(25) (a) Li, T. M.; Hook, J. W., 3rd; Drickamer, H. G.; Weber, G. Plurality of pressure-denatured forms in chymotrypsinogen and lysozyme. *Biochemistry* **1976**, *15* (25), 5571–80. (b) Ruan, K.; Weber, G. Hysteresis and conformational drift of pressure-dissociated glyceraldehydephosphate dehydrogenase. *Biochemistry* **1989**, *28* (5), 2144–53. (c) Mohana-Borges, R.; Silva, J. L.; Ruiz-Sanz, J.; de Prat-Gay, G. Folding of a pressure-denatured model protein. *Proc. Natl. Acad. Sci. U. S. A.* **1999**, *96* (14), 7888–93.

(26) Lakowicz, J. R.; Kusba, J.; Wiczak, W.; Gryczynski, I.; Szmajcinski, H.; Johnson, M. L. Resolution of the conformational distribution and dynamics of a flexible molecule using frequency-domain fluorometry. *Biophys. Chem.* **1991**, *39* (1), 79–84.

(27) Orm, M.; Cubitt, A. B.; Kallio, K.; Gross, L. A.; Tsien, R. Y.; Remington, S. J. Crystal structure of the *Aequorea victoria* green fluorescent protein. *Science* **1996**, *273* (5280), 1392–5.

(28) Choe, S.; Bennett, M. J.; Fujii, G.; Curmi, P. M. G.; Kantardjiev, K. A.; Collier, R. J.; Eisenberg, D. The Crystal-Structure of Diphtheria-Toxin. *Nature* **1992**, *357* (6375), 216–222.

(29) Sanchez, J. M.; Nolan, V.; Perillo, M. A. beta-galactosidase at the membrane-water interface: a case of an active enzyme with non-native conformation. *Colloids Surf., B* **2013**, *108*, 1–7.

(30) Wang, J.; Liu, K.; Xing, R.; Yan, X. Peptide self-assembly: thermodynamics and kinetics. *Chem. Soc. Rev.* **2016**, *45* (20), 5589–5604.

(31) (a) Yeates, T. O. Geometric Principles for Designing Highly Symmetric Self-Assembling Protein Nanomaterials. *Annu. Rev. Biophys.* **2017**, *46*, 23–42. (b) de Pinho Favaro, M. T.; Sanchez-García, L.; Sanchez-Chardi, A.; Roldán, M.; Unzueta, U.; Serna, N.; Cano-Garrido, O.; Azzoni, A. R.; Ferrer-Mirallès, N.; Villaverde, A.; Vazquez, E. Protein nanoparticles are nontoxic, tuneable cell stressors. *Nanomedicine* **2018**, *13* (3), 255–268.

(32) (a) Zou, Q.; Abbas, M.; Zhao, L.; Li, S.; Shen, G.; Yan, X. Biological Photothermal Nanodots Based on Self-Assembly of Peptide-Porphyrin Conjugates for Antitumor Therapy. *J. Am. Chem. Soc.* **2017**, *139* (5), 1921–1927. (b) Liu, K.; Yuan, C.; Zou, Q.; Xie, Z.; Yan, X. Self-Assembled Zinc/Cystine-Based Chloroplast Mimics Capable of Photoenzymatic Reactions for Sustainable Fuel Synthesis. *Angew. Chem., Int. Ed.* **2017**, *56* (27), 7876–7880.

(33) Tarasov, S. G.; Gaponenko, V.; Howard, O. M.; Chen, Y.; Oppenheim, J. J.; Dyba, M. A.; Subramanian, S.; Lee, Y.; Michejda, C.; Tarasova, N. I. Structural plasticity of a transmembrane peptide allows self-assembly into biologically active nanoparticles. *Proc. Natl. Acad. Sci. U. S. A.* **2011**, *108* (24), 9798–803.

(34) Noble, J. E.; De Santis, E.; Ravi, J.; Lamarre, B.; Castelletto, V.; Mantell, J.; Ray, S.; Ryadnov, M. G. A De Novo Virus-Like Topology for Synthetic Virions. *J. Am. Chem. Soc.* **2016**, *138* (37), 12202–10.

(35) (a) De Santis, E.; Alkassam, H.; Lamarre, B.; Faruqi, N.; Bella, A.; Noble, J. E.; Micale, N.; Ray, S.; Burns, J. R.; Yon, A. R.; Hoogenboom, B. W.; Ryadnov, M. G. Antimicrobial peptide capsids of de novo design. *Nat. Commun.* **2017**, *8* (1), 2263. (b) Castelletto, V.; de Santis, E.; Alkassam, H.; Lamarre, B.; Noble, J. E.; Ray, S.; Bella, A.; Burns, J. R.; Hoogenboom, B. W.; Ryadnov, M. G. Structurally plastic peptide capsules for synthetic antimicrobial viruses. *Chem. Sci.* **2016**, *7* (3), 1707–1711.

(36) Pesarrodona, M.; Ferrer-Mirallès, N.; Unzueta, U.; Gener, P.; Tatkiewicz, W.; Abasolo, I.; Ratera, J.; Schwartz, S., Jr.; Villaverde, A.; Vazquez, E. Intracellular targeting of CD44+ cells with self-assembling, protein only nanoparticles. *Int. J. Pharm.* **2014**, *473* (1–2), 286–95.

(37) Diaz, R.; Pallares, V.; Cano-Garrido, O.; Serna, N.; Sanchez-García, L.; Falgas, A.; Pesarrodona, M.; Unzueta, U.; Sanchez-Chardi, A.; Sanchez, J. M.; Casanova, I.; Vazquez, E.; Mangues, R.; Villaverde, A. Selective CXCR4(+) Cancer Cell Targeting and Potent Antineoplastic Effect by a Nanostructured Version of Recombinant Ricin. *Small* **2018**, *14* (26), 1800665.

(38) (a) Frokjaer, S.; Otzen, D. E. Protein drug stability: a formulation challenge. *Nat. Rev. Drug Discovery* **2005**, *4* (4), 298–306.

(b) Schellekens, H. Bioequivalence and the immunogenicity of biopharmaceuticals. *Nat. Rev. Drug Discovery* **2002**, *1* (6), 457–62.

(39) Manges, R.; Vazquez, E.; Villaverde, A. Targeting in Cancer Therapies. *Med. Sci.* **2016**, *4* (1), 6.

ANNEX 4: ARTICLE 5

Selective CXCR4⁺ cancer cell targeting and potent antineoplastic effect by a nanostructured version of recombinant ricin

Raquel Díaz, Victor Pallares, Olivia Cano-Garrido, Naroa Serna, **Laura Sánchez-García**, Aida Falgas, Mireia Pesarrodona, Ugutz Unzueta, Alejandro Sanchez-Chardi, Julieta M Sanchez, Isolda Casanova, Esther Vázquez, Ramón Mangues and Antonio Villaverde

Small (2018) 14: 1800665

Impact factor 9.598 MATERIALS SCIENCE, MULTIDISCIPLINARY (22/285) D1

Selective CXCR4⁺ Cancer Cell Targeting and Potent Antineoplastic Effect by a Nanostructured Version of Recombinant Ricin

Raquel Díaz, Victor Pallarès, Olivia Cano-Garrido, Naroa Serna, Laura Sánchez-García, Aïda Falgàs, Mireia Pesarrodona, Ugutz Unzueta, Alejandro Sánchez-Chardi, Julieta M. Sánchez, Isolda Casanova,* Esther Vázquez, Ramón Mangués, and Antonio Villaverde*

Under the unmet need of efficient tumor-targeting drugs for oncology, a recombinant version of the plant toxin ricin (the modular protein T22-mRTA-H6) is engineered to self-assemble as protein-only, CXCR4-targeted nanoparticles. The soluble version of the construct self-organizes as regular 11 nm planar entities that are highly cytotoxic in cultured CXCR4⁺ cancer cells upon short time exposure, with a determined IC50 in the nanomolar order of magnitude. The chemical inhibition of CXCR4 binding sites in exposed cells results in a dramatic reduction of the cytotoxic potency, proving the receptor-dependent mechanism of cytotoxicity. The insoluble version of T22-mRTA-H6 is, contrarily, moderately active, indicating that free, nanostructured protein is the optimal drug form. In animal models of acute myeloid leukemia, T22-mRTA-H6 nanoparticles show an impressive and highly selective therapeutic effect, dramatically reducing the leukemia cells affection of clinically relevant organs. Functionalized T22-mRTA-H6 nanoparticles are then promising prototypes of chemically homogeneous, highly potent antitumor nanostructured toxins for precise oncotherapies based on self-mediated intracellular drug delivery.

1. Introduction

Cancer is a major, growing, and unsolved health problem worldwide, with an incidence of 454.8 new cases per 100 000 (men and women) per year, and a mortality of 207.9 per 100 000 men and 145.4 per 100 000 women (U.S. data; <https://www.cancer.gov/about-cancer/understanding/statistics>). Only in 2018, 1 735 350 new cancer cases and 609 640 cancer deaths are projected to occur in the United States.^[1] Conventional cancer treatments continue to be based on potent small molecular weight chemicals administered systemically. Since these drugs are not targeted to cancer cells they do not preferentially accumulate in tumor or metastasis. Biodistributed across healthy tissues, they promote severe hepatic and renal damage that often results in numerous life-threatening side effects.^[2] In the line

R. Díaz, Dr. O. Cano-Garrido, N. Serna, L. Sánchez-García, Dr. M. Pesarrodona, Dr. J. M. Sánchez, Dr. E. Vázquez, Prof. A. Villaverde
Institut de Biotecnologia i de Biomedicina
Universitat Autònoma de Barcelona
Bellaterra, 08193 Barcelona, Spain
E-mail: Antoni.Villaverde@uab.cat

R. Díaz, Dr. O. Cano-Garrido, N. Serna, L. Sánchez-García, Dr. M. Pesarrodona, Dr. E. Vázquez, Prof. A. Villaverde
Departament de Genètica i de Microbiologia
Universitat Autònoma de Barcelona
Bellaterra, 08193 Barcelona, Spain

R. Díaz, Dr. O. Cano-Garrido, N. Serna, L. Sánchez-García, A. Falgàs, Dr. M. Pesarrodona, Dr. U. Unzueta, Dr. I. Casanova, Dr. E. Vázquez, Prof. R. Mangués, Prof. A. Villaverde
CIBER de Bioingeniería
Biomateriales y Nanomedicina (CIBER-BBN)
Bellaterra, 08193 Barcelona, Spain
E-mail: ICasanova@santpau.cat

Dr. V. Pallarès, A. Falgàs, Dr. U. Unzueta, Dr. I. Casanova, Prof. R. Mangués
Biomedical Research Institute Sant Pau (IIB-Sant Pau) and Josep Carreras Research Institute
Hospital de la Santa Creu i Sant Pau
08025 Barcelona, Spain

Dr. A. Sánchez-Chardi
Servei de Microscòpia
Universitat Autònoma de Barcelona
Bellaterra, 08193 Barcelona, Spain

Dr. J. M. Sánchez
Instituto de Investigaciones Biológicas y Tecnológicas (IIBYT) (CONICET-Universidad Nacional de Córdoba), ICTA and Cátedra de Química Biológica
Departamento de Química
FCEfYN, UNC, Av. Velez Sarsfield 1611, X 5016GCA Córdoba, Argentina

 The ORCID identification number(s) for the author(s) of this article can be found under <https://doi.org/10.1002/smll.201800665>.

DOI: 10.1002/smll.201800665

with the development of new and improved drugs, drug nanoconjugates, therapeutic antibodies, antibody–drug conjugates, tumor-targeted nanoscale vehicles, and tumor-targeted toxins (such as immunotoxins) are being designed to gain specificity and potency, with still limited therapeutic improvement.^[3] The nanoscale size of the drug, potentially reachable by coupling to a vehicle, minimizes renal clearance and favors the enhanced permeability and retention (EPR) effect.^[4] Among the set of tested new drugs, protein toxins emerge as a very appealing alternative.^[3] Proteins are biocompatible macromolecules, easily produced by recombinant DNA technologies, and more than 400 protein species have been already approved for use in humans.^[5] As versatile molecules, they are suitable for fine tuning through protein fusion technologies, to incorporate relevant functions for use as targeted drugs (such as ligands to specific cell surface tumoral markers).^[6] Engineered versions of natural protein toxins have become promising antitumor agents. The *Corynebacterium diphtheriae* toxin fused to interleukin-2 (Denileukin difitox, ONTAK) is an FDA-approved drug that targets leukemia and lymphoma cell types that display IL-2 receptors.^[7] The exotoxin A from *Pseudomonas aeruginosa* has also been produced through recombinant methodologies in different versions (SS1P, LMB-2, or BL22), which are under clinical trials for the treatment of mesothelioma and leukemia.^[8,9]

Compared to microbial toxins, plant toxins are extremely potent molecules.^[3,10,11] Many of them (such as ricin, saporin, abrin, trichosanthin, bouganin, and gelonin) are ribosome inactivating proteins (RIPs). Being N-glycosidases, they irreversibly depurinate a single adenine residue in the 23S/25S/28S rRNA stem-loop. This action blocks protein translation and leads to fast cell death. Ricin, a RIP originally extracted from the seeds of *Ricinus communis* of ~65 kDa, consists of two chains linked by a disulfide bond; the chain A (RTA) with N-glycosidase enzymatic activity and the chain B (RTB) with lectin properties which binds carbohydrate ligands on target cell surface.^[12] A single ricin molecule is estimated to inactivate 1500–2000 ribosomes per minute,^[13] being very promising as highly active cytotoxic protein drug. We have previously identified the peptide T22, an efficient ligand of the cell surface marker CXCR4 (a cytokine receptor selectively overexpressed in metastatic cells of many cancer types^[14–19]), as a targeting agent for the precise tumor delivery of protein-only self-assembling nanoparticles.^[20,21] Some of these constructs have been built by the controlled oligomerization of proteins with cytotoxic activity, such as pro-apoptotic factors,^[22] anticancer peptides,^[22] and microbial toxins.^[23] In this context, we intended to confer CXCR4⁺ cell-targeted delivery of ricin assembled as protein nanoparticles to determine their selectivity in cell internalization and their performance as cytotoxic drugs. This has been done through in vivo administration of either soluble CXCR4-targeted protein nanoparticles formed by ricin as building blocks or to particular protein-releasing amyloid aggregates formed by CXCR4-targeted ricin, named bacterial inclusion bodies (IBs),^[24] that might represent a steady source of functional protein for advanced therapies.^[25–27]

2. Results

The recombinant T22-mRTA-H6 (Figure 1A) was successfully produced in *Escherichia coli* Origami B, purified by

His-based one-step affinity chromatography and detected as a single protein species with the expected molecular mass of 35.91 kDa (Figure 1B) that was fully confirmed by mass spectrometry (not shown). The pure protein was straightforwardly observed by both, dynamic light scattering (DLS) and field emission scanning electron microscopy (FESEM), as ~11 nm entities occurring in the storage buffer without further treatment (Figure 1C,D), indicating the spontaneous formation of self-assembled nanoparticles. This was the expected outcome as the combination of cationic peptides at the amino terminus and polyhistidines at the carboxy terminus has been proved to be optimal to promote protein oligomerization as regular nanostructures,^[28] irrespective of the core protein segment (ricin, in the case of T22-mRTA-H6, Figure 1A). Treating the material with SDS resulted in monomers of 5.5 nm (Figure 1C), which represented the probable building blocks of the nanoparticles. In the related self-assembling protein T22-GFP-H6, in which the sizes of the building block and the assembled version are both equivalent to those of T22-mRTA-H6, the use of small-angle X-ray scattering and other sophisticated analytical methods^[29] as well as in silico modeling^[30] have revealed that the nanoparticle was formed by ~10 monomers. Being estimative, this figure also fits to T22-mRTA-H6. The analysis of T22-mRTA-H6 nanoparticles by circular dichroism (CD) revealed a structural composition in which α -helix predominates (29.2%, Figure 1E). However, a Thioflavin T (Th T) assay has also revealed the occurrence of intermolecular β -sheet interactions (Figure 1F) that might contribute to the stability of protein nanoparticles, and that is also compatible with the extent of important β -sheet structure found in the CD (Figure 1E). Since the nanostructured ricin was intended to be delivered in tumoral tissues, we wondered if the nanoparticles could still be stable in the abnormal pH values observed in the tumor environment that have been reported to range from ~6.3 (intracellular) to 7.4 (extracellular).^[31,32] As observed, T22-mRTA-H6 remained fully assembled under these conditions (Figure 1F), what supports the usability of construct from the stability point of view.

In order to test the functionality of the recombinant ricin in such assembled form, cultured CXCR4⁺ HeLa cells were exposed to different concentrations of ricin-based nanoparticles. These materials showed a potent, dose-dependent cytotoxicity that essentially abolished cell viability at 100×10^{-9} M (Figure 2A). After 72 h of exposure, the IC50 was determined to be $13 \pm 0.5 \times 10^{-9}$ M. To confirm if, as expected, T22-mRTA-H6-mediated cell death was dependent on its cell binding and internalization of the protein via the cell surface receptor CXCR4 and its ligand T22, we tested if a potent CXCR4 antagonist, AMD3100,^[33] could be able to recover cell viability when used as a competitor of the toxin, at a molar ratio of 10:1. As observed (Figure 2B), AMD3100 dramatically enhanced cell viability in T22-mRTA-H6-treated cells proving a specific, receptor-mediated penetration of the nanoparticles into target cells. To further confirm such precision cell entry mechanism, we decided to expose nontumoral (CXCR4⁻) 3T3 cells and representative CXCR4⁻ and CXCR4⁺ tumoral cell lines to T22-mRTA-H6, and also to a conventional chemical drug used in the treatment of several cancer types but specially of acute myeloid leukemia (AML), namely, cytosine arabinoside

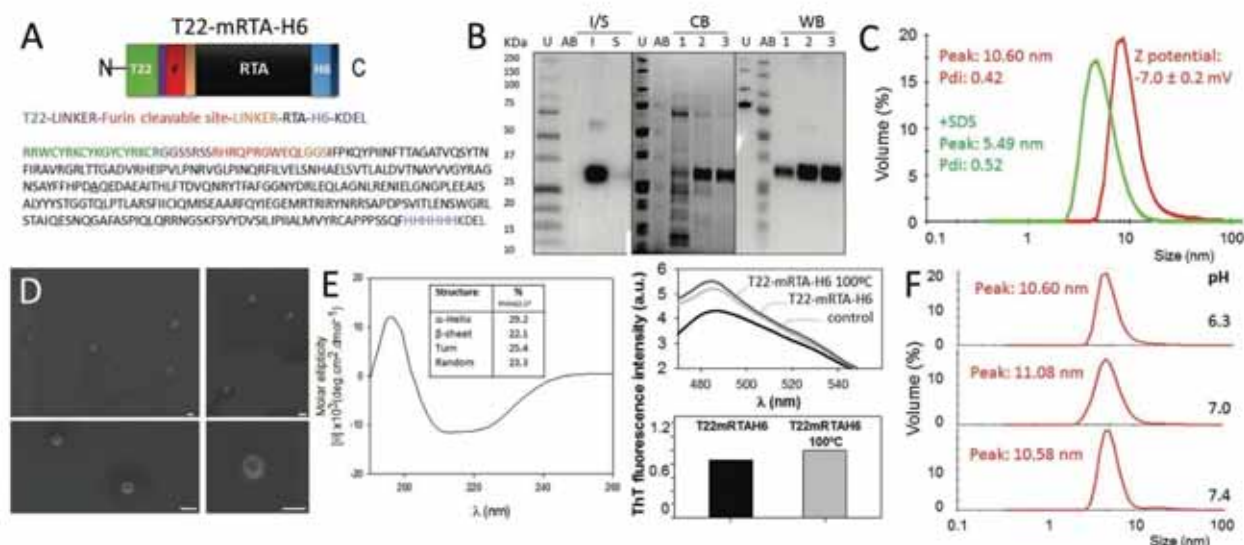


Figure 1. Physicochemical properties of T22-mRTA-H6. A) Modular scheme and amino acid sequence of T22-mRTA-H6. mRTA is the modified fragment A of ricin, described in the Experimental Section, in which the Asn residue 132 has been replaced by Ala (underlined). Sizes of the boxes are only indicative. B) Fractioning between insoluble (I) and soluble (S) cell fractions in total cell extracts, revealed by WB, upon protein production at 37 °C for 3 h. SDS-PAGE analysis of T22-mRTA-H6 upon one-step affinity purification, revealed by Coomassie blue (CB) staining and by Western blot (WB) using an anti-his antibody. U and AB stand for Unstained and All Blue markers, respectively (Bio-Rad, Refs. 161-0363 and 161-0373), and 1, 2, and 3 indicate, respectively, the unspecific elution peak and two peaks with increasing level of purity. Protein in peak 3 was used in further experiments. C) Hydrodynamic size (and Z potential) of T22-mRTA-H6 nanoparticles formed spontaneously upon purification (red line), determined by DLS. Pdi is polydispersity index, and all figures indicate nm. The size of the monomer, determined upon disassembling the material with 1% SDS for 40 min, is also indicated (green line). D) FESEM imaging, at different magnifications, of T22-mRTA-H6 nanoparticles. Bars represent 20 nm. E) Far UV CD of T22-mRTA-H6 in sodium carbonate-bicarbonate buffer at pH 8 measured at 25 °C. In the middle plot, ThT fluorescence emission spectra alone (black line) or in the presence of T22-mRTA-H6 (light grey line) and T22-mRTA-H6 previously heated at 100 °C (dark grey line). $\lambda_{ex} = 450$ nm. In the plot at the bottom, ThT fluorescence emission at 490 nm of T22-mRTA-H6 (black bar) and T22-mRTA-H6 previously heated at 100 °C (gray bars). F) Size of T22-mRTA-H6 nanoparticles dialyzed against 51×10^{-3} M sodium phosphate, 158.6×10^{-3} M trehalose dehydrate, 0.01% polysorbate-20 buffer at different pH values, determined by DLS.

(Ara-C).^[34] These cell lines, with different levels of CXCR4 expression (Figure 2C), supported different levels of protein internalization mediated by the specific interaction between T22 and CXCR4 (Figure 2D). This was determined through the uptake of T22-GFP-H6, a self-assembling fluorescent protein closely related to T22-mRTA-H6 that contains the same ligand of CXCR4 also accommodated at the amino terminus of the polypeptide.^[28] It must be noted that as predicted, CXCR4 expression and T22-mediated protein internalization showed a parallel behavior (compare Figure 2C,D). Then, when they were finally comparatively tested, the ricin-based protein nanoparticle promoted specific cell death only in CXCR4⁺ cancer cells but not in normal cells, at a dose (100×10^{-9} M) at which Ara-C did not show any toxic effect on any of these cell lines (Figure 2E). This observation proved not only the effective targeting of the protein drug but also its superior cytotoxicity compared to an equimolar dose of the model chemical drug.

At this stage, we wanted to confirm that the cytotoxicity promoted by T22-mRTA-H6 was linked to the uptake of the nanoparticles inside CXCR4⁺ cells, and triggered from within. This was reached by exposing HeLa cells to ATTO-labeled nanoparticles and monitoring internalization. As observed (Figure 3A), nanoparticles were internalized by cells at least up to 24 h. As expected for an active version of ricin, apoptosis was detected through both annexin affinity assay and by Hoechst

staining (Figure 3B), and the number of apoptotic cells seemed to peak at around 15–24 h postexposure. In addition, mitochondrial damage was confirmed by the significant increase in the number of cells with lowered JC-1 red fluorescence at 15 and 24 h after treatment with T22-mRTA-H6 (Figure 3C), indicative of a depolarization in the mitochondrial $\Delta\Psi$ linked to apoptotic induction. Interestingly, cell damage occurred without a detectable increase in reactive oxygen species (ROS, Figure 3D), while the formation of apoptotic bodies in ricin-exposed HeLa cells was clearly caspase-dependent (Figure 3E). The combination of these data indicates that T22-mRTA-H6-mediated cell death occurs by a classical caspase-dependent apoptosis pathway.

The suitable cell-targeting of the nanostructured version of ricin conferred by the peptide T22 (Figure 2), and the fact that most of the T22-mRTA-H6 protein was obtained in insoluble form (Figure 1B), prompted us to evaluate if the insoluble version of ricin might also exhibit cell-targeted cytotoxicity. In this context, we have recently described how the presence of T22 and other cell ligands, in recombinant proteins that form bacterial IBs,^[27] allow an efficient and specific cell penetration of the whole protein clusters. In the same conceptual line, bacterial IBs formed by self-assembling proteins might contain quasi-native forms of nanoparticles or assembling precursors.^[36] IB proteins retain functionalities of the soluble protein version and can be gradually released from the

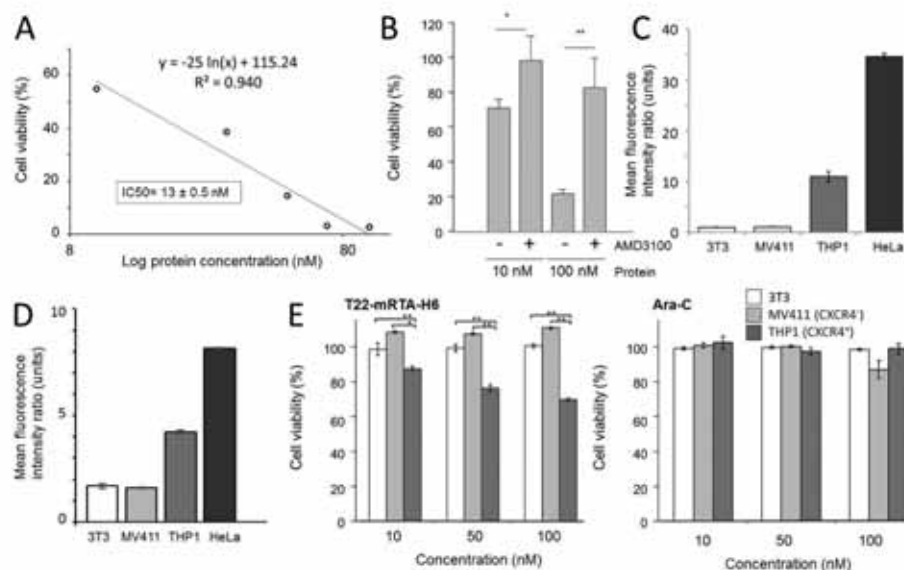


Figure 2. Cytotoxicity and CXCR4 specificity of T22-mRTA-H6 nanoparticles. A) Viability of cultured CXCR4⁺ HeLa cells upon 72 h of exposure to T22-mRTA-H6 nanoparticles at different concentrations, presented as a dose–response curve. B) Inhibition of cell death in HeLa cells exposed to different concentrations of T22-mRTA-H6 nanoparticles for 72 h, mediated by the CXCR4 antagonist AMD3100 (always at an excess molar ratio of 10:1). C) Levels of CXCR4 membrane protein determined by flow cytometry of different cell lines (3T3, MV411, THP1 and HeLa), expressed as mean fluorescence intensity ratio \pm SE. D) Extent of internalization of 100×10^{-9} M T22-GFP-H6 in the different cell lines at 1 h of exposure. Results are expressed as mean fluorescence intensity ratio \pm SE. E) Viability of cultured CXCR4⁺ 3T3 cells upon 48 h of exposure to T22-mRTA-H6 nanoparticles and the small molecular weight antitumoral drug Ara-C, at different concentrations. The commercial CXCR4⁺ and CXCR4⁺ human AML cell lines (MV411 and THP1, respectively) are included as controls. Ara-C showed cytotoxicity above 100×10^{-9} M (not shown). The standard error is represented in all bars. The level of significance is indicated by superscripts (* $p < 0.05$, ** $p < 0.01$).

aggregates when exposed to cells^[26] or when implanted in vivo by local injection.^[25] The ultrastructural morphometry of insoluble version of T22-mRTA-H6 was observed in a nearly native state by FESEM as conventional IBs, namely, pseudo-spherical protein clusters with an average diameter size ranging from 400 to 600 nm (Figure 4A).

When exposing HeLa cells to increasing amounts of T22-mRTA-H6 IBs, a mild cytotoxic effect was indeed observed (Figure 4B), although the differences in cell viability, when comparing with untreated cell cultures, were in the limits of significance. In addition, the insoluble version of T22-GFP-H6 (forming similar IBs^[27]), a self-assembling CXCR4-targeted protein devoid of any cytotoxic domain, also promoted a transient and mild reduction of cell viability. However, in this case, cells showed an immediate recovery at longer time exposures that, in contrast, was not found associated to T22-mRTA-H6. Despite previous data about the potential of functional protein release from IBs,^[25] the biological effect of T22-mRTA-H6 IBs was, in our hands, only moderate.

The antitumor effect of both T22-mRTA-H6 soluble nanoparticles and T22-mRTA-H6 IBs was evaluated in a disseminated AML animal model. NSG mice were injected with THP1-Luci cells to generate leukemia dissemination in mice. 2 d after cell injection through the vein tail, we performed a single-dose injection in the mice hypodermis (SC) of 1 mg of T22-mRTA-H6 IBs in two mice (IB-T22mRTA group). In a different mouse group, we started daily intravenous administrations of 10 μ g of soluble T22-mRTA-H6 (T22mRTA group) to one mouse or buffer alone (VEHICLE group) to three mice, for

a total of ten doses. No effects on mice weight were observed during the treatments (data not shown). The progression and dissemination of leukemia was assessed by monitoring BLI using the IVIS Spectrum. From day 6 and until the end of the experiment, the mouse treated with soluble T22-mRTA-H6 (T22mRTA) showed lower luminescence emission than the VEHICLE group (Figure 5A). Thus, as measured by BLI, treatment with soluble T22-mRTA-H6 inhibited the dissemination of AML cells in mice, compared to the vehicle group, after the fourth, sixth, eighth, and tenth doses of T22-mRTA-H6 at 10 μ g per dose (which corresponded to day 6, 8, 10, or 13 after injection of cells, respectively). In contrast, no differences in BLI were found between mice treated with T22-mRTA-H6 IBs (IB-T22mRTA) and the control VEHICLE mice (Figure 5A).

In a next step, the antitumor activity of nanoparticles was analyzed in affected organs *ex vivo* 14 d after the injection of cells when mice presented signs of advanced disease. The analyses with the IVIS Spectrum showed that the treatment with soluble T22-mRTA-H6 nanoparticles (T22mRTA) decreased BLI in the bone marrow (backbone and hindlimbs), liver, and spleen, in contrast to the findings in mice treated with buffer alone (VEHICLE) (Figure 5B). However, the treatment with T22-mRTA-H6 IBs (IB-T22mRTA) did not show changes in BLI in the same tissues in comparison to control mice (VEHICLE) (Figure 5B).

In addition, we evaluated the dissemination of leukemic cells in the affected organs of the animal by IHC of CD45, a human leukocyte marker that detects AML THP1 cells. Results correlated with BLI analyses showing that treatment with soluble T22-mRTA-H6, differently from those registered after

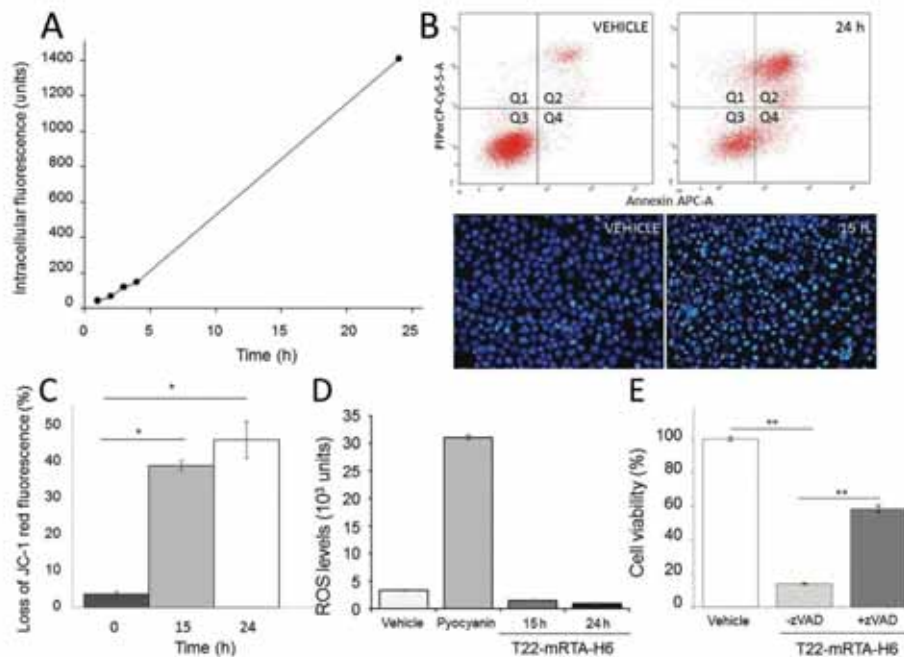


Figure 3. Cell penetrability and intracellular toxicity of T22-mRTA-H6 nanoparticles. A) Intracellular fluorescence in cultured HeLa cells exposed to 100×10^{-9} M of ATTO488 stained T22-mRTA-H6. Extracellular fluorescence was fully removed by a hash trypsin treatment as described.^[35] B) Under the same conditions, the externalized phosphatidylserine was detected by Annexin V Detection Kit (APC, eBioscience) in cells exposed to nonstained T22-mRTA-H6. Dead cells were spotted with propidium iodide (PI). Quadrant Q1 shows HeLa cells marked with PI. Q2 shows cells marked with Annexin V and PI. Q3 shows cells without PI nor Annexin V. Q4 shows cells marked with Annexin V. Therefore, dead cells are shown in Q1 and Q2 while living cells in Q3 and Q4. Apoptotic cells are shown in Q4. At the bottom, Hoechst staining of HeLa cell under the above conditions. Images were obtained by fluorescence microscopy ($\times 400$). C) Loss of JC-1 Red fluorescence in T22-mRTA-H6-treated cells as described above, indicative of a change in the mitochondrial $\Delta\psi$. D) Levels of cellular ROS detected with a fluorescence microplate assay. HeLa cells were treated with either buffer, T22-mRTA-H6 (100×10^{-9} M, for 15 or 24 h) or 100×10^{-6} M Pyocyanin (1 h) as a positive control. Values are expressed as relative fluorescence units \pm SE. E) Inhibition of caspases with zVAD-fmk reverses the antitumor activity of T22-mRTA-H6 in HeLa cells. Cells were pretreated for 1 h with 100×10^{-6} M zVAD-fmk and then exposed to 100×10^{-9} M T22-mRTA-H6 for 48 h. Cell viability is expressed as the percentage of cell survival compared with the control. Values are mean \pm SE. *Vehicle* indicates treatment with buffer. The level of significance is indicated ($^*p < 0.05$, $^{**}p < 0.01$).

T22-mRTA-H6 IBs treatment, reduced the dissemination in the infiltrated tissues, by detecting lower number of CD45 positive cells in bone marrow, liver, and spleen in the mouse treated with soluble T22-mRTA-H6 (Figure 5C). Finally, we performed H&E staining of the infiltrated organs and additional organs

not affected by leukemia cells. We did not observe any sign of toxicity in any of the affected or unaffected tissues, neither with the soluble T22-mRTA-H6 nor with the T22-mRTA-H6 IBs treatments (Figure 6). As it occurred in vitro, IBs caused, if any, just a mild biological effect.

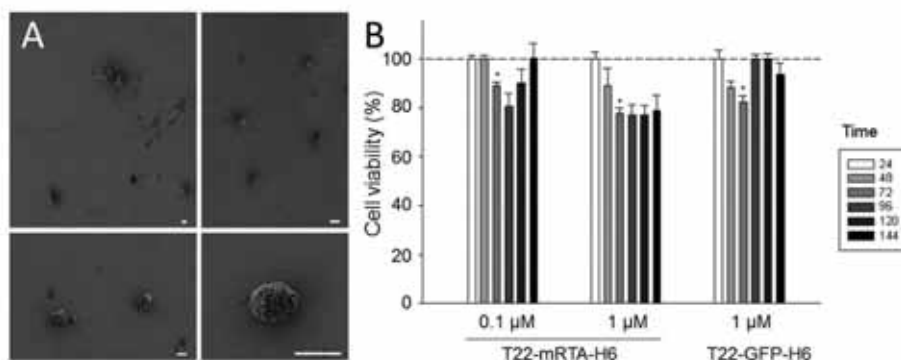


Figure 4. Properties of T22-mRTA-H6 IBs. A) FESEM images of isolated T22-mRTA-H6 IBs at different magnifications. Bars indicate 1 μ m. B) Viability of cultured CXCR4⁺ HeLa cells upon different times of exposure to T22-mRTA-H6 IBs and to control, nonfunctional IBs formed by the related protein T22-GFP-H6. Exposure time is indicated in hours. The standard error is represented by a black line. The level of significance is indicated by superscripts ($^*p < 0.05$).

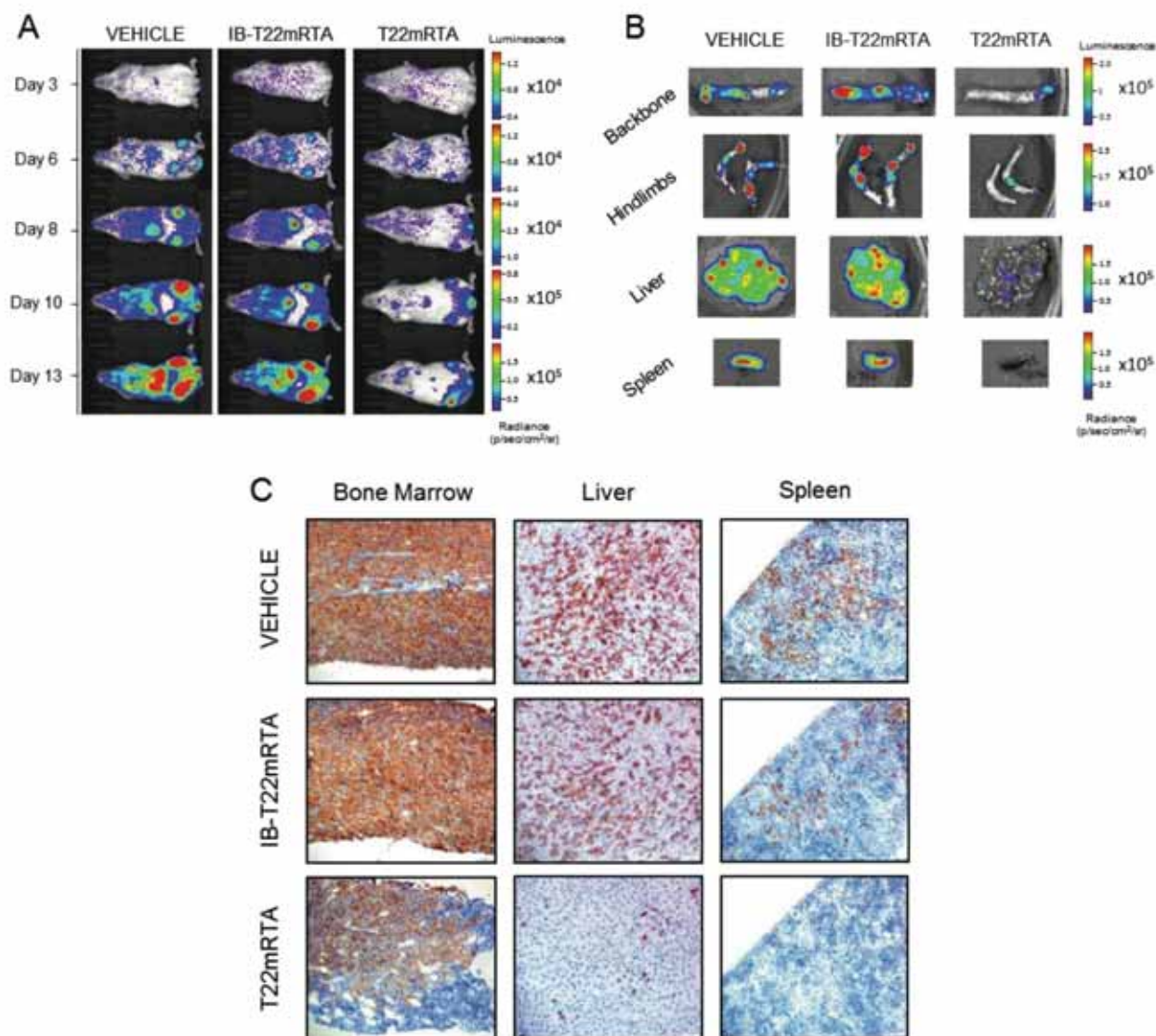


Figure 5. Antitumor activity of T22-mRTA-H6 in a disseminated AML mouse model. A) Follow-up of bioluminescence emitted by mice treated with soluble T22-mRTA-H6 nanoparticles (T22mRTA), T22-mRTA-H6 IBs (IB-T22mRTA), or buffer (VEHICLE) during the 14 d of the experiment, analyzed by IVIS Spectrum. B) Levels of luminescence detected ex vivo in IVIS Spectrum in the tissues infiltrated with leukemic cells such as backbone, hindlimbs, liver, and spleen of mice treated with buffer (VEHICLE), T22-mRTA-H6 IB (IB-T22mRTA), or soluble T22-mRTA-H6 (T22mRTA). C) Detection of CD45 positive cells by IHQ in spleen, liver, and bone marrow of mice treated with buffer (VEHICLE), T22-mRTA-H6 IBs (IB-T22mRTA), or soluble T22-mRTA-H6 nanoparticles (T22mRTA). T22mRTA, mouse treated with soluble T22-mRTA-H6; IB-T22mRTA, mouse group treated with T22-mRTA-H6 IBs; VEHICLE, group treated with vehicle. Bars indicate 50 μ m.

3. Discussion

Functional recruitment in single-chain modular polypeptides is a promising strategy for the generation of self-targeted and self-delivered drugs that are chemically homogenous and produced in a single step in recombinant cell factories.^[37] Protein drugs represent a big sector in the pharmacological market.^[5] Their easy industrial biofabrication and scalability combined with the intrinsic biocompatibility and functional versatility, approachable by genetic engineering, make proteins a very convenient category of tunable pharmaceuticals.^[38,39] In

oncology, cytotoxic proteins selected from nature have been engineered and adapted to act as antitumor agents, by means of different approaches that must necessarily consider cell targeting.^[13] Immunotoxins are relevant representatives of how protein toxins can be targeted by simple fusion technologies in monovalent complexes, with relevant potential for precise cell killing.^[40–42] However, proper targeting is not regularly achieved in current nanomedicine^[43] and the amount of cell targeted drugs that reach the intended tumor tissues, especially in oncology, is rather limited (usually <1%).^[44] Specifically, immunotoxins have not so far fulfilled the requirements regarding a

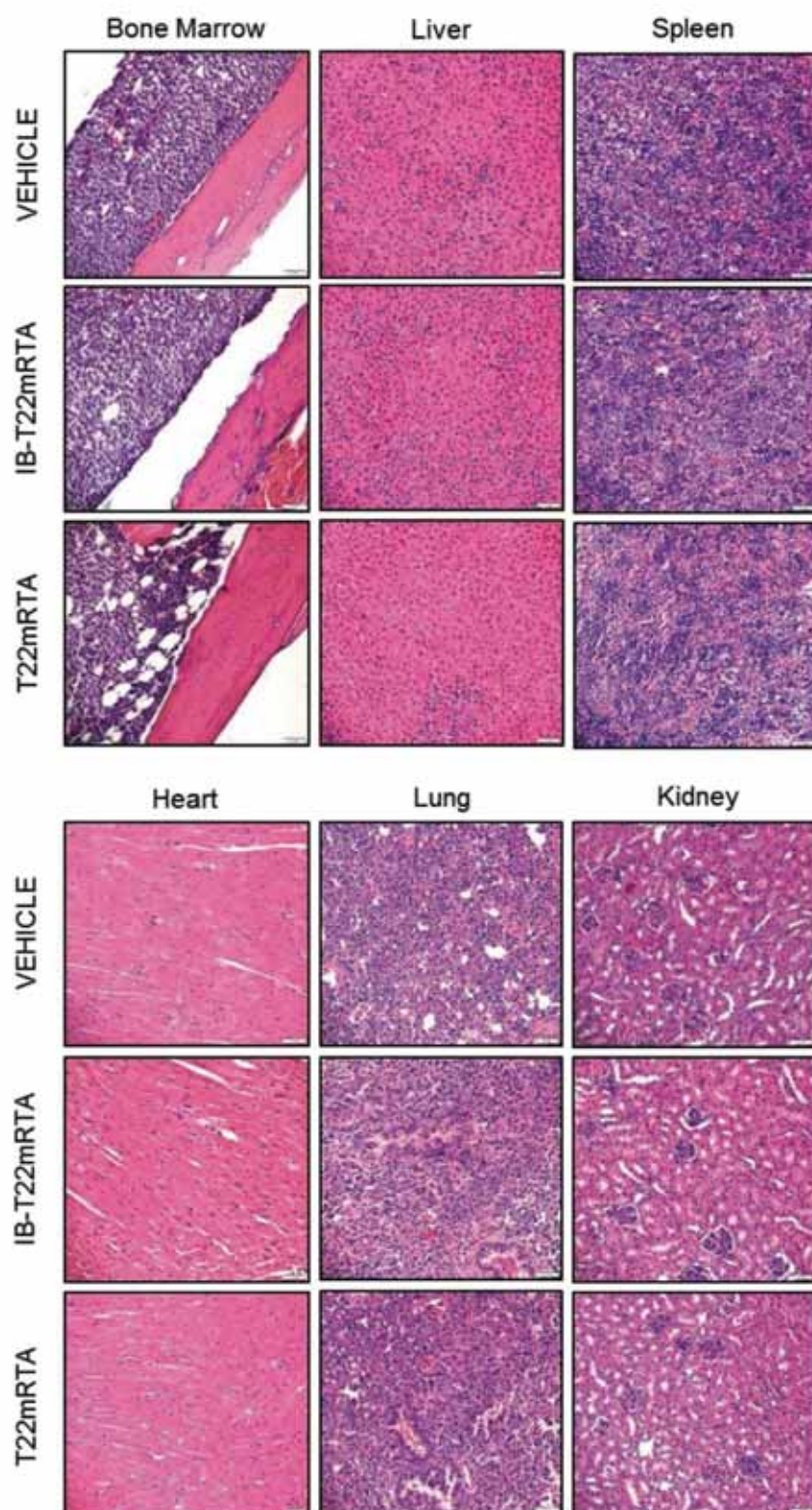


Figure 6. Histopathology in the disseminated AML mouse model after a treatment with T22-mRTA-H6. Hematoxylin and eosin staining of normal (heart, lung, kidney) and leukemia infiltrated organs

convenient therapeutic index, as side toxicity is still relevant.^[3] The combination of highly potent toxins with effective targeting is then necessary for a highly precise and selective cell killing that might still be optimized by a regular and multivalent display of the targeting agent on the surface of the drug.^[45] Also, formulating a protein drug within the nanoscale size should favor the enhanced permeability and retention effects,^[4] minimizing the biological barriers in the drug delivery process.

Under these premises, we have engineered the highly potent plant toxin ricin as a CXCR4-targeted, protein-only nanoscale drug with a multivalent presentation of the ligand, the peptide T22, reached through the regular self-assembling of ricin as stable 11 nm nanoparticles (Figure 1D,F). A related modular protein, namely, T22-GFP-H6, that self-assembles as 12 nm nanoparticles, has been modeled as oligomerizing in ~10 subunits accommodated in a toroid architecture, thus ensuring a sufficient multivalent display of the ligand.^[29,30] According to the similarities in the molecular mass of the building block and in the final size of the resulting nanoparticles, T22-mRTA-H6 seems to self-arrange in a similar pattern (Figure 1). Ricin has been largely considered as a drug component in cancer therapies,^[46] and previously explored in form of immunotoxins with moderate efficacy.^[47–49] In the nanoconstruct generated here, ricin is highly active and fully potent on target cells, indicative of that oligomerization is not preventing functionality.

This particular approach highly increases the selectivity of the cytotoxic potential of ricin against CXCR4⁺ cancer cells because of the combination of three main and critical effects.

(bone marrow, liver, spleen). Images were taken in the microscope with a 20x objective and an Olympus DP72 digital camera. H&E, hematoxylin and eosin; T22mRTA, mouse treated with soluble T22-mRTA-H6; IB-T22mRTA, mouse group treated with T22-mRTA-H6 IBs; VEHICLE, mouse group treated with buffer. Bars indicate 50 μ m.

First, the specific uptake of the therapeutic protein was achieved because of the multivalent display of the CXCR4 ligand, T22, on the nanoparticle and exclusive CXCR4 receptor overexpression in the target cancer cell membranes. This fact prevents internalization and toxicity on normal cells with low or negligible levels of CXCR4. Second, the avoidance of the severe side effects that appeared on previous clinical trials testing ricin anticancer effect that led to their discontinuation.^[13,46] Specifically, we incorporated the mutant (N132A) ricin A chain as functional building block of the nanoparticle, to suppress the potential vascular leak syndrome. We also excluded the use of ricin B-chain to block the severe toxicity associated with its nonspecific binding to glycoproteins or mannose receptors expressed on the membrane of nontumor cells (e.g., Kupffer cells of the liver sinusoids). Finally, the enhanced delivery of the biologically active ricin A chain to the cytosol of target cells (Figure 3A) was reached because of the addition of the furin cleavage site that releases the active domain from the nanoparticle in the endoplasmic reticulum, and a KDEL sequence which allows the translocation of the biologically active toxin to the cytosol, avoiding its lysosomal degradation. The endosomal delivery of the protein drug would also prevent the development of multidrug resistance that mainly relates to drug efflux by cancer cells through the ATP-binding cassette (ABC) transporters activity, overexpression of ABC transporters associating with poor response to therapy.^[50] Low molecular weight drugs enter cells by diffusion across membranes, which renders them vulnerable to their efflux by ABC transporters. In contrast, the nanoscale size of oligomeric ricin is expected to avoid passive diffusion. Entering CXCR4⁺ cells through endocytic vesicles, the protein achieves high intracellular concentration in absence of (or reversing) the multidrug resistance phenotype that might have been observed for a free small drug. This effect, associated with the entry route, has been reported for doxorubicin-loaded polymeric nanoparticles and doxorubicin-polymer conjugates, among others.^[51,52]

The combination of these three crucial effects in basic cellular pathways makes for a dramatic increase of ricin A anti-neoplastic activity. Thus, the previously reported IC50 of untargeted ricin A in HeLa cells (IC50 36 $\mu\text{g mL}^{-1}$ (1×10^{-6} M))^[53] is here reduced about 100-fold (IC50 = 13×10^{-9} M) because of selective CXCR4 cancer cell targeting, KDEL sequence, and furin site incorporation into the nanoparticle. The reached IC50 (Figure 2) is in the same nM range than that described by other highly lethal toxins (such as diphtheria toxin derivatives,^[54–56] *Pseudomonas* exotoxin,^[57] or neurotoxins^[58]). However, this engineered version is highly promising for the further development of the present prototype as an efficient oncological nanostructured drug, since it keeps the full selectivity for the cell surface cytokine receptor CXCR4 (Figure 2) while keeping a nanostructured organization with a multivalent presentation of the surface receptor (Figure 1). In addition, in a molar basis, T22-mRTA-H6 is more cytotoxic on AML CXCR4⁺ cells than Ara-C (Figure 2E), a basic chemical drug included in most AML treatment protocols.^[34] Importantly, the precise cytotoxic activity of T22-mRTA-H6 nanoparticles is conserved in vivo after systemic administration, which leads to a dramatic blockade of leukemic cell affectation in the clinically relevant organs (bone marrow, liver, and spleen) in the CXCR4⁺ AML

model (Figure 5). These findings were associated with absence of any detectable systemic (not shown) or histological toxicity in off-target organs during the experiment time (Figure 6). It could not be fully excluded that in longer treatments ricin (as well as other recombinant toxins or therapeutic fusion proteins) may induce an immune response, that if involving antigens shared with endogenous protein might lead to adverse effects.^[59,60] However, the modified version of ricin used here avoids the vascular leak syndrome (VLS), the major concern in the clinical trial of a ricin A-antibody (CD19/CD12) immunotoxin (<https://clinicaltrials.gov/ct2/show/NCT01408160>). In this context, further de-immunization might be feasible, if required, to improve the clinical performance of T22-mRTA-H6 or derived drugs, ensuring low immunogenicity and avoidance of autoimmune diseases. This could be done by an approach similar to that carried out for diphtheria and *P. aeruginosa* toxins. These microbial proteins, components of most of third generation immunotoxins under clinical evaluation, are successfully engineered by the removal of nonessential sequences and by the genetic elimination of antigenic T and B cell epitopes, without compromising their antitumor activity.^[60]

Combining the impressive therapeutic effects observed in vivo and the fact that CXCR4 is a tumoral marker relevant in more than 20 human neoplasias,^[61] its overexpression correlating with aggressiveness,^[62–66] T22-mRTA-H6 nanoparticles combine selectivity, cytotoxicity, nanoscale size, and multivalent display in a chemically homogeneous entity devoid of any external carrier or vehicle that might impose limitations to the biocompatibility of the whole construct.^[4]

4. Conclusion

One of the most potent toxins in nature, ricin, has been genetically instructed to self-assemble as stable 11 nm homomeric nanoparticles and to selectively kill CXCR4-overexpressing cells, by using a promising protein engineering toolkit. The resulting nanoscale material has been shown as highly cytotoxic and highly selective over CXCR4⁺ cells, resulting in an unusually strong and efficient antitumor activity in a mouse model of the difficult-to-treat disseminated acute myeloid leukemia, in complete absence of side toxicity. This analysis opens a plethora of possibilities to combine highly toxic proteins with a highly selective tumor-targeting platform, that within the nanoscale, would fulfill the emerging concept of self-assembled, self-targeted vehicle-free recombinant drugs for precision medicines.

5. Experimental Section

Genetic Design and Protein Production: The recombinant protein T22-mRTA-H6 (Figure 1A) was designed to include the highly specific CXCR4 ligand T22^[20] at the amino terminus followed by a mutated version of the ricin A chain, and a hexahistidine tail at the carboxy terminus. The mutation N132A was introduced to suppress the vascular leak syndrome in potential future in vivo administrations, keeping the cytotoxic activity. In addition, a furin cleave site was also incorporated to allow the release of the accessory N-terminal region in the endosome and the intracellular activity of ricin in a quasi-native sequence format. A KDEL motif was also incorporated to favor endosomal escape.^[67] The plasmid construct

pET22b-T22-mRTA-H6, encoding the protein under the control of the bacteriophage T7 promoter, was generated by GeneArt and transformed into *E. coli* Origami B cells.

Production and Purification of Soluble Protein: Recombinant bacteria were cultured in lysogeny broth (LB) medium with 100 $\mu\text{g mL}^{-1}$ ampicillin, 15 $\mu\text{g mL}^{-1}$ kanamycin, and 12.5 $\mu\text{g mL}^{-1}$ of tetracycline, at 37 °C and 250 rpm. The recombinant gene expression was induced by adding 0.1 $\times 10^{-3}$ M isopropyl- β -thiogalactopyranoside (IPTG) when the OD of the culture reached a value between 0.5 and 0.7. Cultures were subsequently incubated overnight at 20 °C and 250 rpm. Cells were harvested and centrifuged (5000 g, 15 min, 4 °C). The cell pellet was resuspended in wash buffer (51 $\times 10^{-3}$ M sodium phosphate buffer, pH = 8, 158.6 $\times 10^{-3}$ M trehalose dihydrate, 0.01% Polysorbate-20, 15 $\times 10^{-3}$ M imidazole, 300 $\times 10^{-3}$ M NaCl) in presence of protease inhibitor cocktail Complete EDTA-Free (Roche). Bacterial cells were sonicated twice at 10% amplitude and once at 15% of amplitude for 10 min each round, centrifuged (15 000 g, 45 min, 4 °C) and soluble fraction purified by affinity chromatography with a HiTrap Chelating HP column in an AKTA purifier FPLC (GE Healthcare). After the samples were filtered (0.22 μm) and injected into the column, the fractions to be collected were eluted at \sim 30% elution buffer (51 $\times 10^{-3}$ M sodium phosphate, pH = 8, 158.6 $\times 10^{-3}$ M trehalose dihydrate, 0.01% Polysorbate-20, 500 $\times 10^{-3}$ M imidazole, 300 $\times 10^{-3}$ M NaCl). The buffer exchange was done in Centricon Centrifugal Tubes Ultracel 10000 NMWL. T22-mRTA-H6 was found to be highly stable in 51 $\times 10^{-3}$ M sodium phosphate pH = 6.2, 60 mg mL⁻¹ α -trehalose dehydrate, 0.01% polysorbate-20. Protein purity was analyzed by SDS electrophoresis on TGX Stain-Free gels (Bio-Rad), followed by Western blotting using an anti-His monoclonal antibody (Santa Cruz Biotechnology). Sodium dodecyl sulfate polyacrylamide gel electrophoresis (SDS-PAGE) on TGX Stain-Free Gels (Bio-Rad) was conducted to analyze the protein. Samples were diluted in denaturing buffer (0.53 M Tris Base, 5.52 M glycerol, 0.27 M SDS, 2.84 M β -mercaptoethanol, 7.99 M urea) at a 3:1 molar ratio, boiled at 96 °C for 10 min and loaded into the gels lanes. For the Western blot, an anti-His monoclonal antibody was used (Santa Cruz Biotechnology) followed by a goat anti-mouse IgG (H+L)-HRP secondary antibody (Ref. 170-6516) conjugate (Bio-Rad, Ref. 170-6516). Images were observed using ChemiDoc Touch Imaging System. Protein production has been partially performed by the ICTS "NANBIOSIS," more specifically by the Protein Production Platform of CIBER-BBN/ IBB (<http://www.nanbiosis.es/unit/u1-protein-production-platform-ppp/>)

Production and Purification of Insoluble Protein: Recombinant bacteria were cultured in LB at 37 °C and 250 rpm until the OD reached between 0.5 and 0.7, and gene expression was induced by 1 $\times 10^{-3}$ M IPTG. Then, cells were further incubated to allow gene expression for 3 h at 37 °C and 250 rpm. After sedimentation (5000 g, 15 min, 4 °C), the pellet was resuspended in 0.22 μm filtered lysis buffer (Tris 1 M pH = 8, NaCl 4 M, EDTA 50 $\times 10^{-3}$ M) in presence of protease inhibitor cocktail Complete EDTA-Free (Roche), the protease inhibitor phenylmethane sulfonyl fluoride (PMSF, 100 $\times 10^{-3}$ M), and 50 $\mu\text{g mL}^{-1}$ lysozyme mL⁻¹, followed by an incubation at 37 °C and 250 rpm for 2 h. Cells were disrupted in a French Press (5 rounds at 1200 psi) and kept at -80 °C overnight. Samples were thawed and treated 0.2 μL Triton X-100 mL⁻¹ cell culture for 1 h at room temperature with agitation. Then, after sedimentation (15 000 g, 15 min, 4 °C), pellets were resuspended in the same volume of filtered lysis buffer. The following reagents were then added to the sample: 1 μL MgSO₄ (1 M) mL⁻¹ cell culture, 1 μg DNase mL⁻¹ cell culture. The culture was then incubated for 1 h at 37 °C and 250 rpm agitation. As a sterility assay, LB plates were seeded with 100 μL of culture at 37 °C, overnight, and the suspension of insoluble protein was frozen at -80 °C overnight. The suspension was frozen and thawed daily until no bacterial colonies appeared in the plates. Then, after sedimentation (15 000 g, 15 min, 4 °C), the supernatant was discarded, and each pellet was resuspended in filtered ultrapure water and aliquots were made. Finally, after sedimentation of insoluble material (15 000 g, 15 min, 4 °C), supernatants were discarded and pellets were stored at -80 °C.

Quantitative Protein Analysis: Protein purity was analyzed by SDS-PAGE on a Chemi Doc Touch Imaging System (Bio-Rad). Briefly, both

soluble and insoluble samples were mixed with in denaturing buffer (0.53 M Tris Base, 5.52 M glycerol, 0.27 M SDS, 2.84 M β -mercaptoethanol, 7.99 M urea) at a ratio 3:1, boiled for 5 or 45 min, respectively, and loaded onto the gels. For the Western blot, an anti-His monoclonal antibody was used (Santa Cruz Biotechnology) followed by a goat anti-mouse IgG (H+L)-HRP secondary antibody conjugate (Bio-Rad). Gels were scanned at high resolution and bands were quantified with Quantity One Software (Bio-Rad) using a known protein standard of soluble recombinant T22-mRTA-H6.

Quantitative and Qualitative Analyses of Soluble Protein: Protein molecular weight was verified by mass spectrometry (MALDI-TOF), and concentration determined by Bradford assay (Dye Reagent Concentrate Bio-Rad kit). Volume size distribution of protein nanoparticles was determined by DLS. For that, a 50 μL aliquot (stored at -80 °C) was thawed and the volume size distribution of nanoparticles was immediately determined at 633 nm (Zetasizer Nano ZS, Malvern Instruments Ltd.). Far-UV CD was determined at 25 °C in a Jasco J-715 spectropolarimeter to assess the secondary structure of T22-mRTA-H6, which was dissolved at 0.35 mg mL⁻¹ in 166 $\times 10^{-3}$ M sodium bicarbonate buffer, pH 8. The CD spectra were obtained in a 1 mm path-length cuvette over a wavelength range of 190–260 nm, at a scan rate of 50 nm min⁻¹, a response of 1 s, and a bandwidth of 1 nm. Six scans were accumulated. The magnitude of secondary structure was analyzed using the JASCO spectra-manager analysis software. To investigate potential intermolecular β -sheet structure in the protein nanoparticles, conventional methods for Thioflavin T (ThT) staining were adapted. Briefly, protein aliquots (10 μL) were added to 90 μL of 50 $\times 10^{-6}$ M (Sigma Aldrich) in phosphate buffered saline (PBS), pH 7.4 and stirred for 1 min. The final protein concentration was 0.17 mg mL⁻¹. ThT was excited at 450 nm and the fluorescence emission spectra were recorded in the range of 460–565 nm with a Varian Cary Eclipse spectrofluorimeter. The cross- β -sheet structure was monitored by the enhancement of the free dye fluorescence emission.

Cell Culture and Determination of Cell Viability and Apoptosis: HeLa cells (ATCC-CCL-2) were cultured at 37 °C in a 5% CO₂ humidified atmosphere in MEM- α media supplemented with 10% fetal calf serum (Gibco Thermo Fisher Scientific (TFS)). They were seeded in an opaque 96-well plate (3 $\times 10^4$ cells/well) for 24 h. When insoluble T22-mRTA-H6 was assayed, the media was supplemented with 2% penicillin, 10 000 U mL⁻¹ streptomycin (Gibco, TFS). The next day soluble T22-mRTA-H6 was added and cells were exposed for 24, 48, and 72 h. Cells were also exposed to insoluble protein version during 24, 48, 72, 96, 120, and 144 h. Cell viability was determined by CellTiterGlo Luminescent Cell Viability Assay (Promega) in a Multilabel Plater Reader Victor3 (Perkin Elmer). For the CXCR4 specificity assay, the CXCR4 antagonist AMD3100³³ was added at 10:1 molar ratio 1 h before the incorporation of the protein. Antagonist and protein were incubated in a final volume of 10 μL that were mixed with 90 μL of culture media. All soluble protein experiments were done in triplicate and insoluble protein with six replicates.

On the other hand, the AML cell lines THP1 (ACC-16) and MV411 (ACC-102), as well as 3T3 mouse fibroblasts (ACC-173), were purchased from DSMZ (Leibniz Institute DSMZ-German Collection of Microorganisms and Cell Cultures, Braunschweig, Germany). THP1 was cultured in RPMI-1640 medium supplemented with 10% FBS, 10 mmol L⁻¹ L-glutamine 100 U mL⁻¹ penicillin, 10 mg mL⁻¹ streptomycin, and 0.45 $\mu\text{g mL}^{-1}$ fungizone. (Gibco, TFS). 3T3 cells were cultured with DMEM medium adding the same supplements. Cells were kept at 37 °C in a humidified atmosphere of 5% CO₂. Cell viability assays with these cell lines were performed using the XTT Cell Viability Kit II (Roche Diagnostics) and absorbance was read in a spectrophotometer at 490 nm (BMG Labtech). The effect of the caspase inhibitor zVAD-fmk was evaluated pretreating for 1 h cells seeded on 96-well plates (at 100 $\times 10^{-6}$ M zVAD-fmk) and then exposing them to 100 $\times 10^{-9}$ M T22-mRTA-H6 for 48 h. The antitumor drug Ara-C (cytosine β -D-arabinofuranoside hydrochloride) was purchased from Sigma Aldrich. To allow the follow-up of AML in mice, THP1 AML cell line was transfected with a plasmid encoding the luciferase gene that confers

bioluminescence that can be noninvasively imaged (BLI) to the cells. Briefly, THP1 cells were harvested in 24-well plates, treated with 0.5 μg of DNA plasmid and mixed with Lipofectamine LTX and PLUS reagents (A12621, Invitrogen, TFS) in Opti-MEM Reduced Serum Medium (Gibco, TFS) according to the manufacturer's instructions. 48 h later BLI levels were tested incubating cells with luciferin in an IVIS Spectrum In Vivo Imaging System (PerkinElmer, Waltham, MA). Finally, transfected cells were selected with 1.5 mg mL^{-1} geneticin (G418 Sulfate, Gibco, TFS) and BLI was analyzed periodically to check the preservation of the plasmid in cells, called THP1-Luci cells. Internalization of T22-GFP-H6^[20] in 3T3, MV411, THP1, and HeLa was determined by fluorescence-activated cell sorting (FACS Calibur, BD). Cells were exposed for 1 h to T22-GFP-H6 at 100×10^{-9} M. Then, cells were washed with PBS and trypsinized (1 mg mL^{-1} trypsin, Life Technologies) in order to remove nonspecific binding of nanoparticles to the cell membrane. Finally, levels of intracellular GFP fluorescence were quantified by flow cytometry. Mean fluorescence intensity ratios are given as mean fluorescence intensity of the treated samples divided by the mean fluorescence intensity of the vehicles.

To evaluate cell apoptosis, nuclear staining was performed with the Hoescht 3342 dye (Sigma-Aldrich) in HeLa cells exposed to 100×10^{-9} M T22-mRTA-H6 or buffer for different times. Once the incubation was finished, the media was collected and centrifuged to obtain the suspended cells. They were rinsed with PBS and centrifuged again. The adhered cells were trypsinized and pulled together with those previously obtained. These cells were fixed (3.7% *p*-formaldehyde in PBS, pH 7.4) for 10 min at -20°C , washed with PBS and resuspended in 10 μL of PBS. Finally, cells were mounted on a slide with ProLong Gold Antifade Mountant with DAPI and observed for the appearance of the nuclei under a fluorescence microscope. In addition, externalized phosphatidylserine protein-exposed cells were detected by Annexin V Detection Kit (APC, eBioscience) while dead cells were spotted with propidium iodide (PI), according to supplier instructions. Cell internalization was monitored using ATTO-labeled protein as described elsewhere.^[23]

Determination of ROS Levels and Mitochondrial Damage: On the other hand, levels of cellular ROS were measured with the Cellular ROS Detection Assay Kit (Abcam). In brief, HeLa cells were exposed to 100×10^{-9} M T22-mRTA-H6 (15 or 24 h) or buffer. Then, cells were washed and incubated with ROS Detection Solution for 1 h at 37°C , in the dark, adding 100×10^{-6} M Pyocyanin (1 h) to the positive controls. Afterward, levels of fluorescence were read with a microplate reader (BMG Labtech) at $\text{Ex} = 488$ nm and $\text{Em} = 520$ nm. Values were expressed as relative fluorescence units after subtracting the background fluorescence of blanks. Finally, to measure mitochondrial membrane potential ($\Delta\psi\text{m}$), a mitochondrial potential detection kit (BD MitoScreen, BD Biosciences) according to manufacturer's instructions was used. Labeled cells were analyzed by flow cytometry and the data were expressed as percentage of cells containing depolarized mitochondria (loss of JC-1 red fluorescence).

Flow Cytometry: CXCR4 membrane expression was determined by fluorescence-activated cell sorting (FACS Calibur, BD). Cells were washed with PBS 0.5% BSA and incubated either with PE-Cy5 mouse anti-CXCR4 monoclonal antibody (BD Biosciences) or PE-Cy5 Mouse IgG2a isotype (BD Biosciences) as control. Results of fluorescence emission were analyzed with software Cell Quest Pro and expressed as the ratio between the mean fluorescence intensity of each sample and the isotype values.

Electron Microscopy: The ultrastructure of soluble (in form of nanoparticles) and insoluble (in form of IBs) T22-mRTA-H6 was observed by FESEM). Insoluble protein was resuspended in PBS and sonicated at 10% amplitude 0.5 s ON/OFF for 1 min. Drops of 10 μL of either soluble protein in storage buffer or insoluble protein in PBS were deposited during 1 min on silicon wafers (Ted Pella), excess of liquid eliminated, and air dried. Samples without coating were observed with an in-lens detector in a FESEM Zeiss Merlin (Zeiss) operating at 1 kV. Representative images were obtained at a wide range of magnifications (from 100 000x to 450 000x).

Antineoplastic Effect in a Disseminated AML Mouse Model: NSG (NOD-scid IL2R γ gammanull) female mice (five weeks old) were obtained from Charles River Laboratories (Wilmington, MA) and housed in microisolator units with sterile food and water *ad libitum*. After one week in quarantine, NSG mice were intravenously (IV) injected with luciferase-transfected THP1 cells (THP1-Luci; 1×10^6 cells/200 μL) and divided randomly into three different experimental groups. One group (VEHICLE; $n = 3$) was IV injected with NaCO_3H pH = 8 buffer, a second group (T22mRTA; $n = 1$) was administered with 10 μg of T22-mRTA-H6. Both groups were injected with a daily dose for a total of ten doses. A third group (IB-T22mRTA; $n = 2$) was subcutaneously (SC) injected once with 1 mg of T22-mRTA-H6 IBs. These treatments started 2 d after the IV injection of THP1-Luci cells in mice, which generated the disseminated AML model. Evolution of AML dissemination was monitored in IVIS Spectrum three times per week until the day of the euthanasia. Weight of the animals was measured the same day of BLI analysis. All mice were euthanized the day that the first of them presented relevant signs of disease such as 10% weight loss or lack of mobility. Animals were intraperitoneally injected with luciferin, and after 5 min mice were killed by cervical dislocation. Tissues were excised and the BLI levels of the organs *ex vivo* analyzed. After that, they were preserved in formaldehyde 3.7% and paraffin embedded for further immunohistochemistry analyses. The analysis and detection of BLI was performed using radiance photons in Living Image 4.4 Software both in *in vivo* and *ex vivo* studies. All procedures were conducted in accordance with the guidelines approved by the institutional animal Ethics Committee of Hospital Sant Pau.

Histopathology and Immunohistochemical Staining: Sections of paraffin-embedded samples of infiltrated (liver, spleen, hindlimbs, and backbone) and normal (lung, heart, and kidney) organs were hematoxylin and eosin (H&E) stained and the presence of toxicity was analyzed. Moreover, in order to detect AML cells in infiltrated tissues, immunohistochemical analysis with anti-human CD45 antibody (DAKO) was done in paraffin-embedded tissue samples. Staining was performed in a Dako Autostainer Link 48, following the manufacturer's instructions. Two independent observers evaluated all samples, using an Olympus BX51 microscope (Olympus). Images were acquired using an Olympus DP72 digital camera and processed with CellD Imaging 3.3 software (Olympus).

Statistical Analysis: Quantitative data are expressed as mean \pm standard error (SE). Previously to perform statistical analyses, all variables were tested for normality and homogeneity of variances employing the Shapiro-Wilk and the Levene test, respectively. Comparisons of soluble protein cytotoxicity effects and competition assays were made with Tukey's test. Meanwhile, protein cytotoxicity assays were assessed by Mann-Whitney U tests. Significance was accepted at $p < 0.05$.

Acknowledgements

R.D. and V.P. contributed equally to this work. The authors are indebted to Agencia Estatal de Investigación (AEI) and to Fondo Europeo de Desarrollo Regional (FEDER) (Grant No. BIO2016-76063-R, AEI/FEDER, UE), AGAUR (2017SGR-229), and CIBER-BBN (project VENOM4CANCER) granted to A.V. The authors are also indebted to the Networking Research Center on Bioengineering, Biomaterials and Nanomedicine (CIBER-BBN) that is an initiative funded by the VI National R&D&I Plan 2008–2011, Iniciativa Ingenio 2010, Consolider Program, CIBER Actions and financed by the Instituto de Salud Carlos III, with assistance from the European Regional Development Fund. Protein production was partially performed by the ICTS "NANBIOSIS," more specifically by the Protein Production Platform of CIBER-BBN/IBB (<http://www.nanbiosis.es/unit/u1-protein-production-platform-ppp/>) and the nanoparticle size analysis by the Biomaterial Processing and Nanostructuring Unit. The authors are also indebted to SCAC (UAB) for cell culture facilities and assistance. R.D. received an overseas

predoctoral fellowship from Conacyt (Gobierno de México, 2016). L.S.-G. and A.F. were supported by AGAUR (2017FI_B100063 and 2017FI_B00680), N.S. by a predoctoral fellowship from the Government of Navarra, V.P. received a postdoctoral fellowship from the Spanish Foundation of Hematology and Hemotherapy (FEHH), and U.U. a Sara Borrell postdoctoral fellowship from ISCIII. A.V. holds an ICREA ACADEMIA award.

Conflict of Interest

Some of the authors hold a patent on the use of the peptide T22 as cell-targeted delivery agent.

Keywords

acute myeloid leukemia, nanoparticles, protein engineering, self-assembling, targeted drug delivery

Received: February 17, 2018

Revised: April 24, 2018

Published online: May 29, 2018

- [1] R. L. Siegel, K. D. Miller, A. Jemal, *CA: Cancer J. Clin.* **2018**, *68*, 7.
- [2] B. Vincenzi, G. Armento, M. S. Ceruso, G. Catania, M. Lealos, D. Santini, G. Minotti, G. Tonini, *Expert Opin. Drug Saf.* **2016**, *15*, 1219.
- [3] N. Serna, L. Sanchez-Garcia, U. Unzueta, R. Diaz, E. Vazquez, R. Mangués, A. Villaverde, *Trends Biotechnol.* **2018**, *36*, 318.
- [4] J. Shen, J. Wolfram, M. Ferrari, H. Shen, *Mater. Today* **2017**, *20*, 95.
- [5] L. Sanchez-Garcia, L. Martin, R. Mangués, N. Ferrer-Miralles, E. Vazquez, A. Villaverde, *Microb. Cell Fact.* **2016**, *15*, 33.
- [6] J. R. Kintzing, M. V. F. Interrante, J. R. Cochran, *Trends Pharmacol. Sci.* **2016**, *37*, 993.
- [7] G. Manoukian, F. Hagemeister, *Expert Opin. Biol. Ther.* **2009**, *9*, 1445.
- [8] R. Hassan, E. Sharon, A. Thomas, J. Zhang, A. Ling, M. Miettinen, R. J. Kreitman, S. M. Steinberg, K. Hollevoet, I. Pastan, *Cancer* **2014**, *120*, 3311.
- [9] R. J. Kreitman, I. Pastan, *Best Pract. Res., Clin. Haematol.* **2015**, *28*, 236.
- [10] L. Polito, A. Djemil, M. Bortolotti, *Biomedicines* **2016**, *4*, 12.
- [11] U. Wittstock, J. Gershenzon, *Curr. Opin. Plant Biol.* **2002**, *5*, 300.
- [12] R. D. Cummings, in *Essentials of Glycobiology* (Eds: A. Varki, R. D. Cummings, J. D. Esko, P. Stanley, G. W. Hart, M. Aebi, A. G. Davill, T. Kinoshita, N. H. Packer, J. H. Prestegard, R. L. Schnaar, P. H. Seeberger), Cold Spring Harbor Laboratory Press, Cold Spring Harbor, New York **2015**, pp. 401–412.
- [13] M. Moshiri, F. Hamid, L. Etemad, *Rep. Biochem. Mol. Biol.* **2016**, *4*, 60.
- [14] H. Kulbe, N. R. Levinson, F. Balkwill, J. L. Wilson, *Int. J. Dev. Biol.* **2004**, *48*, 489.
- [15] T. Murakami, A. R. Cardones, S. T. Hwang, *J. Dermatol. Sci.* **2004**, *36*, 71.
- [16] F. Balkwill, *Semin. Cancer Biol.* **2004**, *14*, 171.
- [17] J. Kim, H. Takeuchi, S. T. Lam, R. R. Turner, H. J. Wang, C. Kuo, L. Foshag, A. J. Bilchik, D. S. Hoon, *J. Clin. Oncol.* **2005**, *23*, 2744.
- [18] J. A. Burger, T. J. Kipps, *Blood* **2006**, *107*, 1761.
- [19] J. Kim, T. Mori, S. L. Chen, F. F. Amersi, S. R. Martinez, C. Kuo, R. R. Turner, X. Ye, A. J. Bilchik, D. L. Morton, D. S. Hoon, *Ann. Surg.* **2006**, *244*, 113.
- [20] U. Unzueta, M. V. Cespedes, N. Ferrer-Miralles, I. Casanova, J. Cedano, J. L. Corchero, J. Domingo-Espin, A. Villaverde, R. Mangués, E. Vazquez, *Int. J. Nanomed.* **2012**, *7*, 4533.
- [21] M. V. Cespedes, U. Unzueta, P. Alamo, A. Gallardo, R. Sala, I. Casanova, M. A. Pavon, M. A. Mangués, M. Trias, A. Lopez-Pousa, A. Villaverde, E. Vazquez, R. Mangués, *Nanomed.: Nanotechnol., Biol. Med.* **2016**, *12*, 1987.
- [22] N. Serna, M. V. Cespedes, L. Sánchez-García, U. Unzueta, R. Sala, A. Sánchez-Chardi, F. Cortés, N. Ferrer-Miralles, R. Mangués, E. Vázquez, A. Villaverde, *Adv. Funct. Mater.* **2017**, *27*, 1700919.
- [23] L. Sanchez-Garcia, N. Serna, P. Alamo, R. Sala, M. V. Cespedes, M. Roldan, A. Sanchez-Chardi, U. Unzueta, I. Casanova, R. Mangués, E. Vazquez, A. Villaverde, *J. Controlled Release* **2018**, *274*, 81.
- [24] N. Gonzalez-Montalban, E. Garcia-Fruitos, A. Villaverde, *Nat. Biotechnol.* **2007**, *25*, 718.
- [25] M. V. Cespedes, Y. Fernandez, U. Unzueta, R. Mendoza, J. Seras-Franzoso, A. Sanchez-Chardi, P. Alamo, V. Toledo-Rubio, N. Ferrer-Miralles, E. Vazquez, S. Schwartz, I. Abasolo, J. L. Corchero, R. Mangués, A. Villaverde, *Sci. Rep.* **2016**, *6*, 35765.
- [26] J. Seras-Franzoso, A. Sanchez-Chardi, E. Garcia-Fruitos, E. Vazquez, A. Villaverde, *Soft Matter* **2016**, *12*, 3451.
- [27] U. Unzueta, J. Seras-Franzoso, M. V. Cespedes, P. Saccardo, F. Cortes, F. Rueda, E. Garcia-Fruitos, N. Ferrer-Miralles, R. Mangués, E. Vazquez, A. Villaverde, *Nanotechnology* **2017**, *28*, 015102.
- [28] U. Unzueta, N. Ferrer-Miralles, J. Cedano, X. Zikung, M. Pesarrodonna, P. Saccardo, E. Garcia-Fruitos, J. Domingo-Espin, P. Kumar, K. C. Gupta, R. Mangués, A. Villaverde, E. Vazquez, *Biomaterials* **2012**, *33*, 8714.
- [29] M. Pesarrodonna, E. Crosas, R. Cubarsi, A. Sanchez-Chardi, P. Saccardo, U. Unzueta, F. Rueda, L. Sanchez-Garcia, N. Serna, R. Mangués, N. Ferrer-Miralles, E. Vazquez, A. Villaverde, *Nanoscale* **2017**, *9*, 6427.
- [30] F. Rueda, M. V. Cespedes, O. Conchillo-Sole, A. Sanchez-Chardi, J. Seras-Franzoso, R. Cubarsi, A. Gallardo, M. Pesarrodonna, N. Ferrer-Miralles, X. Daura, E. Vazquez, E. Garcia-Fruitos, R. Mangués, U. Unzueta, A. Villaverde, *Adv. Mater.* **2015**, *27*, 7816.
- [31] B. A. Webb, M. Chimenti, M. P. Jacobson, D. L. Barber, *Nat. Rev. Cancer* **2011**, *11*, 671.
- [32] C. Corbet, O. Feron, *Nat. Rev. Cancer* **2017**, *17*, 577.
- [33] Y. H. Jung, D. Y. Lee, W. Cha, B. H. Kim, M. W. Sung, K. H. Kim, S. H. Ahn, *Head Neck* **2016**, *38*, 1479.
- [34] R. L. Momparler, *Exp. Hematol. Oncol.* **2013**, *2*, 20.
- [35] J. P. Richard, K. Melikov, E. Vives, C. Ramos, B. Verbeure, M. J. Gait, L. V. Chernomordik, B. Lebleu, *J. Biol. Chem.* **2003**, *278*, 585.
- [36] M. Pesarrodonna, Y. Fernandez, L. Foradada, A. Sanchez-Chardi, O. Conchillo-Sole, U. Unzueta, Z. Xu, M. Roldan, S. Villegas, N. Ferrer-Miralles, S. Schwartz Jr., U. Rinas, X. Daura, I. Abasolo, E. Vazquez, A. Villaverde, *Biofabrication* **2016**, *8*, 025001.
- [37] E. Vazquez, R. Mangués, A. Villaverde, *Nanomedicine* **2016**, *11*, 1333.
- [38] I. M. Tomlinson, *Nat. Biotechnol.* **2004**, *22*, 521.
- [39] D. Agyei, I. Ahmed, Z. Akram, H. M. Iqbal, M. K. Danquah, *Protein Pept. Lett.* **2017**, *24*, 94.
- [40] G. Aruna, *J. Stem Cells Regen. Med.* **2006**, *1*, 31.
- [41] C. Alewine, R. Hassan, I. Pastan, *Oncologist* **2015**, *20*, 176.
- [42] B. Akbari, S. Farajnia, S. Ahdi Khosroshahi, F. Safari, M. Yousefi, H. Dariushnejad, L. Rahbarnia, *Int. Rev. Immunol.* **2017**, *36*, 207.
- [43] R. Duncan, R. Gaspar, *Mol. Pharm.* **2011**, *8*, 2101.
- [44] S. Wilhelm, A. J. Tavares, Q. Dai, S. Ohta, J. Audet, H. F. Dvorak, W. C. W. Chan, *Nat. Rev. Mater.* **2016**, *1*, 16014.
- [45] U. Unzueta, M. V. Cespedes, E. Vazquez, N. Ferrer-Miralles, R. Mangués, A. Villaverde, *Trends Biotechnol.* **2015**, *33*, 253.
- [46] N. Tyagi, M. Tyagi, M. Pachauri, P. C. Ghosh, *Tumor Biol.* **2015**, *36*, 8239.

- [47] G. Bellisola, G. Fracasso, R. Ippoliti, G. Menestrina, A. Rosen, S. Solda, S. Udali, R. Tomazzolli, G. Tridente, M. Colombatti, *Biochem. Pharmacol.* **2004**, *67*, 1721.
- [48] R. Schnell, P. Borchmann, J. O. Staak, J. Schindler, V. Ghetie, E. S. Vitetta, A. Engert, *Ann. Oncol.* **2003**, *14*, 729.
- [49] J. M. Lambert, V. S. Goldmacher, A. R. Collinson, L. M. Nadler, W. A. Blattler, *Cancer Res.* **1991**, *51*, 6236.
- [50] M. M. Gottesman, T. Fojo, S. E. Bates, *Nat. Rev. Cancer* **2002**, *2*, 48.
- [51] S. Kapse-Mistry, T. Govender, R. Srivastava, M. Yergeri, *Front. Pharmacol.* **2014**, *5*, 159.
- [52] A. R. Kirtane, S. M. Kalscheuer, J. Panyam, *Adv. Drug Delivery Rev.* **2013**, *65*, 1731.
- [53] R. Wales, L. M. Roberts, J. M. Lord, *J. Biol. Chem.* **1993**, *268*, 23986.
- [54] D. A. Vallera, H. Chen, A. R. Sicheneder, A. Panoskaltis-Mortari, E. P. Taras, *Leukemia Res.* **2009**, *33*, 1233.
- [55] Y. Yamada, A. Aoyama, G. Tocco, S. Boskovic, O. Nadazdin, A. Alessandrini, J. C. Madsen, A. B. Cosimi, G. Benichou, T. Kawai, *J. Immunol.* **2012**, *188*, 6063.
- [56] J. R. Murphy, J. C. vanderSpek, *Semin. Cancer Biol.* **1995**, *6*, 259.
- [57] M. Onda, M. Willingham, Q. C. Wang, R. J. Kreitman, Y. Tsutsumi, S. Nagata, I. Pastan, *J. Immunol.* **2000**, *165*, 7150.
- [58] D. L. Newton, P. J. Nicholls, S. M. Rybak, R. J. Youle, *J. Biol. Chem.* **1994**, *269*, 26739.
- [59] S. Porter, *J. Pharm. Sci.* **2001**, *90*, 1.
- [60] Y. Grinberg, I. Benhar, *Biomedicines* **2017**, *5*, 28.
- [61] Y. Wang, Y. Xie, D. Oupicky, *Curr. Pharmacol. Rep.* **2016**, *2*, 1.
- [62] D. Heckmann, P. Maier, S. Laufs, F. Wenz, W. J. Zeller, S. Fruehauf, H. Allgayer, *Transl. Oncol.* **2013**, *6*, 124.
- [63] W. T. Choi, Y. Yang, Y. Xu, *J. An. Curr. Top. Med. Chem.* **2014**, *14*, 1574.
- [64] K. Philipp-Abbrederis, K. Herrmann, S. Knop, M. Schottelius, M. Eiber, K. Luckerath, E. Pietschmann, S. Habringer, C. Gerngross, K. Franke, M. Rudelius, A. Schirbel, C. Lapa, K. Schwamborn, S. Steidle, E. Hartmann, A. Rosenwald, S. Kropf, A. J. Beer, C. Peschel, H. Einsele, A. K. Buck, M. Schwaiger, K. Gotze, H. J. Wester, U. Keller, *EMBO Mol. Med.* **2015**, *7*, 477.
- [65] T. E. Goranova, S. S. Bozhanov, V. S. Lozanov, V. I. Mitev, R. P. Kaneva, E. I. Georgieva, *Neoplasma* **2015**, *62*, 27.
- [66] K. Tamas, U. M. Domanska, T. H. van Dijk, H. Timmer-Bosscha, K. Havenga, A. Karrenbeld, W. J. Sluiter, J. C. Beukema, M. A. van Vugt, E. G. de Vries, G. A. Hospers, A. M. Walenkamp, *Curr. Pharm. Des.* **2015**, *21*, 2276.
- [67] M. Y. Li, R. Bruzzone, P. G. Wang, *Oncotarget* **2015**, *6*, 30425.


ANNEX 5: ARTICLE 6

Engineering multifunctional protein nanoparticles by in vitro disassembling and reassembling of heterologous building blocks

Ugutz Unzueta, Naroa Serna, **Laura Sánchez-García**, Mónica Roldán, Alejandro Sánchez-Chardi, Ramón Mangués, Antonio Villaverde and Esther Vázquez

Nanotechnology (2017) 28: 505102
Impact factor 3.44 PHYSICS, APPLIED (30/146) Q1

Engineering multifunctional protein nanoparticles by *in vitro* disassembling and reassembling of heterologous building blocks

Ugutx Unzueta^{1,2}, Naroa Serna^{2,3,4}, Laura Sánchez-García^{2,3,4},
Mónica Roldán⁵, Alejandro Sánchez-Chardi⁶, Ramón Mangues^{1,2},
Antonio Villaverde^{2,3,4,7}  and Esther Vázquez^{2,3,4,7}

¹Institut d'Investigacions Biomèdiques Sant Pau and Josep Carreras Research Institute, Hospital de la Santa Creu i Sant Pau, E-08025 Barcelona, Spain

²CIBER de Bioingeniería, Biomateriales y Nanomedicina (CIBER-BBN), Spain

³Institut de Biociències i de Biomedicina, Universitat Autònoma de Barcelona, Bellaterra, E-08193 Barcelona, Spain

⁴Departament de Genètica i de Microbiologia, Universitat Autònoma de Barcelona, Bellaterra, E-08193 Barcelona, Spain

⁵Unitat de Microscòpia Confocal, Servei d'Anatomia Patològica, Institut Pediàtric de Malalties Rares (IPER), Hospital Sant Joan de Déu, Universitat de Barcelona, Esplugues de Llobregat, E-08950 Barcelona, Spain

⁶Servei de Microscòpia, Universitat Autònoma de Barcelona, Bellaterra, E-08193 Barcelona, Spain

E-mail: Antoni.Villaverde@uab.es and Esther.Vazquez@uab.es

Received 15 September 2017, revised 18 October 2017

Accepted for publication 26 October 2017

Published 22 November 2017



CrossMark

Abstract

The engineering of protein self-assembling at the nanoscale allows the generation of functional and biocompatible materials, which can be produced by easy biological fabrication. The combination of cationic and histidine-rich stretches in fusion proteins promotes oligomerization as stable protein-only regular nanoparticles that are composed by a moderate number of building blocks. Among other applications, these materials are highly appealing as tools in targeted drug delivery once empowered with peptidic ligands of cell surface receptors. In this context, we have dissected here this simple technological platform regarding the controlled disassembling and reassembling of the composing building blocks. By applying high salt and imidazole in combination, nanoparticles are disassembled in a process that is fully reversible upon removal of the disrupting agents. By taking this approach, we accomplish here the *in vitro* generation of hybrid nanoparticles formed by heterologous building blocks. This fact demonstrates the capability to generate multifunctional and/or multiparatopic or multispecific materials usable in nanomedical applications.

Supplementary material for this article is available online

Keywords: recombinant proteins, self-assembling, viral mimetics, cell targeting, multifunctional nanoparticles

(Some figures may appear in colour only in the online journal)

⁷ Authors to whom any correspondence should be addressed.

Introduction

Among the diversity of materials used in nanomedicine, proteins offer full biocompatibility, structural and functional versatility and the possibility to control their oligomerization status to reach defined supramolecular architectures [1–5]. For use as biomaterials, self-assembling can be promoted either by adapting natural oligomerization domains [6] or by the *de novo* design of interacting stretches [5, 7, 8]. Virus-like particles are the paradigm of self-organizing oligomeric structures that directly derive from nature. Produced in recombinant cell factories, selected structural viral proteins spontaneously assemble as nanoscale entities, usually homomeric, that mimic viral capsids and that have applicability as immunogens for vaccination [9] and as drug delivery systems [10]. Cellular elements such as bacterial flagella [11] or mammalian cell vaults [12] are equally produced by recombinant DNA technologies upon convenient tailoring.

Regarding *de novo* designed nanoscale multimers, a diversity of rational and semi-rational approaches are available [3]. In this context, we have previously described an oligomerization platform based on the fusion of an N-terminal cationic peptide plus a C-terminal histidine-rich peptide, to diverse central polypeptides that act as a core of the whole fusion [13, 14]. Both end-terminal tails promote protein–protein contacts between the building blocks that render a category of non-toxic planar nanoparticles [15], whose formation and final architecture is modulated by the number of cationic residues at the N-terminus and by the electrostatic charge distribution in the building block [16, 17]. Mimicking viral properties, these materials are highly convenient as drug carriers [18]. When the N-terminal cationic peptide is a specific ligand of a cell surface tumoral marker (such as binders of cell surface proteins CD44 or CXCR4), this protein segment contributes to the self-assembling but it also endorses the penetration of the whole construct in a receptor-specific way, as demonstrated *in vivo* in breast and colorectal cancer models [17, 19–21]. In particular, T22-GFP-H6 is a paradigmatic construct that self-assembles as 12 nm nanoparticles, and in which the cationic peptide T22 acts as a specific ligand of CXCR4, both *in vitro* and *in vivo* [13, 20]. Envisaging the clinically appealing possibility to generate hybrid nanoparticles made of different building blocks or displaying different cell-targeting agents in multiparatopic or multi-specific constructs [22], we have explored here the generation of multifunctional hybrid materials based on this oligomerization platform. This has been successfully achieved through novel but simple procedures that allow the reversible disassembling of protein homomeric oligomers and their controlled re-association, upon convenient ratiometric mixing, to form regular but heteromeric multifunctional nanoparticles.

Methods

Protein design, production and purification

The gene encoding T22-BFP-H6 was designed in house, provided by Gencart (Invitrogen) and cloned in pET22b

(Novagen). The construction of the related gene fusions encoding T22-GFP-H6 and R9-GFP-H6 had been described previously [16, 23]. Proteins were produced in *Escherichia coli* Origami B overnight at 20 °C upon addition of 0.1 mM IPTG for T22-GFP-H6 and T22-BFP-H6 and in *Escherichia coli* Rosetta, overnight at 25 °C, upon addition of 1 mM of IPTG for R9-GFP-H6. These strains were selected because of their less reducing cytoplasm that ensure the formation of the two disulphide bridges of T22, necessary for T22-CXCR4 interaction. Cells were then centrifuged for 10 min (5000 g) and resuspended in Tris buffer (20 mM Tris, 500 mM NaCl, 10 mM Imidazole) in presence of the protease inhibitor Complete EDTA-Free (Roche). Cells were then disrupted by three rounds at 1200 psi in a French Press (Thermo) and subsequently purified by IMAC affinity chromatography using HiTrap Chelating HP 1 ml column in an ÄKTA pure (GE Healthcare). Proteins were eluted by a linear gradient of elution buffer (20 mM Tris, 500 mM NaCl, 500 mM Imidazole) and once collected, they were dialysed against sodium carbonate buffer (166 mM NaCO₃H pH = 8) for T22-GFP-H6 and T22-BFP-H6 and against Tris Dextrose buffer (20 mM Tris + 5% Dextrose pH = 8) for R9-GFP-H6. Protein purity was determined by polyacrylamide gel electrophoresis (SDS-PAGE) and Western blot immunodetection with anti-His monoclonal antibody (Santa Cruz Biotechnology). Finally, protein integrity was determined by MALDI-TOF mass spectrometry.

Production of hybrid nanoparticles

T22-GFP-H6, T22-BFP-H6 and R9-GFP-H6 protein nanoparticles (at 1.5 mg ml⁻¹) were disassembled by adding NaCl (500 mM Na⁺ final concentration) and Imidazole (300 mM final concentration) into their respective buffers. T22-GFP-H6/T22-BFP-H6 and R9-GFP-H6/T22-BFP-H6 hybrid nanoparticles were generated by mixing T22-GFP-H6 and T22-BFP-H6 monomers and R9-GFP-H6 and T22-BFP-H6 monomers respectively in a 1:1 molar ratio and subsequently dialyzing them against a low Na⁺ and Imidazole buffer (166 mM NaCO₃H pH = 8 and 20 mM Tris + 5% Dextrose pH = 8 respectively).

Dynamic light scattering (DLS)

Volume size distribution of parental and hybrid protein nanoparticles at 1.5 mg ml⁻¹ and under different buffer conditions was determined by DLS at 633 nm in a Zetasizer Nano ZS (Malvern).

Field emission scanning electron microscopy (FESEM)

Native ultrastructure of the nanoparticles was evaluated with a microscope Zeiss Merlin (Zeiss) operating at 2 kV. Drops of 3 µl of each sample (T22-GFP-H6, R9-GFP-H6, T22-BFP-H6, T22-GFP-H6/T22-BFP-H6 and R9-GFP-H6/T22-BFP-H6) were directly deposited on silicon wafers (Ted Pella Inc.) for 1 min, excess blotted with Whatman filter paper number 1 (GE Healthcare), air dried, and observed without coating with a high resolution in-lens secondary electron detector.

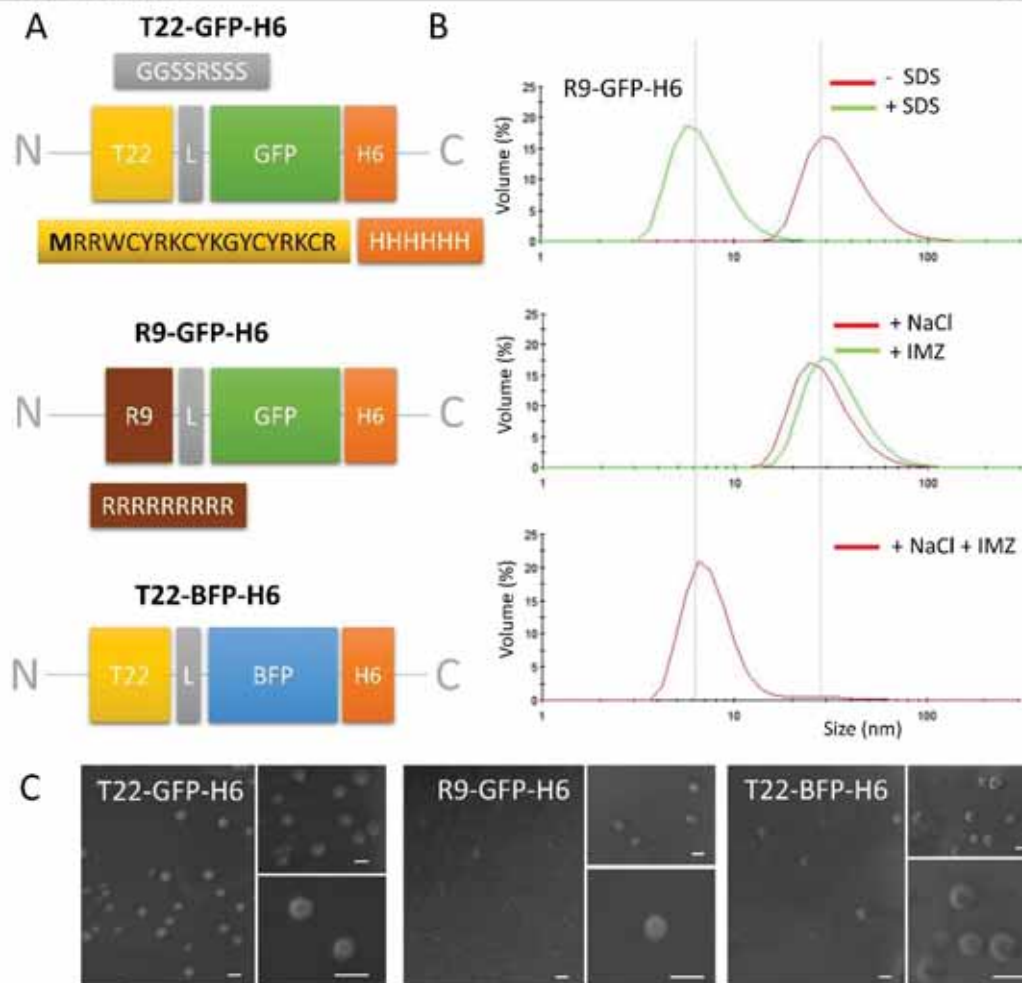


Figure 1. Architecture of protein nanoparticles. (A) Modular organization of the protein building blocks, indicating the relevant amino acid stretches. Box sizes and proportions are only indicative. (B) DLS analysis of R9-GFP-H6 nanoparticles, in the native assembled state or disassembled upon incubation with SDS 0.1%. The sizes of the material treated with imidazole (300 mM, IMZ) and incubated in high salt (500 mM, Na⁺) buffer are also indicated. Raw data for R9-GFP-H6 and for T22-GFP-H6 and T22-BFP-H6 are shown in table 1. The vertical lines indicate the expected location of assembled and unassembled materials. (C) FESEM imaging of the resulting nanoparticles at different magnifications. Bars represent 20 nm.

Table 1. Size of protein nanoparticles under different buffer conditions.

Buffer ^{a,b}	Na ⁺ (mM) ^c	Imidazole (mM)	T22-GFP-H6		R9-GFP-H6		T22-BFP-H6	
			Size (nm)	Pdi	Size (nm)	Pdi	Size (nm)	Pdi
Buffer ^{a,h,i,d}	166 ^a /0 ^b	0	11.01/9.1 ^e	0.454	36.02/19.7 ^e	0.150	8.6/9.0 ^e	0.500
+NaCl	500	0	10.17	0.798	29.7	0.486	8.8	0.495
+IMZ	166 ^a /0 ^b	300	10.79	0.411	34.3	0.129	8.5	0.395
+NaCl +IMZ	500	300	6.5	0.561	7.50	0.734	6.8	0.451
+SDS (0.1%)	166 ^a /0 ^b	0	7.9	0.332	6.9	0.225	6.91	0.198

^a NaCO₃H buffer has been used to dissolve T22-GFP-H6 and T22-BFP-H6.

^b Tris Dextrose has been used for R9-GFP-H6.

^c Total Na⁺ concentration reached in buffer.

^d The parental GFP-H6 sizes 7.0 nm^a and 7.2 nm^b in the same buffers.

^e Size peak of particles reassembled in the original buffer after Na⁺ +IMZ-mediated disassembling. IMZ, Imidazole.

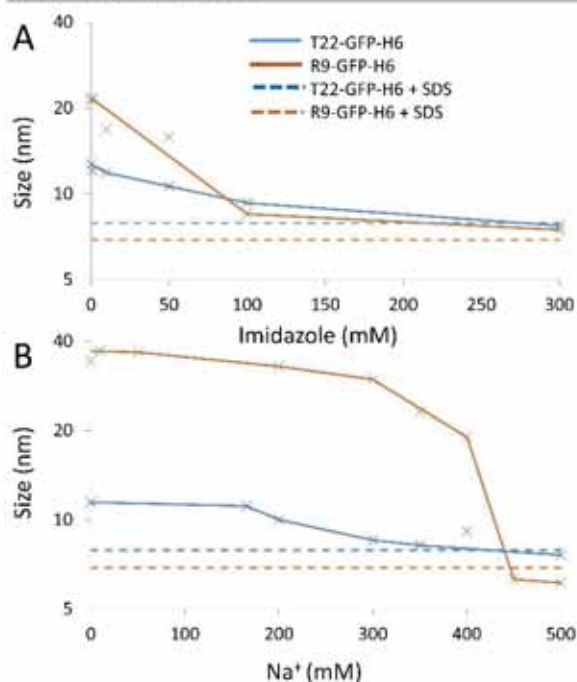


Figure 2. Controlled disassembling of T22-GFP-H6 and R9-GFP-H6 nanoparticles. Disassembling is mediated by increasing concentrations of either imidazole ((A), in 500 mM Na⁺) or salt ((B), in 300 mM imidazole), keeping the rest of conditions constant. The monomer size upon SDS-mediated disassembly is indicated in each case by horizontal dashed lines.

FRET determination

Fluorescence emission spectrum (400–600 nm) of hybrid protein nanoparticles in different buffers was measured in a Cary Eclipse fluorescence spectrophotometer (Agilent Technologies) upon excitation at 387 nm. Acceptor photobleaching experiments were performed on a TCS SP5 Leica Spectral confocal microscope (Leica Microsystems) equipped with a HCX PL Apo CS lambda blue 63×/1.4NA oil objective. We used BFP as the donor fluorochrome paired with GFP as the acceptor fluorochrome. BFP was excited with the 405 nm line (diode laser) and the emission was collected at 420–475 nm. GFP was excited with the 488 nm line of the argon laser and the emission was collected at 500–550 nm. In the presence of FRET, bleaching of the acceptor (GFP) resulted in a significant increase in fluorescence of the donor (BFP). Selective photobleaching of GFP was performed by repeatedly scanning a region of the sample (10 × 10 μm) with the 488 nm argon laser set at 100% intensity to photobleach at least 85% of the original acceptor fluorescence. Pre-bleach and post-bleach images were collected sequentially. To minimize the effect of photobleaching caused by imaging, images were collected at low laser intensity. The amount of proteins used in all these experiments was equivalent to prevent potential influences of protein concentration on FRET efficiency.

The FRET efficiency using the acceptor photobleaching paradigm is calculated as the percentage of increased BFP

emission after GFP photobleaching:

$$\% \text{ FRET efficiency} = \frac{\text{BFP post} - \text{BFP pre}}{\text{BFP post}} \times 100,$$

where BFP_{pre} and BFP_{post} are the BFP emission before and after GFP photobleaching, respectively. Positive and negative controls were used as measure of the highest and lowest percentage of FRET possible, respectively. Mean FRET efficiencies ± standard error were reported ($n \geq 6$). FRET image is presented in pseudocolor for better visualization.

Cell culture and nanoparticle internalization

HeLa cells were obtained from the American Type Culture Collection (reference CCL-2) and cultured in 24 well plates in MEM ALPHA medium (Gibco) supplemented with 10% foetal bovine serum (Gibco), and incubated at 37 °C in a 5% CO₂ humidified atmosphere. For internalization assays 1 μM of hybrid nanoparticles were added in presence of serum free Optipro medium (Gibco) 24 h before flow cytometer analysis. Cells were then analysed after 15 min treatment with 1 mg ml⁻¹ trypsin (Gibco) on a FACS-Canto system (Becton Dickinson) at 488 nm excitation with a 15 mW air-cooled argon ion laser and a D detector (530/30 nm band pass filter). For competition assays, 5 μM of the CXCR4 receptor-specific antagonist AMD3100 (octohydrochloride hydrate, Sigma) was added to the cells 1 h before nanoparticle addition.

For confocal analysis, cells were grown on MatTek culture dishes (MatTek Corporation) and protein nanoparticles added in presence of serum free Optipro medium (Gibco) 24 h before analysis. Cell membranes were then labelled with 2.5 μg ml⁻¹ CellMask™ deep red (Molecular Probes) and nuclei with 0.2 μg ml⁻¹ Hoechst 33342 (molecular probes) for 10 min. Cells were finally washed in PBS (Sigma) and analysed by TCS-SP5 confocal laser scanning microscopy (Leica Microsystems) using a HCX PL Apo CS lambda blue 63×/1.4NA oil objective. A blue diode (405 nm) was used for Hoechst and BFP excitation, an Ar laser (488 nm) for GFP excitation and a HeNe laser (633 nm) for CellMask™ excitation. To localize the protein materials inside the cells, Z stacks of different sections were acquired along the cell thickness following Nyquist criterion. Final images were processed using LAS AF™ software (Leica Microsystems, Heidelberg, Germany) and 3D models were generated using Imaris x64 v7.2.1 software (Bitplane, Zurich Switzerland) with Surpass Mode.

Statistical analyses

Quantitative data of competition assays and FRET analyses are expressed as mean ± standard error. Data of competition assays were log transformed and checked for normal distribution and homogeneity of variances with Kolmogorov–Smirnov and Levene tests, respectively. Then, pairwise comparisons were performed using Student *t* tests. FRET data were compared using Mann–Whitney U tests. Statistical differences were assumed at $p < 0.05$. All statistical analyses were performed with SPSS 15.0 software (SPSS Inc.).

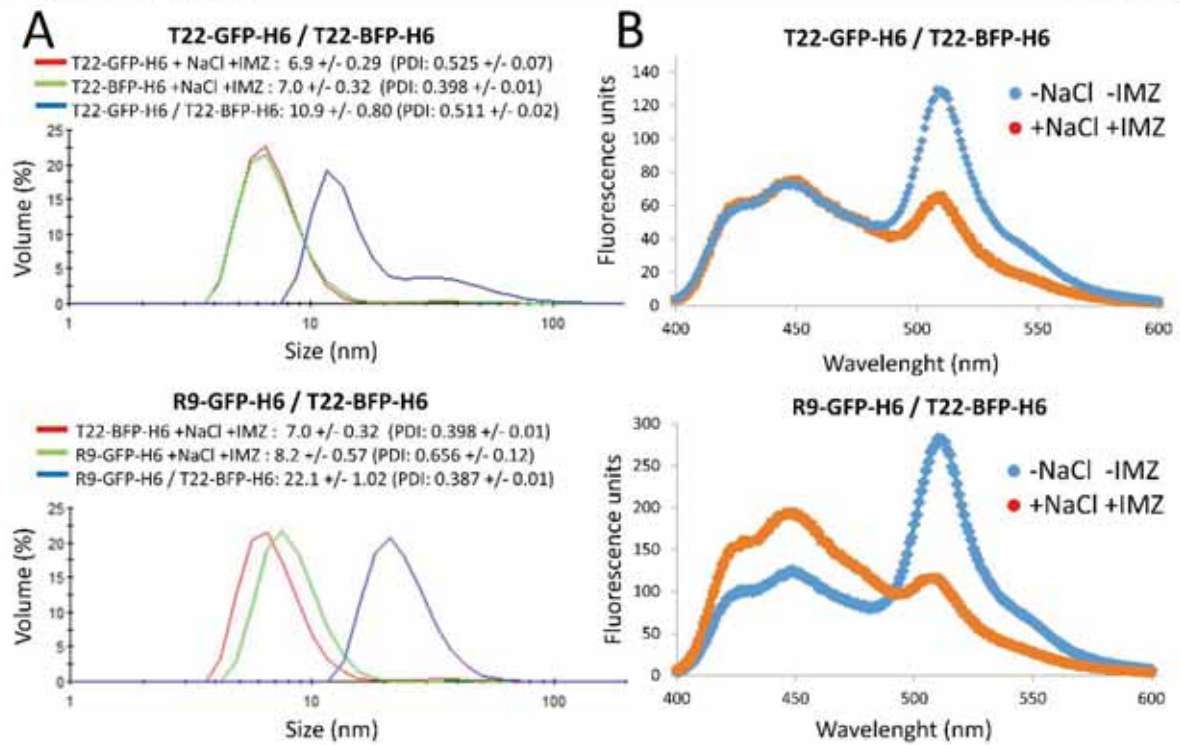


Figure 3. Controlled formation of hybrid materials. Reconstitution of hybrid T22-GFP-H6/T22-BFP-H6 and R9-GFP-H6/ T22-BFP-H6 nanoparticles monitored by DLS (A) and FRET (B) determinations. DLS size of starting building blocks (A) and NaCl and Imidazole-mediated loss of FRET (B) are shown as references. Peak sizes and pdi values are shown for all DLS plots and expressed as mean +/- standard error.

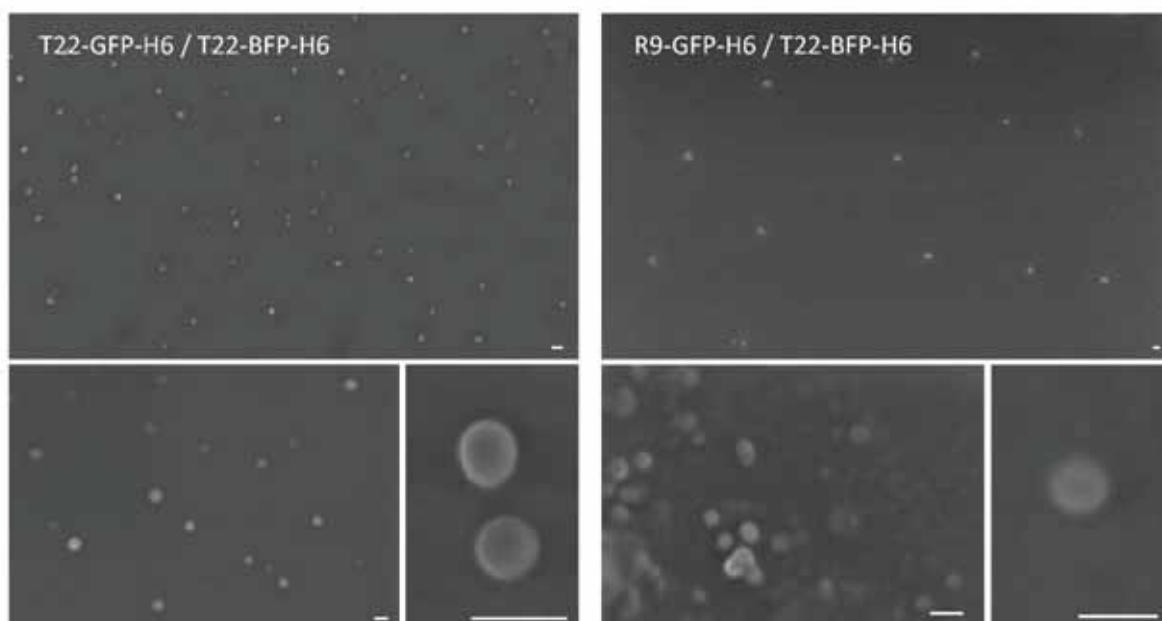


Figure 4. Morphometric analysis of hybrid nanoparticles. FESEM determinations of T22-BFP-H6/T22-GFP-H6 and R9-GFP-H6/T22-BFP-H6 materials, at increasing levels of magnification. White bars indicate 20 nm.

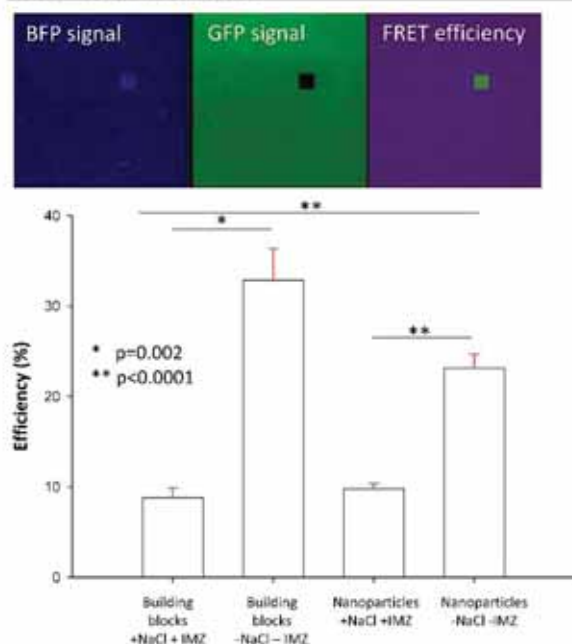


Figure 5. FRET analyses of T22-GFP-H6/T22-BFP-H6 particles and building blocks. Confocal images of T22-GFP-H6/T22-BFP-H6 after photobleaching of GFP molecules showing an increase in fluorescence intensity of donor BFP in the rectangle area, also evident by pseudocolor FRET image (top). Average FRET efficiency of different conditions of building blocks and nanoparticles. Both mixed T22-GFP-H6 and T22-BFP-H6 building blocks and assembled T22-GFP-H6/T22-BFP-H6 nanoparticles were incubated either under low salt conditions in absence of imidazole, or in a high salt buffer in presence of imidazole (bottom).

Results

T22-GFP-H6, T22-BFP-H6 and R9-GFP-H6 fusion proteins were easily produced as full-length polypeptides in bacteria without signs of proteolysis (supplementary figure 1 is available online at stacks.iop.org/NANO/28/505102/mmedia). R9 and in particular T22, are potent ligands of the cell surface protein CXCR4 [21, 24, 25], both acting in the fusion proteins as oligomerization agents but also as cell surface cell ligands. Each of these polypeptides assemble as regular homomeric nanoparticles (figures 1(A)–(C)) because of the combination of cationic peptides and polyhistidines. Upon systemic injection, they show high structural stability, reaching target organs in absence of evident disassembling [17]. Such architectonic robustness was challenged *in vitro* under high salt content conditions (what promotes charge neutralization) or in presence of imidazole (competing for ligands of reactive histidine residues). None of these conditions alone, within the tested ranges, disassembled the oligomers (table 1). However, the combination of both high salt and imidazole disrupted all the materials into smaller building blocks, as realized by denaturing concentrations of SDS (table 1, figure 1(B)).

These data indicated that both architectonic tags (the cationic peptide and the H6 tail) probably have a combined role in nanoparticle formation. The contribution of each end-terminal segment in the material stability was further dissected by keeping constant one disassembling condition while increasing the strength of the secondary parameter. At 500 mM Na⁺, between 100 and 300 mM imidazole (the whole buffer composition slightly influencing the threshold) translated both T22-GFP-H6 and R9-GFP-H6 nanoparticles into single building blocks (table 1, figure 2(A)). On the other hand, at 300 mM imidazole, T22-GFP-H6 was disassembled by 350 mM Na⁺ while R9-GFP-H6 required up to 450 mM (figure 2(B)). Once the disassembling conditions were set, we wondered if hybrid nanoparticles formed by heterologous building blocks might be generated by mixing distinct disassembled materials and dialysing then against a physiological buffer to allow the formation of hybrid oligomers. In this context, we tested the combinations involving T22-GFP-H6 with T22-BFP-H6 (same targeting agent but different building block) and R9-GFP-H6 with T22-BFP-H6 (different targeting agent and building block), that should both allow observing FRET between green and blue fluorescence as an assessment of the hybrid materials being formed.

Reconstitution of nanoparticles was indeed successful, resulting in materials with defined DLS profiles and relatively low polydispersion (figure 3(A)). The intrinsic hybrid nature of the materials was demonstrated by the occurrence of FRET, which was immediately disrupted upon incubation in high salt buffer with imidazole (figure 3(B)). R9-GFP-H6/T22-BFP-H6 materials peaked at 22 nm as a monodisperse population of nanoparticles (figures 3, 4), while T22-GFP-H6/T22-BFP-H6 materials peaked at 10 nm, with a secondary peak at around 30 nm. The prevalence of the 10 nm oligomers was confirmed by FESEM (figure 4), that offered images similar to the parental materials. FRET appearance and disappearance upon disassembling was fully assessed for T22-GFP-H6/T22-BFP-H6, by acceptor photo-bleaching under confocal microscopy (figure 5).

The successful generation of hybrid nanoparticles prompted us to explore their ability to internalize target cells in a stable and specific way. For that, cultured CXCR4⁺ HeLa cells were exposed to T22-GFP-H6/T22-BFP-H6 and R9-GFP-H6/T22-BFP-H6 nanoparticles and investigated for internalization. As observed (figure 6(A)), both materials penetrated HeLa cells after 24 h of exposure. In addition, their uptake was inhibited by the specific chemical ligand of CXCR4, AMD3100 (figure 6(B)). AMD3100-mediated inhibitory effect was observed to be milder in the case of particles containing R9, that acts as both CXCR4 ligand [24] but also as a potent cell penetrating peptide [26,27, 28]. Probably, both internalization mechanisms (CXCR4-dependent and CXCR4-independent) were active in the case of R9-GFP-H6/T22-BFP-H6, while penetration appeared as exclusively CXCR4-dependent in the case of T22-GFP-H6/T22-BFP-H6. The intracellular localization of T22-GFP-H6/T22-BFP-H6 hybrid materials (revealed by the co-localization of blue and green signals in confocal reconstructions) was revealed to be perinuclear (figures 6(C), (D)). This is the same

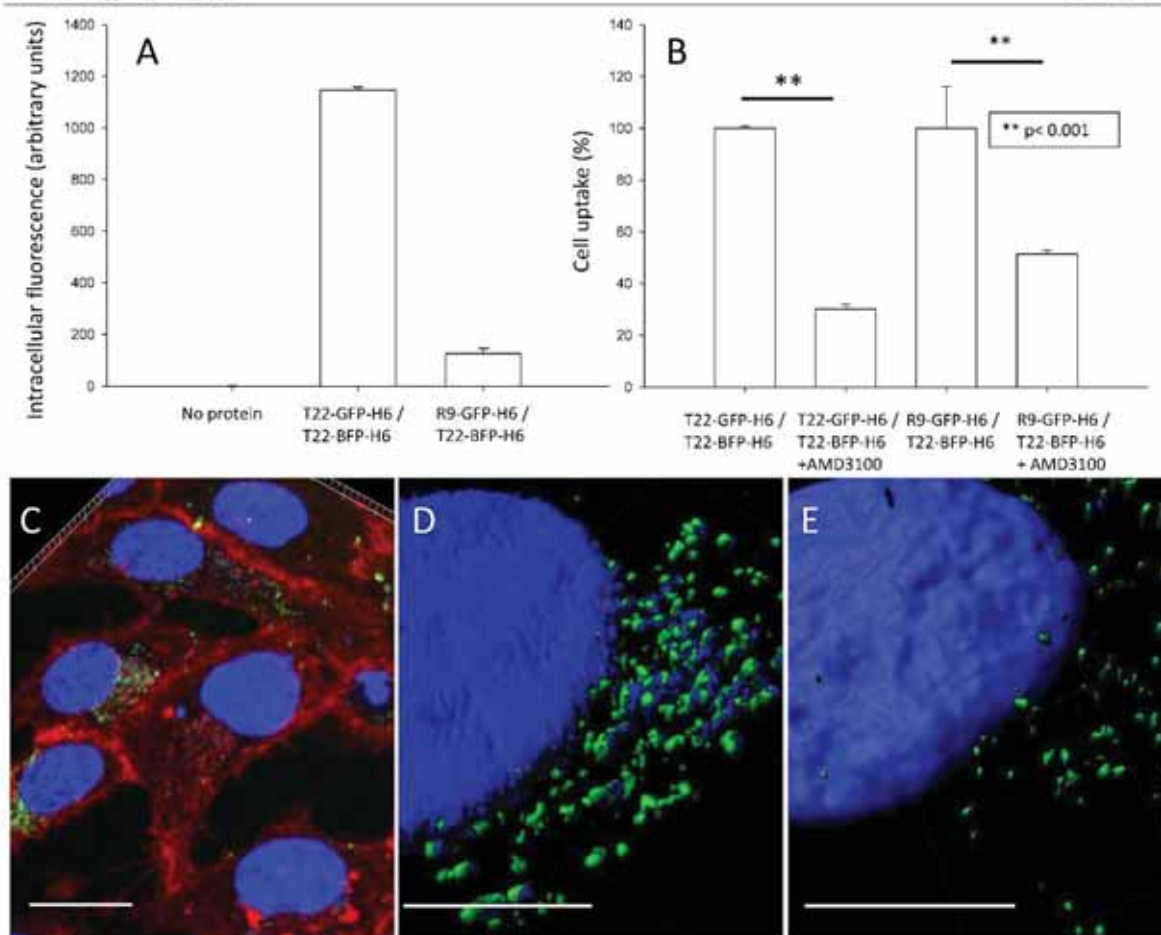


Figure 6. Cell internalization of hybrid nanoparticles. (A) Uptake of hybrid nanoparticles (1 μM) in CXCR4⁺ HeLa cells upon exposure for 24 h. (B). AMD3100-mediated inhibition of cell internalization. (C) Confocal imaging of cultured CXCR4⁺ HeLa cells exposed to T22-GFP-H6/T22-BFP-H6 nanoparticles during 24 h. Blue and green fluorescence of the materials are apparent. Membranes are stained in red and nuclear DNA in blue. The bar indicates 20 μm . (D) Z axis stack and 3D reconstruction of internalized T22-GFP-H6/T22-BFP-H6 nanoparticles, probably clustered in endosomes, showing mutual embedment of blue and green fluorescence. The bar indicates 10 μm . (E) Z axis stack and 3D reconstruction of control, internalized T22-GFP-H6 nanoparticles, showing only green fluorescent signal. The bar indicates 10 μm .

location reached by homogeneous, green fluorescent T22-GFP-H6 constructs [16] (figure 6(E)).

Discussion

We have demonstrated here the possibility to disassemble toroid protein nanoparticles formed by modular proteins that cross-interact through cationic and histidine-rich end terminal peptides (figure 1). These materials fall within the category of cyclic assemblies, that allow the multivalent display of peptide motives in highly symmetric lattices [15]. Importantly, this configuration is highly convenient for cell-targeted vehicles for drug delivery [18], since it empowers the constructs to act as viral mimetics regarding their interaction with target cells. The disruption of the homomeric materials was fully reversible upon dialysis against physiological buffers,

proving that the disassembling buffer breaks specific cross-protein interactions without affecting the global conformation of the building block. The exclusive impact of high salt combined with imidazole proves that nanoparticles based on cationic peptides and polyhistidines might result from synergies between both type of tags, accounting for the high *in vivo* stability of these materials [17]. Controlling the disassembling and reassembling in this platform has allowed the *in vitro* generation of heteromeric nanoparticles (figures 3, 4) that keep the cell targeting properties mediated by the end terminal cationic ligand of CXCR4 (T22, figure 6), a cell-surface receptor linked to several aggressive human cancers [29, 30]. However, these targeting activities might result combined with the cell penetration properties of an additional cell ligand (R9) incorporated in the heteromeric particles. The robustness of the materials formed by heterogeneous building blocks proves the possibility to incorporate diverse biological

activities into multifunctional vehicles, illustrated here by the blue and green fluorescence emission. In addition, it also proves the possibility to integrate different cell ligands with targeted or non-targeted cell penetrating peptides (supplementary figure 2, illustrated here by the simultaneous display of T22 and R9), what represents a promising strategy in the development of smart and biocompatible materials in nanomedicine. Among other applications, the potential for a controlled combination of distinct cell-ligands fits with the increasing interest in the design of bispecific or biparatopic vehicles for drug delivery [31–34]. This dual target strategy, still in early conceptual stages, might dramatically improve the specificity and efficacy of drug delivery in therapeutic fields such as cancer and inflammation. In a related context, cell-targeted protein-only building blocks with intrinsic therapeutic activities have been recently developed, formed by antimicrobial peptides [35] or by pro-apoptotic peptides [36] in addition to fluorescent proteins. These self-assembling protein drugs, reaching a nanoscale organization, exploit the emerging concept of vehicle-free nanoscale drugs [37]. The combination of different building blocks might allow the ratiometric administration of synergistically acting protein drugs or fluorescent probes, in a new approach to combined therapies or theragnosis (supplementary figure 2). Finally, the possibility to generate protein-only self-assembling nanoparticles in endotoxin-free microorganisms such as *Lactococcus lactis* [38] or endotoxin-free strains of *Escherichia coli* [39] prompts to envisage protein-based hybrid nanoparticles as flexible and promising tools for the generation of multifunctional agents for *in vivo* biomedical applications, such as drug delivery, imaging or theragnosis, fields that had been in the past dominated by the use of non-biological materials such as ceramics, metals and polymers [2].

Conclusions

We have here described a methodological approach to generate protein nanoparticles in the viral size range and formed by heterologous building blocks. The structural robustness of these materials proves the feasibility to recruit diverse biological activities into multifunctional vehicles, which would serve as an appealing approach to simultaneously deliver synergistically acting drugs, in a defined ratio, at the cell level. In addition, it also demonstrates the possibility to incorporate, in single nanoscale vehicles, different cell ligands to easily approach the emerging challenge in targeted drug delivery regarding the design of multiparatopic or multi-specific drugs.

Acknowledgments

We are indebted to AGAUR (2014SGR-132) and CIBER-BBN (project NANOPROTHER) granted to AV, Marató de TV3 foundation (TV32013-3930) and ISCIII (PI15/00272 co-founding FEDER) to EV and ISCIII (PI15/00378 and PIE15/00028, co-founding FEDER), Marató de TV3 foundation

(TV32013-2030) and AGAUR 2014-PROD0005 to RM. Protein production has been partially performed by the ICTS 'NANBIOSIS', more specifically by the Protein Production Platform of CIBER-BBN/ IBB (<http://nanbiosis.es/unit/u1-protein-production-platform-ppp/>). LSG was supported by AGAUR (2017FI_B100063), NS by a predoctoral fellowship from the Government of Navarra, UU received a Sara Borrell postdoctoral fellowship from ISCIII and AV an ICREA ACADEMIA award.

ORCID iDs

Antonio Villaverde  <https://orcid.org/0000-0002-2615-4521>

References

- [1] Kumar V A, Wang B K and Kanahara S M 2016 Rational design of fiber forming supramolecular structures *Exp. Biol. Med.* **241** 899–908
- [2] Webber M J, Appel E A, Meijer E W and Langer R 2016 Supramolecular biomaterials *Nat. Mater.* **15** 13–26
- [3] Corchero J L, Vazquez E, Garcia-Fruitos E, Ferrer-Miralles N and Villaverde A 2014 Recombinant protein materials for bioengineering and nanomedicine *Nanomedicine* **9** 2817–28
- [4] Ferrer-Miralles N, Rodriguez-Carmona E, Corchero J L, Garcia-Fruitos E, Vazquez E and Villaverde A 2015 Engineering protein self-assembling in protein-based nanomedicines for drug delivery and gene therapy *Crit. Rev. Biotechnol.* **35** 209–21
- [5] Yeates T O, Liu Y and Laniado J 2016 The design of symmetric protein nanomaterials comes of age in theory and practice *Curr. Opin. Struct. Biol.* **39** 134–43
- [6] Engel J and Kammerer R A 2000 What are oligomerization domains good for? *Matrix Biol.* **19** 283–8
- [7] Doll T A P F, Dey R and Burkhard P 2015 Design and optimization of peptide nanoparticles *J. Nanobiotechnol.* **13** 73
- [8] Li D *et al* 2014 Structure-based design of functional amyloid materials *J. Am. Chem. Soc.* **136** 18044–51
- [9] Lua L H, Connors N K, Sainsbury F, Chuan Y P, Wibowo N and Middelberg A P 2014 Bioengineering virus-like particles as vaccines *Biotechnol. Bioeng.* **111** 425–40
- [10] Molino N M and Wang S W 2014 Caged protein nanoparticles for drug delivery *Curr. Opin. Biotechnol.* **28** 75–82
- [11] Deng L *et al* 2017 Protein nanoparticle vaccine based on flagellin carrier fused to influenza conserved epitopes confers full protection against influenza A virus challenge *Virology* **509** 82–9
- [12] Benner N L *et al* 2017 Vault nanoparticles: chemical modifications for imaging and enhanced delivery *ACS Nano* **11** 872–81
- [13] Rueda F *et al* 2015 Bottom-up instructive quality control in the biofabrication of smart protein materials *Adv. Mater.* **27** 7816–22
- [14] Pesarrodona M *et al* 2017 Intrinsic functional and architectonic heterogeneity of tumor-targeted protein nanoparticles *Nanoscale* **9** 6427–35
- [15] Goodsell D S and Olson A J 2000 Structural symmetry and protein function *Annu. Rev. Biophys. Biomol. Struct.* **29** 105–53

- [16] Unzueta U *et al* 2012 Non-amyloidogenic peptide tags for the regulatable self-assembling of protein-only nanoparticles *Biomaterials* **33** 8714–22
- [17] Cespedes M V *et al* 2014 *In vivo* architectonic stability of fully *de novo* designed protein-only nanoparticles *ACS Nano* **8** 4166–76
- [18] Unzueta U, Cespedes M V, Vazquez E, Ferrer-Miralles N, Mangues R and Villaverde A 2015 Towards protein-based viral mimetics for cancer therapies *Trends Biotechnol.* **33** 253–8
- [19] Pesarrodonna M *et al* 2014 Intracellular targeting of CD44⁺ cells with self-assembling, protein only nanoparticles *Int. J. Pharm.* **473** 286–95
- [20] Cespedes M V *et al* 2016 Cancer-specific uptake of a liganded protein nanocarrier targeting aggressive CXCR4⁺ colorectal cancer models *Nanomed.: Nanotechnol., Biol., Med.* **12** 1987–96
- [21] Unzueta U *et al* 2012 Intracellular CXCR4(+) cell targeting with T22-empowered protein-only nanoparticles *Int. J. Nanomed.* **7** 4533–44
- [22] Chari R V 2016 Expanding the reach of antibody-drug conjugates *ACS Med. Chem. Lett.* **7** 974–6
- [23] Vazquez E *et al* 2010 Protein nanodisk assembling and intracellular trafficking powered by an arginine-rich (R9) peptide *Nanomedicine* **5** 259–68
- [24] Tanaka G *et al* 2012 CXCR4 stimulates macropinocytosis: implications for cellular uptake of arginine-rich cell-penetrating peptides and HIV *Chem. Biol.* **19** 1437–46
- [25] Unzueta U *et al* 2017 Engineering tumor cell targeting in nanoscale amyloid materials *Nanotechnology* **28** 015102
- [26] Alhakamy NA and Berckland CJ 2013 Polyarginine molecular weight determines transfection efficiency of calcium condensed complexes *Mol. Pharmaceutics* **10** 1940–8
- [27] Bilichak A, Luu J and Eudes F 2015 Intracellular delivery of fluorescent protein into viable wheat microspores using cationic peptides *Frontiers Plant Sci.* **6** 666
- [28] Liu B R, Lin M D, Chiang H J and Lee H J 2012 Arginine-rich cell-penetrating peptides deliver gene into living human cells *Gene* **505** 37–45
- [29] Balkwill F 2004 The significance of cancer cell expression of the chemokine receptor CXCR4 *Seminars Cancer Biol.* **14** 171–9
- [30] Kim J *et al* 2006 Chemokine receptor CXCR4 expression in patients with melanoma and colorectal cancer liver metastases and the association with disease outcome *Ann. Surg.* **244** 113–20
- [31] Vazquez-Lombardi R, Phan T G, Zimmermann C, Lowe D, Jermutus L and Christ D 2015 Challenges and opportunities for non-antibody scaffold drugs *Drug Discovery Today* **20** 1271–83
- [32] Kontermann R E 2012 Dual targeting strategies with bispecific antibodies *mAbs* **4** 182–97
- [33] Weidle U H, Kontermann R E and Brinkmann U 2014 Tumor-antigen-binding bispecific antibodies for cancer treatment *Seminars Oncol.* **41** 653–60
- [34] Kontermann R E and Brinkmann U 2015 Bispecific antibodies *Drug Discovery Today* **20** 838–47
- [35] Serna N *et al* 2017 Protein-only, antimicrobial peptide-containing recombinant nanoparticles with inherent built-in antibacterial activity *Acta Biomater.* **60** 256–63
- [36] Serna N *et al* 2017 Peptide-based nanostructured materials with intrinsic proapoptotic activities in CXCR4⁺ solid tumors *Adv. Funct. Mater.* **27** 1700919
- [37] Shen J, Wolfram J, Ferrari M and Shen H 2017 Taking the vehicle out of drug delivery *Mater. Today* **20** 95–7
- [38] Cano-Garrido O *et al* 2016 CXCR4(+) targeted protein nanoparticles produced in the food-grade bacterium *Lactococcus lactis* *Nanomedicine* **11** 2387–98
- [39] Rueda F *et al* 2016 Structural and functional features of self-assembling protein nanoparticles produced in endotoxin-free *Escherichia coli* *Microbial Cell Factories* **15** 59

Supporting Information: Engineering multifunctional protein nanoparticles by *in vitro* disassembling and reassembling of heterologous building blocks

Ugutx Unzueta ^{1,2}, Naroa Serna ^{2,3,4}, Laura Sánchez-García ^{2,3,4}, Mónica Roldán ⁵, Alejandro Sánchez-Chardi ⁶, Ramón Mangués ^{1,2}, Antonio Villaverde ^{2,3,4}*, Esther Vázquez ^{2,3,4}*

¹ Institut d'Investigacions Biomèdiques Sant Pau and Josep Carreras Research Institute, Hospital de la Santa Creu i Sant Pau, 08025 Barcelona, Spain.

² CIBER de Bioingeniería, Biomateriales y Nanomedicina (CIBER-BBN), Spain

³ Institut de Biotecnologia i de Biomedicina, Universitat Autònoma de Barcelona, Bellaterra, 08193 Barcelona, Spain

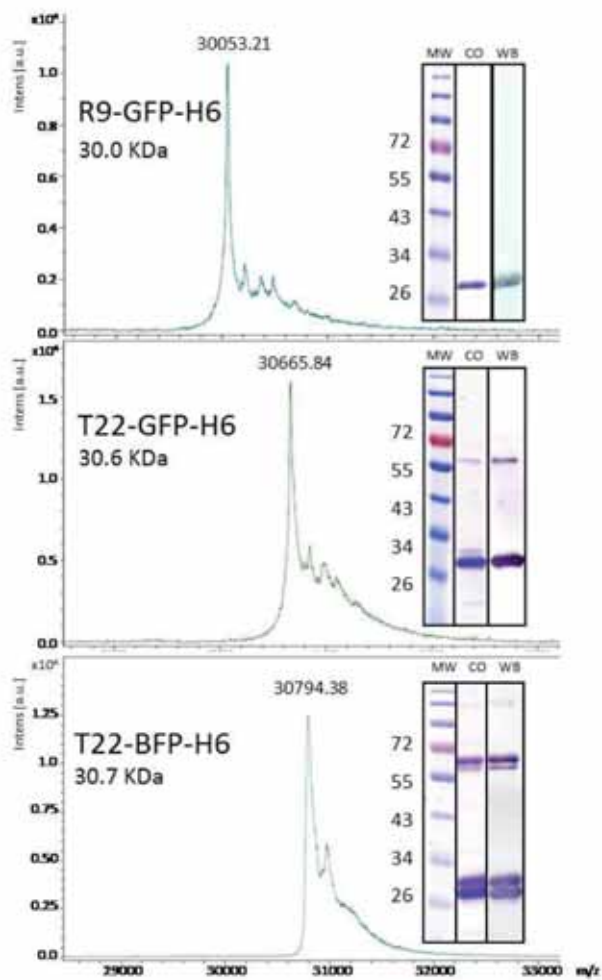
⁴ Departament de Genètica i de Microbiologia, Universitat Autònoma de Barcelona, Bellaterra, 08193 Barcelona, Spain

⁵ Unitat de Microscòpia Confocal. Servei d'Anatomia Patològica, Institut Pediàtric de Malalties Rares (IPER). Hospital Sant Joan de Déu, Universitat de Barcelona, Esplugues de Llobregat, 08950 Barcelona, Spain

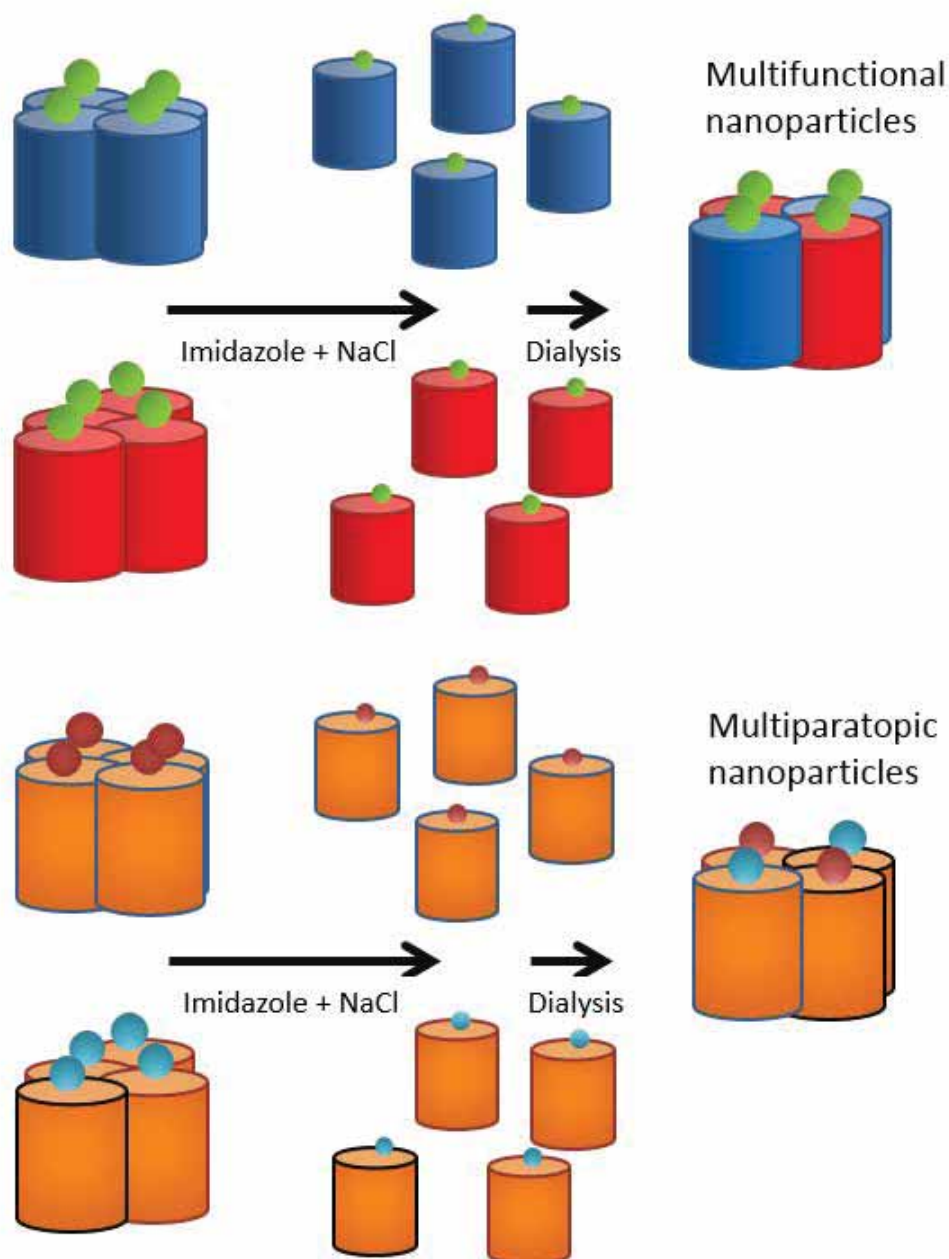
⁶ Servei de Microscòpia, Universitat Autònoma de Barcelona, Bellaterra, 08193 Barcelona, Spain

*Corresponding authors:

AV, Antoni.Villaverde@uab.es; EV, Esther.Vazquez@uab.es



Supplementary Figure 1. Characterization of recombinant R9-GFP-H6, T22-GFP-H6 and T22-BFP-H6 building blocks. MALDI-TOF analyses of recombinant proteins upon purification from bacterial cell extracts. Figures below protein names indicate the expected molecular masses. In the insets, Coomassie-blue staining (CO) and Western (WB) blot detection upon PAGE-SDS. The molecular mass (in KDa) of the most relevant molecular weight markers (MW) are indicated. Note the absence of proteolysis and the tendency to oligomerization of the proteins, especially those based on T22, that might also show isoforms related to sulphide bridge formation.



Supplementary Figure 2. Design of multifunctional and/or multiparatopic/multispecific protein nanoparticles. The procedures proposed here allow the controlled and reversible disassembly of homomeric protein nanoparticles produced in bacteria by recombinant DNA technologies. By mixing heteromeric building blocks during the reassembling process, hybrid nanoparticles with distinct building blocks (coloured cylinders) are generated. This can render multifunctional proteins provided these polypeptides exhibit different functionalities (such as cytotoxicity, enzymatic activities or fluorescence). On the other hand, multiparatopic or multispecific materials can also be produced by recruiting different peptidic ligands, binding to the same or to different cell surface receptors (coloured spheres). This is expected to increase the cell selectivity of the nanoparticles and the precision in the delivery process. Of course, both approaches are simultaneously possible, rendering more complex multifunctional and multiparatopic/multispecific materials. Precise models that account protein-protein interactions can be found elsewhere [13].

References

- [1] Kumar VA, Wang BK, Kanahara SM. Rational design of fiber forming supramolecular structures. *Exp Biol Med*. 2016;241:899-908.
- [2] Webber MJ, Appel EA, Meijer EW, Langer R. Supramolecular biomaterials. *Nature materials*. 2016;15:13-26.
- [3] Corchero JL, Vazquez E, Garcia-Fruitos E, Ferrer-Miralles N, Villaverde A. Recombinant protein materials for bioengineering and nanomedicine. *Nanomedicine*. 2014;9:2817-28.
- [4] Ferrer-Miralles N, Rodriguez-Carmona E, Corchero JL, Garcia-Fruitos E, Vazquez E, Villaverde A. Engineering protein self-assembling in protein-based nanomedicines for drug delivery and gene therapy. *Critical reviews in biotechnology*. 2015;35:209-21.
- [5] Yeates TO, Liu Y, Laniado J. The design of symmetric protein nanomaterials comes of age in theory and practice. *Current opinion in structural biology*. 2016;39:134-43.
- [6] Engel J, Kammerer RA. What are oligomerization domains good for? *Matrix Biol*. 2000;19:283-8.
- [7] Doll TAPF, Dey R, Burkhard P. Design and optimization of peptide nanoparticles. *J Nanobiotechnol*. 2015;13.
- [8] Li D, Jones EM, Sawaya MR, Furukawa H, Luo F, Ivanova M, et al. Structure-Based Design of Functional Amyloid Materials. *Journal of the American Chemical Society*. 2014;136:18044-51.
- [9] Lua LH, Connors NK, Sainsbury F, Chuan YP, Wibowo N, Middelberg AP. Bioengineering virus-like particles as vaccines. *Biotechnology and bioengineering*. 2014;111:425-40.
- [10] Molino NM, Wang SW. Caged protein nanoparticles for drug delivery. *Current opinion in biotechnology*. 2014;28:75-82.
- [11] Deng L, Kim JR, Chang TZ, Zhang H, Mohan T, Champion JA, et al. Protein nanoparticle vaccine based on flagellin carrier fused to influenza conserved epitopes confers full protection against influenza A virus challenge. *Virology*. 2017;509:82-9.
- [12] Benner NL, Zang X, Buehler DC, Kickhoefer VA, Rome ME, Rome LH, et al. Vault Nanoparticles: Chemical Modifications for Imaging and Enhanced Delivery. *ACS nano*. 2017;11:872-81.
- [13] Rueda F, Cespedes MV, Conchillo-Sole O, Sanchez-Chardi A, Seras-Franzoso J, Cubarsi R, et al. Bottom-Up Instructive Quality Control in the Biofabrication of Smart Protein Materials. *Advanced materials*. 2015;27:7816-22.
- [14] Pesarrodonna M, Crosas E, Cubarsi R, Sanchez-Chardi A, Saccardo P, Unzueta U, et al. Intrinsic functional and architectonic heterogeneity of tumor-targeted protein nanoparticles. *Nanoscale*. 2017;9:6427-35.
- [15] Goodsell DS, Olson AJ. Structural symmetry and protein function. *Annual review of biophysics and biomolecular structure*. 2000;29:105-53.
- [16] Unzueta U, Ferrer-Miralles N, Cedano J, Zikung X, Pesarrodonna M, Saccardo P, et al. Non-amyloidogenic peptide tags for the regulatable self-assembling of protein-only nanoparticles. *Biomaterials*. 2012;33:8714-22.
- [17] Cespedes MV, Unzueta U, Tatkiewicz W, Sanchez-Chardi A, Conchillo-Sole O, Alamo P, et al. In vivo architectonic stability of fully de novo designed protein-only nanoparticles. *ACS nano*. 2014;8:4166-76.
- [18] Unzueta U, Cespedes MV, Vazquez E, Ferrer-Miralles N, Mangues R, Villaverde A. Towards protein-based viral mimetics for cancer therapies. *Trends in biotechnology*. 2015;33:253-8.
- [19] Pesarrodonna M, Ferrer-Miralles N, Unzueta U, Gener P, Tatkiewicz W, Abasolo I, et al. Intracellular targeting of CD44+ cells with self-assembling, protein only nanoparticles. *International journal of pharmaceutics*. 2014;473:286-95.
- [20] Cespedes MV, Unzueta U, Alamo P, Gallardo A, Sala R, Casanova I, et al. Cancer-specific uptake of a liganded protein nanocarrier targeting aggressive CXCR4+ colorectal cancer models. *Nanomedicine : nanotechnology, biology, and medicine*. 2016;12:1987-96.

- [21] Unzueta U, Cespedes MV, Ferrer-Miralles N, Casanova I, Cedano J, Corchero JL, et al. Intracellular CXCR4(+) cell targeting with T22-empowered protein-only nanoparticles. *International journal of nanomedicine*. 2012;7:4533-44.
- [22] Chari RV. Expanding the Reach of Antibody-Drug Conjugates. *ACS medicinal chemistry letters*. 2016;7:974-6.
- [23] Vazquez E, Roldan M, Díez-Gil C, Unzueta U, Domingo-Espin J, Cedano J, et al. Protein nanodisk assembling and intracellular trafficking powered by an arginine-rich (R9) peptide. *Nanomedicine*. 2010;5:259-68.
- [24] Tanaka G, Nakase I, Fukuda Y, Masuda R, Oishi S, Shimura K, et al. CXCR4 stimulates macropinocytosis: implications for cellular uptake of arginine-rich cell-penetrating peptides and HIV. *Chemistry & biology*. 2012;19:1437-46.
- [25] Unzueta U, Seras-Franzoso J, Cespedes MV, Saccardo P, Cortes F, Rueda F, et al. Engineering tumor cell targeting in nanoscale amyloid materials. *Nanotechnology*. 2017;28:015102.
- [26] Ugutz Unzueta JS-F, María Virtudes Céspedes, Paolo Saccardo, Francisco Cortes, Fabian Rueda, Elena García-Fruitós, Neus Ferrer-Miralles, Ramon Mangues, Esther Vazquez, Antonio Villaverde. . Engineering tumor cell targeting in nanoscale amyloid materials. *Nanotechnology*. 2016;in press.
- [27] Bilichak A, Luu J, Eudes F. Intracellular delivery of fluorescent protein into viable wheat microspores using cationic peptides. *Frontiers in plant science*. 2015;6:666.
- [28] Liu BR, Lin MD, Chiang HJ, Lee HJ. Arginine-rich cell-penetrating peptides deliver gene into living human cells. *Gene*. 2012;505:37-45.
- [29] Balkwill F. The significance of cancer cell expression of the chemokine receptor CXCR4. *Seminars in cancer biology*. 2004;14:171-9.
- [30] Kim J, Mori T, Chen SL, Amersi FF, Martinez SR, Kuo C, et al. Chemokine receptor CXCR4 expression in patients with melanoma and colorectal cancer liver metastases and the association with disease outcome. *Annals of surgery*. 2006;244:113-20.
- [31] Vazquez-Lombardi R, Phan TG, Zimmermann C, Lowe D, Jeremias L, Christ D. Challenges and opportunities for non-antibody scaffold drugs. *Drug discovery today*. 2015;20:1271-83.
- [32] Kontermann RE. Dual targeting strategies with bispecific antibodies. *mAbs*. 2012;4:182-97.
- [33] Weidle UH, Kontermann RE, Brinkmann U. Tumor-antigen-binding bispecific antibodies for cancer treatment. *Seminars in oncology*. 2014;41:653-60.
- [34] Kontermann RE, Brinkmann U. Bispecific antibodies. *Drug discovery today*. 2015;20:838-47.
- [35] Serna N, Sanchez-García L, Sanchez-Chardi A, Unzueta U, Roldan M, Mangues R, et al. Protein-only, antimicrobial peptide-containing recombinant nanoparticles with inherent built-in antibacterial activity. *Acta biomaterialia*. 2017;60:256-63.
- [36] Naroa Serna MVC, Laura Sánchez-García, Ugutz Unzueta, Rita Sala, Alejandro Sánchez-Chardi, Francisco Cortés, Neus Ferrer-Miralles, Ramón Mangues, Esther Vázquez and Antonio Villaverde. Peptide-Based Nanostructured Materials with Intrinsic Proapoptotic Activities in CXCR4+ Solid Tumors. *Advanced Functional Materials*. 2017.
- [37] Shen J, Wolfram J, Ferrari M, Shen H. Taking the vehicle out of drug delivery. *Materials today*. 2017;20:95-7.
- [38] Cano-Garrido O, Cespedes MV, Unzueta U, Saccardo P, Roldan M, Sanchez-Chardi A, et al. CXCR4(+)-targeted protein nanoparticles produced in the food-grade bacterium *Lactococcus lactis*. *Nanomedicine*. 2016;11:2387-98.
- [39] Rueda F, Cespedes MV, Sanchez-Chardi A, Seras-Franzoso J, Pesarrodonna M, Ferrer-Miralles N, et al. Structural and functional features of self-assembling protein nanoparticles produced in endotoxin-free *Escherichia coli*. *Microbial cell factories*. 2016;15:59.

ANNEX 6: OTHER PUBLICATIONS

1. Pesarrodonna M, Crosas E, Cubarsi R, Sánchez-Chardi A, Saccardo P, Unzueta U, Rueda F, Sanchez-García L, Serna N, Mangues R, Ferrer-Miralles N, Vázquez E, Villaverde A. Intrinsic functional and architectonic heterogeneity of tumor-targeted protein nanoparticles. *Nanoscale*. **2017**, *9*(19), 6427-6435.
2. Serna N, Sánchez-García L, Sánchez-Chardi A, Unzueta U, Roldán M, Mangues R, Vázquez E, Villaverde A. Protein-only, antimicrobial peptide-containing recombinant nanoparticles with inherent built-in antibacterial activity. *Acta Biomater*. **2017**, *60*, 256-263.
3. de Pinho Favaro MT, Sánchez-García L, Sánchez-Chardi A, Roldán M, Unzueta U, Serna N, Cano-Garrido O, Azzoni AR, Ferrer-Miralles N, Villaverde A, Vázquez E. Protein nanoparticles are nontoxic, tuneable cell stressors. *Nanomedicine (Lond)*. **2018**, *13*(3), 255-268.
4. Unzueta U, Cespedes MV, Sala R, Alamo P, Sánchez-Chardi A, Pesarrodonna M, Sánchez-García L, Cano-Garrido O, Villaverde A, Vázquez E, Mangues R, Seras-Franzoso J. Release of targeted protein nanoparticles from functional bacterial amyloids: A death star-like approach. *J. Control Release*. **2018**, *279*, 29-39.
5. Favaro MTP, Serna N, Sánchez-García L, Cubarsi R, Roldán M, Sánchez-Chardi A, Unzueta U, Mangues R, Ferrer-Miralles N, Azzoni AR, Vázquez E, Villaverde A. Switching cell penetrating and CXCR4-binding activities of nanoscale-organized arginine-rich peptides. *Nanomedicine*. **2018**, *14*(6), 777-1786.
6. Serna N, Sanchez JM, Unzueta U, Sánchez-García L, Sánchez-Chardi A, Mangues R, Vázquez E, Villaverde A. Recruiting potent membrane penetrability in tumor cell-targeted protein-only nanoparticles. *Nanotechnology*. **2018**. Available online.
7. López-Laguna H, Unzueta U, Conchillo-Solé O, Sánchez-Chardi A, Pesarrodonna M, Cano-Garrido O, Voltà E, Sánchez-García L, Serna N, Saccardo P, Mangues R, Villaverde A, Vázquez E. Assembly of histidine-rich protein materials controlled through divalent cations. *Acta Biomater*. **2019**, *83*, 257-264.
8. Díaz R, Sánchez-García L, Serna N, Sánchez-Chardi A, Cano-Garrido O, Sánchez JM, Unzueta U, Vazquez E, Villaverde A. Engineering a recombinant chlorotoxin as cell-targeted cytotoxic nanoparticles. *Sci. China Mater*. **2019**. Available online.

ANNEX 7: EUROPEAN PATENT

NANOSTRUCTURED PROTEINS AND USES THEREOF

FIELD OF THE INVENTION

The present invention relates to the field of nanostructured protein materials, more specifically to fusion proteins which can be used for therapy.

BACKGROUND OF THE INVENTION

The systemic administration of drugs in form of nanoconjugates benefits from enhanced drug stability when compared to free molecules. Valuable additional properties such as cell targeting might be also merged into a given hybrid composite through the chemical incorporation of functional groups in nanoscale vehicles, taking profit from the high surface/volume ratio of nanomaterials. When administered systemically, the resulting drug loaded conjugates sizing between ~8 and 100 nm escape from renal filtration in absence of aggregation in lung or other highly vascularized organs. This fact, combined with appropriate physicochemical properties of the material might result in extended circulation time and prolonged drug exposure to target organs, thus enhancing the therapeutic impact and benefits for the patient.

Among the diversity of materials under investigation as drug carriers, that includes metals, ceramics, polymers and carbon nanotubes, proteins offer unique properties regarding biocompatibility and degradability that, in the context of rising nanotoxicological concerns, make them especially appealing.

However, many protein species are themselves, efficient drugs usable in human therapy, as attested by more than 400 protein-based products approved by main medicines agencies. Therefore, the engineering of protein drugs as self-organizing building blocks, that exhibit intrinsic therapeutic activities upon self-assembling as nanoparticles, constitutes an advantageous concept. Thus, this methodology excludes the need of further activation and drug conjugation, as the nanomaterial itself acts as a nanoscale

drug (desirably between 8 and 100 nm). In that way, chemically homogenous protein nanoparticles, showing intrinsic therapeutic activities (like the current plain protein species used in human medicine -e.g, hormones, growth factors, vaccines etc.) can be biologically produced in a single step (as nanoscale assembled entities). Since the material itself acts as a drug, the possibility of drug leakage during circulation, an undesired possibility especially worrying in the case of cytotoxic agents, can be completely abolished, which becomes a significant advantage with respect to the state of the art.

The inventors previously probed into the field by applying a nanoarchitectonic principle based on the addition, to a core protein, of a cationic N-terminal domain plus a C-terminal poly-histidine. [Serna, N. et al. 2016. *Nanomedicine*, 12:1241-51]. It has been described in the art that these end-terminal tags and the resulting charge balance in the whole fusion promote self-assembling and oligomerization of monomeric proteins as robust toroid nanoparticles, stable in plasma [Cespedes, M. V. et al. 2014. *ACS Nano.*, 8:4166-4176] and with high cellular penetrability if empowered with cell-targeting peptides. [Xu, Z. K. et al. 2015. *Materials Letters*, 154:140-3] Nonetheless, the building blocks of these protein structures might also contain functional peptides such as cell-targeting agents, endosomolytic agents or nuclear localization signals, in form of fused stretches with modular organization.

Therefore, to take advantage of such easy protein engineering will be highly beneficial, since a need persists in the art for drug delivery systems with enhanced selectivity and biodisponibility.

SUMMARY OF THE INVENTION

In a first aspect, the invention relates to a fusion protein comprising

- (i) a polycationic peptide,
- (ii) an intervening polypeptide region and
- (iii) a positively charged amino acid-rich region,

wherein the intervening polypeptide region is not a fluorescent protein alone or human p53.

In a second aspect, the invention relates to a method to prepare nanoparticles comprising multiple copies of the fusion protein according to the first aspect of the invention comprising placing a preparation of said fusion protein in a low salt buffer.

In further aspects, the invention relates to a polynucleotide encoding a fusion protein according to the first aspect of the invention, a vector comprising said polynucleotide, and a host cell comprising either said polynucleotide or said vector.

In an additional aspect, the invention relates to a nanoparticle comprising multiple copies of the fusion protein of the invention or a nanoparticle which has been obtained by the method of the invention to prepare nanoparticles.

In yet another additional aspect, the invention relates to a fusion protein, a polynucleotide, a vector, a host cell or a nanoparticle according to the invention for use in medicine.



Acknowledgement of receipt

We hereby acknowledge receipt of your request for grant of a European patent as follows:

Submission number	5255596	
Application number	EP17169722.0	
File No. to be used for priority declarations	EP17169722	
Date of receipt	05 May 2017	
Your reference	T-2017-018EP2	
Applicant	UNIVERSITAT AUTONOMA DE BARCELONA	
Country	ES	
Title	NANOSTRUCTURED PROTEINS AND USES THEREOF	
Documents submitted	package-data.xml application-body.xml OLF-ARCHIVE.zip\Functionalized cellulose fabrics_UAB_Final version.zip SPECEPO-2.pdf\T-2017-018EP Claims.pdf (5 p.) SPECEPO-4.pdf\T-2017-018EP Figs.pdf (17 p.) f1002-1.pdf (2 p.)	ep-request.xml ep-request.pdf (5 p.) SPECEPO-1.pdf\T-2017-018EP Description.pdf (65 p.) SPECEPO-3.pdf\T-2017-018EP Abstract.pdf (1 p.) SEQLTXT.txt\Sequence Listing - T-2017-018.txt
Submitted by	CN=Xavier Vallvé Sanchez 24825	
Method of submission	Online	

Date and time
receipt generated

05 May 2017, 13:58 (CEST)

Message Digest

B7:88:E5:60:51:F6:E3:7C:B3:60:DB:11:1B:D1:1D:08:AB:BB:BC:95

Correction by the EPO of errors in debit instructions filed by eOLF

Errors in debit instructions filed by eOLF that are caused by the editing of Form 1038E entries or the continued use of outdated software (all forms) may be corrected automatically by the EPO, leaving the payment date unchanged (see decision T 152/82, OJ EPO 1984, 301 and point 6.3 ff ADA, Supplement to OJ EPO 10/2007).

/European Patent Office/

Form 1002 - 1: Public inventor(s)

Designation of inventor

User reference: T-2017-018EP2
 Application No:

Public

	<p>Inventor</p> <p>The applicant has acquired the right to the European patent:</p>	<p>Name: VILLAVERDE CORRALES, Mr. ANTONIO Company: UAB Department: IBB Address: IBB Campus de la UAB s/n 08193 Cerdanyola del Vallès Spain</p> <p>As employer</p>
	<p>Inventor</p> <p>The applicant has acquired the right to the European patent:</p>	<p>Name: VÁZQUEZ GÓMEZ, Ms. ESTHER Company: UAB Department: IBB Address: Campus de la UAB s/n 08193 Cerdanyola del Vallès Spain</p> <p>As employer</p>
	<p>Inventor</p> <p>The applicant has acquired the right to the European patent:</p>	<p>Name: Serna Romero, Ms. Naroa Company: Universitat Autònoma de Barcelona Department: IBB Address: IBB Campus de la UAB s/n 08193 Cerdanyola del Vallès Spain</p> <p>As employer</p>
	<p>Inventor</p> <p>The applicant has acquired the right to the European patent:</p>	<p>Name: Sánchez García, Ms. Laura Company: Universitat Autònoma de Barcelona Department: IBB Address: IBB Campus de la UAB s/n 08193 Cerdanyola del Vallès Spain</p> <p>As employer</p>

User reference: T-2017-018EP2
 Application No:

Inventor	Name: Company: Address:	UNZUETA ELORZA, Mr. UGUTZ Hospital de la Santa Creu i Sant Pau Antoni M ^a Claret, 167 08025 Barcelona Spain
The applicant has acquired the right to the European patent:		As employer
Inventor	Name: Company: Address:	MANGUES BAFALLUY, Mr. RAMON Hospital de la Santa Creu i Sant Pau Antoni M ^a Claret, 167 08025 Barcelona Spain
The applicant has acquired the right to the European patent:		As employer
Inventor	Name: Company: Address:	CÉSPEDES NAVARRO, Ms. MARÍA VIRTUDES Hospital de la Santa Creu i Sant Pau Antoni M ^a Claret, 167 08025 Barcelona Spain
The applicant has acquired the right to the European patent:		As employer
Inventor	Name: Company: Address:	CASANOVA RIGAT, Ms. ISOLDA Centro de Investigación Biomédica en Red c/ Monforte de Lemos, 5 08025 Barcelona Spain
The applicant has acquired the right to the European patent:		As employer

Signature(s)

Place: Bellaterra
 Date: 05 May 2017
 Signed by: /Armando Sanchez Bonastre/
 Capacity: (Applicant: UNIVERSITAT AUTONOMA DE BARCELONA)
 Function of person signing: Vicerector for Research and Technology Transfer

The image features a large purple 3D cube on the right and a smaller orange 3D cube on the left. The word "REFERENCES" is written in a bold, dark blue font with a white outline, positioned between the two cubes.

REFERENCES

REFERENCES

1. World Health Organization: <http://www.who.int>
2. Global Cancer Observatory: <http://gco.iarc.fr>
3. National Cancer Institute: <https://www.cancer.gov>
4. Xu, X.; Ho, W.; Zhang, X.; Bertrand, N.; Farokhzad, O. Cancer nanomedicine: from targeted delivery to combination therapy. *Trends Mol. Med.* **2015**, *21* (4), 223-232.
5. Senapati, S.; Mahanta, A. K.; Kumar, S.; Maiti, P. Controlled drug delivery vehicles for cancer treatment and their performance. *Signal. Transduct. Target Ther.* **2018**, *3*, 7.
6. Bobo, D.; Robinson, K. J.; Islam, J.; Thurecht, K. J.; Corrie, S. R. Nanoparticle-Based Medicines: A Review of FDA-Approved Materials and Clinical Trials to Date. *Pharm. Res.* **2016**, *33* (10), 2373-2387.
7. Wang, A. Z.; Langer, R.; Farokhzad, O. C. Nanoparticle delivery of cancer drugs. *Annu. Rev. Med.* **2012**, *63*, 185-198.
8. Rodriguez-Carmona, E.; Villaverde, A. Nanostructured bacterial materials for innovative medicines. *Trends Microbiol.* **2010**, *18* (9), 423-430.
9. Sanvicens, N.; Marco, M. P. Multifunctional nanoparticles-properties and prospects for their use in human medicine. *Trends Biotechnol.* **2008**, *26* (8), 425-433.
10. Park, K. Controlled drug delivery systems: past forward and future back. *J. Control Release* **2014**, *190*, 3-8.
11. Ngandeu Neubi, G. M.; Opoku-Damoah, Y.; Gu, X.; Han, Y.; Zhou, J.; Ding, Y. Bio-inspired drug delivery systems: an emerging platform for targeted cancer therapy. *Biomater. Sci.* **2018**, *6* (5), 958-973.
12. Stylianopoulos, T. EPR-effect: utilizing size-dependent nanoparticle delivery to solid tumors. *Ther. Deliv.* **2013**, *4* (4), 421-423.
13. Ma, N.; Ma, C.; Li, C.; Wang, T.; Tang, Y.; Wang, H.; Moul, X.; Chen, Z.; Hel, N. Influence of nanoparticle shape, size, and surface functionalization on cellular uptake. *J. Nanosci. Nanotechnol.* **2013**, *13* (10), 6485-6498.

REFERENCES

14. Jiang, Y.; Huo, S.; Mizuhara, T.; Das, R.; Lee, Y. W.; Hou, S.; Moyano, D. F.; Duncan, B.; Liang, X. J.; Rotello, V. M. The Interplay of Size and Surface Functionality on the Cellular Uptake of Sub-10 nm Gold Nanoparticles. *ACS Nano*. **2015**, *9*(10), 9986-9993.
15. Guo, P.; Liu, D.; Subramanyam, K.; Wang, B.; Yang, J.; Huang, J.; Auguste, D. T.; Moses, M. A. Nanoparticle elasticity directs tumor uptake. *Nat. Commun.* **2018**, *9*(1), 130.
16. Dreaden, E. C.; Austin, L. A.; Mackey, M. A.; El-Sayed, M. A. Size matters: gold nanoparticles in targeted cancer drug delivery. *Ther. Deliv.* **2012**, *3*(4), 457-478.
17. Chou, L. Y.; Ming, K.; Chan, W. C. Strategies for the intracellular delivery of nanoparticles. *Chem. Soc. Rev.* **2011**, *40*(1), 233-245.
18. Toy, R.; Peiris, P. M.; Ghaghada, K. B.; Karathanasis, E. Shaping cancer nanomedicine: the effect of particle shape on the in vivo journey of nanoparticles. *Nanomedicine. (Lond)* **2014**, *9*(1), 121-134.
19. Blanco, E.; Shen, H.; Ferrari, M. Principles of nanoparticle design for overcoming biological barriers to drug delivery. *Nat. Biotechnol.* **2015**, *33*(9), 941-951.
20. Jiang, W.; Kim, B. Y.; Rutka, J. T.; Chan, W. C. Nanoparticle-mediated cellular response is size-dependent. *Nat. Nanotechnol.* **2008**, *3*(3), 145-150.
21. Albanese, A.; Tang, P. S.; Chan, W. C. The effect of nanoparticle size, shape, and surface chemistry on biological systems. *Annu. Rev. Biomed. Eng* **2012**, *14*, 1-16.
22. Yuan, Y. Y.; Mao, C. Q.; Du, X. J.; Du, J. Z.; Wang, F.; Wang, J. Surface charge switchable nanoparticles based on zwitterionic polymer for enhanced drug delivery to tumor. *Adv. Mater.* **2012**, *24*(40), 5476-5480.
23. Zhang, Y. R.; Lin, R.; Li, H. J.; He, W. L.; Du, J. Z.; Wang, J. Strategies to improve tumor penetration of nanomedicines through nanoparticle design. *WIREs Nanomed. Nanobi.* **2019**, *11*(1), e1519.
24. Sharma, A.; Madhunapantula, S. V.; Robertson, G. P. Toxicological considerations when creating nanoparticle-based drugs and drug delivery systems. *Expert. Opin. Drug Met.* **2012**, *8*(1), 47-69.
25. Naqvi, S.; Samim, M.; Abdin, M.; Ahmed, F. J.; Maitra, A.; Prashant, C.; Dinda, A. K. Concentration-dependent toxicity of iron oxide nanoparticles mediated by increased oxidative stress. *Int. J. Nanomedicine.* **2010**, *5*, 983-989.
26. Park, E. J.; Choi, J.; Park, Y. K.; Park, K. Oxidative stress induced by cerium oxide nanoparticles in cultured BEAS-2B cells. *Toxicology* **2008**, *245*(1), 90-100.

27. Knudsen, K. B.; Northeved, H.; Kumar, P. E.; Permin, A.; Gjetting, T.; Andresen, T. L.; Larsen, S.; Wegener, K. M.; Lykkesfeldt, J.; Jantzen, K.; Loft, S.; Moller, P.; Roursgaard, M. In vivo toxicity of cationic micelles and liposomes. *Nanomedicine*. **2015**, *11* (2), 467-477.
28. Rosenblum, D.; Joshi, N.; Tao, W.; Karp, J. M.; Peer, D. Progress and challenges towards targeted delivery of cancer therapeutics. *Nat. Commun.* **2018**, *9* (1), 1410.
29. Hossen, S.; Hossain, M. K.; Basher, M. K.; Mia, M. N. H.; Rahman, M. T.; Uddin, M. J. Smart nanocarrier-based drug delivery systems for cancer therapy and toxicity studies: A review. *J. Adv. Res.* **2019**, *15*, 1-18.
30. Torchilin, V. P. Multifunctional, stimuli-sensitive nanoparticulate systems for drug delivery. *Nat. Rev. Drug Discov.* **2014**, *13* (11), 813-827.
31. Etheridge, M. L.; Campbell, S. A.; Erdman, A. G.; Haynes, C. L.; Wolf, S. M.; McCullough, J. The big picture on nanomedicine: the state of investigational and approved nanomedicine products. *Nanomedicine*. **2013**, *9*(1), 1-14.
32. Ragelle, H.; Danhier, F.; Preat, V.; Langer, R.; Anderson, D. G. Nanoparticle-based drug delivery systems: a commercial and regulatory outlook as the field matures. *Expert. Opin. Drug Deliv.* **2017**, *14* (7), 851-864.
33. Bertrand, N.; Leroux, J. C. The journey of a drug-carrier in the body: an anatomophysiological perspective. *J. Control Release* **2012**, *161* (2), 152-163.
34. Maeda, H.; Wu, J.; Sawa, T.; Matsumura, Y.; Hori, K. Tumor vascular permeability and the EPR effect in macromolecular therapeutics: a review. *J. Control Release* **2000**, *65* (1-2), 271-284.
35. Wilhelm, S.; Tavares, A. J.; Dai, Q.; Ohta, S.; Audet, J.; Dvorak, H. F.; Chan, W. C. W. Analysis of nanoparticle delivery to tumours. *Nat. Rev. Mater* **2016**, *1*, 16014.
36. Mirshafiee, V.; Mahmoudi, M.; Lou, K.; Cheng, J.; Kraft, M. L. Protein corona significantly reduces active targeting yield. *Chem. Commun. (Camb.)* **2013**, *49*(25), 2557-2559.
37. Stepien, G.; Moros, M.; Perez-Hernandez, M.; Monge, M.; Gutierrez, L.; Fratila, R. M.; Las, H. M.; Menao, G. S.; Puente Lanzarote, J. J.; Solans, C.; Pardo, J.; de la Fuente, J. M. Effect of Surface Chemistry and Associated Protein Corona on the Long-Term Biodegradation of Iron Oxide Nanoparticles In Vivo. *ACS Appl. Mater. Interfaces*. **2018**, *10* (5), 4548-4560.

REFERENCES

38. Charbgoon, F.; Nejabat, M.; Abnous, K.; Soltani, F.; Taghdisi, S. M.; Alibolandi, M.; Thomas, S. W.; Steele, T. W. J.; Ramezani, M. Gold nanoparticle should understand protein corona for being a clinical nanomaterial. *J. Control Release* **2018**, *272*, 39-53.
39. Lesniak, A.; Fenaroli, F.; Monopoli, M. P.; Aberg, C.; Dawson, K. A.; Salvati, A. Effects of the presence or absence of a protein corona on silica nanoparticle uptake and impact on cells. *ACS Nano*. **2012**, *6*(7), 5845-5857.
40. Monopoli, M. P.; Walczyk, D.; Campbell, A.; Elia, G.; Lynch, I.; Bombelli, F. B.; Dawson, K. A. Physical-chemical aspects of protein corona: relevance to in vitro and in vivo biological impacts of nanoparticles. *J. Am. Chem. Soc.* **2011**, *133*(8), 2525-2534.
41. Caracciolo, G. Liposome-protein corona in a physiological environment: challenges and opportunities for targeted delivery of nanomedicines. *Nanomedicine*. **2015**, *11*(3), 543-557.
42. Bertrand, N.; Grenier, P.; Mahmoudi, M.; Lima, E. M.; Appel, E. A.; Dormont, F.; Lim, J.; Karnik, R.; Langer, R.; Farokhzad, O. C. Mechanistic understanding of in vivo protein corona formation on polymeric nanoparticles and impact on pharmacokinetics. *Nat. Commun.* **2017**, *8*, 777.
43. Wolfram, J.; Yang, Y.; Shen, J.; Moten, A.; Chen, C.; Shen, H.; Ferrari, M.; Zhao, Y. The nano-plasma interface: Implications of the protein corona. *Colloids Surf. B*. **2014**, *124*, 17-24.
44. Gref, R.; Domb, A.; Quellec, P.; Blunk, T.; Muller, R. H.; Verbavatz, J. M.; Langer, R. The controlled intravenous delivery of drugs using PEG-coated sterically stabilized nanospheres. *Adv. Drug Deliv. Rev.* **1995**, *16*(2-3), 215-233.
45. Palchetti, S.; Colapicchioni, V.; Digiacomo, L.; Caracciolo, G.; Pozzi, D.; Capriotti, A. L.; La, B. G.; Lagana, A. The protein corona of circulating PEGylated liposomes. *Biochim. Biophys. Acta* **2016**, *1858*(2), 189-196.
46. Hadjidemetriou, M.; Al-Ahmady, Z.; Kostarelos, K. Time-evolution of in vivo protein corona onto blood-circulating PEGylated liposomal doxorubicin (DOXIL) nanoparticles. *Nanoscale*. **2016**, *8*(13), 6948-6957.
47. Gref, R.; Luck, M.; Quellec, P.; Marchand, M.; Dellacherie, E.; Harnisch, S.; Blunk, T.; Muller, R. H. 'Stealth' corona-core nanoparticles surface modified by polyethylene glycol (PEG): influences of the corona (PEG chain length and surface density) and of the core composition on phagocytic uptake and plasma protein adsorption. *Colloids Surf. B*. **2000**, *18*(3), 301-313.

48. Parodi, A.; Quattrocchi, N.; van de Ven, A. L.; Chiappini, C.; Evangelopoulos, M.; Martinez, J. O.; Brown, B. S.; Khaled, S. Z.; Yazdi, I. K.; Enzo, M. V.; Isenhardt, L.; Ferrari, M.; Tasciotti, E. Synthetic nanoparticles functionalized with biomimetic leukocyte membranes possess cell-like functions. *Nat. Nanotechnol.* **2013**, *8* (1), 61-68.
49. Hu, C. M.; Zhang, L.; Aryal, S.; Cheung, C.; Fang, R. H.; Zhang, L. Erythrocyte membrane-camouflaged polymeric nanoparticles as a biomimetic delivery platform. *Proc. Natl. Acad. Sci. U. S. A* **2011**, *108* (27), 10980-10985.
50. Rao, L.; Meng, Q. F.; Bu, L. L.; Cai, B.; Huang, Q.; Sun, Z. J.; Zhang, W. F.; Li, A.; Guo, S. S.; Liu, W.; Wang, T. H.; Zhao, X. Z. Erythrocyte Membrane-Coated Upconversion Nanoparticles with Minimal Protein Adsorption for Enhanced Tumor Imaging. *ACS Appl. Mater. Interfaces.* **2017**, *9*(3), 2159-2168.
51. Fu, Q.; Lv, P.; Chen, Z.; Ni, D.; Zhang, L.; Yue, H.; Yue, Z.; Wei, W.; Ma, G. Programmed co-delivery of paclitaxel and doxorubicin boosted by camouflaging with erythrocyte membrane. *Nanoscale.* **2015**, *7*(9), 4020-4030.
52. Rodriguez, P. L.; Harada, T.; Christian, D. A.; Pantano, D. A.; Tsai, R. K.; Discher, D. E. Minimal "Self" peptides that inhibit phagocytic clearance and enhance delivery of nanoparticles. *Science* **2013**, *339*(6122), 971-975.
53. Longmire, M.; Choyke, P. L.; Kobayashi, H. Clearance properties of nano-sized particles and molecules as imaging agents: considerations and caveats. *Nanomedicine. (Lond)* **2008**, *3* (5), 703-717.
54. Toporkiewicz, M.; Meissner, J.; Matuszewicz, L.; Czogalla, A.; Sikorski, A. F. Toward a magic or imaginary bullet? Ligands for drug targeting to cancer cells: principles, hopes, and challenges. *Int. J. Nanomedicine.* **2015**, *10*, 1399-1414.
55. Peer, D.; Karp, J. M.; Hong, S.; Farokhzad, O.; Margalit, R.; Langer, R. Nanocarriers as an emerging platform for cancer therapy. *Nat. Nanotechnol.* **2007**, *2*, 751-760.
56. Bertrand, N.; Wu, J.; Xu, X.; Kamaly, N.; Farokhzad, O. C. Cancer nanotechnology: the impact of passive and active targeting in the era of modern cancer biology. *Adv. Drug Deliv. Rev.* **2014**, *66*, 2-25.
57. Diamantis, N.; Banerji, U. Antibody-drug conjugates--an emerging class of cancer treatment. *Br. J. Cancer* **2016**, *114* (4), 362-367.
58. Lambert, J. M.; Berkenblit, A. Antibody-Drug Conjugates for Cancer Treatment. *Annu. Rev. Med.* **2018**, *69*, 191-207.

REFERENCES

59. Sievers, E. L.; Senter, P. D. Antibody-drug conjugates in cancer therapy. *Annu. Rev. Med.* **2013**, *64*, 15-29.
60. Hamann, P. R.; Hinman, L. M.; Hollander, I.; Beyer, C. F.; Lindh, D.; Holcomb, R.; Hallett, W.; Tsou, H. R.; Upeslakis, J.; Shochat, D.; Mountain, A.; Flowers, D. A.; Bernstein, I. Gemtuzumab ozogamicin, a potent and selective anti-CD33 antibody-calicheamicin conjugate for treatment of acute myeloid leukemia. *Bioconjug. Chem.* **2002**, *13* (1), 47-58.
61. Beck, A.; Goetsch, L.; Dumontet, C.; Corvaia, N. Strategies and challenges for the next generation of antibody-drug conjugates. *Nat. Rev. Drug Discov.* **2017**, *16* (5), 315-337.
62. Lu, J.; Jiang, F.; Lu, A.; Zhang, G. Linkers Having a Crucial Role in Antibody-Drug Conjugates. *Int. J. Mol. Sci.* **2016**, *17* (4), 561.
63. Tsuchikama, K.; An, Z. Antibody-drug conjugates: recent advances in conjugation and linker chemistries. *Protein Cell* **2018**, *9* (1), 33-46.
64. Tang, Z.; Li, D.; Sun, H.; Guo, X.; Chen, Y.; Zhou, S. Quantitative control of active targeting of nanocarriers to tumor cells through optimization of folate ligand density. *Biomaterials* **2014**, *35* (27), 8015-8027.
65. Poon, Z.; Chen, S.; Engler, A. C.; Lee, H. I.; Atas, E.; von, M. G.; Bhatia, S. N.; Hammond, P. T. Ligand-clustered "patchy" nanoparticles for modulated cellular uptake and in vivo tumor targeting. *Angew. Chem. Int. Ed Engl.* **2010**, *49* (40), 7266-7270.
66. Muro, S. Challenges in design and characterization of ligand-targeted drug delivery systems. *J. Control Release* **2012**, *164* (2), 125-137.
67. Lee, S. H.; Sato, Y.; Hyodo, M.; Harashima, H. Size-Dependency of the Surface Ligand Density of Liposomes Prepared by Post-insertion. *Biol. Pharm. Bull.* **2017**, *40* (7), 1002-1009.
68. Colombo, M.; Fiandra, L.; Alessio, G.; Mazzucchelli, S.; Nebuloni, M.; De, P. C.; Kantner, K.; Pelaz, B.; Rotem, R.; Corsi, F.; Parak, W. J.; Prospero, D. Tumour homing and therapeutic effect of colloidal nanoparticles depend on the number of attached antibodies. *Nat. Commun.* **2016**, *7*, 13818.
69. Maxfield, F. R.; Yamashiro, D. J. Endosome acidification and the pathways of receptor-mediated endocytosis. *Adv. Exp. Med. Biol.* **1987**, *225*, 189-198.
70. Hou, K. K.; Pan, H.; Schlesinger, P. H.; Wickline, S. A. A role for peptides in overcoming endosomal entrapment in siRNA delivery - A focus on melittin. *Biotechnol. Adv.* **2015**, *33*, 931-940.
71. Ogris, M.; Carlisle, R. C.; Bettinger, T.; Seymour, L. W. Melittin enables efficient vesicular escape and enhanced nuclear access of nonviral gene delivery vectors. *J. Biol. Chem.* **2001**, *276* (50), 47550-47555.

72. Ahmad, A.; Ranjan, S.; Zhang, W.; Zou, J.; Pyykko, I.; Kinnunen, P. K. Novel endosomolytic peptides for enhancing gene delivery in nanoparticles. *Biochim. Biophys. Acta* **2015**, *1848* (2), 544-553.
73. Jia, L. T.; Zhang, L. H.; Yu, C. J.; Zhao, J.; Xu, Y. M.; Gui, J. H.; Jin, M.; Ji, Z. L.; Wen, W. H.; Wang, C. J.; Chen, S. Y.; Yang, A. G. Specific tumoricidal activity of a secreted proapoptotic protein consisting of HER2 antibody and constitutively active caspase-3. *Cancer Res.* **2003**, *63* (12), 3257-3262.
74. Kakimoto, S.; Hamada, T.; Komatsu, Y.; Takagi, M.; Tanabe, T.; Azuma, H.; Shinkai, S.; Nagasaki, T. The conjugation of diphtheria toxin T domain to poly(ethylenimine) based vectors for enhanced endosomal escape during gene transfection. *Biomaterials* **2009**, *30* (3), 402-408.
75. Michiue, H.; Tomizawa, K.; Wei, F. Y.; Matsushita, M.; Lu, Y. F.; Ichikawa, T.; Tamiya, T.; Date, I.; Matsui, H. The NH2 terminus of influenza virus hemagglutinin-2 subunit peptides enhances the antitumor potency of polyarginine-mediated p53 protein transduction. *J. Biol. Chem.* **2005**, *280* (9), 8285-8289.
76. Simeoni, F.; Morris, M. C.; Heitz, F.; Divita, G. Insight into the mechanism of the peptide-based gene delivery system MPG: implications for delivery of siRNA into mammalian cells. *Nucleic Acids Res.* **2003**, *31* (11), 2717-2724.
77. Hatakeyama, H.; Ito, E.; Akita, H.; Oishi, M.; Nagasaki, Y.; Futaki, S.; Harashima, H. A pH-sensitive fusogenic peptide facilitates endosomal escape and greatly enhances the gene silencing of siRNA-containing nanoparticles in vitro and in vivo. *J. Control Release* **2009**, *139* (2), 127-132.
78. Min, S. H.; Lee, D. C.; Lim, M. J.; Park, H. S.; Kim, D. M.; Cho, C. W.; Yoon, D. Y.; Yeom, Y. I. A composite gene delivery system consisting of polyethylenimine and an amphipathic peptide KALA. *J. Gene Med.* **2006**, *8* (12), 1425-1434.
79. Varkouhi, A. K.; Scholte, M.; Storm, G.; Haisma, H. J. Endosomal escape pathways for delivery of biologicals. *J. Control Release* **2011**, *151* (3), 220-228.
80. Mateos-Timoneda, M. A.; Lok, M. C.; Hennink, W. E.; Feijen, J.; Engbersen, J. F. Poly(amido amine)s as gene delivery vectors: effects of quaternary nicotinamide moieties in the side chains. *ChemMedChem.* **2008**, *3* (3), 478-486.
81. Meng, Z.; Luan, L.; Kang, Z.; Feng, S.; Meng, Q.; Liu, K. Histidine-enriched multifunctional peptide vectors with enhanced cellular uptake and endosomal escape for gene delivery. *J. Mater. Chem. B* **2017**, *5*, 74-84.
82. Ferrer-Miralles, N.; Corchero, J. L.; Kumar, P.; Cedano, J. A.; Gupta, K. C.; Villaverde, A.; Vazquez, E. Biological activities of histidine-rich peptides; merging biotechnology and nanomedicine. *Microb. Cell Fact.* **2011**, *10*, 101.

REFERENCES

83. Benjaminsen, R. V.; Matthebjerg, M. A.; Henriksen, J. R.; Moghimi, S. M.; Andresen, T. L. The possible "proton sponge " effect of polyethylenimine (PEI) does not include change in lysosomal pH. *Mol. Ther.* **2013**, *21* (1), 149-157.
84. Akinc, A.; Thomas, M.; Klibanov, A. M.; Langer, R. Exploring polyethylenimine-mediated DNA transfection and the proton sponge hypothesis. *J. Gene Med.* **2005**, *7*(5), 657-663.
85. Cronin, K. A.; Lake, A. J.; Scott, S.; Sherman, R. L.; Noone, A. M.; Howlader, N.; Henley, S. J.; Anderson, R. N.; Firth, A. U.; Ma, J.; Kohler, B. A.; Jemal, A. Annual Report to the Nation on the Status of Cancer, part I: National cancer statistics. *Cancer* **2018**, *124* (13), 2785-2800.
86. Feng, Y.; Broder, C. C.; Kennedy, P. E.; Berger, E. A. HIV-1 entry cofactor: functional cDNA cloning of a seven-transmembrane, G protein-coupled receptor. *Science* **1996**, *272* (5263), 872-877.
87. The Human Protein Atlas: <https://www.proteinatlas.org/>
88. Chatterjee, S.; Behnam, A. B.; Nimmagadda, S. The intricate role of CXCR4 in cancer. *Adv. Cancer Res.* **2014**, *124*, 31-82.
89. Vazquez, E.; Mangues, R.; Villaverde, A. Functional recruitment for drug delivery through protein-based nanotechnologies. *Nanomedicine. (Lond)* **2016**, *11* (11), 1333-1336.
90. Shen, J.; Wolfram, J.; Ferrari, M.; Shen, H. Taking the vehicle out of drug delivery. *Mater. Today (Kidlington.)* **2017**, *20* (3), 95-97.
91. Li, W.; Yang, Y.; Wang, C.; Liu, Z.; Zhang, X.; An, F.; Diao, X.; Hao, X.; Zhang, X. Carrier-free, functionalized drug nanoparticles for targeted drug delivery. *Chem. Commun. (Camb.)* **2012**, *48* (65), 8120-8122.
92. Zhao, Y.; Wang, W.; Guo, S.; Wang, Y.; Miao, L.; Xiong, Y.; Huang, L. PolyMetformin combines carrier and anticancer activities for in vivo siRNA delivery. *Nat. Commun.* **2016**, *7*, 11822.
93. Jung, Y. D.; Ellis, L. M. Inhibition of tumour invasion and angiogenesis by epigallocatechin gallate (EGCG), a major component of green tea. *Int. J. Exp. Pathol.* **2001**, *82* (6), 309-316.
94. Chung, J. E.; Tan, S.; Gao, S. J.; Yongvongsoontorn, N.; Kim, S. H.; Lee, J. H.; Choi, H. S.; Yano, H.; Zhuo, L.; Kurisawa, M.; Ying, J. Y. Self-assembled micellar nanocomplexes comprising green tea catechin derivatives and protein drugs for cancer therapy. *Nat. Nanotechnol.* **2014**, *9* (11), 907-912.
95. Pieters, B. J. G. E.; van Eldijk, M. B.; Nolte, R. J. M.; Mecnovic, J. Natural supramolecular protein assemblies. *Chem. Soc. Rev.* **2016**, *45*, 24-39.

96. Ferrer-Miralles, N.; Domingo-Espin, J.; Corchero, J. L.; Vazquez, E.; Villaverde, A. Microbial factories for recombinant pharmaceuticals. *Microb. Cell Fact.* **2009**, *8*, 17.
97. Cano-Garrido, O.; Sanchez-Chardi, A.; Pares, S.; Giro, I.; Tatkievicz, W. I.; Ferrer-Miralles, N.; Ratera, I.; Natalello, A.; Cubarsi, R.; Veciana, J.; Bach, A.; Villaverde, A.; Aris, A.; Garcia-Fruitos, E. Functional protein-based nanomaterial produced in microorganisms recognized as safe: A new platform for biotechnology. *Acta Biomater.* **2016**, *43*, 230-239.
98. Taguchi, S.; Ooi, T.; Mizuno, K.; Matsusaki, H. Advances and needs for endotoxin-free production strains. *Appl. Microbiol. Biotechnol.* **2015**, *99* (22), 9349-9360.
99. Cano-Garrido, O.; Seras-Franzoso, J.; Garcia-Fruitos, E. Lactic acid bacteria: reviewing the potential of a promising delivery live vector for biomedical purposes. *Microb. Cell Fact.* **2015**, *14*, 137.
100. Cano-Garrido, O.; Cespedes, M. V.; Unzueta, U.; Saccardo, P.; Roldan, M.; Sanchez-Chardi, A.; Cubarsi, R.; Vazquez, E.; Mangues, R.; Garcia-Fruitos, E.; Villaverde, A. CXCR4(+)-targeted protein nanoparticles produced in the food-grade bacterium *Lactococcus lactis*. *Nanomedicine. (Lond)* **2016**, *11* (18), 2387-2398.
101. Rueda, F.; Cespedes, M. V.; Sanchez-Chardi, A.; Seras-Franzoso, J.; Pesarrodonna, M.; Ferrer-Miralles, N.; Vazquez, E.; Rinas, U.; Unzueta, U.; Mamat, U.; Mangues, R.; Garcia-Fruitos, E.; Villaverde, A. Structural and functional features of self-assembling protein nanoparticles produced in endotoxin-free *Escherichia coli*. *Microb. Cell Fact.* **2016**, *15*, 59.
102. Unzueta, U.; Seras-Franzoso, J.; Cespedes, M. V.; Saccardo, P.; Cortes, F.; Rueda, F.; Garcia-Fruitos, E.; Ferrer-Miralles, N.; Mangues, R.; Vazquez, E.; Villaverde, A. Engineering tumor cell targeting in nanoscale amyloidal materials. *Nanotechnology.* **2017**, *28* (1), 015102.
103. Mamat, U.; Wilke, K.; Bramhill, D.; Schromm, A. B.; Lindner, B.; Kohl, T. A.; Corchero, J. L.; Villaverde, A.; Schaffer, L.; Head, S. R.; Souvignier, C.; Meredith, T. C.; Woodard, R. W. Detoxifying *Escherichia coli* for endotoxin-free production of recombinant proteins. *Microb. Cell Fact.* **2015**, *14*, 57.
104. Celik, E.; Calik, P. Production of recombinant proteins by yeast cells. *Biotechnol. Adv.* **2012**, *30* (5), 1108-1118.
105. Nielsen, J. Production of biopharmaceutical proteins by yeast: advances through metabolic engineering. *Bioengineered.* **2013**, *4* (4), 207-211.
106. Contreras-Gomez, A.; Sanchez-Miron, A.; Garcia-Camacho, F.; Molina-Grima, E.; Chisti, Y. Protein production using the baculovirus-insect cell expression system. *Biotechnol. Prog.* **2014**, *30* (1), 1-18.

REFERENCES

107. Hamilton, S. R.; Gerngross, T. U. Glycosylation engineering in yeast: the advent of fully humanized yeast. *Curr. Opin. Biotechnol.* **2007**, *18* (5), 387-392.
108. Lai, T.; Yang, Y.; Ng, S. K. Advances in Mammalian cell line development technologies for recombinant protein production. *Pharmaceuticals (Basel)* **2013**, *6* (5), 579-603.
109. Lalonde, M. E.; Durocher, Y. Therapeutic glycoprotein production in mammalian cells. *J. Biotechnol.* **2017**, *251*, 128-140.
110. Garcia-Fruitos, E.; Gonzalez-Montalban, N.; Morell, M.; Vera, A.; Ferraz, R. M.; Aris, A.; Ventura, S.; Villaverde, A. Aggregation as bacterial inclusion bodies does not imply inactivation of enzymes and fluorescent proteins. *Microb. Cell Fact.* **2005**, *4*, 27.
111. Garcia-Fruitos, E. Inclusion bodies: a new concept. *Microb. Cell Fact.* **2010**, *9*, 80.
112. de, M. A.; Ferrer-Miralles, N.; Garcia-Fruitos, E.; Mitraki, A.; Peternel, S.; Rinas, U.; Trujillo-Roldan, M. A.; Valdez-Cruz, N. A.; Vazquez, E.; Villaverde, A. Bacterial inclusion bodies are industrially exploitable amyloids. *FEMS Microbiol. Rev.* **2019**, *43* (1), 53-72.
113. Garcia-Fruitos, E.; Sabate, R.; de Groot, N. S.; Villaverde, A.; Ventura, S. Biological role of bacterial inclusion bodies: a model for amyloid aggregation. *FEBS J.* **2011**, *278* (14), 2419-2427.
114. Martinez-Alonso, M.; Gonzalez-Montalban, N.; Garcia-Fruitos, E.; Villaverde, A. Learning about protein solubility from bacterial inclusion bodies. *Microb. Cell Fact.* **2009**, *8*, 4.
115. Rinas, U.; Garcia-Fruitos, E.; Corchero, J. L.; Vazquez, E.; Seras-Franzoso, J.; Villaverde, A. Bacterial Inclusion Bodies: Discovering Their Better Half. *Trends Biochem. Sci.* **2017**, *42* (9), 726-737.
116. Garcia-Fruitos, E.; Seras-Franzoso, J.; Vazquez, E.; Villaverde, A. Tunable geometry of bacterial inclusion bodies as substrate materials for tissue engineering. *Nanotechnology.* **2010**, *21* (20), 205101.
117. Seras-Franzoso, J.; Diez-Gil, C.; Vazquez, E.; Garcia-Fruitos, E.; Cubarsi, R.; Ratera, I.; Veciana, J.; Villaverde, A. Bioadhesiveness and efficient mechanotransduction stimuli synergistically provided by bacterial inclusion bodies as scaffolds for tissue engineering. *Nanomedicine (Lond)* **2012**, *7* (1), 79-93.
118. Unzueta, U.; Cespedes, M. V.; Sala, R.; Alamo, P.; Sanchez-Chardi, A.; Pesarrodonna, M.; Sanchez-Garcia, L.; Cano-Garrido, O.; Villaverde, A.; Vazquez, E.; Mangues, R.; Seras-Franzoso, J. Release of targeted protein nanoparticles from functional bacterial amyloids: A death star-like approach. *J. Control Release* **2018**, *279*, 29-39.

119. Lee, E. J.; Lee, N. K.; Kim, I. S. Bioengineered protein-based nanocage for drug delivery. *Adv. Drug Deliv. Rev.* **2016**, *106*, 157-171.
120. Frietze, K. M.; Peabody, D. S.; Chackerian, B. Engineering virus-like particles as vaccine platforms. *Curr. Opin. Virol.* **2016**, *18*, 44-49.
121. Ong, H. K.; Tan, W. S.; Ho, K. L. Virus like particles as a platform for cancer vaccine development. *PeerJ.* **2017**, *5*, e4053.
122. Kushnir, N.; Streatfield, S. J.; Yusibov, V. Virus-like particles as a highly efficient vaccine platform: diversity of targets and production systems and advances in clinical development. *Vaccine* **2012**, *31* (1), 58-83.
123. Palladini, A.; Thrane, S.; Janitzek, C. M.; Pihl, J.; Clemmensen, S. B.; de Jongh, W. A.; Clausen, T. M.; Nicoletti, G.; Landuzzi, L.; Penichet, M. L.; Balboni, T.; Ianzano, M. L.; Giusti, V.; Theander, T. G.; Nielsen, M. A.; Salanti, A.; Lollini, P. L.; Nanni, P.; Sander, A. F. Virus-like particle display of HER2 induces potent anti-cancer responses. *Oncoimmunology.* **2018**, *7* (3), e1408749.
124. Ma, Y.; Nolte, R. J.; Cornelissen, J. J. Virus-based nanocarriers for drug delivery. *Adv. Drug Deliv. Rev.* **2012**, *64* (9), 811-825.
125. Rohovie, M. J.; Nagasawa, M.; Swartz, J. R. Virus-like particles: Next-generation nanoparticles for targeted therapeutic delivery. *Bioeng. Transl. Med.* **2017**, *2* (1), 43-57.
126. Fan, X. Z.; Naves, L.; Siwak, N. P.; Brown, A.; Culver, J.; Ghodssi, R. Integration of genetically modified virus-like-particles with an optical resonator for selective bio-detection. *Nanotechnology.* **2015**, *26* (20), 205501.
127. Unzueta, U.; Cespedes, M. V.; Vazquez, E.; Ferrer-Miralles, N.; Mangues, R.; Villaverde, A. Towards protein-based viral mimetics for cancer therapies. *Trends Biotechnol.* **2015**, *33* (5), 253-258.
128. Lapenta, F.; Aupic, J.; Strmsek, Z.; Jerala, R. Coiled coil protein origami: from modular design principles towards biotechnological applications. *Chem. Soc. Rev.* **2018**, *47* (10), 3530-3542.
129. Padilla, J. E.; Colovos, C.; Yeates, T. O. Nanohedra: using symmetry to design self assembling protein cages, layers, crystals, and filaments. *Proc. Natl. Acad. Sci. U. S. A* **2001**, *98* (5), 2217-2221.
130. Vazquez, E.; Villaverde, A. Engineering building blocks for self-assembling protein nanoparticles. *Microb. Cell Fact.* **2010**, *9*, 101.
131. Unzueta, U.; Ferrer-Miralles, N.; Cedano, J.; Zikung, X.; Pesarrodona, M.; Saccardo, P.; Garcia-Fruitos, E.; Domingo-Espin, J.; Kumar, P.; Gupta, K. C.; Mangues, R.; Villaverde, A.; Vazquez, E. Non-amyloidogenic peptide tags for the regulatable self-assembling of protein-only nanoparticles. *Biomaterials* **2012**, *33* (33), 8714-8722.

REFERENCES

132. Serna, N.; Cespedes, M. V.; Saccardo, P.; Xu, Z.; Unzueta, U.; Alamo, P.; Pesarrodonna, M.; Sanchez-Chardi, A.; Roldan, M.; Mangues, R.; Vazquez, E.; Villaverde, A.; Ferrer-Miralles, N. Rational engineering of single-chain polypeptides into protein-only, BBB-targeted nanoparticles. *Nanomedicine*. **2016**, *12* (5), 1241-1251.
133. Cespedes, M. V.; Unzueta, U.; Tatkiwicz, W.; Sanchez-Chardi, A.; Conchillo-Sole, O.; Alamo, P.; Xu, Z.; Casanova, I.; Corchero, J. L.; Pesarrodonna, M.; Cedano, J.; Daura, X.; Ratera, I.; Veciana, J.; Ferrer-Miralles, N.; Vazquez, E.; Villaverde, A.; Mangues, R. In vivo architectonic stability of fully de novo designed protein-only nanoparticles. *ACS Nano*. **2014**, *8* (5), 4166-4176.
134. Vazquez, E.; Roldan, M.; Diez-Gil, C.; Unzueta, U.; Domingo-Espin, J.; Cedano, J.; Conchillo, O.; Ratera, I.; Veciana, J.; Daura, X.; Ferrer-Miralles, N.; Villaverde, A. Protein nanodisk assembling and intracellular trafficking powered by an arginine-rich (R9) peptide. *Nanomedicine. (Lond)* **2010**, *5* (2), 259-268.
135. Pesarrodonna, M.; Fernandez, Y.; Foradada, L.; Sanchez-Chardi, A.; Conchillo-Sole, O.; Unzueta, U.; Xu, Z.; Roldan, M.; Villegas, S.; Ferrer-Miralles, N.; Schwartz S Jr; Rinas, U.; Daura, X.; Abasolo, I.; Vazquez, E.; Villaverde, A. Conformational and functional variants of CD44-targeted protein nanoparticles bio-produced in bacteria. *Biofabrication*. **2016**, *8* (2), 025001.
136. Pesarrodonna, M.; Ferrer-Miralles, N.; Unzueta, U.; Gener, P.; Tatkiwicz, W.; Abasolo, I.; Ratera, I.; Veciana, J.; Schwartz S Jr; Villaverde, A.; Vazquez, E. Intracellular targeting of CD44+ cells with self-assembling, protein only nanoparticles. *Int. J. Pharm.* **2014**, *473* (1-2), 286-295.
137. Cespedes, M. V.; Unzueta, U.; Avino, A.; Gallardo, A.; Alamo, P.; Sala, R.; Sanchez-Chardi, A.; Casanova, I.; Mangues, M. A.; Lopez-Pousa, A.; Eritja, R.; Villaverde, A.; Vazquez, E.; Mangues, R. Selective depletion of metastatic stem cells as therapy for human colorectal cancer. *EMBO Mol. Med.* **2018**, *10* (10).
138. de Pinho Favaro, M. T.; Sanchez-Garcia, L.; Sanchez-Chardi, A.; Roldan, M.; Unzueta, U.; Serna, N.; Cano-Garrido, O.; Azzoni, A. R.; Ferrer-Miralles, N.; Villaverde, A.; Vazquez, E. Protein nanoparticles are nontoxic, tuneable cell stressors. *Nanomedicine. (Lond)* **2018**, *13* (3), 255-268.
139. Serna, N.; Cespedes, M. V.; Saccardo, P.; Xu, Z.; Unzueta, U.; Alamo, P.; Pesarrodonna, M.; Sanchez-Chardi, A.; Roldan, M.; Mangues, R.; Vazquez, E.; Villaverde, A.; Ferrer-Miralles, N. Rational engineering of single-chain polypeptides into protein-only, BBB-targeted nanoparticles. *Nanomedicine*. **2016**, *12* (5), 1241-1251.

140. Unzueta, U.; Cespedes, M. V.; Ferrer-Miralles, N.; Casanova, I.; Cedano, J.; Corchero, J. L.; Domingo-Espin, J.; Villaverde, A.; Mangués, R.; Vázquez, E. Intracellular CXCR4(+) cell targeting with T22-empowered protein-only nanoparticles. *Int. J. Nanomedicine*. **2012**, *7*, 4533-4544.
141. Serna, N.; Cespedes, M. V.; Sanchez-Garcia, L.; Unzueta, U.; Sala, R.; Sanchez-Chardi, A.; Cortes, F.; Ferrer-Miralles, N.; Mangués, R.; Vázquez, E.; Villaverde, A. Peptide-based nanostructured materials with intrinsic proapoptotic activities in CXCR4+ solid tumors. *Adv. Funct. Mater.* **2017**, *27*(32), 1700919.
142. Lopez-Laguna, H.; Unzueta, U.; Conchillo-Sole, O.; Sanchez-Chardi, A.; Pesarrodonna, M.; Cano-Garrido, O.; Volta, E.; Sanchez-Garcia, L.; Serna, N.; Saccardo, P.; Mangués, R.; Villaverde, A.; Vázquez, E. Assembly of histidine-rich protein materials controlled through divalent cations. *Acta Biomater.* **2019**, *83*, 257-264.
143. Rueda, F.; Cespedes, M. V.; Conchillo-Sole, O.; Sanchez-Chardi, A.; Seras-Franzoso, J.; Cubarsi, R.; Gallardo, A.; Pesarrodonna, M.; Ferrer-Miralles, N.; Daura, X.; Vázquez, E.; Garcia-Fruitos, E.; Mangués, R.; Unzueta, U.; Villaverde, A. Bottom-Up Instructive Quality Control in the Biofabrication of Smart Protein Materials. *Adv. Mater.* **2015**, *27*(47), 7816-7822.
144. Ma, R.; Mahadevappa, R.; Kwok, H. F. Venom-based peptide therapy: insights into anti-cancer mechanism. *Oncotarget*. **2017**, *8*(59), 100908-100930.
145. Chaisakul, J.; Hodgson, W. C.; Kuruppu, S.; Prasongsook, N. Effects of Animal Venoms and Toxins on Hallmarks of Cancer. *J. Cancer* **2016**, *7*(11), 1571-1578.
146. Grinberg, Y.; Benhar, I. Addressing the Immunogenicity of the Cargo and of the Targeting Antibodies with a Focus on Demmunized Bacterial Toxins and on Antibody-Targeted Human Effector Proteins. *Biomedicines*. **2017**, *5*(2).
147. Hardwick, J. M.; Soane, L. Multiple functions of BCL-2 family proteins. *Cold Spring Harb. Perspect. Biol.* **2013**, *5*(2).
148. Shamas-Din, A.; Kale, J.; Leber, B.; Andrews, D. W. Mechanisms of action of Bcl-2 family proteins. *Cold Spring Harb. Perspect. Biol.* **2013**, *5*(4), 008714.
149. Walsh, M. J.; Dodd, J. E.; Hautbergue, G. M. Ribosome-inactivating proteins: potent poisons and molecular tools. *Virulence*. **2013**, *4*(8), 774-784.
150. Wang, Z.; Zheng, Q.; Zhang, H.; Bronson, R. T.; Madsen, J. C.; Sachs, D. H.; Huang, C. A.; Wang, Z. Ontak-like human IL-2 fusion toxin. *J. Immunol. Methods* **2017**, *448*, 51-58.

REFERENCES

151. Hollevoet, K.; Mason-Osann, E.; Liu, X. F.; Imhof-Jung, S.; Niederfellner, G.; Pastan, I. In vitro and in vivo activity of the low-immunogenic antimesothelin immunotoxin RG7787 in pancreatic cancer. *Mol. Cancer Ther.* **2014**, *13* (8), 2040-2049.
152. Allahyari, H.; Heidari, S.; Ghamgosha, M.; Saffarian, P.; Amani, J. Immunotoxin: A new tool for cancer therapy. *Tumour. Biol.* **2017**, *39* (2), 1010428317692226.
153. Pastan, I.; Hassan, R.; Fitzgerald, D. J.; Kreitman, R. J. Immunotoxin therapy of cancer. *Nat. Rev. Cancer* **2006**, *6* (7), 559-565.
154. Liu, D.; Auguste, D. T. Cancer targeted therapeutics: From molecules to drug delivery vehicles. *J. Control Release* **2015**, *219*, 632-643.
155. Lammers, T.; Hennink, W. E.; Storm, G. Tumour-targeted nanomedicines: principles and practice. *Br. J. Cancer* **2008**, *99* (3), 392-397.
156. Yang, Y.; Luo, Z.; Qin, Y.; Zhou, Y.; Gong, L.; Huang, J.; Wang, H. Production of bFGF monoclonal antibody and its inhibition of metastasis in Lewis lung carcinoma. *Mol. Med. Rep.* **2017**, *16* (4), 4015-4021.
157. Makita, S.; Tobinai, K. Antibody therapy targeting CD19 for B-cell non-Hodgkin's lymphoma. *Ann. Oncol.* **2018**, *29* (5), 1086-1089.
158. Rimawi, M. F.; Schiff, R.; Osborne, C. K. Targeting HER2 for the treatment of breast cancer. *Annu. Rev. Med.* **2015**, *66*, 111-128.
159. Cespedes, M. V.; Unzueta, U.; Alamo, P.; Gallardo, A.; Sala, R.; Casanova, I.; Pavon, M. A.; Mangués, M. A.; Trias, M.; Lopez-Pousa, A.; Villaverde, A.; Vazquez, E.; Mangués, R. Cancer-specific uptake of a liganded protein nanocarrier targeting aggressive CXCR4(+) colorectal cancer models. *Nanomedicine.* **2016**, *12* (7), 1987-1996.
160. Duncan, R.; Gaspar, R. Nanomedicine(s) under the microscope. *Mol. Pharm.* **2011**, *8* (6), 2101-2141.
161. Mbanya, J. C.; Sandow, J.; Landgraf, W.; Owens, D. R. Recombinant human insulin in global diabetes management - Focus on clinical efficacy. *Eur. Endocrinol.* **2017**, *13* (1), 21-25.
162. Vajo, Z.; Fawcett, J.; Duckworth, W. C. Recombinant DNA technology in the treatment of diabetes: insulin analogs. *Endocr. Rev.* **2001**, *22* (5), 706-717.
163. Swiech, K.; Picanco-Castro, V.; Covas, D. T. Production of recombinant coagulation factors: Are humans the best host cells? *Bioengineered.* **2017**, *8* (5), 462-470.
164. Powell, J. S. Lasting power of new clotting proteins. *Hematology. Am. Soc. Hematol. Educ. Program.* **2014**, *2014* (1), 355-363.

165. Johnson, I. S. Human insulin from recombinant DNA technology. *Science* **1983**, *219*(4585), 632-637.
166. Anonymous. Human insulin receives FDA approval. *FDA. Drug Bull.* **1982**, *12* (3), 18-19.
167. Ferrer-Miralles, N.; Villaverde, A. Bacterial cell factories for recombinant protein production; expanding the catalogue. *Microb. Cell Fact.* **2013**, *12*, 113.
168. Bandaranayake, A. D.; Almo, S. C. Recent advances in mammalian protein production. *FEBS Lett.* **2014**, *588* (2), 253-260.
169. Manoukian, G.; Hagemester, F. Denileukin diftitox: a novel immunotoxin. *Expert Opin. Biol. Ther.* **2009**, *9*(11), 1445-1451.
170. Chung, C.; Pherwani, N. Ziv-aflibercept: a novel angiogenesis inhibitor for the treatment of metastatic colorectal cancer. *Am. J. Health Syst. Pharm.* **2013**, *70*(21), 1887-1896.
171. Perkins, S. L.; Cole, S. W. Ziv-aflibercept (Zaltrap) for the treatment of metastatic colorectal cancer. *Ann. Pharmacother.* **2014**, *48*(1), 93-98.
172. Choi, H. S.; Liu, W.; Misra, P.; Tanaka, E.; Zimmer, J. P.; Itty, I. B.; Bawendi, M. G.; Frangioni, J. V. Renal clearance of quantum dots. *Nat. Biotechnol.* **2007**, *25*(10), 1165-1170.
173. Wang, J.; Liu, G. Imaging Nano-Bio Interactions in the Kidney: Toward a Better Understanding of Nanoparticle Clearance. *Angew. Chem. Int. Ed Engl.* **2018**, *57*(12), 3008-3010.
174. Peigneur, S.; Tytgat, J. Toxins in Drug Discovery and Pharmacology. *Toxins. (Basel)* **2018**, *10*(3).
175. Calvete, J. J.; Sanz, L.; Angulo, Y.; Lomonte, B.; Gutierrez, J. M. Venoms, venomics, antivenomics. *FEBS Lett.* **2009**, *583* (11), 1736-1743.
176. Schmohl, J. U.; Todhunter, D.; Oh, S.; Vallera, D. A. Mutagenic Deimmunization of Diphtheria Toxin for Use in Biologic Drug Development. *Toxins. (Basel)* **2015**, *7*(10), 4067-4082.
177. Onda, M.; Nagata, S.; FitzGerald, D. J.; Beers, R.; Fisher, R. J.; Vincent, J. J.; Lee, B.; Nakamura, M.; Hwang, J.; Kreitman, R. J.; Hassan, R.; Pastan, I. Characterization of the B cell epitopes associated with a truncated form of *Pseudomonas* exotoxin (PE38) used to make immunotoxins for the treatment of cancer patients. *J. Immunol.* **2006**, *177*(12), 8822-8834.
178. Juliano, R. L.; Alam, R.; Dixit, V.; Kang, H. M. Cell-targeting and cell-penetrating peptides for delivery of therapeutic and imaging agents. *WIREs Nanomed. Nanobi.* **2009**, *1* (3), 324-335.

REFERENCES

179. Vives, E.; Schmidt, J.; Pelegrin, A. Cell-penetrating and cell-targeting peptides in drug delivery. *Biochim. Biophys. Acta* **2008**, *1786* (2), 126-138.
180. LeCher, J. C.; Nowak, S. J.; McMurry, J. L. Breaking in and busting out: cell-penetrating peptides and the endosomal escape problem. *Biomol. Concepts* **2017**, *8* (3), 131-141.
181. Barati, S.; Chegini, F.; Hurtado, P.; Rush, R. A. Hybrid tetanus toxin C fragment-diphtheria toxin translocation domain allows specific gene transfer into PC12 cells. *Exp. Neurol.* **2002**, *177* (1), 75-87.
182. Oliveira, S.; van, R., I; Kranenburg, O.; Storm, G.; Schiffelers, R. M. Fusogenic peptides enhance endosomal escape improving siRNA-induced silencing of oncogenes. *Int. J. Pharm.* **2007**, *331* (2), 211-214.
183. Ferrer-Miralles, N.; Rodriguez-Carmona, E.; Corchero, J. L.; Garcia-Fruitos, E.; Vazquez, E.; Villaverde, A. Engineering protein self-assembling in protein-based nanomedicines for drug delivery and gene therapy. *Crit. Rev. Biotechnol.* **2015**, *35* (2), 209-221.
184. Gelain, F.; Unsworth, L. D.; Zhang, S. Slow and sustained release of active cytokines from self-assembling peptide scaffolds. *J. Control Release* **2010**, *145* (3), 231-239.
185. Aruna, G. Immunotoxins: a review of their use in cancer treatment. *J. Stem Cells Regen. Med.* **2006**, *1* (1), 31-36.
186. Leopold, P. L.; Ferris, B.; Grinberg, I.; Worgall, S.; Hackett, N. R.; Crystal, R. G. Fluorescent virions: dynamic tracking of the pathway of adenoviral gene transfer vectors in living cells. *Hum. Gene Ther.* **1998**, *9* (3), 367-378.
187. Wagner, E.; Plank, C.; Zatloukal, K.; Cotten, M.; Birnstiel, M. L. Influenza virus hemagglutinin HA-2 N-terminal fusogenic peptides augment gene transfer by transferrin-polylysine-DNA complexes: toward a synthetic virus-like gene-transfer vehicle. *Proc. Natl. Acad. Sci. U. S. A* **1992**, *89* (17), 7934-7938.
188. Skehel, J. J.; Cross, K.; Steinhauer, D.; Wiley, D. C. Influenza fusion peptides. *Biochem. Soc. Trans.* **2001**, *29*, 623-626.
189. Han, X.; Bushweller, J. H.; Cafiso, D. S.; Tamm, L. K. Membrane structure and fusion-triggering conformational change of the fusion domain from influenza hemagglutinin. *Nat. Struct. Biol.* **2001**, *8* (8), 715-720.
190. Lee, Y. J.; Johnson, G.; Pellois, J. P. Modeling of the endosomolytic activity of HA2-TAT peptides with red blood cells and ghosts. *Biochemistry* **2010**, *49* (36), 7854-7866.

191. Liou, J. S.; Liu, B. R.; Martin, A. L.; Huang, Y. W.; Chiang, H. J.; Lee, H. J. Protein transduction in human cells is enhanced by cell-penetrating peptides fused with an endosomolytic HA2 sequence. *Peptides* **2012**, *37* (2), 273-284.
192. Serna, N.; Sanchez, J. M.; Unzueta, U.; Sanchez-Garcia, L.; Sanchez-Chardi, A.; Mangues, R.; Vazquez, E.; Villaverde, A. V. Recruiting potent membrane penetrability in tumor cell-targeted protein-only nanoparticles. *Nanotechnology*. **2018**. Available online.
193. Rosenkilde, M. M.; Gerlach, L. O.; Jakobsen, J. S.; Skerlj, R. T.; Bridger, G. J.; Schwartz, T. W. Molecular mechanism of AMD3100 antagonism in the CXCR4 receptor: transfer of binding site to the CXCR3 receptor. *J. Biol. Chem.* **2004**, *279* (4), 3033-3041.
194. Kawaguchi, A.; Orba, Y.; Kimura, T.; Iha, H.; Ogata, M.; Tsuji, T.; Aina, A.; Sata, T.; Okamoto, T.; Hall, W. W.; Sawa, H.; Hasegawa, H. Inhibition of the SDF-1alpha-CXCR4 axis by the CXCR4 antagonist AMD3100 suppresses the migration of cultured cells from ATL patients and murine lymphoblastoid cells from HTLV-I Tax transgenic mice. *Blood* **2009**, *114* (14), 2961-2968.
195. Kim, H. Y.; Hwang, J. Y.; Kim, S. W.; Lee, H. J.; Yun, H. J.; Kim, S.; Jo, D. Y. The CXCR4 Antagonist AMD3100 Has Dual Effects on Survival and Proliferation of Myeloma Cells In Vitro. *Cancer Res. Treat.* **2010**, *42* (4), 225-234.
196. Tietz, P. S.; Yamazaki, K.; LaRusso, N. F. Time-dependent effects of chloroquine on pH of hepatocyte lysosomes. *Biochem. Pharmacol.* **1990**, *40* (6), 1419-1421.
197. Lonn, P.; Kacsinta, A. D.; Cui, X. S.; Hamil, A. S.; Kaulich, M.; Gogoi, K.; Dowdy, S. F. Enhancing Endosomal Escape for Intracellular Delivery of Macromolecular Biologic Therapeutics. *Sci. Rep.* **2016**, *6*, 32301.
198. Leshchiner, E. S.; Braun, C. R.; Bird, G. H.; Walensky, L. D. Direct activation of full-length proapoptotic BAK. *Proc. Natl. Acad. Sci. U. S. A.* **2013**, *110* (11), e986-e995.
199. Holinger, E. P.; Chittenden, T.; Lutz, R. J. Bak BH3 peptides antagonize Bcl-xL function and induce apoptosis through cytochrome c-independent activation of caspases. *J. Biol. Chem.* **1999**, *274* (19), 13298-13304.
200. Dai, H.; Pang, Y. P.; Ramirez-Alvarado, M.; Kaufmann, S. H. Evaluation of the BH3-only protein Puma as a direct Bak activator. *J. Biol. Chem.* **2014**, *289* (1), 89-99.
201. Park, S. Y.; Jeong, M. S.; Jang, S. B. In vitro binding properties of tumor suppressor p53 with PUMA and NOXA. *Biochem. Biophys. Res. Commun.* **2012**, *420* (2), 350-356.

REFERENCES

202. Zhang, Y.; Xing, D.; Liu, L. PUMA promotes Bax translocation by both directly interacting with Bax and by competitive binding to Bcl-X L during UV-induced apoptosis. *Mol. Biol. Cell* **2009**, *20* (13), 3077-3087.
203. Yu, J.; Zhang, L.; Hwang, P. M.; Kinzler, K. W.; Vogelstein, B. PUMA induces the rapid apoptosis of colorectal cancer cells. *Mol. Cell* **2001**, *7* (3), 673-682.
204. Chen, H. C.; Kanai, M.; Inoue-Yamauchi, A.; Tu, H. C.; Huang, Y.; Ren, D.; Kim, H.; Takeda, S.; Reyna, D. E.; Chan, P. M.; Ganesan, Y. T.; Liao, C. P.; Gavathiotis, E.; Hsieh, J. J.; Cheng, E. H. An interconnected hierarchical model of cell death regulation by the BCL-2 family. *Nat. Cell Biol.* **2015**, *17* (10), 1270-1281.
205. Ansari, A. M.; Ahmed, A. K.; Matsangos, A. E.; Lay, F.; Born, L. J.; Marti, G.; Harmon, J. W.; Sun, Z. Cellular GFP Toxicity and Immunogenicity: Potential Confounders in in Vivo Cell Tracking Experiments. *Stem Cell Rev.* **2016**, *12* (5), 553-559.
206. Zhan, C.; Li, C.; Wei, X.; Lu, W.; Lu, W. Toxins and derivatives in molecular pharmaceuticals: Drug delivery and targeted therapy. *Adv. Drug Deliv. Rev.* **2015**, *90*, 101-118.
207. Foss, F. M. DAB(389)IL-2 (ONTAK): a novel fusion toxin therapy for lymphoma. *Clin. Lymphoma* **2000**, *1* (2), 110-116.
208. Wong, B. Y.; Gregory, S. A.; Dang, N. H. Denileukin diftitox as novel targeted therapy for lymphoid malignancies. *Cancer Invest.* **2007**, *25* (6), 495-501.
209. Clinical trials (NCT01829711): <http://clinicaltrials.gov>
210. Clinical trials (NCT00321555): <http://clinicaltrials.gov>
211. Labyntsev, A. J.; Korotkevych, N. V.; Kolybo, D. V.; Komisarenko, S. V. Effect of diphtheria toxin T-domain on endosomal pH. *Ukr. Biochem. J.* **2015**, *87* (4), 13-23.
212. Tyagi, N.; Tyagi, M.; Pachauri, M.; Ghosh, P. C. Potential therapeutic applications of plant toxin-ricin in cancer: challenges and advances. *Tumour. Biol.* **2015**, *36* (11), 8239-8246.
213. Moshiri, M.; Hamid, F.; Etemad, L. Ricin Toxicity: Clinical and Molecular Aspects. *Rep. Biochem. Mol. Biol.* **2016**, *4* (2), 60-65.
214. Wales, R.; Roberts, L. M.; Lord, J. M. Addition of an endoplasmic reticulum retrieval sequence to ricin A chain significantly increases its cytotoxicity to mammalian cells. *J. Biol. Chem.* **1993**, *268* (32), 23986-23990.
215. Liu, D.; Auguste, D. T. Cancer targeted therapeutics: From molecules to drug delivery vehicles. *J. Control Release* **2015**, *219*, 632-643.

216. Endres, M. J.; Clapham, P. R.; Marsh, M.; Ahuja, M.; Turner, J. D.; McKnight, A.; Thomas, J. F.; Stoebenau-Haggarty, B.; Choe, S.; Vance, P. J.; Wells, T. N.; Power, C. A.; Sutterwala, S. S.; Doms, R. W.; Landau, N. R.; Hoxie, J. A. CD4-independent infection by HIV-2 is mediated by fusin/CXCR4. *Cell* **1996**, *87*(4), 745-756.



Departament de Genètica i Microbiologia
Facultat de Biociències
Laura Sánchez García
PhD Thesis 2019

